Ultrastructural Analysis of Proteins Involved in Synapse

Development and Function

BY
Laura Manning
B.S., University of Illinois at Urbana Champaign, 2012

THESIS

Submitted as partial fulfillment of the requirements
for the degree of Doctor of Philosophy in Biological Sciences
in the Graduate College of the
University of Illinois at Chicago, 2017

Chicago, Illinois

Defense Committee:

Liang-Wei Gong, Chair
Janet Richmond, Advisor
Chiou-Fen Chuang
Simon Alford, Anatomy and Cell Biology
Hongkyun Kim, Rosalind Franklin University of Medicine and Science

ACKNOWLEDGEMENTS

Thank you to my advisor, Janet Richmond, who gave me every opportunity to succeed and grow as a scientist. You have helped me develop confidence that is rooted in exceptional training in technique and understanding of the field, and you have worked tirelessly to support my success. Thanks also to my committee members, Doctors Liang-Wei Gong, Simon Alford, Chiou-Fen Chuang, and Hoky Kim for your guidance and thoughtful discussion throughout the course of my PhD. I am grateful to have worked with outstanding collaborators, including Tyne Miller-Fleming and David Miller, Ken Miller, Peri Kurshan and Kang Shen, and Zhao Xuang and Daniel Colón-Ramos, who provided outstanding grounding and insight for my work.

Thank you also to the talented individuals in my electron microscopy community, especially Szi-chieh Yu for world-class training, Alex Gottschalk and his lab, including Wagner Steuer-Costa, and Alex Oranth, for two lovely summers in Germany, Eddie Hujber and Shigeki Watanabe for assistance with data analysis, and Mei Zhen and Maike Kittelmann for anatomical expertise. A huge thanks to Linda Juarez, Figen Seiler, and Olivia Thomson for assistance with the electron microscope and comradery in that dark basement. Thanks also to Reiner Bleher for assistance with the high-pressure freezer.

A very special thank you to Dr. Dave Featherstone, who I always pictured would read this thesis. You were a wonderful mentor and a very special part of our lab family. I learned so much from you about teaching and science. You are dearly missed.

Thanks to my labmates, fellow graduate students, and department faculty members for your support. A special thank you to Dr. Thom Park and Dan Applegate for making me feel welcome at UIC, Brigitte Browe for countless coffee, lunch, and life dates, and Sarah Zinn, for every time we spent alone together in the lab, singing, dancing, laughing, and crying.

I am deeply grateful for the support of my friends and family over the last five and a half years. Thank you especially to my mother, Mona, father, Marty, sister, Amy, brother Charlie, and brother-in-law Michael, for always letting me know that you are rooting for me. And to my amazing extended family, thank you for being such a strong presence and support network for me. Your love is palpable.

Finally, to my partner, Ricardo. The data analysis in this thesis would not be possible without your expert help in building the code to execute it. Far beyond this, I am infinitely grateful for your support through the many late nights, the challenges, and the triumphs. You are my true partner, and I thank you endlessly for your love.

LM

CONTRIBUTION OF AUTHORS

Laura Manning contributed to experimental conception and design for all projects described in this thesis, performed EM experiments and quantified results, created and edited figures and wrote this thesis, critically revised submitted manuscripts and approved final versions for publication.

Additional contributions to Chapter 2

Zhao Xuan, Jessica Nelson, and Peri T. Kurshan contributed to project conception and design, designed and interpreted experiments and performed genetics, imaging, and behavioral experiments, critically revised the manuscript and approved the final version for publication. Janet E. Richmond contributed to project conception and design, designed and interpreted experiments and performed in vivo electrophysiological measurements, critically revised the manuscript and approved the final version for publication. Daniel Colón-Ramos contributed to project conception and design, designed and interpreted experiments and, critically revised the manuscript and approved the final version for publication. Kang Shen contributed to project conception and design, designed and interpreted experiments, critically revised the manuscript, and approved the final version for publication.

Additional contributions to Chapter 3

Logan M. Morrison, Stacey L. Edwards, and Natalia Stec contributed to project conception and design, designed and interpreted experiments and performed genetics and imaging experiments, critically revised the manuscript and approved the final version for publication. Janet E. Richmond and Kenneth G. Miller contributed to project conception and design, critically revised the manuscript and approved the final version for publication.

Additional contributions to Chapter 4 and Appendix A

Tyne Miller-Fleming, Sarah Petersen, Megan Gornet, Allison Beers, and David Miller III contributed to project conception and design, generated transgenic lines, collected images, and quantified results, wrote the published manuscript, critically revised the manuscript and approved the final version for publication. Cristina Matthewman contributed to project conception and design, performed oocyte electrophysiology assays, critically revised the published manuscript and approved the final version for publication. Sayaka Hori generated the *unc-8 (tm5052)* mutant allele, and critically revised the published manuscript and approved the final version for publication. Shohei Mitani generated the *unc-8 (tm5052)* mutant allele, and critically revised the published manuscript and approved the final version for publication. Laura Bianchi designed and interpreted experiments, critically revised the published manuscript, and approved the final version for publication.

TABLE OF CONTENTS

TABLE OF CONTENTS (continued)

TABLE OF CONTENTS (continued)

LIST OF FIGURES

LIST OF FIGURES (continued)

LIST OF FIGURES (continued)

LIST OF FIGURES (continued)

LIST OF FIGURES (continued)

LIST OF FIGURES (continued)

LIST OF ABBREVIATIONS

ACh	Acetylcholine
AChE	acetylcholinesterase inhibitor
AFS	automatic freeze substitution
AIS	axon initial segment
AMPA	α-amino-3-hydroxy-5-methylisoxazole-4-propionic acid
AP	adaptor protein
ASIC	acid sensing ion channel
AZ	active zone
BRP	bruchpilot
BWM	body wall muscle
CaMKII	calcium/calmodulin-dependent protein kinase II
CAPS	calcium-activated protein for secretion
Cas9	Cas gene 9
CASK	calcium/calmodulin-dependent serine protein kinase 3
CAST	CAZ-associated structural protein
CAT-1	C elegans vesicular monamine transporter
CAZ	cytomatrix at the active zone
CC	coiled coil
CCD	charge-coupled device
CDK-5	cyclin-dependent kinase
cDNA	complementary DNA
CED	cell death
CED-3	Caspase
CED-4/Apaf	Calcineurin addaptor protein
ChR2	channelrhodopsin
CLA-1	Clarinet
CME	clathrin-mediated endocytosis

Cre	site-specific DNA recombinase
CRISPR	Clustered Regularly Interspaced Short Palindromic Repeats.
CSS	CDK, SAD-1, SYD-1, SYD-2 , alternatively core synyapse stability
CTNS-1	lysosomal cysteine transporter
CYY-1	cyclin box-containing protein
DCV	dense core vesicle
DEG	degenerin
DP	dense projection
DUF	domain of unknown function
EGL-21	Carboxypeptidase E
EGTA	ethylene glycol tetraacetic acid
ELKS	Glutamate (E), leucine (L), lysine (K) and serine (S) rich proteins
EM	Electron microscopy
ENaC	Sodium epithelial channel
ET	electron tmography
FLP-13	FMRFAmide-like protein
FS	Freeze substitution
GABA	γ–aminobutyric acid
GAP	GTPase activating protein
GFP	green fluorescent protein
GIT	G protein coupled receptor kinase 2 interacting
GluR1	Glutamate receptor 1
GSNL-1	gelsolin
GTP/GDP	Guanosine-5'-triphosphate/diphosphate
HPF	High-presure freeze
HSN	hermaphrodite specific neuron
INS_22	type-alpha INSulin-like molecule-22
IRX-1	Iroquois family homeodomain transcription factor
JIP3	JNK-interacting protein
JNK	c-Jun N-terminal kinase
kb	kilobase
kDa	kilo Dalton
KIF1A	kinesin family member 1A
L1	larval stage one
LAR	leukocyte antigen related
LH	liprin homology
loxP	Locus of Crossover in P1
LTD	long-term depression
mCh	mCherry

LIST OF ABBREVIATIONS (continued)

MINT	Munc18 interacting protein
NAB-1	neurabin
nm	nanometer
NMDA	N-methyl-D-aspartate,
NMJ	neuromuscular junction
NSF	soluble N-ethylmaleimide sensitive factor
NSM	neurosecretory motor sensory neuron
NUD-2	nuclear distribution protein
PD	presynaptic density
PDZ	post synaptic density protein (PSD95), Drosophila disc large tumor suppressor (Dlg1), and zonula occludens-1 protein (zo-1)
PTV	piccolo/bassoon transport vesicle
PVD	polymodal nociceptive for mechanosensation and thermosensation sensory neuron
Rab	Ras-related in brain
RIM	RAB3-interacting molecule
RIM-BP	RIM-binding protein
RPTP	LCA-related protein tyrosine phosphatase
RRP	Readily-releasable pool
RT-PCR	reverse transcription polymerase chain reaction
SAD	synapse amphid defective
SAM	sterile alpha motif
SEC	self-excising cassette
SNAP-25	synaptosome-associated protein of 25 kDa
SNARE	NSF attachment protein receptors
SNB	synaptobrevin
SNB-1	synaptobrevin 1
ssTEM	serial section TEM
STRN-1	sentryn
STV	SV protein transport vesicle
SV	Synaptic vesicle
SYD	synapse defective
SYN-13	early endosome marker
TAX-6	Calcineurin
TBA-1	tubulin alpha chain
TEM	transmission electron microscopy
TOM-1	tomosyn
um	micromolar
UNC	uncoordinated
UNC-49	GABAa receptor
UNC-57	endophilin

UNC-8	DEG/ENaC channel
VGCC	voltage-gated Ca^{2+} channel
WGS	whole genome sequencing
WT	wildtype
YFP	yellow fluorescent protein

SUMMARY

Understanding the diverse array of pathways and effectors involved in synaptic development and transmission can provide insight into how organisms sense and relay stimuli and coordinate behavior. In combination with robust functional, genetic, and molecular techniques established in the soil nematode *Caenorhabditis elegans*, ultrastructural analysis provides unique insight into the mechanisms that underlie synaptic function. The neuromuscular junction of *C. elegans* is well-suited for examination by high-pressure freeze and freeze substitution electron microscopy. Using this technique, I characterized the ultrastructural phenotypes of mutations in genes critical for organizing and regulating synapses.

Two of these genes encode novel active zone proteins, Clarinet and Sentryn. Clarinet regulates synapse number, vesicle clustering, and release in various neuron classes. Sentryn operates with a specialized class of active zone enriched proteins to capture synaptic and dense core vesicles at synapses. Finally, I examined synaptic ultrastructure in mutants involved in synapse disassembly during developmental synapse remodeling, including transcription factor UNC-55, DEG/ENaC channel UNC-8, and Iroquois homeodomain protein IRX-1. While some synaptic disassembly may be prevented in these mutants, the localization of key active zone proteins are differentially regulated and contribute to functional defects.

I. INTRODUCTION

The nervous system drives all vital processes in organisms. Neurons that comprise this system transmit electrical and chemical signals throughout the organism using specialized structures called synapses. Commonly, chemical synapses feature a presynaptic terminal which contains vesicles filled with signaling molecules, known as neurotransmitters. Incoming electrical signals trigger vesicles to fuse with the plasma membrane of the presynaptic cell in a process called exocytosis, which releases neurotransmitter into the synaptic cleft. These neurotransmitter molecules can then diffuse across the cleft and bind to receptors on the postsynaptic cell, resulting in changes in ion channels or signaling cascades in the target cell. This dynamic process of synaptic transmission can vary widely among different organisms and even synapses within the same organism. Yet the mechanisms of converting electrical signals to chemical signals remains an essential task for most synapses, and decades of research have been devoted to understanding how these processes are linked.

A. SV Cycle

Structural and functional studies have identified various steps in the synaptic vesicle (SV) cycle. First, SVs are filled with small molecule neurotransmitters such as acetylcholine (ACh), γ-Aminobutyric acid (GABA), and glutamate. They are then clustered around the active zone (AZ), a region that contains highly specialized machinery to coordinate their release. SVs selectively "dock" when they contact the plasma membrane and are "primed" to become fusion competent. Primed vesicles make up a readily-releasable pool (RRP) that can rapidly fuse with the plasma membrane upon receiving a Ca^{2+} signal. Fused SVs in the plasma membrane are

subsequently recycled through endocytosis and re-enter the cycle. SVs release is responsible for fast signaling at synapses.

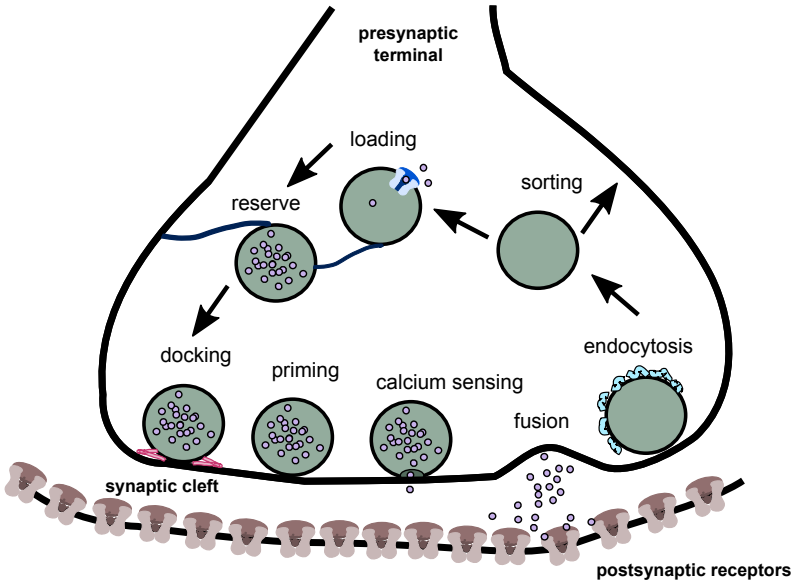

Figure I.1 The synaptic vesicle cycle. Within the presynaptic terminal, synaptic vesicles are loaded with neurotransmitter. A subset of vesicles can be mobilized to the active zone, where they can be docked to the plasma membrane and primed to become fusion competent. Upon sensing an incoming Ca^{2+} signal through voltage-gated calcium channels, vesicles fuse, releasing their neurotransmitter into the synaptic cleft where they can bind to postsynaptic receptors. Figure adapted from Richmond, 2005.

1. Docking

The structural and molecular correlates of docking have been challenging to define. Docked vesicles are described structurally by electron microscopy (EM) as a subset of SVs that contact the presynaptic membrane (reviewed in Zucker, 1996; Robinson and Martin, 1998). This morphological definition of docking, however, cannot distinguish whether a docked vesicle is also primed and is part of the functional RRP. Furthermore, conventional fixation methods for EM result in artificial changes in ultrastructure that have historically prevented clear identification of direct contact between SV and plasma membrane. Thus, structural definitions of docking have varied, including SVs from within 0 to 50 nm of the plasma membrane. Advances in

high-pressure freeze EM (HPF) and freeze substitution (FS) EM have enabled a more accurate understanding of docking and priming. A current model is that docking near the AZ is mediated by interactions among SV-associated GTPase RAB-3, Rab3-interacting molecule RIM/UNC-10, and (Wang et al., 1997; Weimer et al., 2006a; Weimer et al., 2006b; Gracheva et al., 2008).

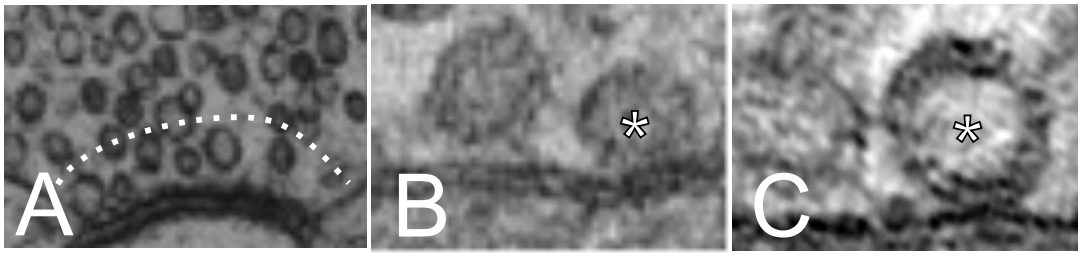

Figure I.2 Representative images showing different classifications of docking. A. Squid giant synapse preserved by conventional fixation, modified from Hess et al.,1993. In this study, docked vesicles were defined as within 50 nm of the plasma membrane, as indicated by the dashed line. **B.** *C. elegans* neuromuscular junction preserved by HPF/FS EM. In (B) and (C), the star indicates a docked vesicle, defined as zero distance to the plasma membrane. **C.** Hippocampal organic slice culture preserved by HPF/FS EM, modified from Imig et al., 2014.

2. Priming

Primed vesicles represent a subset of SVs that comprise the RRP. Vesicles are primed when partial SNARE complexes form between v- (vesicle membrane) and t-SNARES (target membrane). This conserved family of soluble N-ethylmaleimide sensitive factor (NSF) attachment protein receptors consists of small, membrane-associated proteins that are essential for intracellular membrane fusion (Söllner et al., 1993). Both v- and t-SNARES contain a C-terminal transmembrane domain with a characteristic SNARE motif of 60-70 highly conserved amino acids (reviewed in Hong, 2005, Jahn and Scheller, 2006, Koeppler et al., 2007). The conserved SNARE motif residues are alternatively used to classify SNARE proteins. The R-SNARE (arginine) synaptobrevin is an integral SV protein, while Q-SNAREs (glutamine) syntaxin-1 and

SNAP-25 (synaptosome-associated protein of 25 kDa) are localized to the presynaptic membrane. SNARE complexes, also known as SNAREpins, form by binding to each other via α-helical SNARE motifs. The four helices rapidly zipper together from N- to C-terminal into a partial helix bundle, forming a *trans*-SNARE complex that facilitates rapid release upon a Ca^{2+} signal (Fasshauer et al., 1998, Pobbati et al., 2006; Sutton et al., 1998). In fact, clostridial toxins (botulinum and tetanus) that cleave SNARE proteins result in profound loss of release (Blasi et al., 1993a; Blasi et al., 1993b; Schiavo et al., 1992). Furthermore, genetic disruption of any SNARE protein also abolishes release and often results in lethality in both vertebrates and invertebrates (O'Connor et al., 1997; Saifee et al., 1998; Schoch et al., 2001; Washbourne et al., 2001).

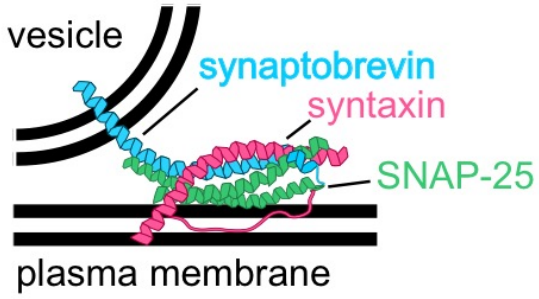

Figure I.3. SNARE complex between vesicle and plasma membrane. A simplified model of SNARE protein interactions. Synaptobrevin (blue) is an integral synaptic vesicle protein. Syntaxin (pink) and SNAP-25 (green) are associated with the plasma membrane. The SNARE motifs of synaptobrevin, syntaxin, and SNAP-24 interact to form a four-helix bundle.

3. Conflicting theories about docking, priming, and the role of SNAREs

Due to the lethality of genetic mutants, SNARE proteins have been difficult to study (Nonet et al., 1998; Saifee et al., 1998). Conventional EM studies in *Drosophila melanogaster*, squid, and mouse suggest that these proteins are not essential for docking (Hunt et al., 1994; Broadie et al., 1995; Deak et al., 2004). However, reanalysis of these mutants using HPF/FS EM and electron tomography (ET) challenge this theory. In *Caenorhabditis elegans* (*C. elegans)* motor neuron synapses, the SNARE protein syntaxin was found to be required for docking,

priming, and fusion (Richmond and Jorgensen., 1999, Hammarlund et al., 2007). Importantly, UNC-13 must be present to stabilize an open conformation of syntaxin and facilitate docking at the AZ (defined in this study as <231 nm from the DP). A constitutively open form of syntaxin was also able to dock vesicles in the absence of the UNC-13, but could not fully rescue release (Hammarlund et al., 2007). While syntaxin (*unc-64*) null mutants arrest in the first larval stage, a mosaic strain expressing *unc-64* in cholinergic motor neurons rescued lethality. Docked SVs were observed in cholinergic, but not GABAergic neurons, which contained no rescued expression of syntaxin. Additionally, normal rates of spontaneous release were detected from cholinergic synapses, whereas in GABAergic motor neurons synaptic activity was absent. Thus, syntaxin is required in *C. elegans* for docking, and docked vesicles require UNC-13 to be primed for release. Syntaxin's role in docking has been confirmed in mouse studies (Gerber et al., 2008; Siksou et al., 2009; Arancillo et al., 2013, Imig et al., 2014). One such study in mouse hippocampal organotypic slice culture indicates that SNAP-25, syntaxin, and synaptobrevin are all required for SV docking, and that docking is a morphological correlate of SV priming (Imig et al., 2014). By carefully classifying vesicle distance to the plasma membrane, the authors argue that SV docking at the plasma membrane enables *trans*-SNARE complex formation and requires all three SNARE proteins. In mutant SNAP-25, syntaxin, and synaptobrevin synapses, they observed drastic reductions in SVs within 0-2 nm of the plasma membrane, and a corresponding increase of SVs 5-20 nm away from the plasma membrane. The reduction in docking correlates with changes in the RRP measured in slice culture (Stevens and Tsujimoto, 1995; Imig et al., 2014; Watanabe et al., 2013). The authors propose that various AZ components recruit SVs to the AZ where they become tethered within ~10 nm of the plasma membrane, and Muc13/RIM/Rab3A interactions

may help localize SVs closer to the membrane to enable *trans*-SNARE interactions for final docking and priming (Imig et al., 2014). A later study performed in mouse hippocampal cultures found that even in synapses with almost no docked SVs, release could be stimulated (Wang et al., 2016). Additional examination of SNARE proteins and other AZ protein effects on docking will be required to clarify the molecular contributions to docking and priming

4. Fusion

While SNARE proteins are sufficient to mediate reconstituted vesicle fusion on the order of hours, a variety of other proteins interact with SNAREs to enable physiological, millisecond rates of fusion (Weber et al., 1998), particularly proteins in the Synaptotagmin, Sec/Munc-18 (SM), and (M)unc-13 families. Syntaxin can exist in a closed confirmation with its N-terminal regulatory domain (H_{abc}) blocking the SNARE domain that participates in SNARE complex formation. Munc-18 stabilizes this closed conformation as Syntaxin is transported to the synapse, and it later promotes fusion by interacting with the assembled SNARE complex (Dulubova et al., 1999; Khvotchev et al., 2007; Ma et al., 2013). UNC-13, on the other hand, stabilizes an open conformation of Syntaxin (Stevens et al., 2005). As described above, UNC-13 is required for vesicle priming and neurotransmission (Betz et al., 1998; Maruyama and Brenner, 1991; Richmond et al., 1999). Finally, Synaptotagmin interacts with the assembled SNARE complex to trigger fusion. When Synaptotagmin binds calcium at its two C2 domains, it inserts four membrane-binding loops into the presynaptic membrane that induce curvature and allow for fusion between vesicle and plasma membrane (Martens et al., 2007). Fusion releases neurotransmitters into the synaptic cleft, where they can diffuse towards postsynaptic receptors

on the target cells. These receptors can be ligand-gated ion channels that depolarize or hyperpolarize the postsynaptic cell or metabotropic receptors that initiate signaling cascades in the cell (Stroud et al., 1990, Gage, 1998, Richmond and Jorgensen, 1999).

5. Endocytosis and vesicle recycling

After fusion, vesicle membrane and proteins are recovered through endocytosis. Synapses often undergo repetitive rounds of SV release, and a lot of time and energy must be used to create *de novo* vesicles. Thus, endocytosis enable recycling of SVs and maintains homeostasis of the plasma membrane surface area (Miller and Heuser, 1984). Several models of endocytosis exist, including kiss-and-run, ultrafast endocytosis, and clathrin-mediated endocytosis (CME) (reviewed in Jung and Haucke, 2007, Rizzoli and Jahn, 2007, Watanabe et al., 2013). During CME, vesicle proteins, including AP180 and AP-2, are recruited to the membrane (Schmid, 1997, Haucke and De Camilli, 1999, Nonet, 1999). They recruit clathrin molecules that promote membrane invagination into the presynaptic terminal. Both endophilin and synaptojanin are likely involved in this process, helping to change membrane composition and curvature (Harris et al., 2000, Huttner and Schmidt, 2000, Farsad et al., 2001, Schuske et al., 2003). The GTPase dynamin polymerizes around the neck of the budding clathrin-coated membrane, and GTP hydrolysis promotes the "pinching off" of this vesicle (Sweitzer and Hinshaw, 1998). The clathrin coat is removed from the vesicle by ATPase Hsc70 (Ungewickell et al., 1995). The energy-dependent process of CME occurs in the peri-active zone of the synapse over tens of seconds. Alternatively, kiss-and-run fusion, in which a transient fusion pore is formed between SV and plasma membrane, can occur near the active zone within one second

(reviewed in Ackermann et al., 2015). The recent discovery of ultrafast endocytosis revealed that endocytosis can occur within 50-100 ms of stimulation at an area adjacent to the active zone. These findings support the idea that exo- and endocytosis are linked (Watanabe et al., 2013). After vesicles have been endocytosed, they must be refilled with neurotransmitter and often follow an endosomal sorting step (Wucherpfennig et al., 2003, Rizzoli et al., 2006).

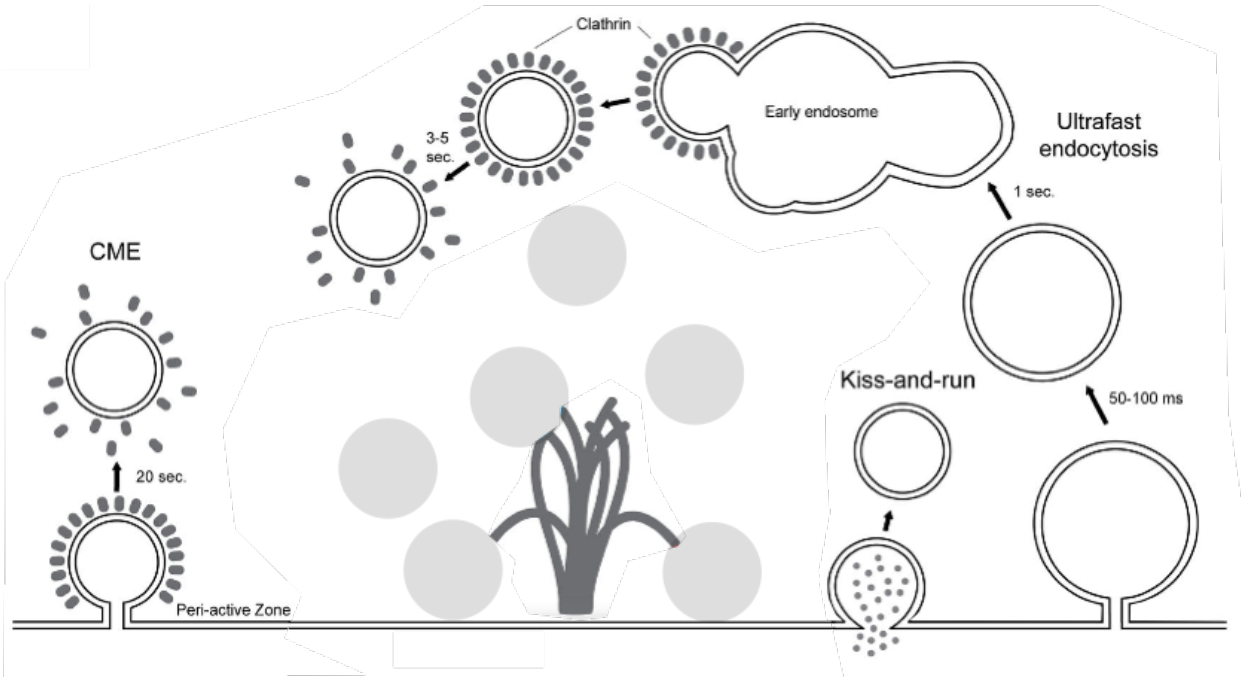

Figure I.4. Models of endocytosis. Following exocytosis, vesicles can be retrieved by various forms of endocytosis. (1) Clathrin-mediated endocytosis (or CME) creates a clathrin-coated pit around the membrane. (2) Kiss-and-run fusion occurs when a transient fusion pore is created, and the original vesicle is retrieved immediately. (3) Ultrafast endocytosis occurs within milliseconds after a stimulus, and large endocytic intermediates are fused with early endosomal compartments, from which new vesicles can be budded off by clathrin.

6. Dense core vesicle release

Dense core vesicles (DCVs) are an additional class of secretory vesicles named for their electron-dense appearance in electron micrographs. In contrast to SVs, DCVs contain a variety of neuropeptides and catecholamines that can modulate both pre- and postsynaptic targets, often

on a longer time scale than SV signaling (Levitan, 2008; Sossin and Scheller, 1991, Banerjee et al., 2017; Bhattacharya and Francis, 2015; Bhattacharya et al., 2014; Chen et al., 2016; Choi et al., 2015; Hu et al., 2011; Lim et al., 2016; Liu et al., 2007, Hu et al., 2015; Kupfermann, 1991). DCVs are frequently identified in SV-containing synapses, though they are not clustered as tightly around the AZ as SVs and are thought to require sustained global Ca^{2+} levels that result from high-frequency stimulation to fuse (Verhage et al., 1991; Bruns and Jahn, 1995; Tandon et al., 1998; Hammarlund 2008; Hammarlund et al., 2007; Hoover et al., 2014; Weimer et al., 2006) whereas SVs fuse in response to higher Ca^{2+} concentrations at discrete nanodomains at the AZ. In addition to SV release machinery syntaxin and SNARE proteins, DCVs require calcium-activated protein for secretion (CAPS) to fuse with presynaptic membrane (Hammarlund et al., 2008: Renden et al., 2001; Sieburth et al., 2006; Speese et al., 2007). Once released, DCVs are not recycled but rather are made *de novo* in the cell body (Li and Kim, 2008).

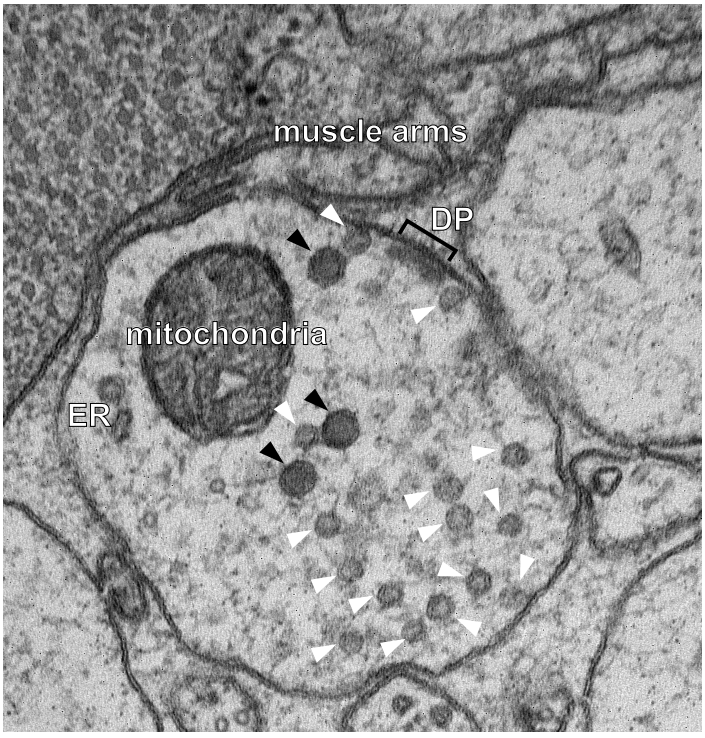

Figure I.5 Electron micrograph of a cholinergic neuromuscular junction in C. elegans. This bouton forms a synapse with the muscle arms indicated in the figure. The dense projection (DP) is thought to be comprised of active zone proteins. Synaptic vesicles (white arrowheads) have a light gray core and an average diameter of ~30 nm. Dense core vesicles (black arrowheads) have a dark core and average diameter of ~60 nm. Mitochondria and endoplasmic reticulum (ER) are also often present in the terminals.

B. The Active Zone

A wide array of synaptic machinery has evolved to coordinate the precise mechanisms of vesicle transport, release, and recycling. The presynaptic AZ contains highly specialized structures that form a cytoskeletal matrix at the active zone (CAZ) opposite to postysynaptic targets. Presynaptic specializations often appear in electron micrographs as electron dense regions know as a presynaptic density (PD) or dense projection (DP). They are thought to spatially organize Ca^{2+}, SVs, and exo/endocytic machinery to ensure rapid release in response to electrical stimuli, as well as position release sites near postsynaptic targets. Furthermore, these proteins can serve as targets for modulation of synaptic strength and disassembly. It is believed that a set of evolutionarily conserved protein families comprise the core of the AZ (reviewed in Sudhof, 2012; Bruckner et al., 2015).

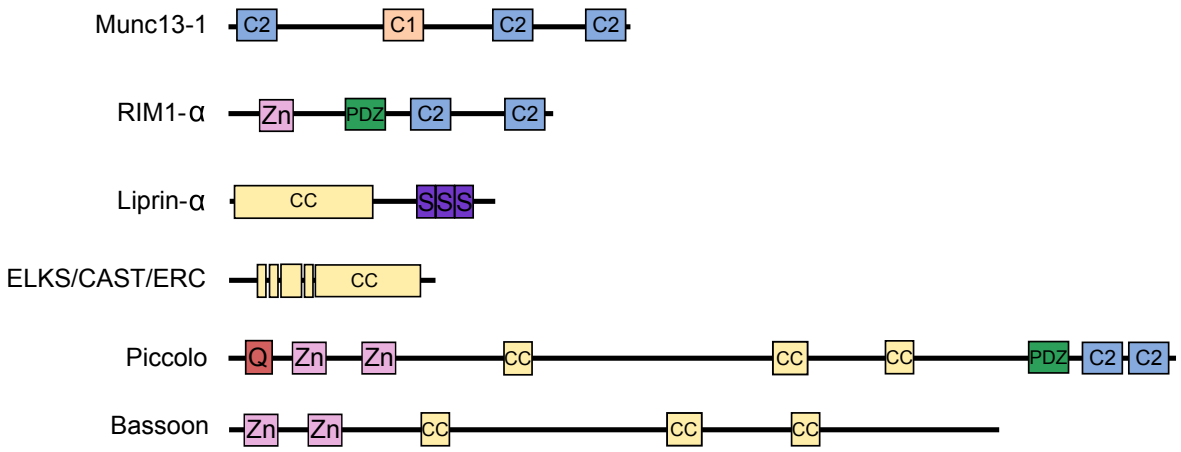

Figure I.6 Protein domain structure of core active zone proteins. Munc13-1 contains three C2-domains and a C1-domain. RIM1α has an N-terminal zinc-finger domain (Zn), a PDZ-domain, and two C2-domains. Liprin-α consists of N-terminal coiled coil domains (CC) and C-terminal sterile-alpha-domains (S). ELKS/CAST/ERC contain repeating coiled-coil (CC) domains. Bassoon and Piccolo share two zinc-finger domains and three coiled-coil (CC) domains. Piccolo also has a PDZ domain, two C2-domains and proline-rich sequences. Adapted from Schoch and Gundelfinger, 2006.

1. UNC-13/Munc-13 proteins

The Munc-13 protein family is a conserved set of vesicle priming proteins that are highly expressed in the nervous system (Aravamudan et al., 1999; Augustin et al., 19999; Richmond et al., 1999). Mutants for *unc-13* are severely uncoordinated (Kohn et al., 2000). Four homologs are expressed in vertebrates, and *C. elegans* expresses a long (*unc-13L)* and short (*unc-13S)* isoform (Koch et al., 2000; Kohn et al., 2000). Munc family proteins share a C1 domain that is homologous to the diacylglycerol (DAG)/phorbel ester-binding region of protein kinase C (PKC), a central MUN domain that can interact with SNARE motifs and Munc18, and two flanking C2 domains that can bind Ca^{2+}, phospholipids, and/or other proteins. ubMunc13-2, and *unc-13L* also contain an N-terminal C2A domain and Calmodulin-binding (CaM) domain. The C2A domain promotes homodimerization, which inhibits SNARE binding at the MUN domain. In *C. elegans*, the C2A domain helps target UNC-13L to the active zone near UNC-10, and it is believed that UNC-10 can form heterodimers with UNC-13, enabling its priming interaction with Syntaxin (Hu et al., 2013). Munc13 proteins are essential for priming in different animals, and mutant synapses lacking Munc13 proteins exhibit severe release defects (Brenner, 1974; Aravamudan et al., 1999). Interestingly, recent evidence suggests that UNC-13L mediates fast, synchronous release in *C. elegans*, and that this effect is partially enabled by the CaM domain. UNC-13S, which does not contain these N-terminal domains, appears to localize distal to the DP, and promotes slower, asynchronous SV release in concert with UNC-13L (Hu et al., 2013). Munc13 proteins may also be targets for synaptic plasticity mechanisms.

2. RIM proteins

RIMs were originally identified as Rab3-interacting-molecules (Wang et al., 1997). Vertebrates express four RIM genes, while *C. elegans* expresses one homolog, *unc-10*. RIMs are highly enriched at the active zones of synapses, and immunoEM has shown that UNC-10 localizes within 100 nm of the DP in *C. elegans* (Weimer et al., 2006). UNC-10, Rim1α, and Rim2α all contain a N-terminal zinc finger (ZF) flanked by two α-helical regions, a central PDZ domain, and two unconventional C2 domains that do not bind Ca^{2+}, linked by a Proline-rich sequence. Various splice isoforms are also expressed that do not contain these regions.

RIMs are organizers of the synapse. The Zn finger region can form heterodimers with (M)unc-13, while the α-helical regions can bind to SV-associated Rab3 in a GTP-dependent manner (Gracheva et al., 2008). In *C. elegans*, *unc-10*, *rab-3*and *unc-10;rab-3* double mutants exhibit a similar depletion of docked vesicles in the region where UNC-10 immunostaining was observed, in addition to similar defects in evoked and spontaneous release (Gracheva et al., 2008). The loss of docked SVs has also been confirmed by tomography (Stigoloher et al., 2011). Mammalian Rab3, RIM, and Munc13 form a tripartite complex (Dulubova et al., 2005) that helps localize and dock SVs at the AZ. A similar function is likely in *C. elegans*, where UNC-10 is thought to recruit SVs near the DP via RAB-3, enabling priming by UNC-13. At the same time, RIM's central PDZ domain can interact with voltage-gated Ca^{2+} channels (VGCCs), and VGCC interaction is facilitated by RIM-binding proteins (RIM-BPs), thus providing spatial proximity to link SVs with Ca^{2+} signal (Liu et al., 2011). In *Drosophila*, RIM-dependent regulation of the RRP underlies presynaptic homeostasis (Muller et al., 2012). RIM family proteins can also interact with

synaptotagmin, SNAP-25, (Coppola et al., 2001), scaffolding proteins and ELKS/CAST (Ohtsuka et al., 2002) and Liprin-α (Schoch et al., 2002).

3. SYD-2/Liprin-α proteins

Liprin-α (LAR-interacting proteins) are scaffolding molecules that regulate AZ organization. Of the four known vertebrate Liprin-α genes, Liprin-α2 and 3 are expressed in the brain. Invertebrate homologs exist in *Drosophila* (Dliprin-α) and *C. elegans* (*synapse defective syd-2*) and are expressed both pre- and postysynaptically (Zhen and Jin, 1999, Kaufman et al., 2002; Li et al., 2014). SYD-2/Liprin-α contains highly conserved N-terminal Liprin Homology (LH) domains within a predicted coiled-coil region, and three C-terminal sterile alpha motif (SAM) domains. The N-terminal region can bind to itself in homodimers and can also interact with RIM (Schoch et al., 2002), ELKS (Ko et al., 2003a), and G protein-coupled receptor kinase-interacting protein (GIT) (Ko et al., 2003b). SYD-2/liprin-α can also interact with the SV motor protein KIF1A/UNC-103 (Shin et al., 2003; Miller et al., 2005) and the postsynaptic glutamate receptor interacting protein (GRIP) (Wyszynski et al., 2002). SYD-2/Liprin-α plays a major role in synapse assembly, as discussed below.

4. ELKS/CAST/ERC proteins

Glutamate (E), leucine (L), lysine (K) and serine (S) rich proteins are enriched at synapses, although they were first identified in papillary thyroid carcinoma (Nakata et al., 1999; Nakata et al., 2002). They include CAZ-associated structural protein CAST and ELKS/Rab6-interacting protein/CAST, which were identified in different screens by their localization or interaction with

synaptic proteins (Ohtsuka et al., 2002; Wang et al., 2002). *Drosophila* Bruchpilot shares homology with ELKS in its N-terminal half, and *C. elegans* expresses a single homolog ELKS-1 (Wagh et al., 2006, Kittel et al., 2006; Fouquet et al., 2009). ELKS contain mostly coiled-coil domains that comprise major structural components of the AZ. The *Drosophila* NMJ shows striking effects of *brp* mutations, including loss of T-bars (the electron-dense presynaptic specialization in *Drosophila*), defective VGCC clustering, and impaired release. It is important to note that BRP is a fusion of N-terminal ELKS-like region and a C-terminal region with plectin-homolgy. This plectin-homology region appears to execute important functional roles of SV recruitment, similar to Piccolo/Bassoon (see below). Deletion of one of three ELKS genes in vertebrates resulted in an increase of inhibitory synaptic transmission (Deng et al., 2009). On the contrary, *elks-1(lf)* mutants in *C. elegans* display normal DP length and shape, as well as normal vesicle clustering, docking, and release (Kittelmann et al., 2013). ELKS can interact with RIM, Munc-13, SYD-2/Liprin-α proteins, and SYD-1, but the extent of those interactions appears to be mediated by other proteins (Ohtsuka et al., 2002; Ko et al., 2003b, Deken et al., 2005, Dai et al., 2006; Patel et al., 2006; Patel and Shen, 2009, Kittelmann et al., 2013). ELKS-1 likely performs a redundant function in worm and other synapses.

5. Piccolo/Bassoon/Fife

Piccolo and Bassoon are well-studied CAZ proteins that help cluster SVs at the active zone, thereby "orchestrating" the synapse. While Piccolo and Bassoon were previously thought to be expressed exclusively in vertebrates, a *Drosophila* homolog, Fife, was recently characterized (Bruckner et al., 2012, 2016). These large, homologous proteins are predicted to

have an N-terminal Zn finger and coiled-coiled domains that mediate protein binding to ELKS, Rab3, and synaptobrevin2/VAMP2 (Fenster et al., 2000; Cases-Langhoff et al., 1996; tom Dieck et al., 1998; Takao-Rikitsu et al., 2004). Piccolo has a C-terminal PDZ domain and two C2 domains that can interact with cAMPGEFII (Shibasaki et al., 2004) and form Ca^{2+}-dependent homodimers and heterodimers with Rim2 (Fujimoto et al., 2002). While Piccolo and Bassoon knockdown do not affect release in mouse neurons, they influence SV clustering and regulate ubiquitination and degradation of presynaptic components (Mukherjee et al., 2010; Waites et al., 2013). Interestingly, fife was recently shown to regulate synaptic strength through interactions with RIM and Ca^{2+} channels, promoting vesicle docking and release (Bruckner et al., 2016). Chapter 2 of this thesis describes a novel, Piccolo-related protein in *C. elegans* named Clarinet.

C. Ultrastructural characterization of the active zone

Ultrastructural characterization of the AZ is an essential complement to molecular and physiological examination. Indeed, understanding defective synaptic transmission in various genetic mutants often requires clarification by analysis of vesicle status (docked/tethered/undocked) and distribution, and DP architecture (Gracheva et al., 2006; Kittelmann et al., 2013). In this thesis, I focus on the ultrastructural analysis of neuromuscular junction (NMJ) synapses in *C. elegans* to understand important processes in synaptic assembly, transmission and development.

1. Presynaptic specializations in different organisms

While the proteins that comprise the AZ are largely conserved, the appearance of presynaptic specializations can vary significantly among organisms and even within different types of synapses. The hallmark of most AZ's is an electron dense DP surrounded by a cloud of SVs. Structural characteristics of the AZ tend to reflect the functional needs of the synapse. In *C. elegans* NMJs, the DP is elongated, with an apparent repeating structure of branched units that form "bays" in which SVs are likely to localize (Kittelman et al., 2013). These structures also exhibit filaments that branch out and often contact SVs, a function that appears to facilitate SV release (Kittelman et al., 2013; Stigloher et al., 2011). The configuration of repeating subunits is like that observed in the frog NMJ, which contains a highly organized structural array of beams and ribs (Harlow et al., 2001). In *Drosophila*, NMJ's were originally characterized by a T-bar shaped DP, which was later understood to be a fixative-induced collapse of filaments that extend into the presynaptic terminal (reviewed in Ackermann et al., 2015). Larger and more complex DP structure has also been observed in in *C. elegans* interneurounal synapses, as well as mammalian sensory synapses such as ribbon synapses in photoreceptor cells and hair cells (reviewed in Ackermann et al., 2015). Interestingly, AZ's in the mammalian central nervous system (CNS) are less complex, and cryo-fixation reveals that a large, electron-dense region is absent, replaced by fine filamentous structures that can contact SVs up to 100 nm away. This structural distinction may reflect the reduced probability of release observed at these synapses (reviewed in Ackermann et al., 2015).

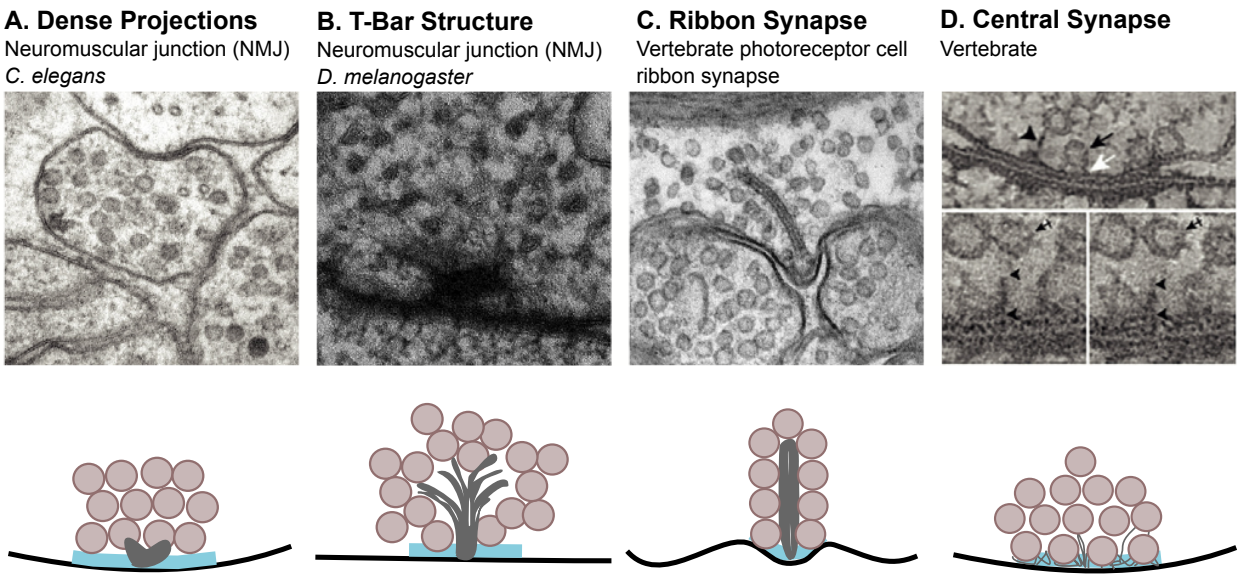

Figure I.7. Synaptic ultrastructure in different organisms. Electron micrographs and cartoon models of synaptic ultrastructure. In each cartoon, synaptic vesicles are shown in light brown and the active zone is shown in blue. A. The *C. elegans* neuromuscular junction is characterized by a dense projection (gray), surrounded by vesicles. B. In *Drosophila*, the presynaptic specialization is known as a T-bar (gray), and exhibits a more complex structure of filaments emanating into the terminal. C. Ribbon synapses are found in sensory neurons such as vertebrate photoreceptor cells. The elongated synaptic ribbon tethers large numbers of vesicles to facilitate rapid and frequent release. D. Synapse in the vertebrate central nervous system do not exhibit large presynaptic densities but rather a multitude of filaments connecting synaptic vesicles to the active zone. Adapted from Ackermann et al., 2015.

2. Components and regulators of the active zone

Identifying the molecular components of the AZ described above, including DP and filaments seen at the EM level, remains a major challenge in the field. This difficulty is partly due to our current understanding that various AZ components form many weak and redundant interactions. Thus, the absence of any one protein may only result in a subtle change in structure (Patel et al., 2006). Still, advances in ultrastructural analysis by EM have provided some clues about the molecular identity of the AZ. One of the most striking of these is the disappearance of T-bars from the NMJs of *Drosophila brp* null mutants. Based on this observation, researchers

have been able to determine that T-bar size is also regulated by fife, and that BRP, fife, RIM/UNC-10, and RBP all recruit VGCCs to the AZ (Kittel et al., 2006; Wagh et al., 2006; Fouquet et al., 2009; Bruckner et al., 2016, Kaeser et al., 2011; Mittelstaedt et al., 2007).

Studies in *C. elegans* reveal a major role for *syd-2/liprin-α* in assembling the AZ. SYD-2 was originally identified in *C. elegans* in a screen for SV clustering defects in motor neurons (Zhen and Jin, 1999) and seems to play an important role in synapse development and DP assembly (Zhen and Jin, 1999; Patel et al., 2006; Dai et al., 2006; Patel and Shen, 2009; Kittelmann et al., 2013). Initial observations by conventional EM noted *syd-2* mutants contained elongated DPs and diffuse SV clusters in GABAergic motor neurons. However, upon reexamination using HPF/FS EM, it was found that *syd-2(lf)* mutants have shorter DPs and fewer docked SVs (Kittelmann et al., 2013; Stigloher et al., 2011). Interestingly, gain-of-function mutations in SYD-2 that enhance LH binding activity were shown to increase the size of DPs, and this effect was dependent on ELKS (Kittelmann et al., 2013). Thus, SYD-2 is thought to regulate DP size by polymerizing DP subunits in an ELKS-dependent mechanism, although loss of *elks-1* alone does not affect DP size (Kittelmann et al., 2013). SYD-2 and UNC-10 also contribute to the filaments that connect SVs to the DP (Stigloher et al., 2011). While SYD-2 may bind and recruit many proteins to the synapse, the exact interactions and mechanisms by which synapses are assembled remain poorly understood. SYD-2 likely exerts influence on a wide variety of mechanisms in synapse assembly, discussed below.

Advances in superresolution imaging and immunoEM also reveal proteins whose localization near the DP may implicate their role in AZ structure. In *C. elegans*, antibodies for UNC-10/RIM and SYD-2 localized mostly within 30 nm of the DP (Weimer et al., 2006). RIM localization near the center of the AZ has been supported in a variety of models through additional imaging techniques including stochastic optical reconstruction microscopy (STORM), photo-activated light microscopy (PALM), and stimulated emission depletion (STED) microscopy (reviewed in Bruckner et al., 2015; Dani et al., 2010). In rat hippocampal cells, immunoEM and ET found that CAST and Bassoon localize ~30 nm and ~70 nm from the plasma membrane of the AZ, respectively (Siksou et al., 2007). The authors propose a model in which CAST anchors bassoon to the AZ, while bassoon and synapsin both contribute to filaments that cluster SVs nearby. In cerebellar synapses, RIM1 and Munc-13 were found ~20 nm from the plasma membrane at the AZ, and Piccolo extended from the distal tip of the DP to up to 80 nm into the presynaptic cytoplasm (Limbach et al., 2011). There is also evidence that Munc-13 functions as a scaffold for Bassoon and ELKS2 (Wang et al., 2009). Taken together, this growing body of work contributes to a model in which Piccolo and Bassoon regulate SVs and synaptic architecture at the peri-AZ, while CAST/ELKS/ERC/BRP, link them to the central AZ. There, Munc13, RIM, and CAST facilitate VGCC localization, priming, and fusion (reviewed in Bruckner et al., 2016). In *C. elegans*, regulators of the DP and AZ are still not fully understood. Chapters 2 and 3 of this thesis describe two novel components of the *C. elegans* AZ that represent missing links in our understanding of synaptic regulation.

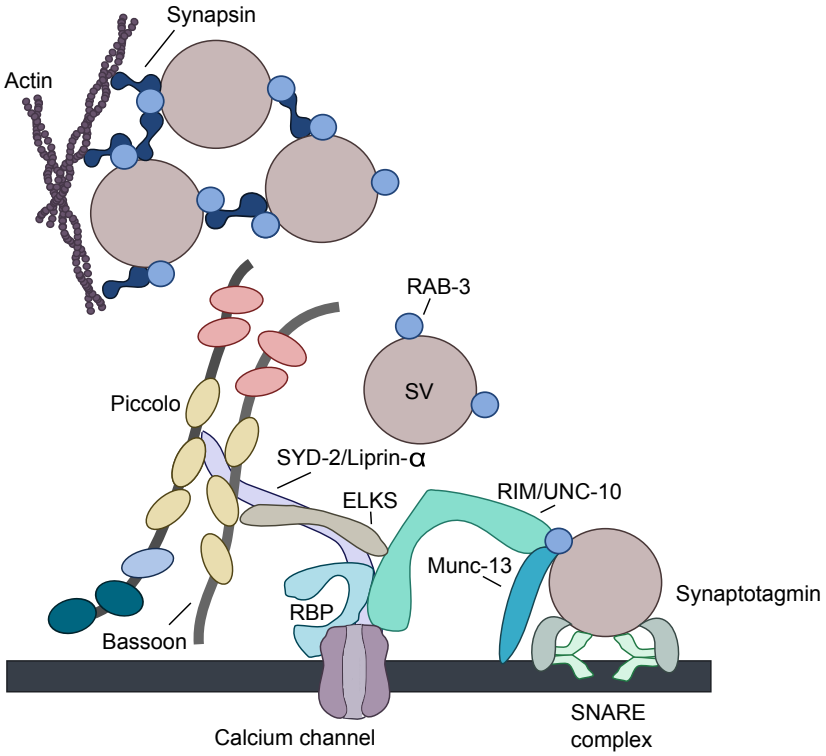

Figure I.7. Active zone protein interactions. Schematic diagram of active zone proteins interacting to cluster synaptic vesicles near voltage-gated calcium channels. The exact interactions and structure of this complex are not precisely resolved. Adapted from Ackermann et al., 2015.

D. Synaptic development

The maturation, assembly, and maintenance of synapses and AZ's require a highly complex group of processes, including axon guidance, adhesion and transsynaptic signaling, cytoskeleton regulation, transport of vesicles and AZ proteins, synapse differentiation, and inhibitory regulation of synaptic assembly. Furthermore, once synapses are established, they are subject to modulation and even disassembly as an organism develops. This thesis will focus on mechanisms for synapse organization and disassembly in Chapters 2, 3, and 4.

1. Synapse assembly

The variation in presynaptic protein composition as well as functional demands across different organisms and synapses likely impacts the mechanisms for synapse assembly. Studies

suggest that components of new synapses are transported in Piccolo-Bassoon transport vesicles (PTVs) (Zhai et al., 2001; Shapira et al., 2003; Maas et al., 2012). Golgi-derived PTVs have been identified that contain AZ proteins Piccolo, Bassoon, RIM1α, and ELKS2/CAST and arrive to nascent synapses early in development. These proteins may be able to self-assemble upon arriving at the synapse. In worms, *in vivo* time-lapse imaging indicated that SVs proteins can be prepackaged into SV protein transport vesicles (STVs) and trafficked to synapses (Wu et al., 2013). ImmunoEM analysis, two-color live imaging, and biochemical studies have revealed that STVs and PTVs, and/or AZ proteins, may be cotransported to synapses, undergoing bidirectional movement and frequent pausing en route to the synaptic region (Tao-Cheng, 2007; Bury and Sabo, 2011; Wu et al., 2013). The presence of SYD-2 prevents STV cargo from disassociating from paused STV/AZ complexes, and enhances pausing of RAB-3 associated with UNC-10. This trafficking is dependent on UNC-104/KIF1A, the anterograde motor in *C. elegans* neurons, whose activity can also be enhanced by SYD-2 (Wagner et al., 2009; Wu et al., 2013). Interactions with the c-Jun N-terminal kinase (JNK) kinase pathway and the Arf-like small G-protein ARL-8 contribute to synaptic patterning by regulating STVs and AZ protein aggregation (Jin and Garner, 2008; Owald and Sigrist, 2009).

SYD-2 can also interact with the CASK/MINT/Veli complex (a secondary AZ protein complex thought to link core AZ proteins to synaptic cell-adhesion molecules) as well as Bassoon, Piccolo, UNC-10, ELKS-1, G protein coupled receptor kinase 2 interacting (GIT), and LAR (reviewed in Patel et al., 2006). In *C. elegans,* SYD-2 influences localization of both AZ structural

proteins and SVs, the latter possibly through interactions with UNC-104 (Miller et al., 2005, Edwards et al., 2015a).

Thoughtful work with *syd-2* mutants has shed light on the hierarchy of synaptic assembly proteins in various neurons. PTP-3A, a conserved isoform of the LAR receptor protein tyrosine phosphatase (RPTP) family, is proposed as an anchor for SYD-2, which acts as a scaffold that regulates size and spatial distribution of synaptic materials. PTP-3A distribution was diffuse in a *syd-2* null mutant nerve cord, although interestingly, proper SYD-2 localization was also dependent on PTP-3A (Ackley et al., 2005). This kind of reciprocal influence is also seen in the interaction between SYD-2 and SYD-1, a unique rho GAP protein (Hallam et al., 2002). SYD-1 regulates neuronal polarity and axon guidance. In *syd-1* null mutants, dendrites accumulated presynaptic machinery that likely represented functional synapses (Hallam et al., 2002). In hermaphrodite specific neurons (HSN), *syd-1* was shown to function upstream of *syd-2* as a positive regulator of synapse assembly (Patel et al., 2006). Despite this hierarchical relationship, *syd-1* and *syd-2* appear to be partially dependent on one another for synaptic localization. Both these proteins function upstream of a wide range of other presynaptic proteins, including UNC-10, UNC-13, UNC-18, UNC-2, UNC-104/KIF1A, and ELKS-1 (Patel et al., 2006).

Interestingly, a gain-of-function mutation in the coiled-coil region of *syd-2* bypassed the requirement for *syd-1* and rescued *syd-1* mutant defects (Patel et al., 2006; Spangler et al., 2013; Wentzel et al., 2013). This effect was dependent on *elks-1*, which was also required to mediate various *syd-2(gf)* mutant phenotypes (Dai et al., 2006; Kittelman et al., 2013). The LH domains of

SYD-2 promotes homodimerization and binding to ELKS, and these interactions play an important role in synapse and DP assembly. In fact, SYD-2 homodimerization is thought to be auto-inhibitory, and additional mechanisms exist to negatively regulate SYD-2 activity, potentially by weakening the interaction between SYD-2 and ELKS-1 (Taru and Jin, 2011; Chia et al., 2013). SYD-2 is thought to recruit SAD-1, which can influence SV clustering (discussed below), but AZ proteins that are important for release are likely to localize independently of one another. While these proteins probably exert different function in different neurons, the importance of SYD-1 and SYD-2 in synapse assembly appears to be conserved in mammals, as evidenced by presynaptic development and release defects observed in mammalian *syd-1* and *liprin-α* mutants (Wentzler et al., 2013).

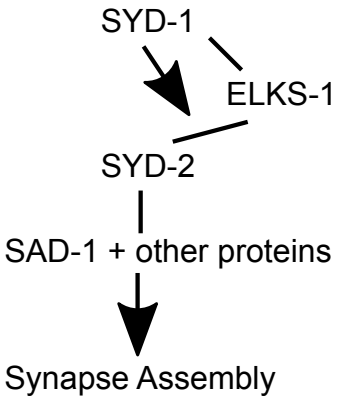

Figure I.8. Hierarchy of synapse assembly in *C. elegans*. SYD-1 operates upstream of SYD-2, which is a major organizer and recruiter of synaptic proteins, including SAD-1. ELKS-1 promotes the function of SYD-2, and this interaction is positively regulated by SYD-1. Adapted from Patel et al., 2006.

2. Guided axonal transport

Trafficking presynaptic components from cell body to synapses must continue throughout the lifespan of an organism to maintain and modulate synaptic circuits. Synaptic components, including SVs and DCVs, are transported along a network of microtubule tracks. In axons, microtubules are oriented with their plus ends out away from the soma (Baas et al., 1998,

2006). In dendrites, polarity is mixed. Most vertebrate dendrites are oriented with the plus-end out, while most dendrites in fly and worm are oriented with the minus-end out (reviewed in Chia et al., 2013). SVs and DCVs travel on these tracks through their interactions with molecular motors Kinesin3/UNC-104/KIF1A, which mediates plus-end-directed transport, and dynein, which mediates minus-end-directed transport (reviewed in Edwards et al., 2015b). Though SVs and DCVs use a common set of machineries to achieve synaptic localization, DCVs are not as tightly associated with the AZ as SVs. During guided axonal transport, both UNC-104/KIF1A and dynein operate on SVs and DCVs, resulting in bidirectional movement along the axon. Yet anterograde movement must dominate to ensure appropriate synaptic levels of vesicles. At the same time, these motors transport lysosomes and early endosomes in the retrograde direction to clear them from axons. The exact mechanisms for regulating SV and DCV trafficking remain unclear, but evidence suggests that SVs and associated proteins are regulated differently than structural AZ proteins such as UNC-10, ELKS-1, UNC-13, and SYD-2.

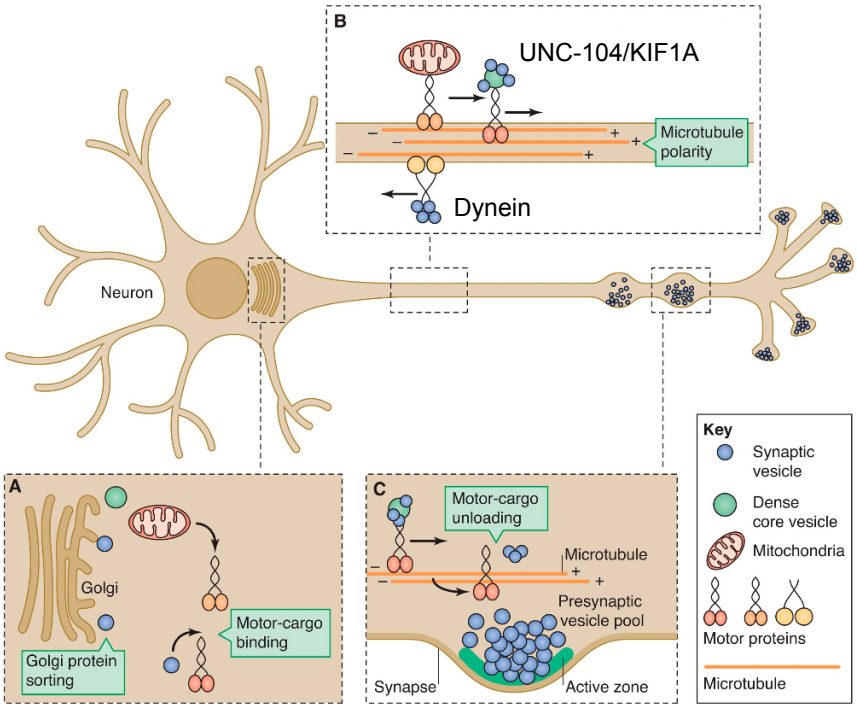

Figure I.9. Guided axonal transport. A. Vesicles are created and sorted in the Golgi apparatus. **B.** Axonal microtubules are oriented with their plus end out toward synapses. The forward motor, UNC-104/KIF1A, mediates anterograde cargo transport to synapses, while the reverse motor, dynein, directs cargo in retrograde transport. Both motors can operate on cargo as they are trafficked, resulting in bidirectional transport. **C.** Cargo must be unloaded at the synaptic region of the neuron and captured at the active zone. Adapted from Chia et al., 2013.

3. UNC-16/JIP3 and the CSS System

Emerging evidence points to UNC-16/JIP3 and the CSS system as important regulators of guided axonal transport. UNC-16/JIP3 is a JNK-interacting protein that promotes both STV transport to the synapse and clearance of endosomal organelles from synapses. In animals lacking *unc-16/JIP3*, lysosomes and early endosomes accumulate at synapses, instead of being transported to cell bodies (Edwards et al., 2015; Miller et al., 2016). A screen for suppressors of this phenotype led to the identification of the CSS system, comprised of CDK-5, SAD-1, SYD-2/Liprin-α, SYD-1 and SAD-1-interacting protein STRADα. CSS proteins are thought to promote

plus-end transport of lysosomes and early endosomes, as well as SVs and DCVs. SAD-1 (synapse amphid defective) is a neuronal serine-threonine kinase that promotes SV clustering and axon termination. While it is recruited to synapses by *syd-2*, it does not require *unc-104* to traffic to synapses (Crump et al., 2001). SAD-1, SYD-2, and SYD-1 have all been previously implicated in regulating neuronal polarity and clustering of synaptic proteins. New findings described in Chapter 3 of this thesis have led to an updated characterization of this system.

4. Synaptic disassembly

Synapses are often eliminated as circuits develop, respond to environmental changes, or are affected by disease. Although relatively little is understood about the mechanisms for synaptic refinement, there has long been an association of activity-dependence with selective synapse removal (Flavell and Greenberg, 2008; Kakizawa et al., 2000; Zuo et al., 2005b). In *Drosophila* and cultured hippocampal neurons, local activity can trigger caspases, which are highly implicated in programmed cell death. It is believed that these caspases may mediate elimination of dendritic spines, as well as internalization of AMPA receptors during long-term depression (LTD) (Erturk et al., 2014; Kuo et al., 2006; Li et al., 2010). On the presynaptic side of synapses, the conserved apoptotic cell death (CED) pathway was recently implicated in synapse removal. CED-3, the *C. elegans* Caspase 3 homolog, can cleave an actin-severing protein gelsolin at a conserved cleavage site. Cleaved gelsolin (GSNL-1) binds to actin filaments at their barbed ends, preventing monomer exchange and severing filaments in a Ca^{2+}-dependent manner (Silacci et al., 2004, Klaavuniemi et al., 2008). Interestingly, in *C. elegans*, F-actin is thought to interact

with SYD-1 and SYD-2 through the adaptor protein neurabin (NAB-1) (Chia et al., 2012; 2014). The role of this pathway in synapse removal will be discussed in depth in Chapter 4.

E. Caenorhabditis elegans as a model organism

Many inroads in our understanding of synaptic structure and function have been derived from the model organism, *Caenorhabditis elegans* (*C. elegans*). This nematode worm was introduced as a model system by Sydney Brenner as a powerful genetic tool with relatively simple anatomy (Brenner et al., 1974). The entire genome of *C. elegans* has been sequenced, and many of the genes represent a single homolog of more complex gene families in other organisms, including humans. Furthermore, *C. elegans* are predominantly hermaphrodites that can self-fertilize and produce a brood of up to ~300 offspring that reach adulthood in about 3 days (Sulston and Brenner, 1974). These features, and their inexpensive, simple maintenance, support robust genetic manipulation such as forward and reverse genetic screens, cell-specific rescue experiments, and more recently, targeted DNA editing by the CRISPR-Cas9 system (Dickinson et al., 2015).

C. elegans also provides a number of advantages for structural investigation. These worms exhibit consistent cell lineages in both somatic and nervous systems. The hermaphrodite nervous system contains 302 neurons with relatively unbranched axons and dendrites. Neurons follow stereotyped position of cells somas, processes, and synapses that form a nerve ring, head and tail ganglia, and dorsal and ventral nerve cords. Early serial EM reconstructions by John White provide a complete wiring and connectivity map of the worm that serves as a cornerstone for the field (White et al., 1986). Finally, worms are the ideal size for HPF EM/FS. The adult worm

is about 1 mm in length and 65 um in diameter, allowing for exquisite preservation by this technique.

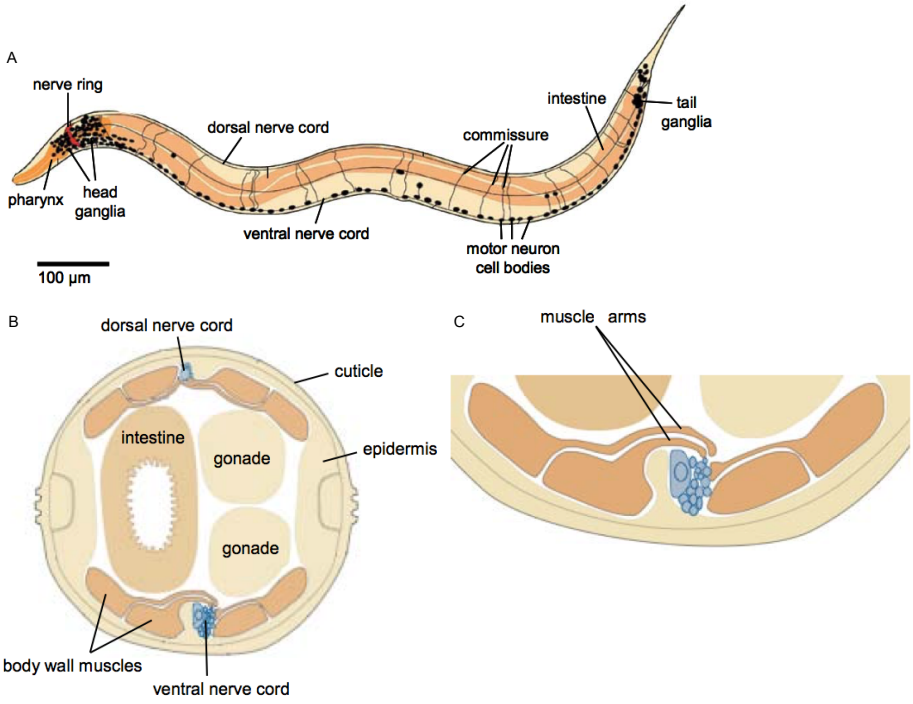

Figure I.10. The nervous system of C. elegans. A. The head of the worm (left) contains the nerve ring and head ganglia. A dorsal and ventral nerve cord extend along the anterior/posterior axis of the worm. Pictured are motor neurons, with cell bodies located in the ventral cord and commissures extending across the worm to the dorsal cord. **B.** Cross section of the worm. The dorsal and ventral nerve cords are located toward exterior edge of the worm. **C.** Muscle arms protrude towards the nerve cord to form neuromuscular junctions. Adapted from Gally and Bessereau, 2003.

1. The motor neuron system in C. elegans

The motor neuron system in *C. elegans* consists of 95 longitudinal body wall muscles (BWM) that are innervated by 113 motor neurons running along the anterior/posterior axis of the worm in dorsal and ventral nerve cords (Sulston and Horvitz, 1977). These muscle cells extend muscle arms towards the nerve cord in four quadrants on either side, in contrast to other

organisms whose neurons project axons towards muscle (Stretton, 1976). NMJs appear as "pearls on a string", forming *en passant* axon swellings along the cord (White et al., 1986).

The ventral nerve cord (VNC) contains all motor neuron cell bodies, and neurons must project axons or dendrites to the dorsal nerve cord (DNC). Motor neurons are classified based on their anatomy and primary neurotransmitters. V-class motor neurons innervate the ventral cord, extending dendrites to the dorsal cord. D-class motor neurons project axons to form synapses in the dorsal cord and localize dendrites in the ventral cord. Within each class, neurons are considered A-type or B-type if they release acetylcholine (ACh), or D-type if they release GABA, onto BWM cells (Richmond and Jorgensen, 1999). Postsynaptic ACh receptors are non-selective cation channels that allow an influx of Na^+ and K^+, resulting in depolarization and muscle contraction. $GABA_A$ receptors are ion channels that pass Cl^- into the muscle cell, resulting in hyperpolarization and relaxation (Richmond and Jorgensen, 1999). The precise wiring of excitatory cholinergic input from VA/VB and DA/DB neurons to body wall muscles on one side of the animal is coupled to inhibitory GABAergic signaling by VD/DD neurons to muscles on the opposite side of the animal. This cross-inhibition allows the motor circuit to execute sinusoidal body movements that propagate along the anterior/posterior axis of the worm. Finally, excitatory cholinergic B-type motor neurons VB and DB mediate forward movement, while A-type VA and DA cholinergic neurons drive reverse movement (reviewed in de Bono and Maricq, 2005).

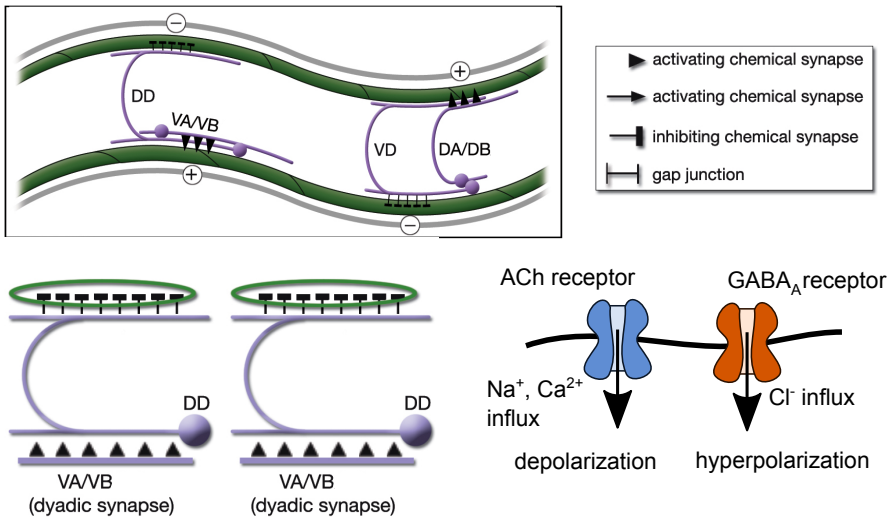

Figure I.11. The motor neuron wiring of C. elegans. VA/VB cholinergic neurons innervate the ventral cord. DA/DB cholinergic neurons innervate the dorsal cord. These neurons release acetylcholine, which binds to receptors and causes a depolarizing influx of Na^+ and Ca^{2+}, causing the muscle to contract. VD GABAergic neurons innervate the ventral cord, while DD GABAergic neurons innervate the dorsal cord. These neurons release GABA onto muscles, which cause $GABA_A$ receptors to open and pass Cl^- into the muscle, allowing it to relax. The cross-wiring of these neurons allows for excitation on one side of the worm linked to inhibition on the other, producing sinusoidal body bends that propagate along length of the animal. Adapted from Altun and Hall, 2011.

These different classes of neurons and synapses can be identified at the EM level based on their stereotyped position and postsynaptic partners. Cholinergic synapses project onto muscle and dendrites of GABAergic neurons, forming dyadic synapses (McIntire et al., 1993). GABAergic synapses exclusively project onto body wall muscles and muscle arms (Schuske et al., 2004; White et al., 1986).

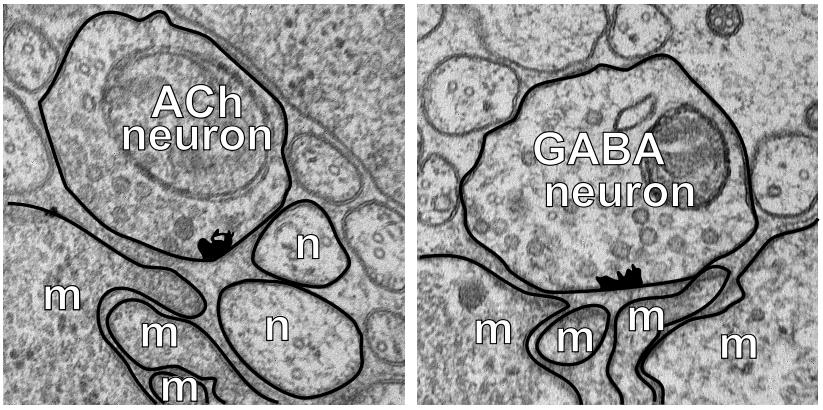

Figure I.12. Cholinergic and GABAergic synapse morphology. Cholinergic neurons (left, ACh) project at an angle to muscle arms (m) and often form dyadic synapses with another neuron (n). GABAergic neurons (right) project exclusively to muscle arms.

The *C. elegans* motor circuit provides a system that is amenable to complementary forms of structural and functional analysis. Locomotion, including response to various stimuli and drug application, can provide a readout of motor neuron activity. Furthermore, whole-cell patch clamp recordings can be recorded from ventromedial muscle cells to measure pre- and postysynaptic function (Richmond and Jorgensen, 1999).

F. Advantage of HPF/FS EM for studying synaptic ultrastructure

Synapses in *C. elegans* are very small, with structures on the order of one to hundreds of nanometers in size. Although advances in superresolution microscopy have come far in their ability to resolve synaptic structures, EM remains the best tool for this important analysis. Unlike light microscopy, electron microscopes use a beam of electrons to illuminate a sample. Because the wavelength of an electron is 100,000 times shorter than that of a photon, this technique can provide resolution down to an atomic level (Erni et al., 2009). In transmission electron microscopy (TEM), electrons either pass through a sample or are scattered by the atomic nucleus or electron shell of a molecule in the sample. Those that pass through can be detected

by a charge-coupled device (CCD) camera and appear as light spots on an electron micrograph, while those that are scattered appear as dark spots. Thus, all structures in a sample may be visible without an artificially expressed marker. Because biological samples are rich in carbon, nitrogen, and hydrogen, which have low atomic numbers, samples are often counterstained with heavy metals, such as uranyl acetate and lead citrate, that deposit metal on proteins and nucleotides and enhance contrast. Additionally, samples must be free of water and generally less than 200 nm thick to be observed in the electron microscope. Thus, a great deal of preparation must be performed to ready a sample for imaging in the electron microscope.

While traditional chemical fixation methods for EM have provided foundational anatomical information, HPF/FS protocols have enabled critical advances in the field. As noted in the discussion above, studies using conventional EM methods have shown different results than those using HPF/FS EM (Zhen and Jin 1999 vs Kittelman et al., 2013; Richmond and Jorgensen, 1999; Weimer et al., 2006; reviewed in Imig et al., 2014). Conventional fixation requires the cuticle of the worm to be breached to increase permeability across this thick structure. Worms must then incubate in highly concentrated fixative for hours before structures are fully immobilized. Both the hyperosmotic conditions associated with these methods and disruption of the worm's hydrostatic pressure result in shrinkage of extracellular space, distortion of membrane and organelle morphology and location, and even degradation of certain structures (Weimer et al., 2006). Additionally, aldehydes that are commonly used to fix tissue can stimulate vesicle exocytosis (Smith and Reese, 1980).

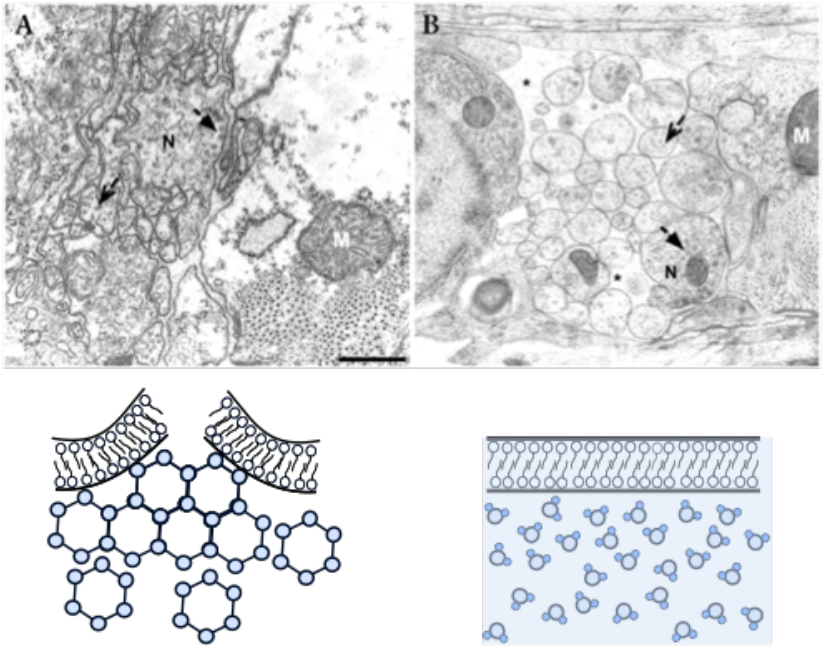

Figure I.13. Conventional and high-pressure freeze fixation. Conventional fixation (A, top left) can result in dehydrated tissue, movement of organelles, and breakage of membranes. High pressure freeze and freeze substitution (B, top right) result in round, well-preserved structures. Water in tissue can form ice crystals that occupy larger space, resulting in changes to morphology (bottom left). Freezing water at high pressure and low temperature forms vitreous ice, which occupies the same space as liquid water (bottom right). Adapted from http://advanced-microscopy.utah.edu/education/electron-micro/.

In contrast, freezing the animal within milliseconds captures the intact worm in a near physiological state and allows fixatives to diffuse into the interior of the worm as it is brought to room temperature over several days. Furthermore, freezing at high pressure (2100 bar) and low temperature (-180°C) in a high-pressure freezer, converts tissue to a vitrified state (Moor, 1987). Vitreous ice in the sample occupies the same space as water, rather than forming larger crystalline ice structures that can cause cellular components to change shape, size, and position during dehydration and chemical fixation. Since water conducts heat poorly, thick tissues may still experience ice crystal formation under these conditions. Fortunately, the ~65um thickness of

an adult worm is within the 200um limit for vitrification, and up to 30 worms can readily be frozen simultaneously.

After freezing, samples undergo stepwise thawing from -180°C to room temperature over 1-7 days while incubated in chemical fixatives. FS can be performed in an automatic freeze substitution (AFS) machine or in makeshift, temperature controlled chambers. A variety of solvents and incubation parameters have been used in FS. Common precipitating fixatives are methanol, anhydrous acetone, uranyl acetate, and tannic acid. These are combined with oxidizing agents such as osmium tetroxide or potassium permanganate that crosslink lipids and deposit heavy metals in the tissue to provide mechanical strength and visual contrast during imaging. Choice of solvents depend on the focus of analysis. A stronger fixative, such as osmium tetroxide, preserves tissue more effectively, improving resolution, but strongly reduces antigenicity. Finally, fixed worms can be embedded in epoxy or methacrylate-based resins which are hardened by heat or UV light. Embedded samples can be trimmed and sectioned with a diamond knife to prepare for imaging.

Specimens prepared using HPF/FS exhibit fewer distortion artifacts due to fixation and dehydration, have improved antigenicity, and result in a more physiologically accurate structural representation of the worm. Ultrathin (~40 nm) serial sections along the nerve cord can be imaged, aligned, and analyzed to reveal reconstructed 3D representations of ultrastructure. While cross sections provide excellent xy-resolution (2 nm), z-resolution is limited to the thickness of the section, in this case ~40 nm. Electron tomography partly circumvents this issue by imaging thicker sections (~200-300 um) at varying angles and then artificially reconstructing

their volumes. Still, serial section reconstructions can provide a wealth of important ultrastructural information.

I used HPF/FS EM and serial section TEM (ssTEM) to analyze active zone structure at the *C. elegans* NMJ. This work provides a crucial component of the characterization of two novel AZ proteins, Clarinet and Sentryn. I also characterized the ultrastructure of mutants involved in a synapse remodeling program. My findings anchor an advanced understanding of how various AZ proteins interact to assemble and disassemble synapses and regulate their function.

G. Clarinet (CLA-1) is a novel active zone protein required for synaptic vesicle clustering and release

Piccolo and Bassoon are active zone proteins that bring SVs from the periphery of the synapse to the AZ. Before the discovery of fife in *Drosophila*, no known invertebrate homologs for these proteins were identified. Chapter 2 of this thesis describes the characterization of a novel, Piccolo-related protein in *C. elegans* that we named Clarinet. Clarinet (CLA-1) is a novel AZ protein that was discovered in a genetic screen for regulators of SV clustering. Clarinet is named based on its homology to vertebrate Piccolo and is also related to vertebrate RIM. *cla-1* encodes a long, medium, and short isoform that share C-terminal PDZ and C2 domains. The long isoform (CLA-1L) appears to have a unique subset of functions. The C-terminus of all isoforms localizes discretely at the AZ and requires SYD-1, SYD-2, and UNC-104 to fully localize to synapses. Interestingly, *cla-1* null mutants also contain reduced levels of endogenous SYD-2::GFP at synapses. While synapse number is reduced, as measured by fluorescently tagged synaptobrevin (SNB-1) and RAB-3, evoked release appears normal. However, spontaneous release frequency

and sustained release in response to repeated stimulation are both reduced. Furthermore, *cla-1* null animals are resistant to the acetylcholinesterase (AChE) inhibitor aldicarb, which is an indirect measure of defective ACh release.

To understand the seemingly inconsistent effects of loss of *cla-1* on SV release, I performed HPF/FS EM analysis of cholinergic motor neuron synapses in *cla-1* null mutants. My results indicate that *cla-1* contributes to the size of the DP as well as the ability of SVs to physically tether to the DP. An increase in docked SVs within 100 nm of the DP led to us to examine *cla-1*'s interaction with *unc-10*, which localizes and functions in this area. We found that while *cla-1;unc-10* double mutants do not exacerbate the reduction of synapses in *cla-1* single mutants, they do exhibit additive defects in evoked and spontaneous release. Taken together, these findings suggest that *unc-10* can compensate for a loss of *cla-1* at the AZ to maintain the RRP.

H. The unique active zone protein Sentryn captures SVs and DCVs in the synaptic region of axons

Before SVs are localized to sites of release at the AZ, they must first be transported out of cell bodies and down long axonal processes to a synaptic region. Interestingly, guided axonal transport must achieve dual roles of both promoting plus-end transport to the synaptic region, and then capturing SVs and DCVs at synapses, thus preventing additional plus-end transport into a distal asynaptic region of the neuron. To understand this functional switch, as well as identify additional regulators in the poorly understood trafficking of DCVs, we conducted a screen for genes involved DCV localization. As presented in Chapter 3, we discovered a novel AZ protein,

Sentryn (STRN-1), that is conserved in all animals and expressed throughout the nervous system. We propose that Sentryn functions as a part of the CSS protein system, which is a unique subset of AZ-enriched proteins.

We analyzed fluorescently tagged SV and DCV proteins to find that *strn-1*, *sad-1*, and *strn-1;sad-1* mutants contained lower levels of axonal SVs and DCVs, which instead accumulated in their cell somas and dendrites. This effect was dynein-dependent, and epistatic experiments suggested that *strn-1* and *sad-1* operate together to enable the function of *syd-2.* Time-lapse imaging of these markers revealed that STRN-1 and SAD-1 promote anterograde transport, with more time spent pausing and less time spent in anterograde movement in mutants for *strn-1*, *sad-1*, and *strn-1;sad-1*. Furthermore, we observed fluorescently tagged SVs and DCVs mislocalized at distal asynaptic regions past the synaptic regions of DA9, suggesting that these CSS proteins influence both transport and synaptic capture of SVs and DCVs.

In order to confirm that these results were not an artifact of over-expressed fluorescent markers, I used HPF/FS EM to examine the native ultrastructure in *strn-1*, *sad-1*, and *strn-1;sad-1* mutants. I observed similar reductions in DCVs and SVs at the synapse as seen at the light level. Importantly, my analysis revealed that all three mutants resulted in a smaller DP length, and fewer SVs were docked in *sad-1* and *strn-1;sad-1* mutants. These results indicate that Sentryn is an important, conserved AZ protein that provides a link between synaptic transport and capture. Thus, we named this protein Sentryn for its purpose to stand guard, like a “sentry,” over SVs and DCVs at the AZ.

I. The DEG/ENaC cation channel protein UNC-8 drives activity-dependent synapse removal in remodeling GABAergic neurons

While a complicated series of molecular players must interact to assemble and maintain synaptic architecture, equally intricate mechanisms exist to dismantle synapses. One such case is the dramatic remodeling program of GABAergic motor neurons that occurs during development. DD cell bodies and synapses first appear in the ventral cord in the embryo. Between larval stages L1 and L2 of development, these neurons disassemble their ventral synapses and relocate them to the dorsal cord of the animal. During L2, VD cell bodies are born and innervate the ventral cord for the remainder of the life cycle. Both DD and VD neurons are programmed for synaptic remodeling. However, VD synapses do not remodel because the transcription factor UNC-55, suppresses the endogenous remodeling program. Of the many potential gene targets suppressed by UNC-55, we investigated the Degenerin/Epithelial Sodium Channel (DEG/ENaC) protein UNC-8. The final chapter of this thesis examines the specific mechanisms that UNC-8 regulates to trigger synapse disassembly in DD motor neurons.

Using a variety of fluorescently-tagged synaptic markers, we determined that UNC-8, a nonselective cation channel, promotes activity-dependent remodeling in DD neurons. In an *unc-55* mutant, VD neurons undergo "ectopic remodeling," resulting in a dramatic loss of ventral GABAergic synapses. An *unc-55;unc-8* double mutant restored some of these synapses to the ventral cord. HPF/FS EM analysis confirmed that while no ventral GABAergic synapses could be found in an *unc-55* mutant, they were readily identifiable in *unc-8* and *unc-8;unc-55* double mutants. Further genetic and pharmacological experiments explored the question of how UNC-8 promotes remodeling. We found that remodeling required at least four additional proteins all

connected to Ca^{2+}, including the VGCC (UNC-2), the calcium/calmodulin-dependent phosphatase Calcineurin (TAX-6), adaptor protein CED-4/Apaf1, and its downstream target, CED-3/caspase. We propose a model in which TAX-6 phosphorylation activates UNC-8. Depolarization through UNC-8 may stimulate local VGCC activity, resulting in a positive feedback loop between TAX-6, UNC-8, and UNC-2 that may function as an activity sensor. The resulting increase in intracellular Ca^{2+} could then trigger canonical apoptotic cell death pathways mediated by adaptor protein CED-4/Apaf1 and its downstream target, CED-3/caspase leading to synapse disassembly.

II. CLARINET (CLA-1), A NOVEL ACTIVE ZONE PROTEIN, REGULATES SYNAPTIC VESICLE RELEASE

Zhao Xuan[1*], Laura Manning[2*], Jessica Nelson[1], Janet E. Richmond[2], Daniel Colón-Ramos[1,4], Kang Shen[3,5] and Peri T. Kurshan[3]

[1]Program in Cellular Neuroscience, Neurodegeneration and Repair, Department of Cell Biology and Department of Neuroscience, Yale University School of Medicine
[2]Department of Biological Sciences, University of Illinois at Chicago, Chicago, IL
[3]Department of Biology, Stanford University, Stanford, CA
[4] Instituto de Neurobiología, Recinto de Ciencias Médicas, Universidad de Puerto Rico
[5]Howard Hughes Medical Institute
* These authors contributed equally.

This chapter has been modified from a manuscript under revision at *eLife*, previously published in *bioRxiv*. All figures have been copied or modified from the manuscript with permission from the authors.

A. Introduction

Neurons communicate by releasing synaptic vesicles in response to an electrical signal. An essential group of conserved proteins act together to coordinate this process. These proteins form a cytomatrix at the active zone of presynaptic boutons and function to bring synaptic vesicles near the plasma membrane, localize calcium channels to release sites, and prime synaptic vesicles for calcium-dependent release. In vertebrates, a core group of these proteins include liprin-α, RIM, RIM-BP, ELKS, and Munc-13 (Sudhof, 2012; Ackermann et al., 2015).

Active zone proteins are largely conserved, with some exceptions. *Drosophila* Bruchpilot is most similar to vertebrate ELKS in its N-terminal sequence homology (Wagh et al., 2006; Kittel

et al., 2006). However, it also contains a large C-terminal half with coiled-coil structures that are thought to tether SVs (Matkovic et al., 2013). Vertebrate synapses also rely on Bassoon and Piccolo to properly cluster synaptic vesicles (Langnaese et al., 1996; Mukherjee et al., 2010). Previously, these two proteins have been considered exclusive to vertebrates. Recently, however, *Drosophila* Fife was discovered based on its PDZ domain sequence homology to vertebrate Piccolo. Fife also contains Zinc finger and C2 domains and is a proposed active zone protein (Bruckner et al., 2012). Studies show that Fife binds to and functions redundantly with RIM to dock synaptic vesicles and increase release probability (Bruckner et al., 2016). Still, homologs for Piccolo, Bassoon, or Fife have remained elusive in *C. elegans*.

In this study, we conducted a forward genetic screen for regulators of synaptic vesicle clustering. From this screen, we identified clarinet (*cla-1*), a unique protein that is required for synapse development and release. *cla-1* encodes six isoforms that fall into three groups (*cla-1(L),* *cla-1(M),* and *cla-1(S)*, that share a C-terminal PDZ and C2 domain. The PDZ domain contains sequence homology to Piccolo and RIM. In a null *cla-1* mutant, fewer synapses are observed, spontaneous release is reduced, and synaptic depression is increased. *cla-1* mutants also exhibit smaller dense projections and a large reduction in the number of SVs contacting those projections, as well as defects in levels of the AZ protein SYD-2/Liprin-α. Based on these findings, we conclude that *cla-1* encodes a novel active zone protein that is important for proper synapse development and function.

B. Results

1. CLA-1 clusters synaptic vesicles in the NSM neuron

To identify regulators of synaptic vesicle clustering, we conducted a forward genetic screen for clustering defects in the serotonergic NSM neuron of *C. elegans* (Figure 1). We observed the fluorescence pattern of the SV protein marker VMAT/CAT-1::GFP, and identified the allele *ola104*, which displayed diffuse SV distribution in NSM (Figure 2.1D-F). Synapses in *ola104* animals showed reduced intensity at puncta and increased extrasynaptic fluorescence.

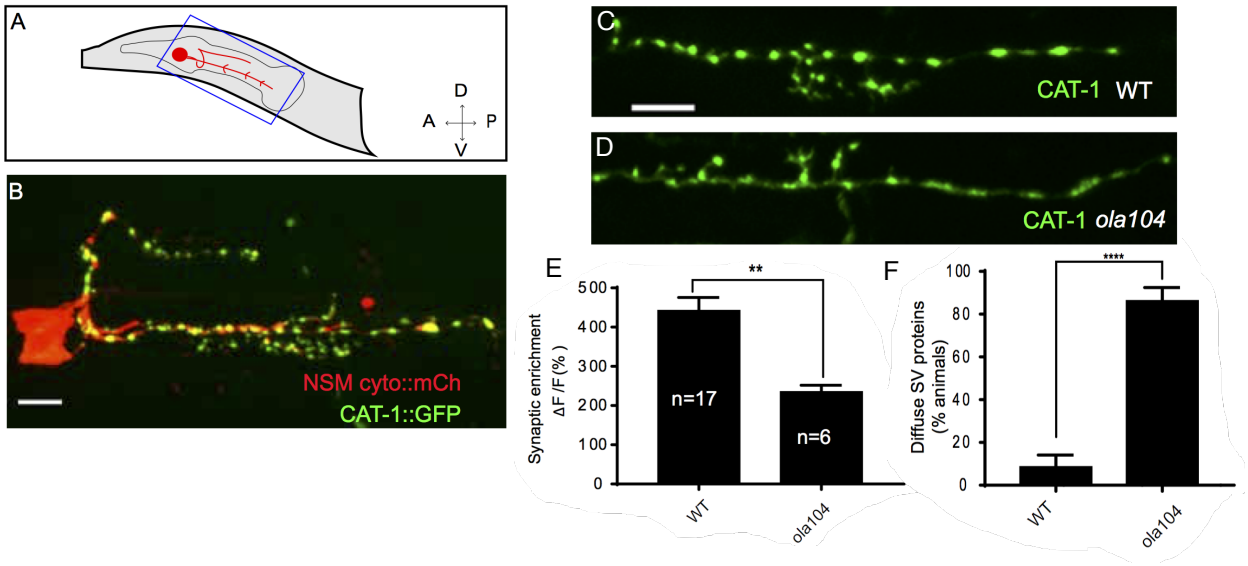

Figure II.1. *ola104* displays disrupted synaptic vesicle clustering in NSM neuron and was identified as a genetic lesion of *cla-1*. A. Schematic diagram of the nematode head and the NSM neuron (highlighted red, boxed in blue). **B.** Cytosolic mCherry and the synaptic vesicle marker CAT-1::GFP expressed cell specifically in NSM. Scale bar = 5 µm. **C-D.** Synaptic vesicle marker CAT-1::GFP in the NSM ventral neurite in wild type (WT; C) and *ola104* (D). Note that *ola104* mutants exhibit diffuse (D and E) rather than the wild-type punctate (C and E) fluorescence patterns. Scale bar = 5 µm **E.** Synaptic enrichment (ΔF/F) of CAT-1::GFP in NSM for wild-type (WT) and *ola104* animals. **F.** Percentage of animals displaying diffuse distribution of CAT-1::GFP in NSM of wild-type (WT) and *ola104* animals. n= 62 for WT; n=63 for *ola104.* Data collected by Zhao Xuan.

We used single nucleotide polymorphism (SNP) mapping to determine that *ola104* is a missense mutation in *cla-1* located on chromosome IV (Figure 2.2A). Complementation testing with the independent allele, *cla-1(ok560)*, showed that the two alleles phenocopied one another and were non-complementary (Figure 2.2B-F).

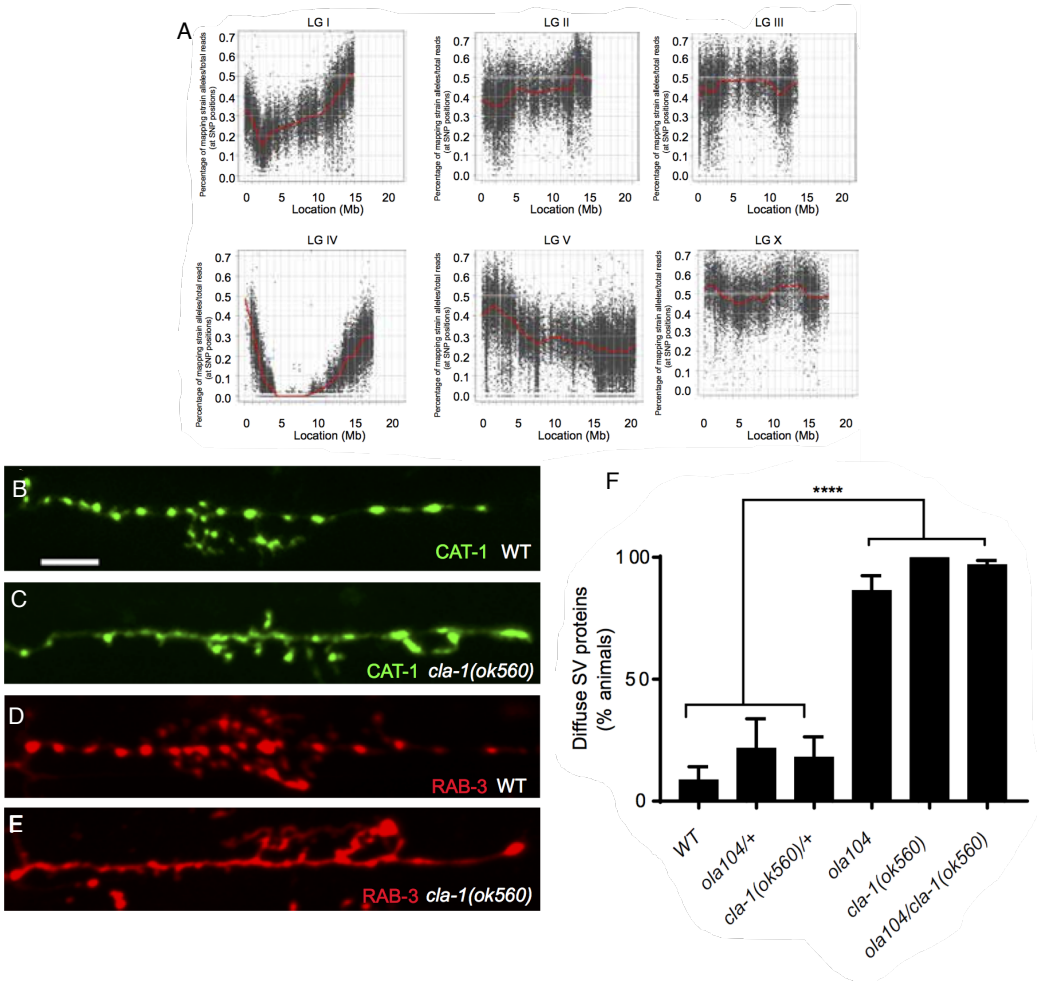

Figure II.2. *ola104* phenocopies *cla-1(ok560)* and is non-complementary. A. Graphic representation of the whole genome sequence SNP data. The positions of SNP loci are depicted as a XY scatter plot, where the ratio of Hawaiian/total number of reads for each SNP is represented. LGI to LGV and LGX are linkage groups/chromosomes of the worm. **B-E.** Synaptic vesicle markers in NSM: CAT-1::GFP (B-C) or RAB-3::mCH (D-E) in the ventral neurite of wild type (WT; B and D) and *cla-1(ok560)* (C and E). Note that *cla-1* mutants exhibit diffuse (C, E) rather than the wild type punctate (B, D) fluorescence patterns. Scale bar = 5 µm. **F**. *cla-1 (ok560)*

animals phenocopy *ola104* and do not complement *ola104* when assayed for CAT-1::GFP distribution in NSM. Data collected by Zhao Xuan.

The *cla-1* gene predicts six different isoforms which can be classified into three groups based on length (Figure 2.3A). CLA-1(L) (long) includes CLA-1a and b; CLA-1(M) (medium) includes CLA-1c and d; and CLA-1(S) (short) includes CLA-1e and f (Figure 3A). We examined SV clustering in five mutant alleles across these isoforms. *cla-1(ok560)* deletes the *cla-1(L)* promoter and part of the *cla-1(L*) coding region and will subsequently be referred to as *cla-1(L)*. *cla-1(wy1048)* is a CRISPR-generated allele that deletes the C-terminal region of *cla-1(L)* and M and most of *cla-1(S)*, including the common PDZ and C2 domains. Since *cla-1(wy1048)* creates a large deletion in all isoforms, we consider it a null allele and will subsequently refer to it as *cla-1(S/M/L).* We used RT-PCR to the C-terminal PDZ domain of *cla-1* to confirm that the *cla-1(L)* deletion mutant still expressed the shorter isoforms (Figure 2.3C). Each of the five mutant alleles we examined showed diffuse CAT-1::GFP fluorescence in the NSM (Figure 2.3B). Since this defect was seen in both the null mutant and *cla-1(L)*, we conclude that CLA-1(L) may play a specific role in SV localization at NSM synapses.

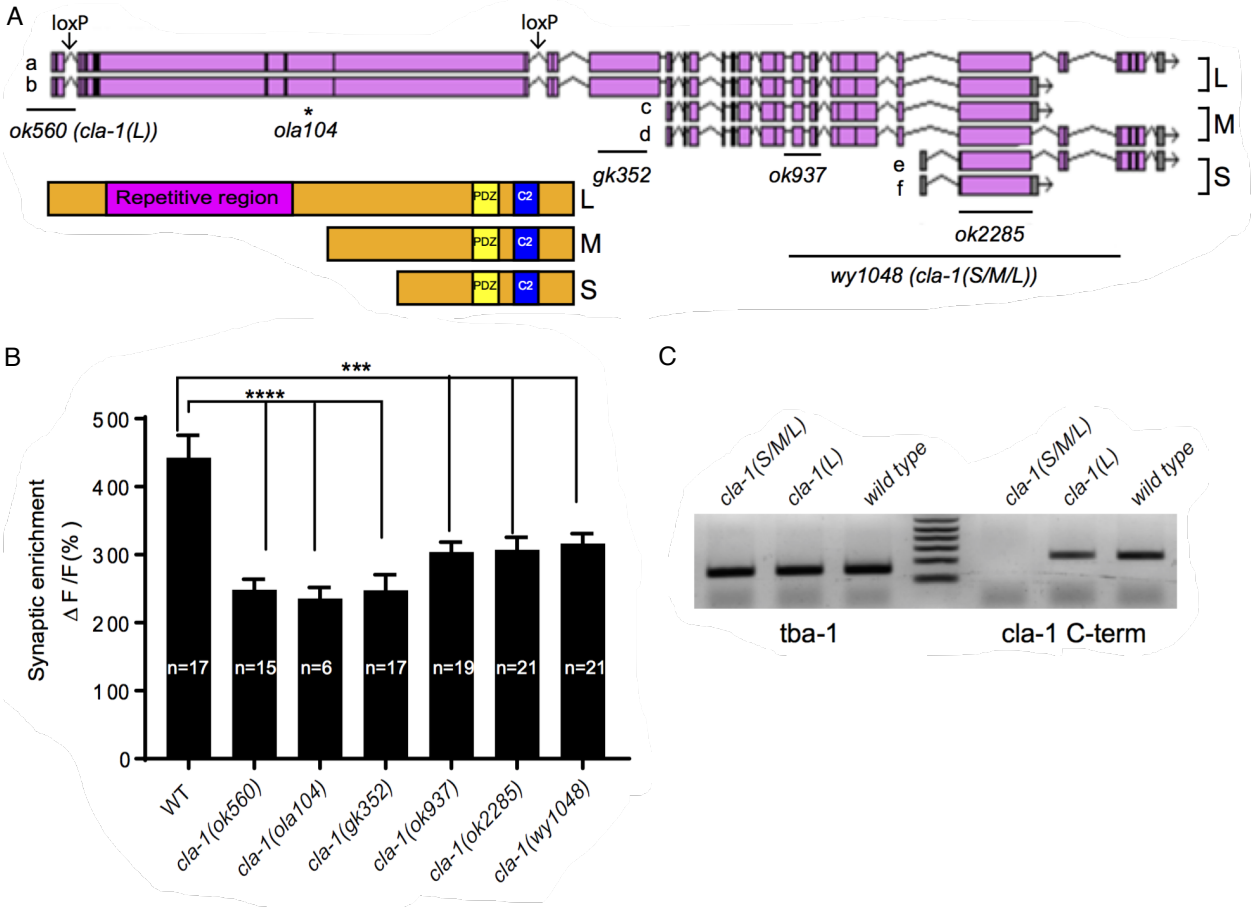

Figure II.3. Different isoforms of CLA-1 promote synaptic enrichment at NSM. A. Schematics of the genomic region of *cla-1* and the structure of three main isoforms of the CLA-1 protein. The locations of loxP sites and the genetic lesions of the *cla-1* alleles examined in this study are indicated. In addition to the common C-terminus, CLA-1(L) contains a large N-terminal repetitive region (see Figure 4A). **B.** Synaptic enrichment (ΔF/F) of CAT-1::GFP in NSM is greatly reduced in all *cla-1* mutants compared to wild type. **C**. RT-PCR shows that the common C-terminus is still expressed in a CLA-1(L) N-terminal deletion mutant (but not after deletion of the C-terminus itself, as in the null allele). *tba-1* (tubulin alpha chain) is used as a positive control. Data collected by Peri Kurshan.

2. CLA-1 is a novel active zone protein most closely related to RIM

cla-1(L) encodes a large ~9000 amino acid long protein, including an extended repetitive region of ~4000 amino acids (Figure 2.3A). The 12kb cDNA for this repetitive region consists of tandem repeats of 282 base pair repeat units (Figure 2.4A). Its predicted secondary structure

contains random coils alternating with alpha helices. The smaller *cla-1(M)* encodes ~3000 amino acids, and *cla-1(S)* encodes ~1000 amino acids. All three CLA-1 isoforms have common C-terminal PDZ and C2 domains, and these domains are conserved with mammalian active zone proteins Piccolo and RIM (Figure 4B). However, we found no other sequence similarities with vertebrate sequences. We performed a phylogenetic analysis of the *cla-1* PDZ domain sequences and found this domain is most closely related to RIM, but within a distinct clade (Figure 2.4B). These results suggest that *cla-1* encodes a novel protein in the active zone family. Because of its demonstrated functional role in SV clustering, we believe it may be functionally homologous to Piccolo, Bassoon, and Fife. Based on this relationship and its large size, we named this protein Clarinet (CLA-1).

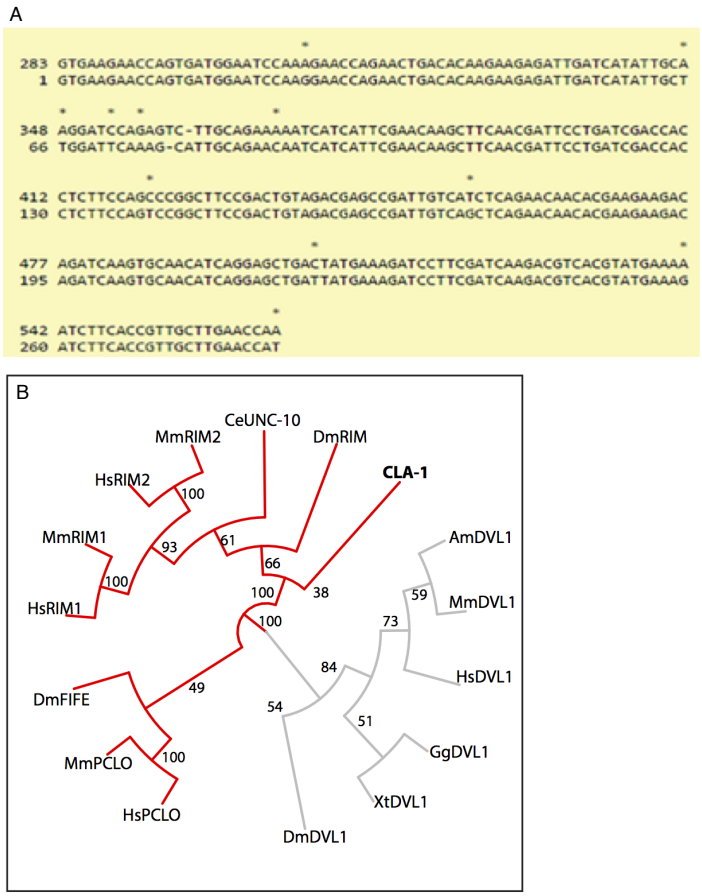

Figure II.4. Genetic structure and classification of CLA-1. A. Repeat unit (282bp) of the repetitive region of *cla-1(L)* cDNA. Note the high similarity between two repeat units shown here. **B.** The PDZ sequence of CLA-1 was aligned to RIM, Piccolo and Fife from *C. elegans* (CeUNC-10), *Drosophila* (DmRIM, DmFIFE), mouse (MmRIM1/2, MmPCLO) and human (HsRIM1/2, HsPCLO) by neighbor joining with 100 bootstrap replicates. PDZ domains of Dishevelled family proteins were used as an outgroup (gray).

We next examined the expression patterns of CLA-1 using GFP reporters fused to likely promoter regions in the 2kb fragments upstream of the L, M, and S isoforms. For each isoform, we observed broad expression that colocalized highly with pan-neuronal RAB-3::mCherry (Figure 2.5A-C).

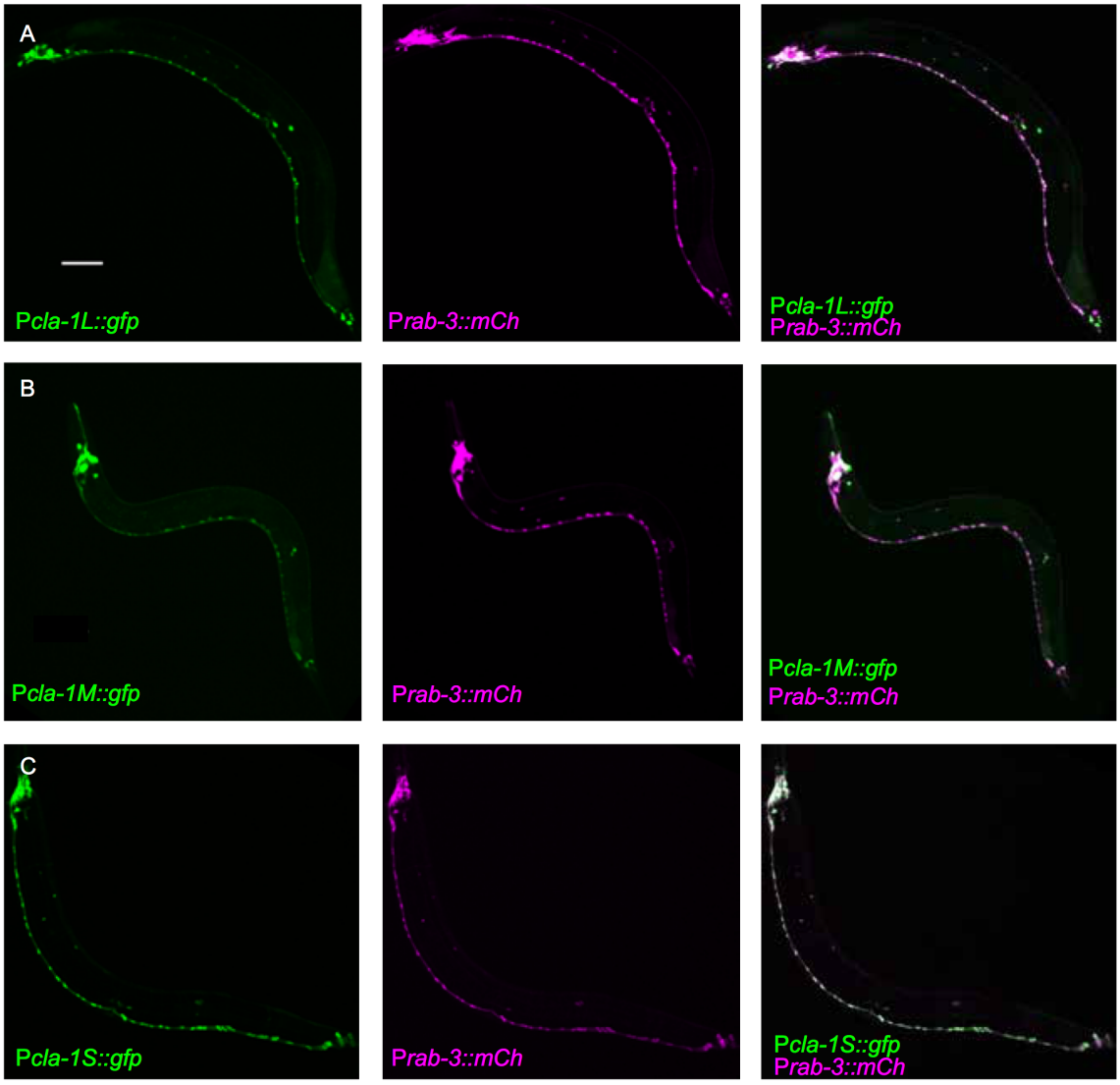

Figure II.5. Expression pattern of CLA-1 isoforms. A-C. Expression pattern of the long (A), medium (B), and short (C) isoforms of CLA-1. Promoter reporter was generated by putting 2kb upstream of start codons of each isoform before gfp cDNA. The GFP reporters under all three promoters are expressed broadly in the nervous system, marked with a mCherry reporter under the rab-3 promoter (middle panels of A-C). Scale bar = 60µm. Data collected by Zhao Xuan.

As an additional test, we used CRISPR to fuse GFP to the N-terminus of the endogenous *cla-1* locus (Figure 2.6A) (Dickinson et al., 2015). We observed expression of homozygous endogenous GFP::CLA-1(L) at synapses in the 3-fold stage of development, when the embryonic nervous system begins forming (Figure 2.6B, C). Its distribution colocalized tightly with a coexpressed

NSM::mCherry::RAB-3 cDNA (Figure 2.6D-F), confirming that CLA-1(L) is present at synapses, at or near SV clusters.

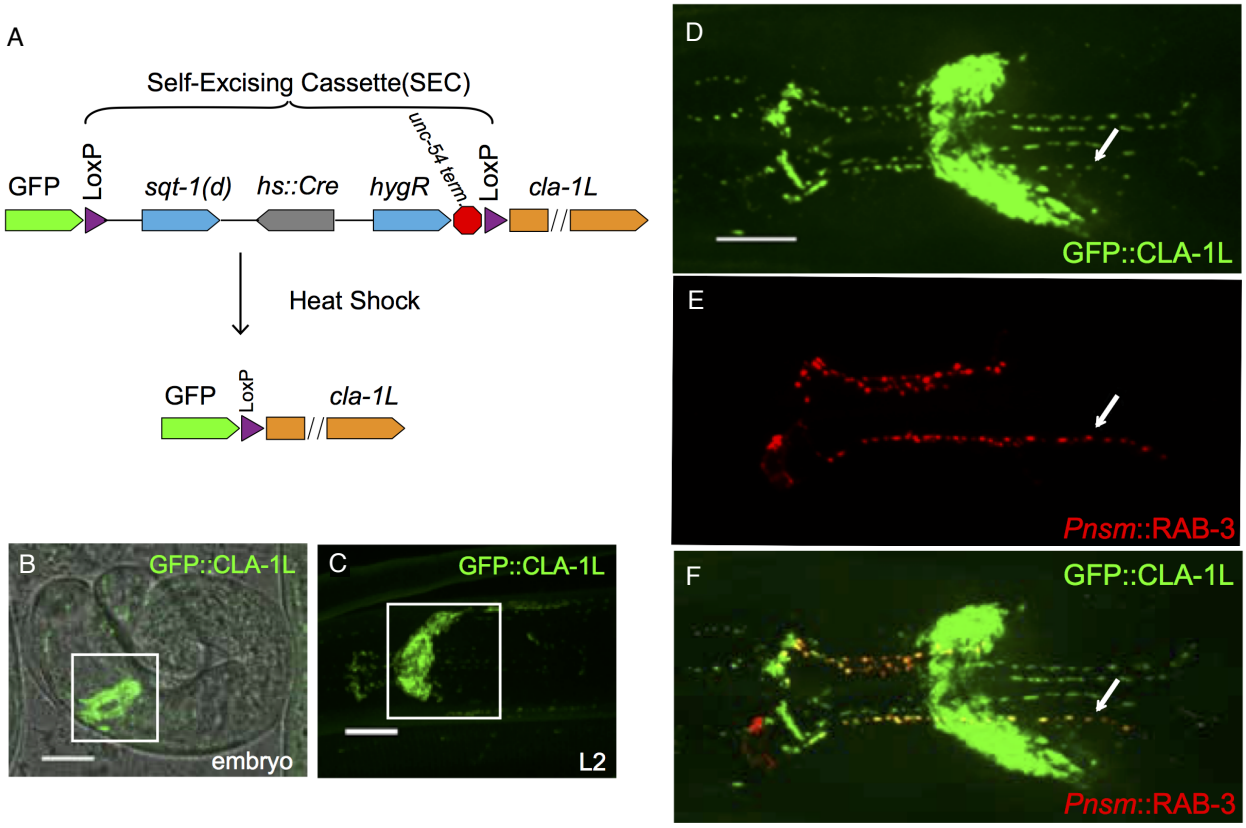

Figure II.6. CLA-1 localizes to synapses and regulates synaptic vesicle clustering in a cell autonomous manner. A. CRISPR strategy for N-terminal GFP tagging of CLA-1(L) (described in methods). Briefly, a GFP followed by a self-excising cassette (SEC) was inserted in front of the cla-1(L) start codon, and then excised upon heat shock. **B-C.** Endogenous expression of GFP::CLA-1(L) during development. GFP::CLA-1(L) is highly expressed in the nerve ring (the synapse-rich region in the nematode head considered the "brain" of the worm; boxed region) during late embryogenesis (B) and during larval stages (C, image taken in L2 larvae but representative of expression pattern seen for all stages of larval development, and adults; boxed region is the nerve ring). Scale bar = 10µm. **D-F.** Endogenous expression of GFP::CLA-1(L) in the nerve ring of adult worms (D) along with NSM-specific expression of mCh::RAB-3 (E). CLA-1(L) colocalizes with RAB-3 in NSM (arrows) (F). Note that in these animals the nerve ring is also labeled with GFP::CLA-1(L), as it represents the endogenous protein expression pattern from the CRISPR lines (see Materials and Methods). Scale bar = 10µm. Data collected by Zhao Xuan.

3. *CLA-1 acts cell-autonomously to regulate SV clustering*

To test whether CLA-1 cell-autonomously regulates SV localization, we employed CRISPR in cell-specific knockout and rescue experiments. First, we generated a transgenic strain with loxP sites at introns flanking exon 3 and exon 13 of *cla-1(L)* (Figure 2.7A). The loxP insertion alone had no effect on SV distribution in NSM, as visualized by CAT-1::GFP (Figure 2.7B, C, E). Then, we expressed Cre specifically in NSM, which should delete CLA-1(L) in this cell exclusively. The resulting CAT-1::GFP fluorescence pattern reflected the disrupted SV clustering phenotype seen previously (Figure 2.7D, E). Thus, *cla-1(L)* is required for SV clustering in NSM and acts cell autonomously.

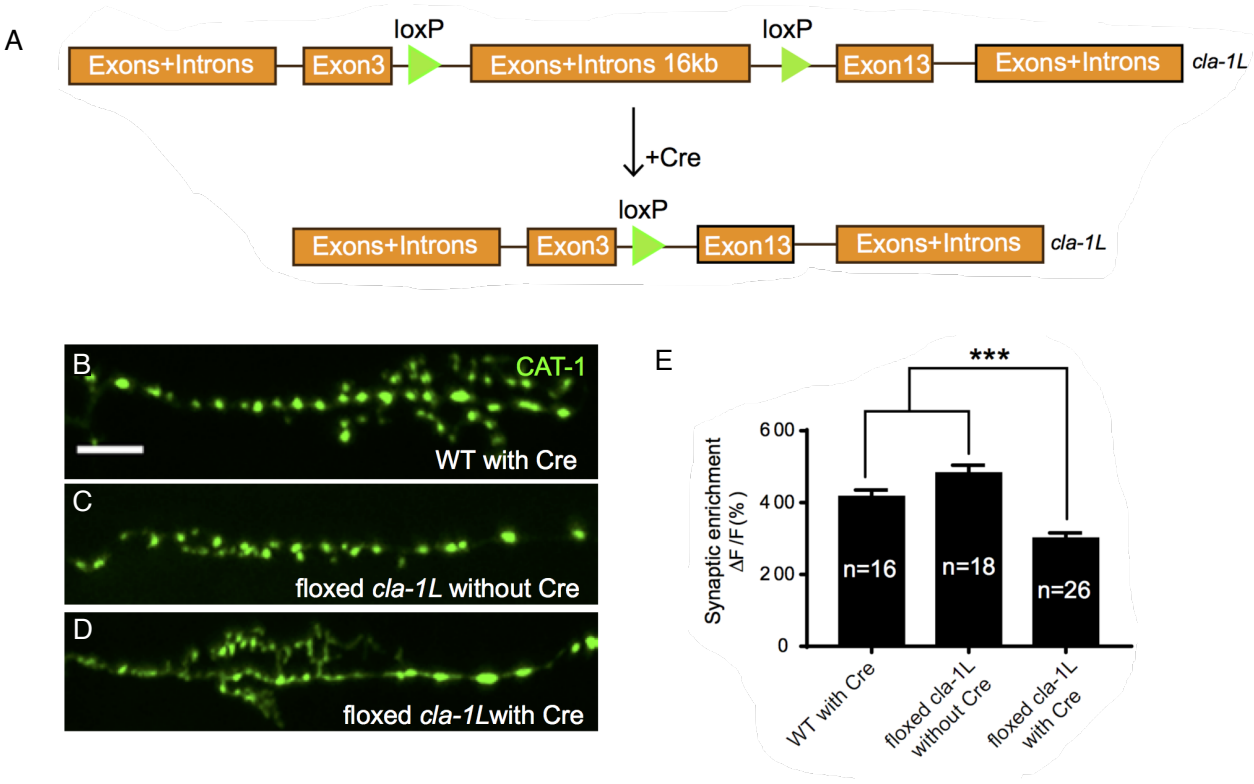

Figure II.7. CLA-1 regulates cell-autonomous defects in synaptic enrichment. A. To determine cell autonomy, loxP sites were inserted into introns between exon 3 and 13 of *cla-1(L)* (fig. 7A) via CRISPR. Cre expression in NSM led to the removal of CLA-1(L) specifically in that neuron. **B-D.** CAT-1::GFP distribution is normal in WT worms expressing Cre recombinase in NSM (B), and in floxed cla-1(L) worms without Cre (C), as expected. However, when Cre is expressed cell-

specifically in NSM in the context of the floxed *cla-1(L)* allele, the synaptic vesicle pattern in NSM phenocopies that of loss of function mutants for *cla-1* (D). Scale bar = 5µm. **E.** Synaptic enrichment (ΔF/F) of CAT-1::GFP in NSM for control animals ("WT with Cre" and "floxed *cla-1(L)* without Cre"), and animals in which *cla-1(L)* was cell-specifically deleted in NSM ("floxed *cla-1(L)* with Cre"). Data collected by Zhao Xuan.

We then performed a cell-specific rescue experiment in the *cla-1* null mutant background. We created a conditional *cla-1(L)*-expressing strain by inserting an N-terminal GFP and transcriptional terminator before the *cla-1(L)* start codon (Figure 2.8A). This alteration should drive expression of GFP under the endogenous *cla-1(L)* promoter while preventing expression of the *cla-1(L)* gene itself. As predicted, we observed GFP expression throughout the nervous system (Figure 2.8B) like the previous CLA-1(L) promoter expression pattern observation (Figure 2.5A-C). Similar to the *cla-1(L)* mutant, RAB-3::mCherry fluorescence was diffuse (Figure 2.8D, arrow). We then used NSM-specific expression of Cre cDNA to remove the terminator cassette in the GFP^CAS^*cla-1(L)* transgene, resulting in an in-frame, functional translational fusion of *cla-1(L)* (Figure 2.8A). In this case, GFP::CLA-1(L) localized in a punctate pattern in NSM (Figure 2.8G), colocalized with the punctate RAB-3 marker (Figure 2.8C) and therefore rescued SV clustering in NSM (Figure 2.8,H). Based on these complementary results from cell-autonomy experiments, we conclude that *cla-1(L)* is both necessary and sufficient to moderate SV clustering in NSM in a cell-autonomous fashion.

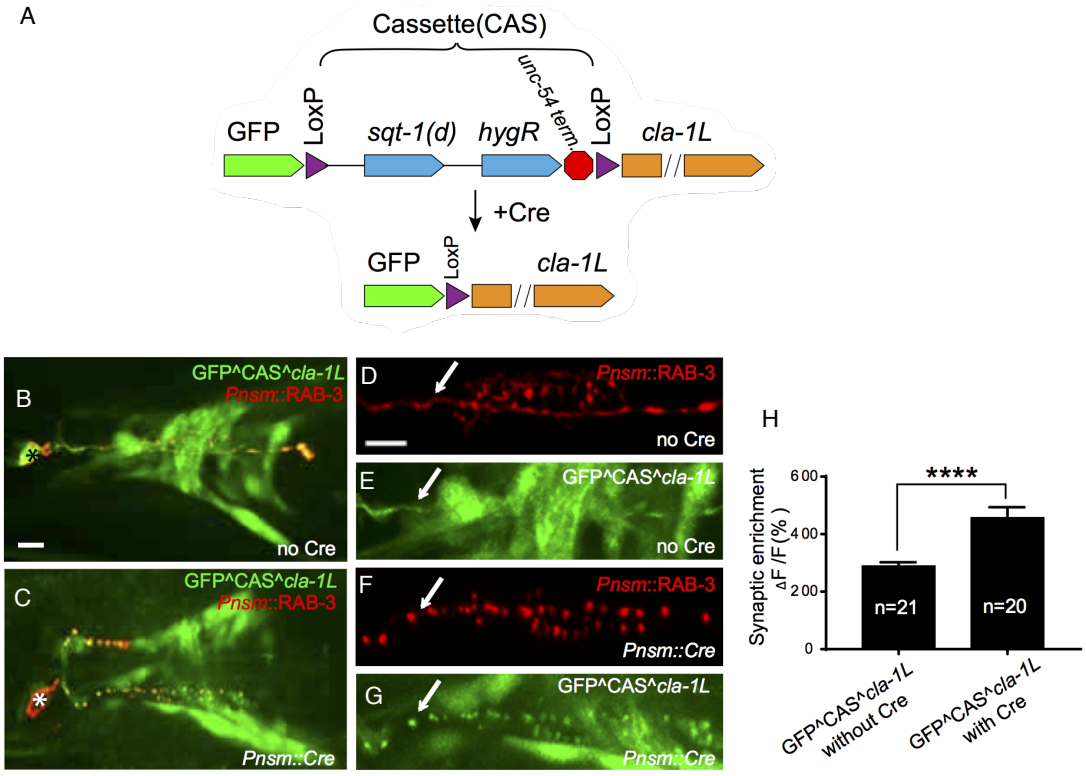

Figure II.8. Targeted expression of CLA-1 can induce synaptic enrichment cell-autonomously. A. Cell specific expression of CLA-1(L). The *cla-1(L)* null allele was generated by inserting GFP and a cassette (CAS) containing a transcriptional terminator before the start codon of *cla-1(L)*. Since the cassette was flanked by loxP sites, cell-specific expression of Cre resulted in cell-specific expression of GFP fused CLA-1(L). **B-G.** Cytosolic GFP driven by the endogenous *cla-1(L)* promoter in place of CLA-1(L) (*Pcla-1(L)*::GFP; B and E) overlaps (arrows in D and E) with RAB-3 expressed under the NSM promoter (*Pnsm*::RAB-3::mCh; C and D). RAB-3 shows defective vesicle clustering before Cre excision of the translation termination sequence (GFP^CAS^*cla-1(L)* without Cre; D; arrow). Upon cell-specific Cre expression in NSM (C,F-G), a functional, translational fusion of GFP:CLA-1(L) (see Materials and Methods and Figure 2.8A) rescues the synaptic pattern in NSM (as determined by punctate distribution of both RAB-3 (F, arrow) and GFP::CLA-1(L) (G, arrow)). Scale bar = 5µm. Asterisk (B and E) corresponds to the location of the cell body of the NSM neurons. **H.** Quantification of the synaptic enrichment (ΔF/F) of CAT-1::GFP in NSM for *cla-1l(L)* null animals ("GFP^CAS^*cla-1L* without Cre") and animals expressing GFP::CLA-1L cell-specifically in NSM ("GFP^CAS^*cla-1L* with Cre"). Data collected by Zhao Xuan.

4. CLA-1 isoforms regulate different aspects of synapse development throughout the nervous system

Having observed CLA-1 expression throughout the nervous system (Figure 2.5A-C), we wondered whether CLA-1 regulates SV clustering in neurons other than NSM. Indeed, we observed defects in fluorescent RAB-3 localization in both AIY and PVD neurons (Figure 2.9).

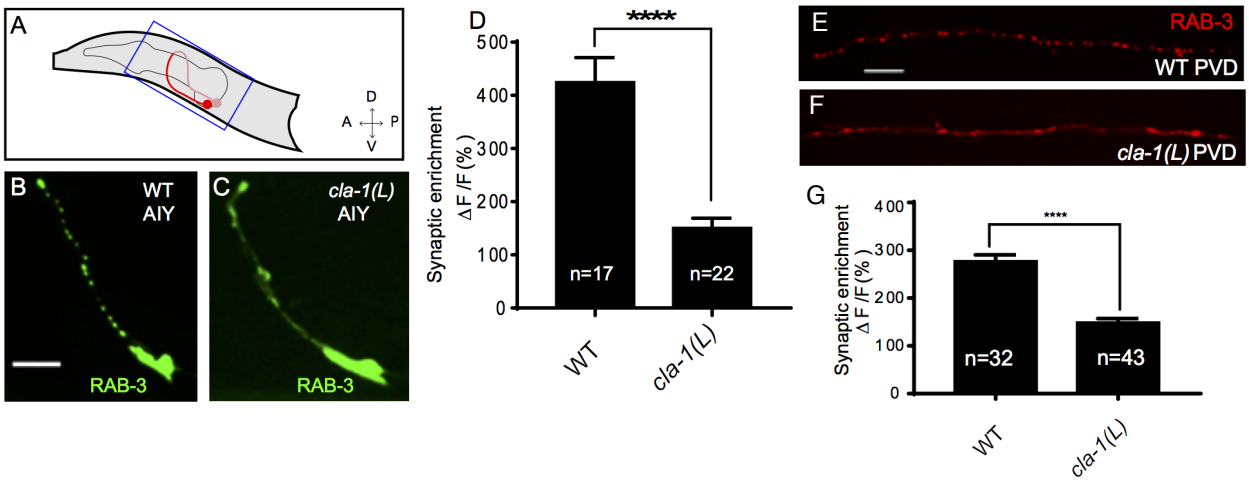

Figure II.9. CLA-1 isoforms have discrete functions in several neuron types. A. Schematic diagram of the bilaterally symmetric AIY interneuron (highlighted in red, boxed in blue) in the worm head. **B-C.** RAB-3::GFP forms discrete presynaptic clusters in AIY of wild type animals (WT; B), but is diffuse in *cla-1(L)* mutants (C). Scale bar = 5µm. **D.** Synaptic enrichment (ΔF/F) of RAB-3::GFP in AIY for wild-type (WT) animals and *cla-1(L)* mutants. **E-F.** RAB-3::GFP forms discrete presynaptic clusters in the mechanosensory neuron PVD of wild type animals (WT; E), but is diffuse in *cla-1(L)* mutants (F). Scale bar = 10µm. **G.** Synaptic enrichment (ΔF/F) of RAB-3::mCh in the PVD axon for wild-type (WT) animals and *cla-1(L)* mutants. Data collected by Zhao Xuan.

Interestingly, *cla-1(L)* mutants did not display a diffuse pattern of SV proteins (SNB-1::GFP or RAB-3::GFP) in GABA or cholinergic motor neurons that innervate body wall muscles (Figure 2.10). These data indicate that CLA-1(L) may have unique roles in different neurons. Since *cla-1(L)* mutants still express M and S isoforms, we next used the *cla-1(wy1048)* null allele, which deletes the PDZ and C2 domains in all three isoforms (Figure 2.3A). *cla-1(S/M/L)* mutants showed

similar synaptic enrichment defects as *cla-1(L)* in NSM (Figure 2.3B). In motor neurons, however, synaptic enrichment appeared normal in *cla-1(S/M/L)*, but with fewer synapses in the given field of view (Figure 2.10A-F). To more carefully examine whether the *cla-1* C-terminus or S/M isoforms regulate synapse number, we quantified RAB-3 fluorescent puncta in the single cholinergic motor neuron, DA9 (Figure 2.10J). We found that *cla-1(S/M/L)* contained fewer synapses than wild-type or *cla-1(L)* animals (Figure 2.10K,L). We also observed a reduction in puncta numbers in *cla-1(L)* mutants, but these effects were variable (Figure 2.10K,L). Taken together, these results indicate that specific isoforms may distinctly regulate SV clustering or synapse number in different neurons.

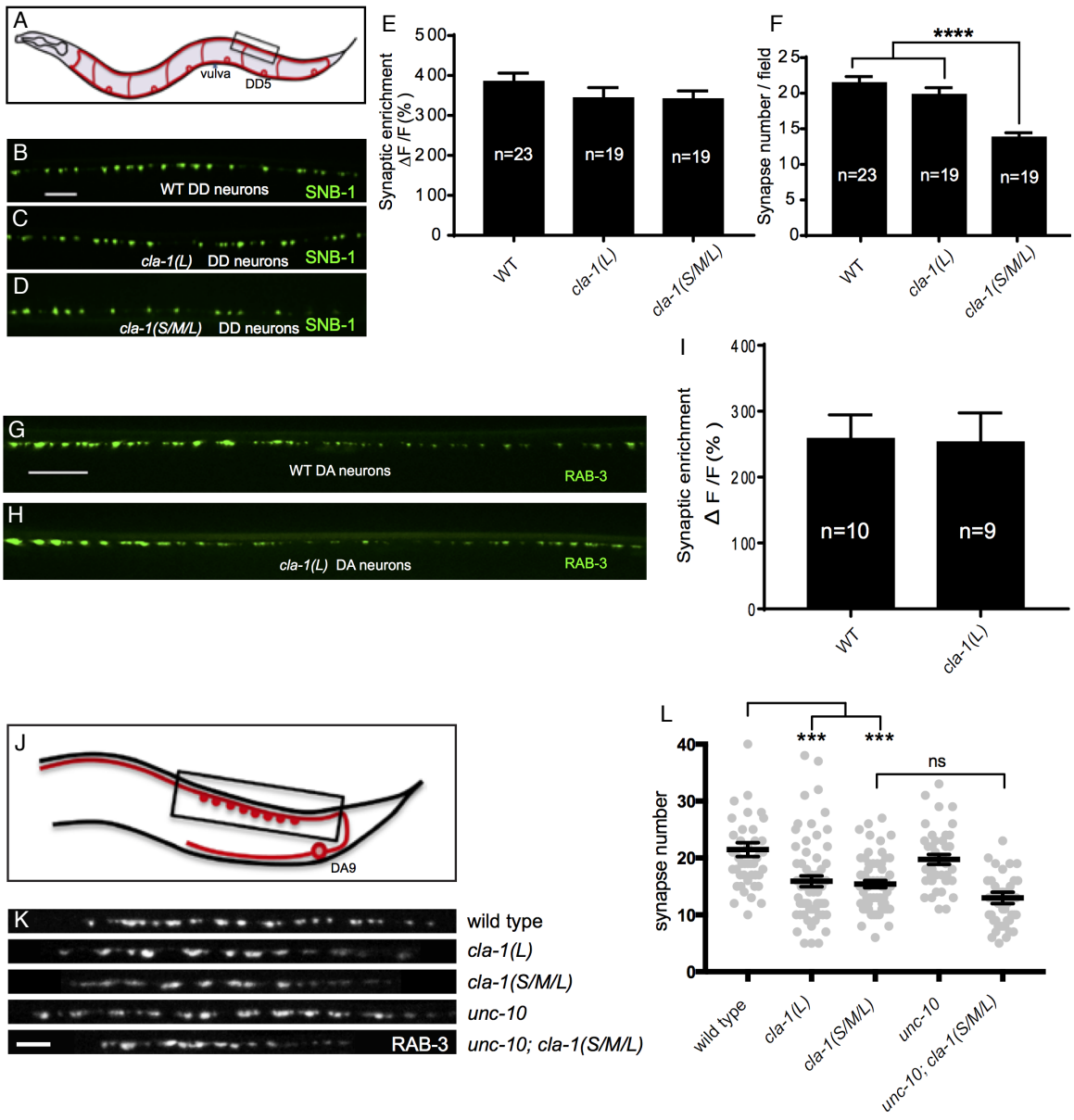

Figure II.10. CLA-1 influences synapse number, but not enrichment at motor neurons. A. Schematic diagram of DD motor neurons. Synaptic vesicle clustering in DD neurons was assessed by examining the localization of SNB-1::GFP in the boxed area. **B-D**. SNB-1::GFP forms discrete presynaptic clusters in DD axons of *cla-1(L)* or *cla-1(S/M/L)* mutants (C-D), similar to the wild-type animals (WT; B). Scale bar = 10µm. **E.** Synaptic enrichment (ΔF/F) of SNB-1::GFP in the DD axons for wild-type (WT) animals and *cla-1(L)* or *cla-1(S/M/L)* mutants . **F.** SNB-1::GFP puncta number in DD axons of *cla-1(S/M/L)* and *cla-1(L)* mutants, compared to wild-type (WT) animals. **G-H.** RAB-3::GFP in DA motor neurons of WT (G) or *cla-1(L)* (H) animals was indistinguishable. Scale bar = 10µm. **I.** Synaptic enrichment (ΔF/F) of RAB-3::GFP in the cholinergic DA motor neurons for wild-type (WT) animals and *cla-1(L)* mutants. All images were taken of the dorsal nerve cord posterior to the vulva. **J.** Schematic of the DA9 cholinergic motor neuron. Synapses (boxed region) labeled by GFP::RAB-3 were examined. **K.** Straightened synaptic domain (boxed

region in J) showing the localization of GFP::RAB-3 in wild-type animals and various mutants. Scale bar = 5µm. **L.** Synapse number was reduced in *cla-1(S/M/L)* as well as *cla-1(L)* mutants compared to wild-type animals (although with greater variability in *cla-1(L)* mutants), but was not significantly different between *cla-1(S/M/L)* single mutants and *cla-1(S/M/L);unc-10* double mutants. Data collected by Zhao Xuan (A-I) and Peri Kurshan (J-L).

5. CLA-1 isoforms localize to distinct areas of synapses

If CLA-1 isoforms do in fact regulate diverse aspects of synapse and SV development, it is possible that they also localize to different regions within the synapse. As discussed above, we observed the endogenous N-terminally tagged CLA-1(L) colocalized tightly with RAB-3::GFP in NSM (Figure 2.6D-F). Next, we examined CLA-1(S) localization by fusing GFP to either the N- or C-terminal end of CLA-1(S) and co-expressing each marker with DA9::RAB-3 (Figure 2.11A and data not shown). Like CLA-1(L), both N- and C- terminally tagged CLA-1(S) localized to the ventral tip of the presynaptic bouton where active zone proteins are known to exist (Stigloher et al., 2011). Indeed, CLA-1(S) colocalized with AZ proteins ELKS-1::GFP and UNC-2::GFP (Figure 2.11B,C). To probe the relationship between CLA-1(S) and CLA-1(L) positioning, we coexpressed a fluorescent N-terminally tagged CLA-1(S) in DA9 with the endogenous N-terminally tagged CLA-1(L) marker (Figure 2.11D). Both markers were present at the presynaptic varicosity, but CLA-1(L) appeared to fill the entire varicosity, while CLA-1(S) appeared in more discrete puncta. We wondered if this difference was due to different localization of this isoform, or if it reflected the large distance between the N- and C-terminals of CLA-1(L). To test this idea, we created an additional endogenous GFP-knock-in tag to the C-terminus of all *cla-1* isoforms. This marker was expressed in a punctate distribution in DA9 and colocalized precisely with the CLA-1(S) tag (Figure 2.11E). These results suggest that while both CLA-1(L) and CLA-1(S) are anchored at the

active zone by their similar C-terminal domains, CLA-1(L)'s N-terminal tag can extend into the remaining synaptic region occupied by SVs.

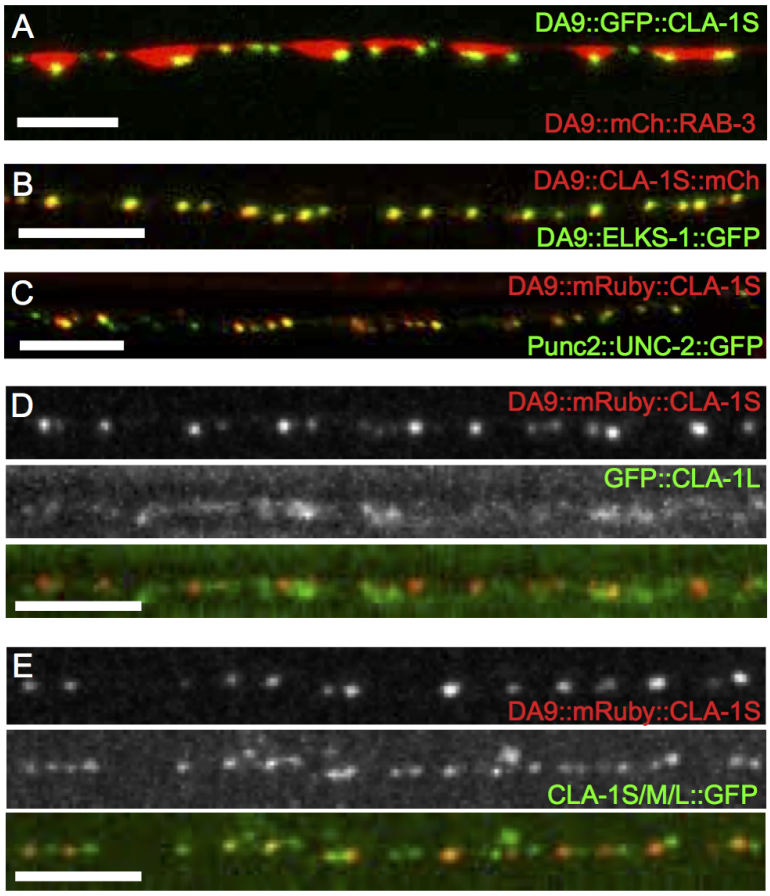

Figure II.11. Subcellular localization of CLA-1 proteins. A-C. CLA-1(S) localizes to the active zone. GFP::CLA-1(S) and mCherry::RAB-3 expressed in DA9 (A) show overlapping expression patterns, with CLA-1(S) fluorescence limited to a subregion of the RAB-3 domain. **B/C.** mRuby::CLA-1(S) expressed in DA9 colocalizes well with ELKS-1::GFP (B) and the N-type calcium channel UNC-2::GFP (C). Scale bars = 5µm. **D**. mRuby3::CLA-1(S) expressed in DA9 along with endogenous expression of N-terminally tagged GFP::CLA-1(L). Scale bar = 5µm. **E**. mRuby3::CLA-1(S) expressed in DA9 along with endogenous expression of C-terminally tagged CLA-1(S)/M/L::GFP. Note that the CLA-1/S/M/L::GFP puncta that do not colocalize with mRuby::CLA-1S are contained in neurons besides DA9. Each mRuBy::CLA-1S puncta colocalizes with a CLA-1S/M/L/::GFP puncta. Scale bar = 5µm. Data collected by Peri Kurshan.

6. cla-1 mutants exhibit ultrastructural defects in dense projection morphology and vesicle localization

Since *cla-1* appears to influence synapse organization at the light level and localizes to the AZ, we next looked at the EM level to see if there were ultrastructural correlates in the *cla-1(S/M/L)* mutant. We collected an average of 148 40-nm serial sections from three worms each of both wild type and *cla-1(S/M/L)* genotypes. We reconstructed these sections and analyzed 19 synapses from wild-type and 12 cholinergic motor neuron synapses from *cla-1(S/M/L)* dorsal cord (Figure 2.12A, Figure 2.14). *cla-1(S/M/L)* synapses exhibited smaller terminal area size (Figure 2.12B) and shorter dense projection lengths than wild-type, although the area of the dense projection in cross section was normal (Figure 2.12C,D). This finding is consistent with our previous data that showed CLA-1(S) is present at the active zone (Figure 2.11). The reduction in dense projection size suggests that CLA-1 may, in fact, be a component of the DP, or influence the localization of other dense projection components. The reduction in dense projection length remained significant when normalized to terminal area (data not shown). The average number of SVs present at *cla-1(S/M/L)* mutant synapses was reduced, but when normalized to terminal size, there was no significant change (Figure 2.12E,F).

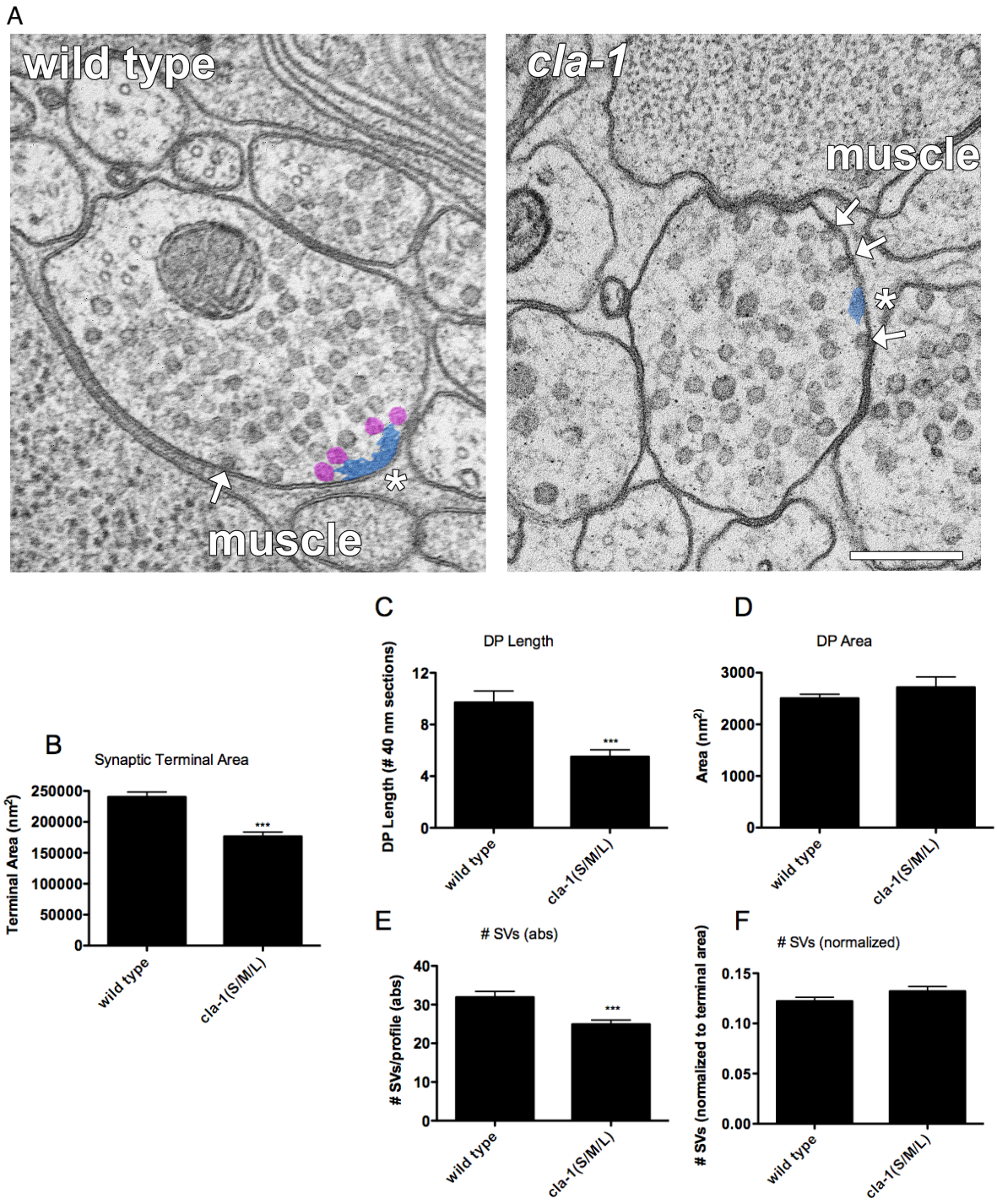

Figure II.12. Ultrastrucutral analysis of *cla-1(S/M/L).* A. Representative micrographs of wild type and *cla-1(S/M/L)* mutant synaptic profiles. Arrows indicate docked vesicles; asterisks indicate the dense projection (DP), which is also colored blue; undocked vesicles touching the dense projection are colored pink. Scale bar = 200nm. B. Synaptic terminal area (measured in nm^2) is reduced in *cla-1(S/M/L)* mutants. C. The length of the dense projection, measured in the number

of profiles in which it is observed, is decreased in *cla-1(S/M/L)* mutants. **D.** The area of the dense projection, measured in cross section, is not changed in *cla-1(S/M/L).* **E.** Total number of synaptic vesicles is reduced in *cla-1(S/M/L)* mutants. **F.** Number of synaptic vesicles normalized to terminal area is unchanged in *cla-1(S/M/L)* mutants (***p<.0001). N = 19 for wild type, 12 for *cla-1(S/M/L).* Data collected by Laura Manning.

If *cla-1* is normally involved in clustering SVs, we might expect to see SVs distributed further from the DP. We measured the distance between every SV (docked or undocked) to the DP and plotted their distribution (Figure 2.13A). The average distance to DP was left-shifted in *cla-1* mutants, indicating that SVs were located closer to the DP. We interpret this result as a consequence of smaller synapses, as evidenced by smaller terminal area and DP, and fewer SVs in *cla-1* synapses. We also observed localization defects in synaptic DCVs. When measured as a total or normalized value, the number of DCVs present in synaptic profiles was dramatically reduced in *cla-1(S/M/L)* mutants (Figure 2.13B,C). While DCVs are typically not clustered near the AZ, they were even further excluded from this region in *cla-1* mutant synapses (Figure 2.13D). These results highlight CLA-1's role in clustering both SVs and DCVs at the active zone, and potentially uncover a role in regulating synapse size.

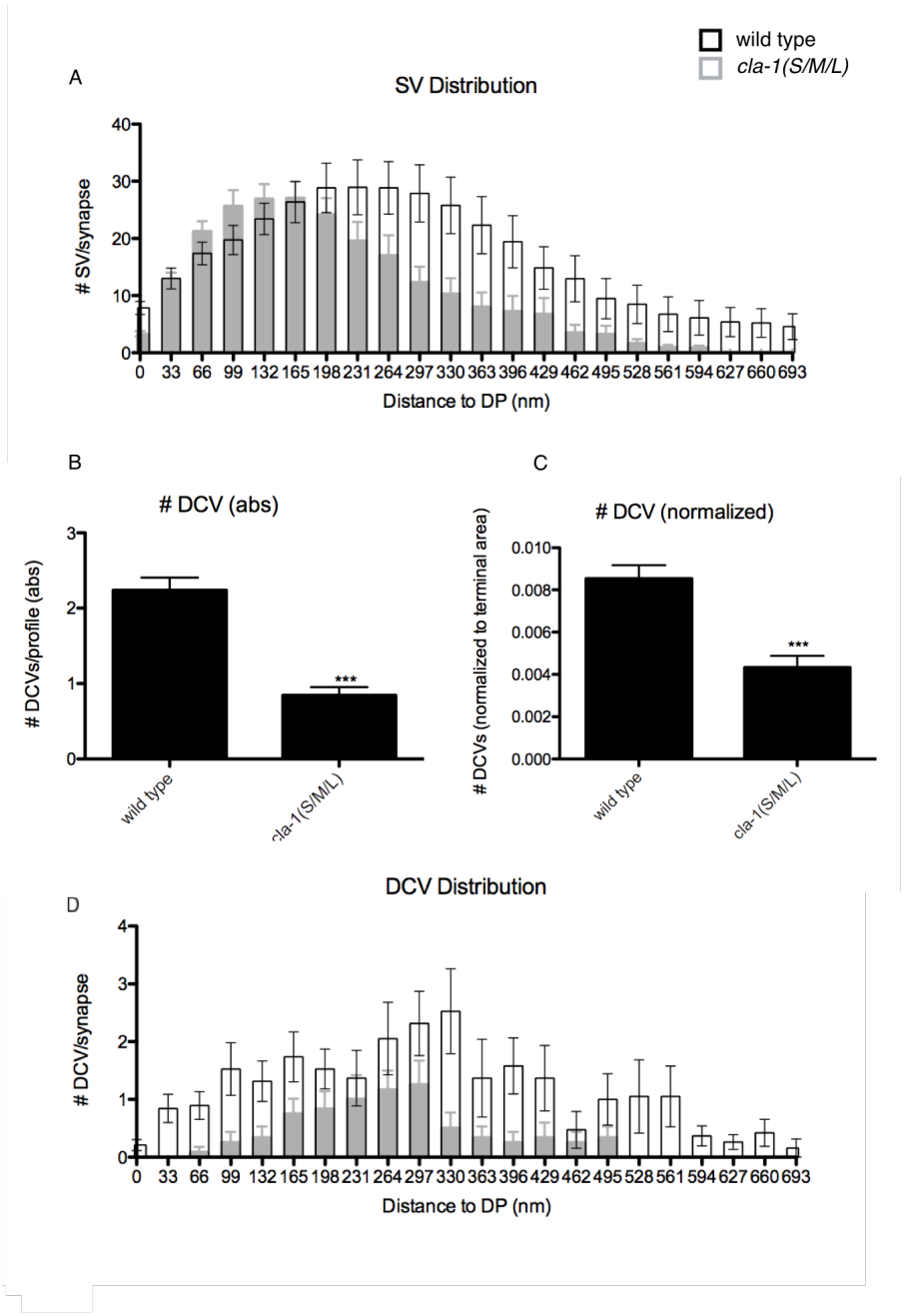

Figure II.13. Vesicle distribution in cla-1(S/M/L) synapses. A. The distance from each synaptic vesicle (docked or undocked) to the dense projection, per profile, was measured and plotted in a frequency distribution. cla-1(S/M/L) synapses (gray) exhibit a shift towards smaller average distances. **B.** The absolute number of dense core vesicles per profile was reduced in cla-1(S/M/L). **C.** The number of dense core vesicles normalized to terminal area was also reduced in cla-1(S/M/L). **D.** The distance from each dense core vesicle to the dense projection, per profile, was measured and plotted in a frequency distribution. cla-1(S/M/L) synapses (gray) exhibit a reduction in DCVs throughout this distribution. (***p<.0001). N = 19 for wild type, 12 for *cla-1(S/M/L).* Data collected by Laura Manning.

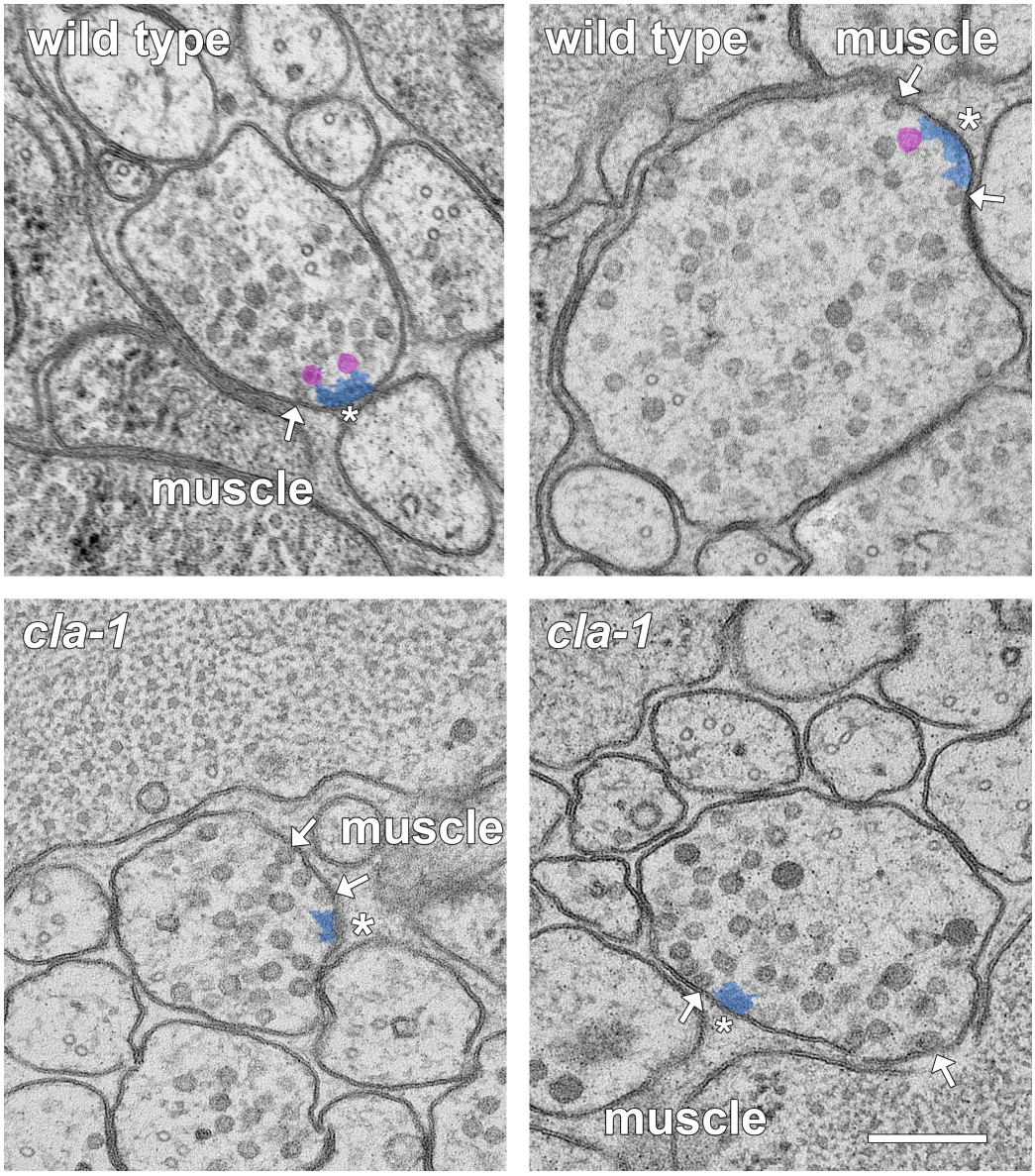

Figure II.14. Images of wild type and *cla-1* mutant synapses. Additional representative EM images of wild type and *cla-1(S/M/L)* mutant synaptic terminals. Arrows indicate docked vesicles; asterisks indicate the dense projection (DP), which is also colored blue; undocked vesicles touching the dense projection are colored pink. Scale bar = 200nm. Data collected by Laura Manning.

While we observed no change in the total or normalized number of docked SVs (Figure 2.15A,B), *cla-1(S/M/L)* mutant synapses showed an altered docked SV distribution (Figure 2.15C). Specifically, within 100 nm of the DP, an area that is crucial for synchronous release, docked SVs were more prevalent in *cla-1(S/M/L)* mutants than in wild type (Figure 2.15C) (Gracheva et al., 2008; Kittelmann et al., 2013).

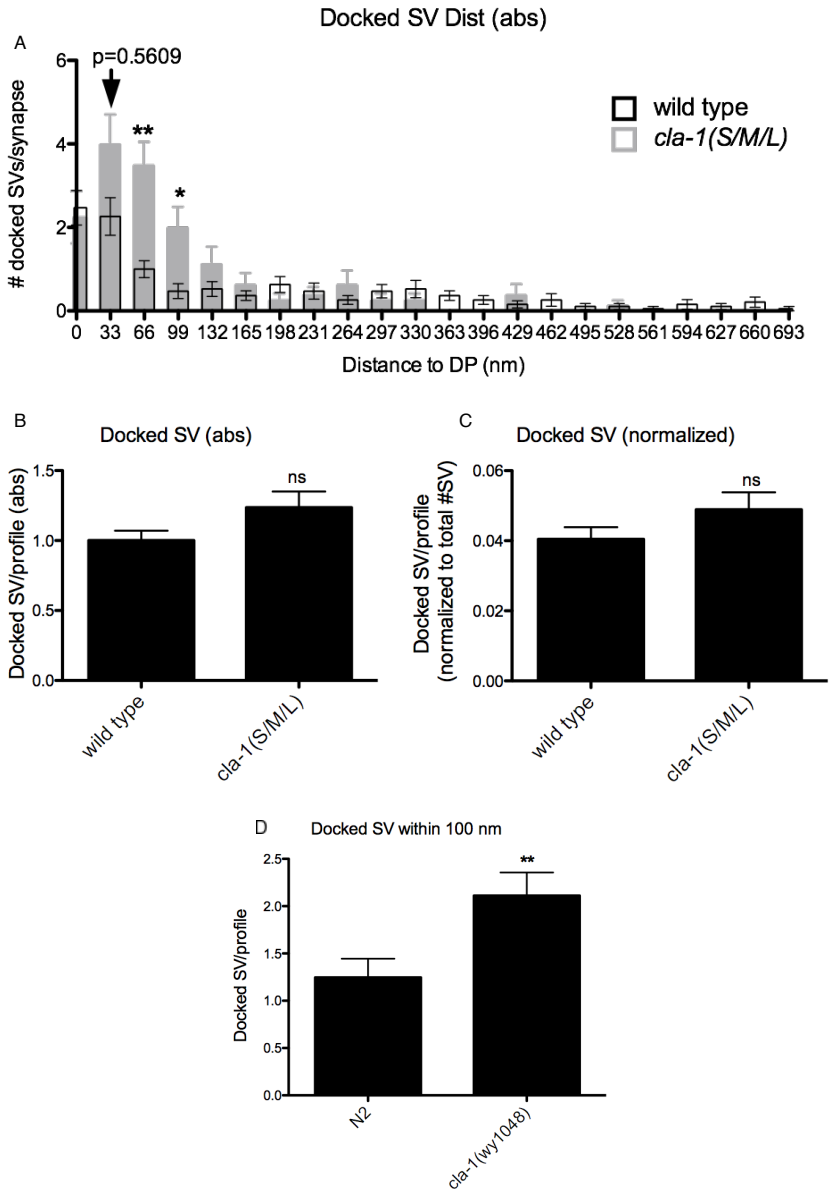

Figure II.15. Ultrastructural analysis reveals a change in synaptic vesicle docking at the active zone. A/D. The distance from each docked vesicle to the dense projection, per profile, was measured and plotted in a frequency distribution. cla-1(S/M/L) synapses (gray) have increased docking within 100 nm of the dense projection. **B/C**. The total number of docked synaptic vesicles per profile (B) and normalized to total number of synaptic vesicles in the profile (**p<0.01, ns = not significant. N = 19 for wild type, 12 for *cla-1(S/M/L).* Data collected by Laura Manning.

Due to this localized increase in docked SV, we found that the total number of docked SVs contacting the DP was similar to wild type (Figure 2.16A, B). However, we observed a dramatic reduction in the number of undocked vesicles contacting the DP (Figure 2.12, Figure 2.14 pink vesicles, Figure 2.16C,D). This result suggests that CLA-1 contributes to SV recruitment from the broader SV pool to the active zone.

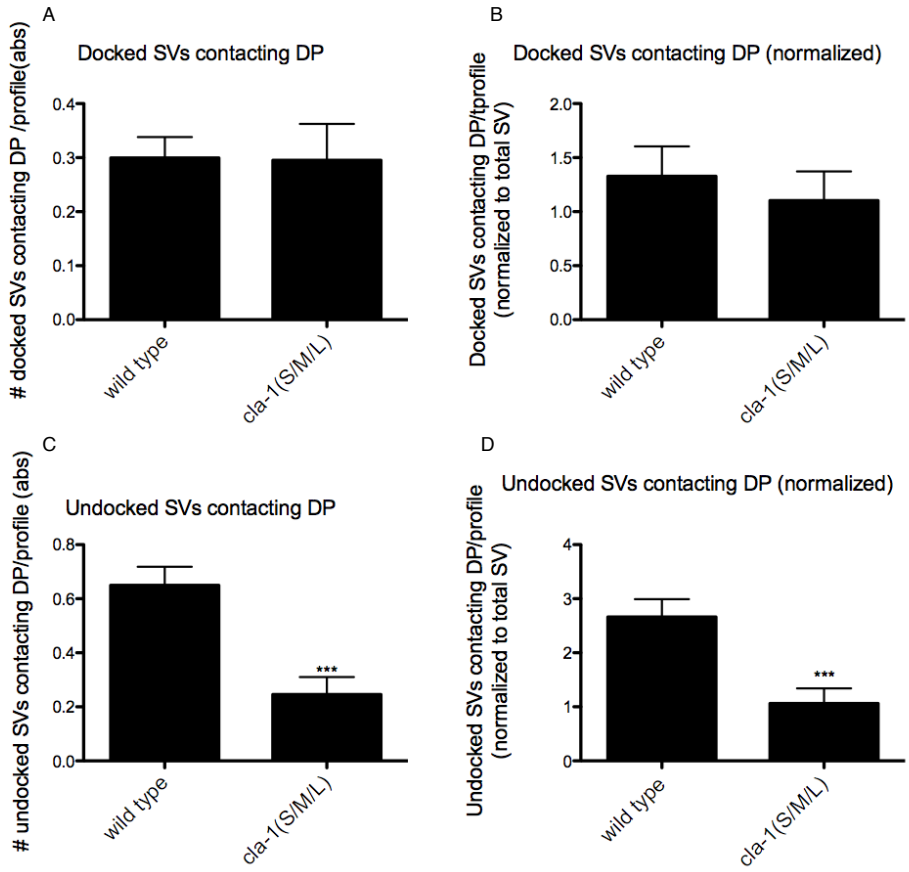

Figure II.16. Undocked vesicles contacting the dense projection are reduced in cla-1(S/M/L) synapses. A/B. The number of docked synaptic vesicles contacting the dense projection per profile, measured as an absolute value (A) or normalized to total synaptic vesicles in that profile (B). **C/D.** The number of undocked synaptic vesicles contacting the dense projection per profile, measured as an absolute value (C) or normalized to total synaptic vesicles in that profile (D). (***p<.0001). N = 19 for wild type, 12 for *cla-1(S/M/L.* Data collected by Laura Manning.

7. cla-1 mutants display neurotransmitter release defects

Based on these structural defects, it is reasonable to think that *cla-1* mutant animals would also exhibit synaptic dysfunction (Zhen and Jin, 1999; Hallam et al., 2002). One test of neurotransmitter release capability is through the acetylcholinesterase inhibitor aldicarb, which exacerbates the effects of ACh released at the NMJ by prolonging signaling (Mahoney et al., 2006). Animals that release less ACh from cholinergic motor neurons show resistance to aldicarb. We observed aldicarb resistance in both *cla-1(L)* and *cla-1(S/M/L)* mutant animals, indicating SV release defects in these animals (Figure 2.17). Interestingly, *cla-1(S/M/L)* animals displayed a more pronounced resistance than *cla-1(L)* alone, indicating that CLA-1(L) may be required for SV release, while the shorter isoforms, or its C-terminus, may be important for other aspects of release.

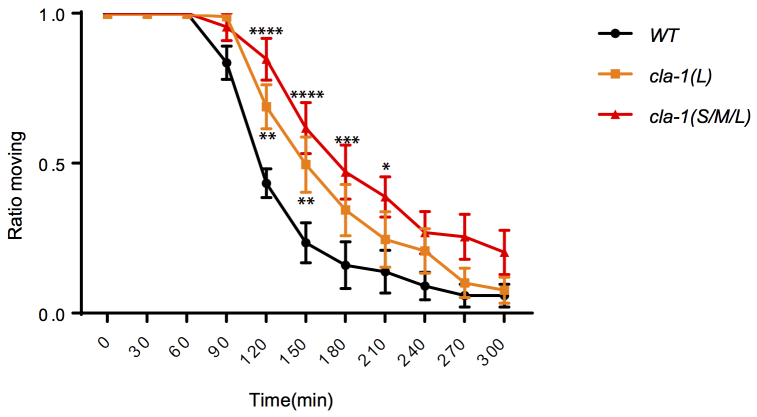

Figure II.17. *cla-1* mutant animals show defects in synaptic transmission. Quantification of the ratio of moving worms from each genotype on 1 mM aldicarb at the indicated exposure time reveals aldicarb resistance in both *cla-1(S/M/L)* and *cla-1(L)* mutants. Data are from five separate blinded experiments with ~25 animals per experiment (see Materials and Methods). Data collected by Zhao Xuang.

To further probe the functional role of CLA-1 isoforms, we recorded postsynaptic currents in voltage-clamped body wall muscles. In *cla-1(S/M/L)* animals, spontaneous postsynaptic "mini" current frequency was reduced by 46% compared to wild-type, though no significant change was observed in *cla-1(L)* (Figure 2.18A,C). This dramatic reduction indicates an important role for CLA-1 in SV release. This change could also be at least partly accounted for by the reduction in synapse number in *cla-1(S/M/L)* animals that is not present in *cla-1(L)* animals (Figure 2.10L). We observed no changes in mini amplitude in *cla-1* mutants, suggesting normal postsynaptic receptor function (Figure 2.18D). A single evoked stimulation elicited normal responses in each of the mutant strains, but a 20Hz stimulation train revealed defects in both *cla-1(L)* and *cla-1(S/M/L)* responses (Figure 2.18B,E). This latter finding was consistent with the aldicarb data. This form of depression represents a reduction in the number of vesicles in the readily releasable pool (Kaeser and Regehr, 2014) and may be due to the reduction in SVs contacting the DP. Interestingly, both alleles show an equally reduced response. Since the commonality between these strain is the missing long isoform, it may be that CLA-1(L) specifically recruits SV during repetitive stimulation.

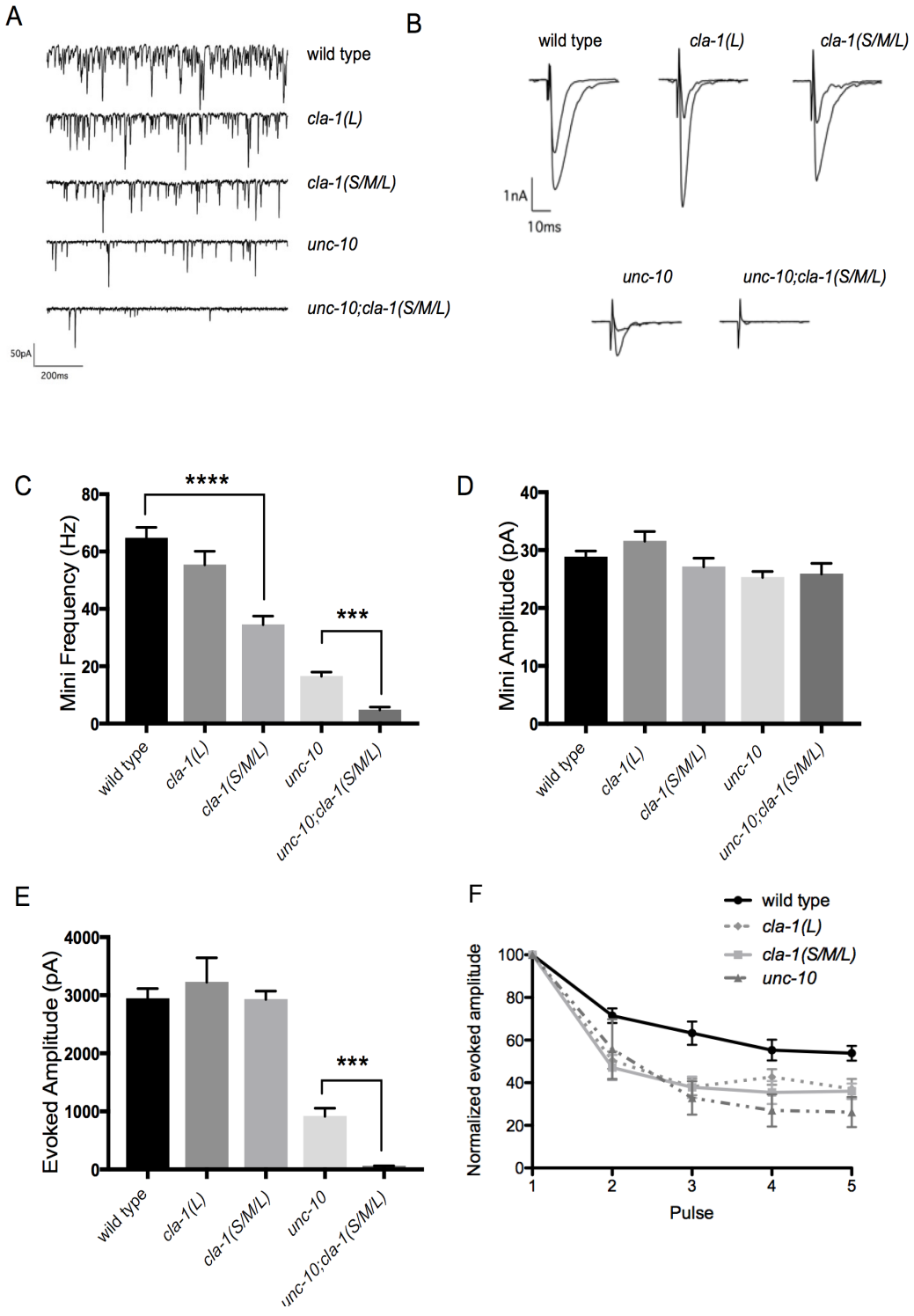

Figure II.18. *cla-1* mutant animals show defects in synaptic transmission. A. Representative traces of spontaneous post-synaptic currents. B. Representative traces of evoked EPSCs, including the first and last trace from a five-stimulus train given at 20 Hz. C. Frequency of spontaneous miniature postsynaptic currents is reduced in *cla-1(S/M/L)* but not *cla-1(L)* mutants, compared to wild type. It is also further reduced in *cla-1(S/M/L);unc-10* double mutants

compared to *unc-10* single mutants. **D**. Amplitude of spontaneous miniature postsynaptic currents is unchanged in *cla-1* mutants. **E**. The amplitude of electrode-evoked responses to a single stimulus is unchanged in *cla-1* mutants compared to wild type, but is dramatically reduced in *cla-1(S/M/L);unc-10* double mutants compared to *unc-10* single mutants. **F**. Normalized amplitude of currents evoked by repeated electrode stimulation (interpulse interval = 50 msec) reveals increased depression in *cla-1(S/M/L)*, *cla-1(L),* and *unc-10* mutants. Data collected by Janet Richmond.

If CLA-1 normally regulates synapse number and recruits SVs to the RRP, why does *cla-1(S/M/L)* exhibit normal evoked release in response to a single stimulus? To answer this question, we relied on our observations of increased docked SVs in the 100 nm near the DP. The AZ protein UNC-10/RIM is known to localize and dock SVs in this location, and to be important for SV release (Gracheva et al., 2008; Weimer et al., 2006; Stigloher et al., 2011). We examined double mutants for *cla-1(S/M/L)* and *unc-10* to see if *unc-10* was compensating for the loss of *cla-1*. Indeed, we saw that double mutants had a dramatically reduced response to a single evoked stimulus than either single mutant alone (Figure 2.18E). Spontaneous release was also reduced in an additive fashion in *cla-1;unc-10* double mutants. Because the evoked release from a single stimulus was so small in these animals, we could not observe synaptic depression from train stimulation. However, we did note that *unc-10* mutants exhibited depression at similar levels as both *cla-1* mutants (Figure 12.8F).

Together, these results indicate that *cla-1* and *unc-10* perform distinct and additive roles in SV release. The fact that *cla-1;unc-10* double mutants exhibit a reduction in synapse number that was similar to *cla-1(S/M/L)* single mutants suggests that CLA-1 specifically regulates synapse number (Figure 2.10L). Yet both *unc*-10 and *cla-1* mutants showed similar levels of depression in response to a stimulus train. This result suggests that *cla-1* and *unc-10* each contribute to release sustainability. This finding is consistent with a similar reduction in undocked vesicles contacting

the DP observed in both *cla-1* (Figure 2.16C, D) and in *unc-10* mutants (Stigloher et al., 2011), suggesting that vesicle tethering to the DP could be important for recruitment to the primed pool during train stimulation. The additivity of the release defects observed in *cla-1;unc-10* mutants may indicate that UNC-10 can compensate for loss of *cla-1*, or, alternatively, that both proteins function together to regulate release.

8. CLA-1 localization requires unc-104/kinesin-3, syd-2/liprin-α, and syd-1

Synaptic proteins interact hierarchically to build the active zone during development (Van Vactor and Sigrist, 2017). While the scaffold molecule SYD-2/Liprin-α and rhoGAP SYD-1/mSYD1A are thought to be among the first proteins to reach a new synapse, many questions remain about active zone protein trafficking and localization (Fouquet et al., 2009; Patel et al., 2006; Patel and Shen, 2009). To test the mechanisms for CLA-1 localization to the synapse, we measured CLA-1(S)::GFP in the single cholinergic motor neuron DA9, in a variety of mutant backgrounds. In a mutant for the synaptic vesicle motor *unc-104/kinesin-3*, SVs are not transported to synapses, as confirmed by the loss of RAB-3::GFP in DA9 synapses (Edwards et al., 2015b) (Figure 2.19A,B). In *unc-104* mutants, we also observed a drastic reduction of CLA-1(S)::GFP signal, although it was not completely eliminated (Figure 2.19A,C). CLA-1(S) was almost completely absent from synapses in a *syd-2/liprin-α* mutant background, and was also greatly reduced in *syd-1/mSYD1A* mutant animals (Figure 2.19A,C). We therefore conclude that CLA-1(S) relies on each of these three proteins to arrive at the synapse. While RAB-3 puncta were severely reduced in a *syd-2* mutant background, they were not further reduced in a *syd-2;cla-1* double mutant, suggesting that SYD-2 operates upstream of CLA-1 (Figure 2.18B,D). We also tested

mutants for *elks-1*, *unc-10/RIM*, *rimb-1/RIM-BP*, and triple mutants for these three (data not shown) and found CLA-1(S) localization intact, suggesting that CLA-1(S) does not require these proteins for proper trafficking.

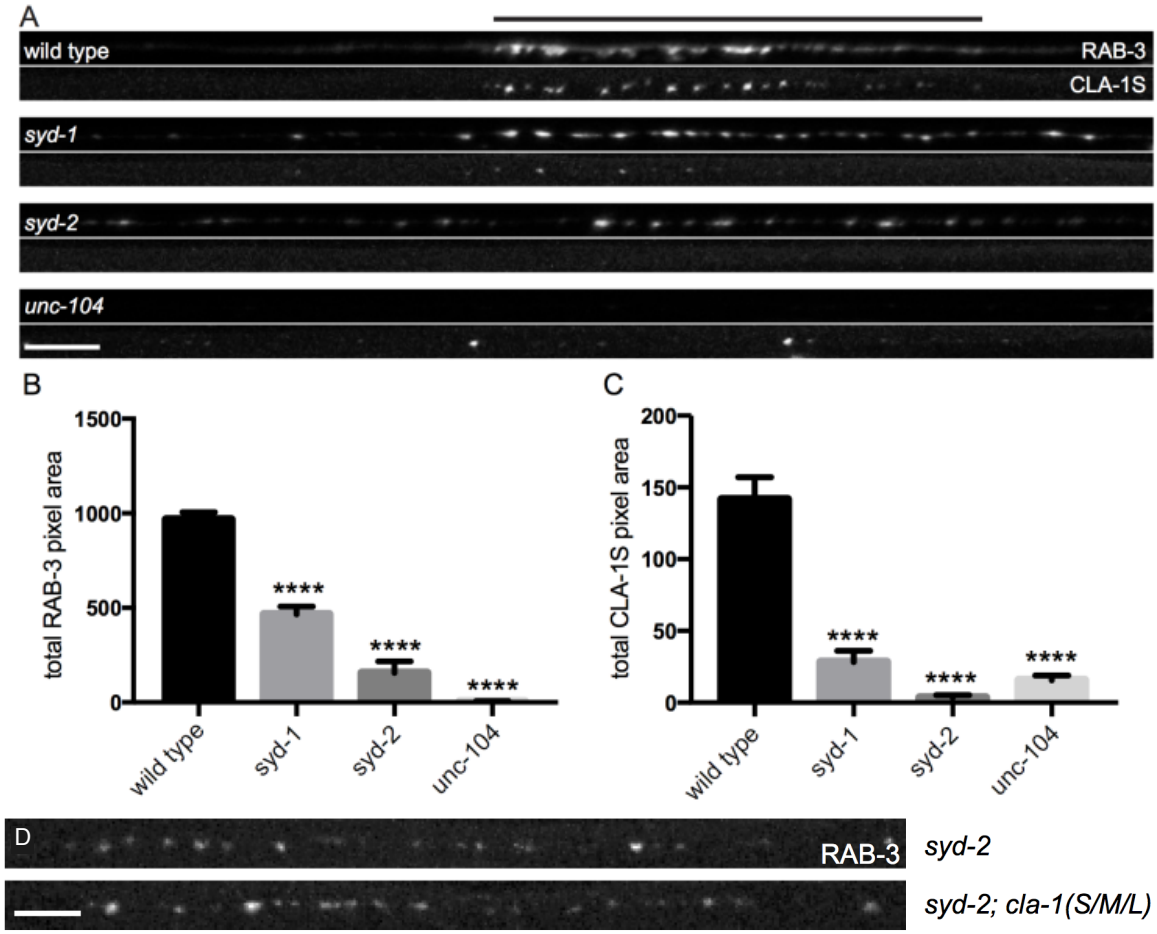

Figure II.19 CLA-1(S) synaptic localization is regulated by UNC-104/Kinesin-3, SYD-2/liprin-α, and SYD-1. A. CLA-1(S)::GFP and mCherry::RAB-3 expression in the DA9 motor neuron of the indicated genotypes. *syd-1* and *syd-2/liprin-α* mutants exhibit smaller synaptic vesicle clusters that are distributed throughout the axon, and greatly reduced (*syd-1*) or absent (*syd-2*) CLA-1(S) puncta. No synaptic vesicles are detected in *unc-104* mutant axons, while the number of CLA-1(S) puncta is greatly diminished. Scale bar = 5 µm. Line above images indicated wild type synaptic domain. **B.** Average total pixel area of mCherry::RAB-3 for wild-type animals and various mutants. **C.** Average total pixel area of CLA-1(S)::GFP for wild-type animals and various mutants. **D.** Synapse assembly as assessed by GFP::RAB-3 puncta distribution and intensity is unchanged between *syd-2* single mutants and *syd-2;cla-1(S/M/L)* double mutants (not quantified). Data collected by Peri Kurshan.

We used a similar method to examine endogenous CLA-1(L) localization at the synapse. Because our GFP::CLA-1(L) strain is an endogenous tag that is expressed in many cells, we could not obtain single-cell resolution. However, we found that CLA-1(L) fluorescence was greatly reduced in the nerve ring of *unc-104/kinesin-3*, *syd-2/liprin-α*, and *syd-1* mutant animals (Figure 2.20B-E). Collectively, these results demonstrate that all isoforms of CLA-1 require UNC-104/KINESIN-3, SYD-2/LIPRIN-α, and SYD-1 but not other active zone proteins such as ELKS-1 and UNC-10/RIM, to traffic to the synapse.

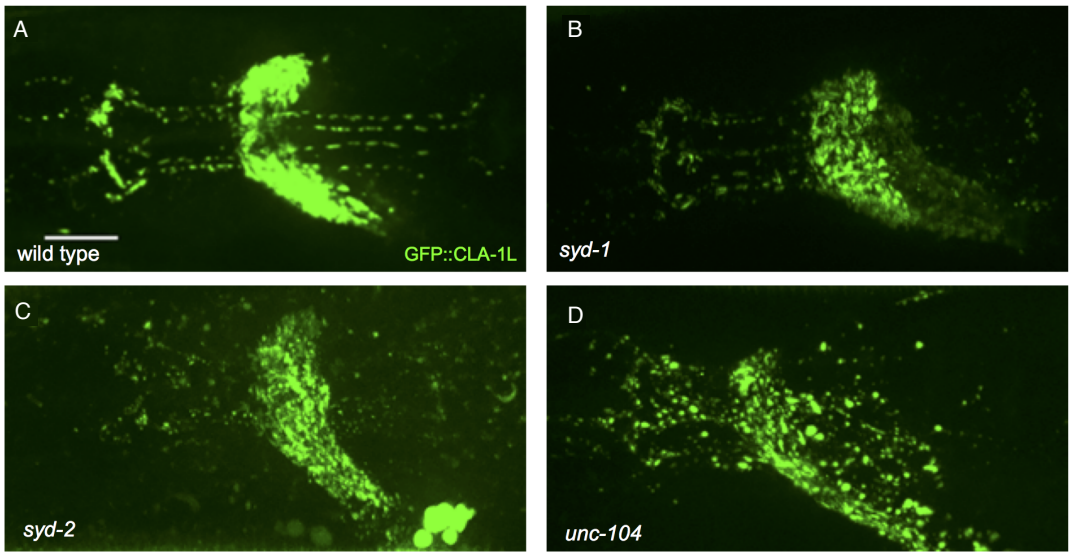

Figure II.20 CLA-1(L) synaptic localization is regulated by UNC-104/Kinesin-3, SYD-2/liprin-α and SYD-1. A-D. The pattern of GFP::CLA-1(L) fluorescence appears perturbed in syd-1 (B), syd-2 (C) and unc-104 (D) mutants compared to wild-type (WT, A) animals. Scale bar = 10. Data collected by Zhao Xuan.

Considering the dramatic shortening of dense projections in *cla-1* mutants, we wondered if *cla-1* impacted localization of any other AZ proteins. We examined endogenously tagged SYD-2::GFP in the *cla-1(S/M/L)* mutant and found that SYD-2 puncta and average fluorescence along the dorsal cord were both dimmer (Figure 2.21).

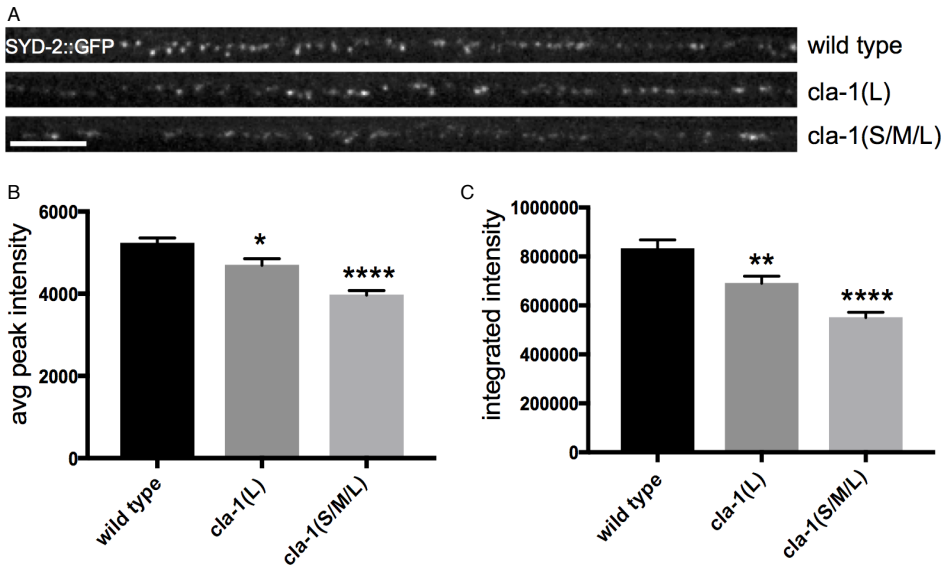

Figure II.21 Endogenous SYD-2 is reduced at cla-1(S/M/L) synapses. A. Endogenous SYD-2::GFP expression in motor neurons of the posterior dorsal nerve cord is reduced in cla-1 mutants. **B.** Average SYD-2::GFP puncta intensity is reduced in cla-1 mutants. **C.** SYD-2::GFP total (integrated) intensity per unit length is reduced in cla-1 mutants. Data collected by Peri Kurshan.

We also imaged tagged SYD-2 and SYD-1 in the single NSM neuron, and found that SYD-2::GFP fluorescence was more diffuse in *cla-1(S/M/L)*, but not in *cla-1(L)* alone. SYD-1::GFP fluorescence was unchanged in both mutants **(Figure 2.21)**. These results suggest that *cla-1* promotes SYD-2 recruitment to active zones.

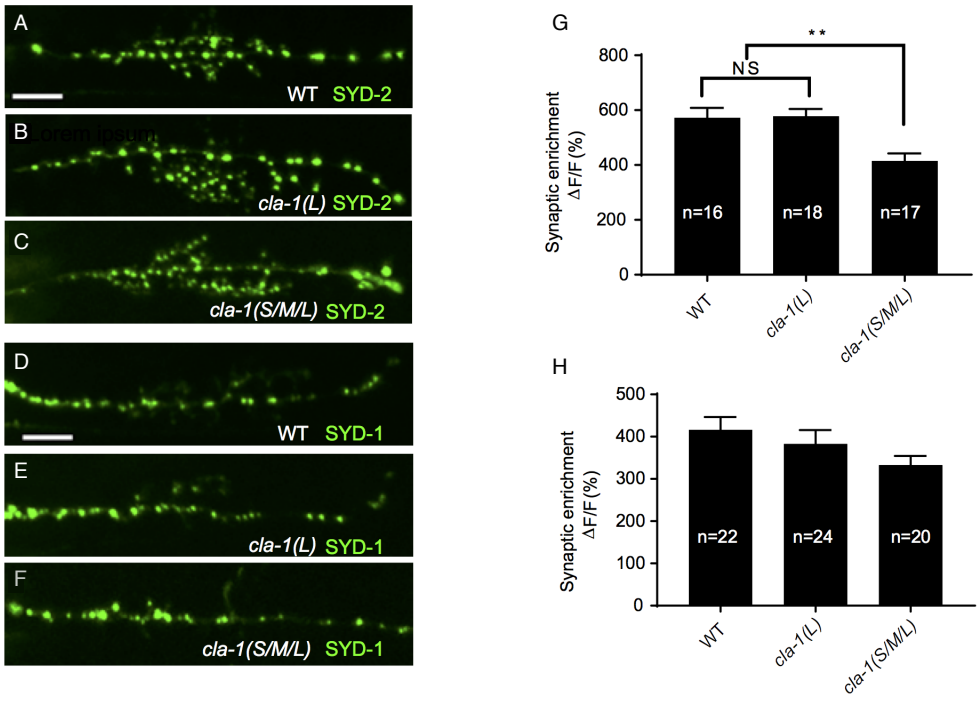

Figure II.22 CLA-1 promotes synaptic of enrichment of SYD-2, but not SYD-1, in NSM. A-C. Active zone marker SYD-2::GFP in the NSM ventral neurite in wild type (A), cla-1(L) (B) and cla-1(S/ML) (C). **G.** Synaptic enrichment (ΔF/F) of SYD-2::GFP in NSM is reduced in cla-1(S/M/L) but not cla-1(L) mutants compared to wild type. **D-F.** Active zone marker SYD-1::GFP in the NSM ventral neurite in wild type (H), cla-1(L) and cla-1(S/ML) **H.** Synaptic enrichment (ΔF/F) of SYD-1::GFP in NSM is not significantly reduced in cla-1 mutants compared to wild type. Data collected by Zhao Xuan.

C. Discussion

In this study, we identify the novel protein Clarinet (CLA-1) in *C. elegans*, comprised of short, medium, and long isoforms. CLA-1 localizes to the AZ where it can influence SV and DCV clustering, synapse number, synaptic ultrastructure and release properties.

CLA-1 isoforms regulate distinct aspects of synapse development and function

To better understand *cla-1* and its different isoforms, we examined two mutant alleles of *cla-1*. *cla-1(L)* deletes the start of the long isoform and does not affect the M/S isoforms. *cla-*

1(S/M/L) deletes the C-terminus present in all isoforms, resulting in complete deletion of *cla-1(S)*. By comparing the phenotypes in these two mutants, we were able to distinguish which were linked to the N-terminal region of the long isoform versus those linked to the C-terminal regions present in the M/S isoforms. We found that *cla-1(S/M/L)* contained fewer synapses in motor neurons and showed reduced spontaneous release. This effect was not present in *cla-1(L),* suggesting that the M/S isoforms, or their shared C-terminal domains, regulate synapse number and SV release in these neurons. All *cla-1* isoforms were required for synaptic vesicle enrichment in sensory neurons, but not motor neurons. Only the long isoform was required for proper synapse number in motor neurons. Both mutant alleles showed aldicarb resistance, with a more severe phenotype in *cla-1(S/M/L)*, as well as reduced responses to repetitive evoked stimuli.

CLA-1 isoforms localize to the active zone

While each CLA-1 isoform colocalized well with RAB-3-labeled synaptic vesicles in the whole animal, we observed an important difference in subcellular localization between CLA-1(S) and CLA-1(L). CLA-1(S) appeared as discrete puncta within the cloud of RAB-3-labeled SVs in DA9 synapses, whether it was N- or C-terminally tagged. CLA-1(S) also colocalized tightly with the active zone protein ELKS-1 and the VGCC UNC-2. Similarly, the endogenous C-terminally tagged CLA-1(L)::GFP colocalized with C-terminal tagged CLA1(S) in discrete puncta. However, the endogenous N-terminally tagged GFP::CLA-1(L) exhibited larger fluorescent puncta. Based on these experiments, we believe that both CLA-1(L) and CLA-1(S) anchor at the active zone through their common C-terminal domains, which are homologous with vertebrate Piccolo and RIM. We hypothesize that the ~9000 amino acids in the CLA-1(L) isoform may extend into the presynaptic

bouton. Similarly, vertebrate Piccolo is thought to be able to extend ~100 nm away from the plasma membrane (Dani et al., 2010) and its coiled-coil structures could stretch up to 750 nm (Limbach et al., 2011). Since Clarinet is nearly twice the size of Piccolo and contains more unstructured areas, it could theoretically extend quite far from the active zone. Ultimately, the results presented here underscore that while Clarinet, BRP, Fife, and Piccolo contain variable N-terminal sequences, their architecture may enable them to link the synaptic vesicle pool to the active zone in a similar manner.

CLA-1 regulates synaptic ultrastructure and function

Building upon light level experiments, we used HPF/FS EM analysis to reveal the extent to which *cla-1* influences synapse morphology. *cla-1(S/M/L)* animals contained smaller dense projections than those in wild-type synapses. This finding implies CLA-1 may be a component of the dense projection. In *C. elegans*, the dense projection is critical for organizing SVs and release machinery (Kittelmann et al., 2013; Stigloher et al., 2011), analogous to the T-bar in *Drosophila* and ribbon structures in the mammalian visual system (Fouquet et al., 2009; Ackermann et al., 2015). At the fly neuromuscular junction, dense projection size is reduced in fife mutants (Bruckner et al., 2016). Interestingly, in *C. elegans*, *syd-2/liprin-α* regulates DP size and is considered a master regulator of synapse assembly (Kittelman et al., 2013; Patel et al., 2006; Dai et al., 2006). *cla-1(S/M/L)* mutants showed reduced synaptic localization of endogenous SYD-2::GFP. It is therefore possible that the smaller dense projection length may be in part due to a reduction of both CLA-1 and SYD-2. Few active zone proteins have been reported to promote SYD-2 localization (Patel and Shen, 2009). Although CLA-1 appears to promote SYD-2 localization,

CLA-1(S) absolutely requires SYD-2 to localize at the active zone. Therefore, SYD-2 probably recruits CLA-1 to the DP. A similar kind of reciprocal relationship has been observed between SYD-1 and SYD-2 in HSN neurons (Patel et al., 2006). A mutation in either *syd-1* or *syd-2* reduced about half of the synaptic localization of the complementary protein. This study implied that SYD-1 and SYD-2 could both still localize to synapses in the absence of the other, but to a lesser extent than normal, and that SYD-1 likely functions upstream of SYD-2 (Patel et al., 2006). On the other hand, CLA-1(S) localization was eliminated in *syd-2* mutants, indicating that it cannot localize without SYD-2. Additionally, both *syd-1* and *syd-2* mutants displayed more severe defects in synapse assembly than *cla-1*. Thus, it is likely that CLA-1 functions downstream of these genes.

Along with shorter dense projection lengths, *cla-1(S/M/L)* cholinergic synapses were smaller than those of the wild type and contained fewer SVs. The reduction in SVs disappeared when the count was normalized to terminal area, suggesting that this observation is likely a reflection of smaller synapse size. The distribution of SVs (both cytosolic and docked) relative to the DP was left-shifted in *cla-1(S/M/L)* mutants, indicating that SVs in these mutant synapses were commonly found closer to the DP than in wild type. This finding was surprising, as we predicted that a loss of *cla-1* might result in more diffuse SV localization, and thus a right shifted, larger average distance to the DP. Still, fluorescently tagged SV-associated RAB-3 did not appear diffuse in cholinergic motor neurons of *cla-1(S/M/L)* mutants. The altered synapse size points to a possible role for AZ proteins in determining the size of the SV pool as well as the size of the presynaptic bouton itself. One component of the presynaptic cytoskeleton is F-actin, which has been linked to Piccolo. In Piccolo knockdown neurons, activity-dependent assembly of F-actin is reduced (Chia et al., 2013; Waites et al., 2011). Regulation of the cytoskeleton could contribute

to the size of the presynaptic bouton. Additionally, this change in synapse size may be reflective of lower levels of SYD-2 in *cla-1* mutant synapses. It is also possible that a reduction in synaptic size caused by *cla-1(S/M/L)* prevents their detection by light microscopy, resulting in a lower synapse number count. Extensive reconstruction of motor neuron axons at the EM level is required to support this theory.

While the total number of docked SVs was unchanged in *cla-1(S/M/L)* mutant synapses, their distribution relative to the DP was altered. Docked SVs accumulated at higher levels within 100 nm of the DP. This area likely contains preferential release sites, as UNC-10 localizes here and enhances docking and evoked release (Weimer et al., 2006; Gracheva et al., 2008; Stigloher et al., 2011). Unlike *unc-10* mutants, which show fewer docked SVs physically contacting the DP, *cla-1(S/M/L)* mutants exhibited wild type levels of this class of SVs. However, the number of undocked vesicles contacting the DP was dramatically reduced. These findings suggest that *cla-1* may help recruit SVs to the active zone, possibly by physically linking them to the DP. In mammalian synapses, Piccolo recruits SVs from the reserve pool via Synapsin (Leal-Ortiz et al., 2008; Waites et al., 2011) and maintains SV clusters at the AZ (Mukherjee et al., 2010).

This ultrastructural analysis of *cla*-1 synapses has been essential to understanding the functional phenotypes we observed. *cla-1(S/M/L)* mutant synapses produced a normal response to a single evoked stimulus, which is supported by our findings that there are normal numbers of total and docked SVs at these synapses. Still, these mutants are unable to sustain release upon repeated stimulation. Furthermore, the rate of spontaneous release is reduced in *cla-1(S/M/L)* mutants, which also show increased resistance to aldicarb. These defects may arise in part from a reduction in SV recruitment to the AZ, as evidenced by fewer undocked SVs contacting the DP.

The number of docked SVs contacting the DP was unaffected in *cla-1(S/M/L)*, which may result from an accumulation of docked SVs within 100 nm of the DP. Because this is an area of the AZ that is known to localize UNC-10, which is required to dock vesicles close the active zone, we constructed *cla-1;unc-10* double mutants and found that they had an additive detrimental effect on both spontaneous and evoked release. Based on these results, it is possible that UNC-10 compensates for the loss of CLA-1, upregulating docking near the DP and facilitating normal release in its absence. Alternatively, docked vesicles may accumulate in this region due to a *cla*-1-dependent release defect. Evidence from *Drosophila* fife and vertebrate RIM mutants have shown a role for these proteins in calcium channel localization. In *Drosophila* fife mutants, the VGCC cacophony is mildly reduced at synapses, and mini release is more sensitive to the Ca^{2+} chelator EGTA, indicating an impairment in coupling of Ca^{2+} channels to SVs. Similar effects have been shown in vertebrate RIM, which can directly interact with VGCCs through its PDZ domain (Kaeser et al., 2011, Han et al., 2011). It is thus possible that *C. elegans* CLA-1 partially redundantly regulates Ca^{2+} channel localization with UNC-10/RIM which would explain the enhanced defects in release in the double mutants.

Our results also indicate the *cla-1* may promote DCV localization at synapses. DCVs were strikingly absent from *cla-1(S/M/L)* mutant synapses, both as an absolute number and when normalized to terminal area. While DCVs normally do not cluster tightly to the AZ (Hammarlund et al., 2007), physical tethers connecting DCVs to the SV pool have been observed by ET (Stigloher et al., 2011). Additionally, SYD-2, in conjunction with other CSS system proteins, is known to promote synaptic capture of DCVs and can interact with UNC-104/KIF1A to promote anterograde vesicle transport (Edwards et al., 2015a,b; Miller et al., 2005; Wagner et al., 2009;

Chapter 3 of this thesis). It is possible that CLA-1, functioning downstream of SYD-2, may participate in capturing DCVs. Although this system also regulates SV capture, we did not observe a loss of SVs from the synapse. It is likely that additional redundant mechanisms exist to maintain the SV pool at synapses (Siksou et al., 2007; Fernandez-Busnadiego et al., 2010; Stavoe and Colon-Ramos, 2012; stavoe et al., 2012; Pechstein and Shupliakov, 2010; Cazares et al., 2016).

CLA-1 plays a role in SV clustering

Synaptic vesicles are recruited to and clustered at synapses by a variety of molecular mechanisms, more of which will be discussed in Chapter 3 of this thesis. While CLA-1 appears to play an important role in clustering SVs in sensory neurons NSM and AIY, it did not influence SV clustering at motor neurons. This finding is not surprising, as the functional demands of different synapses often result in different architecture (Ackermann et al., 2015). For example, DP ultrastructure is much more elongated and complex in interneurons than at the NMJ (Kittelmann et al., 2013). It is possible that varying the timing and extent of CLA-1 expression may result in different effects on SV clustering, as has been observed with LAR-RPTP isoform PTP-3A, a proposed synaptic anchor that can recruit SYD-2 and other scaffolding molecules early in synapse formation (Ackley et al., 2005). The two isoforms PTP-3A and PTP-3B exhibit distinct expression patterns, which likely influence their interacting partners and localization.

CLA-1 isoforms comprise a novel active zone protein with conserved functional roles at the synapse

CLA-1 is a novel active zone protein in *C. elegans* that contains both structural and functional homology to vertebrate active zone proteins RIM, Fife, Piccolo, and Bassoon. Its abnormally large long isoform contains a unique structure, almost half of which is a repetitive region that has no order or homology to known vertebrate proteins. The distribution of CLA-1 isoforms in the presynaptic terminal, as well as its apparent role in recruiting SVs for release, highlight an interesting role for regulation of SV clustering and retrieval. These mechanisms may be conserved in synapse development and function in other organisms.

D. Materials and Methods

Strains and genetics

Worms were raised on NGM plates at 20°C using OP50 *Escherichia coli* as a food source. N2 Bristol was used as the wild-type reference strain. Hawaii CB4856 strain was used for SNP mapping. The following mutant strains were obtained through the Caenorhabditis Genetics Center: *cla-1(ok560)IV, cla-1(gk352)IV, cla-1(ok937)IV, cla-1(ok2285)IV, unc-104(e1265)II, syd-2(ok217)X, syd-2(ju37)X, syd-1(ju82)II*, unc-10(md1117)X, vaIs33 [Punc-2::UNC-2::GFP] and zxIs6 [unc-17p::ChR2(H134R)::YFP + lin-15(+)] V. nuIs168 [Pmyo-2::gfp; Punc-129::Venus::rab-3] was provided by Jihong Bai (Fred Hutchinson Cancer Research Center, Seattle, Washington). juIs137 and [Pflp-13::snb-1::gfp] were provided by Yishi Jin (UCSD, San Diego, CA). kyIs445 [Pdes-2::mCherry::rab-3; Pdes-2:sad-1::gfp] was provided by Cori Bargmann (Rockefeller University, New York, NY). Other strains used in the study are as follows: olaIs1 [Ptph-1::mCherry; Ptph-1::cat-1::gfp], olaEx1106 [Ptph-1:: mCherry:: rab-3; Ptph-1::syd-2::gfp],wyEx505 [Pttx-3::mCherry::erc; Pttx-3::gfp::rab-3], wyIs45 [Pttx-3::rab3::gfp], olaEx2548 [Punc-47::egfp::rab-3],

olaEx791 [Ptph-1::mCherry ; Ptph-1::gfp::syd-1] and zxIs6 [Punc-17::ChR2(H134R)::yfp; lin-15(+)], wyIs85 [Pitr-1::GFP::RAB-3], wyIs574 [Pmig-13::CLA1S::GFP];wyIs226 [Pmig-13::mCherry::RAB-3], wyEx8596 [Pmig-13::mRuby3::CLA-1(S)], wyEx6368 [Pmig-13::CLA-1(S)::mCherry + Pmig-13::GFP::ELKS-1], wyEx9404[Pmig13::FLPase + Pmig13::mRuby3::cla-1];cla-1(wy1186)IV [C-terminal FRT-stop-GFP-FRT].

Molecular biology and transgenic lines

Expression clones were made in the pSM vector (Shen and Bargmann, 2003). The plasmids and transgenic strains (0.5–50 ng/µl) were generated using standard techniques and coinjected with markers Punc122::GFP (15–30 ng/µl), Punc122::dsRed (15–30 ng/µl), Podr-1::RFP (100 ng/µl) or Podr-1::GFP (100 ng/µl).

Screen and SNP mapping coupled with WGS

Worms expressing CAT-1::GFP and cytosolic mCherry in NSM neuron (olaIs1) were mutagenized with ethyl methanesulfonate (EMS) as described previously (Brenner, 1974). The screen was performed as previously described (Nelson et al, 2013; Jang et al., 2016). CAT-1::GFP was diffusely distributed throughout neurites in 6 mutants, including *cla-1(ola104)*. The *ola104* allele was mapped to a 2.1Mbp region on chromosome IV using SNP mapping coupled with whole-genome sequencing (WGS) (Davis et al., 2005; Doitsidou et al., 2010). WGS identified the genetic lesion in ola104 as a missense mutation in cla-1. ola104/cla-1(ok560) trans-heterozygotes were examined for complementation.

Phylogenetic tree creation

We generated a phylogenic tree to determine how related the CLA-1 PDZ domain was to the other family members (Figure 4B). The PDZ domains of Piccolo/Fife-related proteins were identified by SMART (Schultz et al., 1998; Letunic et al., 2012). T-Coffee (M-Coffee) was used for multi-alignment of the sequences (Notredame, 2010). A rooted phylogenetic tree was determined from aligned sequences by neighbor joining with 100 bootstrap replicates using APE (Paradis et al., 2004). PDZ domains of Dishevelled family proteins were used as an outgroup. A circle tree was built using ggtree (Yu et al., 2017).

RT PCR

RNA from wild type, *cla-1(S/M/L)* and *cla-1(L)* worms was prepared by standard protocols. A cDNA library was created by reverse transcription using oligo dTs. PCR amplification was conducted using primers against the C-terminal PDZ domain of *cla-1*, as well as against the housekeeping gene *tba-1*.

Fluorescence microscopy and confocal imaging

Images of fluorescently tagged fusion proteins were captured at room temperature in live *C. elegans*. Mid-L4 through young adult stage hermaphrodite animals were anesthetized using 10 mM levamisole (Sigma-Aldrich) or 50mM muscimol (Abcam) in M9 buffer, mounted on 2-5% agar pads and imaged as follows: Images were taken using a 60x CFI Plan Apochromat VC, NA 1.4, oil objective (Nikon) on an UltraView VoX spinning-disc confocal microscope (PerkinElmer). a Zeiss LSM710 confocal microscope (Carl Zeiss) with a Plan-Apochromat 63x/1.4 NA objective, or

a Zeiss Axio Observer Z1 microscope equipped with a Plan-Apochromat 63 × 1.4 objective and a Yokagawa spinning-disk unit. Maximum-intensity projections were generated using ImageJ (NIH) or ZEN 2009 software and used for all the confocal images. Quantification was performed on maximal projections of raw data.

Quantification of synaptic vesicle clustering and synapse number phenotypes

Quantification of synaptic vesicle clustering active zone protein clustering was based on a previous protocol (Jang et al., 2016). Briefly, fluorescence values for individual neurites (ventral neurite for the NSM and PVD neurons, Zone3 for the AIY neuron, and dorsal neurite for DD GABAergic or cholinergic motor neurons) were obtained through segmented line scans using ImageJ. A sliding window of 2µm was used to identify all the local fluorescence peak values and trough values for an individual neuron. Synaptic enrichment was then calculated as % ΔF/F as previously described (Dittman and Kaplan, 2006; Bai et al., 2010). To measure penetrance, animals were scored as displaying either “punctate” or “diffuse” phenotypes for synaptic vesicles proteins. Percentage of animals displaying diffuse distribution of synaptic vesicle proteins was calculated for each genotype. For each experiment, at least 30 animals were scored for each genotype and at least five independent experiments were performed. The number of synaptic vesicle puncta in DD GABAergic motor neurons was counted by ImageJ with the same settings for all images including threshold, size and circularity. DA9 synapse number and SYD-2::GFP puncta fluorescence was quantified using a Matlab (Mathworks, Natick MA) script that counted and measured peaks above threshold from plot profiles of segmented line scans generated in

ImageJ. To quantify synaptic fluorescence of CLA-1(S) or RAB-3, total integrated intensity of the line scans was analyzed using an ImageJ plugin.

Generation of *cla-1(S/M/L)*

To create *cla-1(wy1048)* we chose sgRNAs ~13kb apart designed to delete most of the M and almost all of the S isoform, including the shared PDZ and C2 domains. sgRNAs were injected at 30ng/µl along with Cas9 plasmid at 50ng/µl and F2 worms were screened by PCR. The resulting deletion is flanked by the following sequences: 5' CCACAACAATCATTCCACCC, 3' AGGTGTCGGCACACGTCATC.

N-terminal endogenous labeling of CLA-1(L)

To endogenously tag CLA-1(L) at the N-terminus, a CRISPR protocol (Dickinson et al., 2015) was used to create cla-1(ola300[gfp:: SEC::cla-1(L)]), in which gfp::SEC (Self-Excising Cassette) was inserted before the start codon of cla-1(L). SEC consists of a hygromycin resistance gene (hygR), a visible marker [sqt-1(d)]) and an inducible Cre recombinase. SEC is flanked by LoxP sites, and heat shock induced Cre expression removed the SEC, leaving GFP fused to CLA-1(L) in *cla-1(ola311[gfp::cla-1(L)])*.

Cell autonomy of CLA-1(L)

Two methods were used to demonstrate cell autonomy of CLA-1(L). In the first method, a CRISPR protocol (Paix et al., 2014; Arribere et al., 2014) was used to create cla-1 (ola324), in which two loxP sites were inserted into two introns of cla-1(L). We used three criteria to ensure that our

insertion sites efficiently and specifically target CLA-1(L). First, we avoided inserting loxP sites into small introns to prevent any effects on splicing. Second, to ensure that CLA-1(M) is unaffected after Cre-loxP recombination, the second loxP site was positioned about 4kb away from the start codon of cla-1(M). Third, the sequence flanked by loxP sites is about 16kb and is close to the start codon of cla-1(L). Thus removal of the sequence should result in a CLA-1(L) null mutation. Cell-specific removal of CLA-1(L) in NSM was achieved with a plasmid driving the expression of cre cDNA under the NSM-specific *tph-1* promoter fragment as described previously (Jang et al., 2016; Nelson and Colon-Ramos, 2013).

In the second method we modified a CRISPR protocol (Dickinson et al., 2015) to create cla-1(ola321[gfp:: CAS::cla-1(L)]), in which CAS consists of a hygromycin resistance gene (hygR) and a visible marker [sqt-1(d)]). Since CAS contains a transcriptional terminator, this strain is a *cla-1(L)* null allele. Since CAS is flanked by loxP sites, Cre-loxp recombination generates functional GFP fused to CLA-1(L). Cell-specific rescue in NSM was achieved with a plasmid driving the expression of cre cDNA under the NSM-specific *tph-1* promoter fragment. Detailed subcloning information will be provided upon request.

C-terminal endogenous tagging of CLA-1 isoforms

A cell-specific CRISPR protocol (Schwartz and Jorgensen, 2016) was used to insert a let-858 3'UTR flanked by FRT sites followed by GFP at the conserved C-terminus of cla-1. Upon crossing to a strain containing cell-specific FLPase, the endogenous stop site and exogenous 3'UTR are excised, leaving the C-terminal GFP inserted in front of the endogenous 3'UTR. To achieve DA9-specific expression of CLA-1::GFP we used a FLPase driven by the Pmig-13 promoter, which has

previously proven to be specific to DA9 within the posterior dorsal cord. However, Pmig-13 seems to express at very low levels in other neurons in this region (enough to generate excision at the FRT sites), as evidenced by the fact that we see CLA-1::GFP puncta outside DA9 driven exogenously expressed CLA-1.

Aldicarb assays

Animals were assayed for acute exposure to aldicarb (Mahoney et al., 2006). Aldicarb (ULTRA scientific) was prepared as a stock solution of 200mM stock in 50% ethanol. Aldicarb sensitivity was measured by transferring 25 animals to plates containing 1mM aldicarb and then assaying the time course of paralysis. Animals were considered paralyzed once they no longer moved even when prodded with a platinum wire three times on the head and tail. The ratio of animals moving to the total number of animals on the plate was calculated for each time point. All strains used for this assay also contained zxIs6 in the background for consistency with electrophysiology assays. All assays were performed blinded to genotype.

Electrophysiology

Electrophysiological recordings were obtained from the *C. elegans* neuromuscular junctions of immobilized and dissected adult worms as previously described (Richmond, 2009). Ventral body wall muscle recordings were acquired in whole-cell voltage-clamp mode (holding potential, -60 mV) using an EPC-10 amplifier, digitized at 1 kHz. Evoked responses were obtained using a 2ms voltage pulse applied to a stimulating electrode positioned on the ventral nerve cord anterior to the recording site. For multiple stimulations, a 5 pulse train was delivered at 20 Hz. The 5mM

Ca^{2+} extracellular solution consisted of 150 mM NaCl, 5 mM KCl, 5 mM $CaCl_2$, 4 mM $MgCl_2$, 10 mM glucose, 5 mM sucrose, and 15 mM HEPES (pH 7.3, ~340 mOsm). The patch pipette was filled with 120 mM KCl, 20 mM KOH, 4 mM $MgCl_2$, 5 mM (N-tris[Hydroxymethyl] methyl-2-aminoethane-sulfonic acid), 0.25 mM $CaCl_2$, 4 mM Na^2ATP, 36 mM sucrose, and 5 mM EGTA (pH 7.2, ~315 mOsm). Data were obtained using Pulse software (HEKA. Subsequent analysis and graphing was performed using mini analysis (Synaptosoft), Igor Pro and Prism (GraphPad).

Electron Mcreaicroscopy

Worms underwent high-pressure freeze (HPF) fixation as described previously (Weimer et al., 2006). Young adult hermaphrodites were placed in specimen chambers filled with *Escherichia coli* and frozen at -180°C and high pressure (Leica SPF HPM 100). Samples then underwent freeze substitution (Reichert AFS, Leica, Oberkochen, Germany). Samples were held at -90°C for 107 h with 0.1% tannic acid and 2% OsO_4 in anhydrous acetone. The temperature was then increased at 5°C/h to -20°C, and kept at -20°C for 14h, and increased by 10°C/h to 20°C. After fixation, samples were infiltrated with 50% Epon/acetone for 4h, 90% Epon/acetone for 18h, and 100% Epon for 5 hours. Finally, samples were embedded in Epon and incubated for 48h at 65°C. All specimens were prepared in the same fixation and subsequently blinded for genotype. Ultra thin (40 nm) serial sections were cut using an Ultracut 6 (Leica) and collected on formvar-covered, carbon-coated copper grids (EMS, FCF2010-Cu). Post-staining was performed using 2.5% aqueous uranyl acetate for 4 min, followed by Reynolds lead citrate for 2 min. Images were obtained on a Jeol JEM-1220 (Tokyo, Japan) transmission electron microscope operating at 80 kV. Micrographs were collected using a Gatan digital camera (Pleasanton, CA) at a magnification

of 100k. Images were quantified blinded to genotype using NIH ImageJ software and macros provided by the Jorgensen lab. Data was analyzed using MATLAB scripts written by the Jorgensen lab and Ricardo Fleury.

Images of the dorsal cord were taken for three animals from each strain. Cholinergic synapses were identified by morphology (White et al., 1986). A synapse was defined as a set of serial sections containing a dense projection and two flanking sections without dense projections from either side. Synaptic vesicles were identified as spherical, light gray structures with an average diameter of ~30 nm. To control for inherent variability in the size of synaptic terminals, we measured the density of synaptic vesicles in the terminal by dividing the number of synaptic vesicles by the area of the terminal in micrometers. A synaptic vesicle was considered docked if it contacted the plasma membrane. Vesicles that were within 1-4 nm of the plasma membrane that exhibited small tethers to the PM were not scored as docked. The total number of undocked vesicles contacting the dense projection were quantified per profile containing a dense projection.

Statistical analyses

Statistics was determined using students t-test, one-way ANOVA or two-way ANOVA with Tukey's post-hoc analysis. Error bars were calculated using standard errors of the mean. * signifies $p<0.05$, ** $p<0.01$, *** $p<0.001$, **** $p<0.0001$.

E. Cited Literature

Ackermann, F., Waites, C. L., & Garner, C. C. (2015). Presynaptic active zones in invertebrates and vertebrates. EMBO Reports, 16(8), 1–16. http://doi.org/10.15252/embr.201540434

Arribere, J. A., Bell, R. T., Fu, B. X. H., Artiles, K. L., Hartman, P. S., & Fire, A. Z. (2014). Efficient marker-free recovery of custom genetic modifications with CRISPR/Cas9 in Caenorhabditis elegans. Genetics, 198(3), 837–846. http://doi.org/10.1534/genetics.114.169730

Bai, J., Z. Hu, J.S. Dittman, E.C. Pym, and J.M. Kaplan. 2010. Endophilin functions as a membrane-bending molecule and is delivered to endocytic zones by exocytosis. Cell. 143:430-441

Brenner, S. (1974). The genetics of Caenorhabditis elegans. Genetics, 77(1), 71–94. http://doi.org/10.1002/cbic.200300625

Bruckner, J. J., Gratz, S. J., Slind, J. K., Geske, R. R., Cummings, A. M., Galindo, S. E., … O'Connor-Giles, K. M. (2012). Fife, a Drosophila Piccolo-RIM homolog, promotes active zone organization and neurotransmitter release. The Journal of Neuroscience : The Official Journal of the Society for Neuroscience, 32(48), 17048–58. http://doi.org/10.1523/JNEUROSCI.3267-12.2012

Bruckner, Joseph J., 1 Zhan, Hong , 2 Gratz, Scott J., 2 Rao, Monica, 1 Ukken, Fiona , 2 Zilberg, Gregory, 2 and O'Connor-Giles, Kate M. , 1, 2, 3. (2016). Fife organizes synaptic vesicles and calcium channels for high-probablility neurotransmitter release. J. Cell Biol, 216(1), 231–246. http://doi.org/10.1083/jcb.201601098

Cazares, V.A., M.M. Njus, A. Manly, J.J. Saldate, A. Subramani, Y. Ben-Simon, M.A. Sutton, U. Ashery, and E.L. Stuenkel. 2016. Dynamic Partitioning of Synaptic Vesicle Pools by the SNARE-Binding Protein Tomosyn. J.Neurosci. 36:11208-11222. doi: 36/44/11208.

Chia, P. H., Li, P., & Shen, K. (2013). Cellular and molecular mechanisms underlying presynapse formation. Journal of Cell Biology, 203(1), 11–22. http://doi.org/10.1083/jcb.201307020

Dai, Y., Taru, H., Deken, S. L., Grill, B., Ackley, B., Nonet, M. L., & Jin, Y. (2006). SYD-2 Liprin-alpha organizes presynaptic active zone formation through ELKS. Nat Neurosci, 9(12), 1479–1487. http://doi.org/nn1808 [pii]\r10.1038/nn1808

Dani, A., Huang, B., Bergan, J., Dulac, C., & Zhuang, X. (2010). Superresolution Imaging of Chemical Synapses in the Brain. Neuron, 68(5), 843–856. http://doi.org/10.1016/j.neuron.2010.11.021

Davis, M. W., Hammarlund, M., Harrach, T., Hullett, P., Olsen, S., & Jorgensen, E. M. (2005). Rapid single nucleotide polymorphism mapping in C. elegans. BMC Genomics, 6, 118. http://doi.org/10.1186/1471-2164-6-118

Dickinson, D. J., Pani, A. M., Heppert, J. K., Higgins, C. D., & Goldstein, B. (2015). Streamlined genome engineering with a self-excising drug selection cassette. Genetics, 200(4), 1035–1049. http://doi.org/10.1534/genetics.115.178335

Dittman, J. S., & Kaplan, J. M. (2006). Factors regulating the abundance and localization of synaptobrevin in the plasma membrane. Proceedings of the National Academy of Sciences of the United States of America, 103(30), 11399–404. http://doi.org/10.1073/pnas.0600784103

Doitsidou, M., Poole, R. J., Sarin, S., Bigelow, H., & Hobert, O. (2010). C. elegans mutant identification with a one-step whole-genome-sequencing and SNP mapping strategy. PLoS ONE, 5(11), 1–7. http://doi.org/10.1371/journal.pone.0015435

Edwards, S. L., Morrison, L. M., Yorks, R. M., Hoover, C. M., Boominathan, S., & Miller, K. G. (2015). UNC-16 (JIP3) acts through synapse-assembly proteins to inhibit the active transport of cell soma organelles to Caenorhabditis elegans motor neuron axons. Genetics, 201(1), 117–141. http://doi.org/10.1534/genetics.115.177345

Edwards, S. L., Yorks, R. M., Morrison, L. M., Hoover, C. M., & Miller, K. G. (2015). Synapse-assembly proteins maintain synaptic vesicle cluster stability and regulate synaptic vesicle transport in Caenorhabditis elegans. Genetics, 2011. Edwa(1), 91–116. http://doi.org/10.1534/genetics.115.177337

Fernández-Busnadiego, R., Zuber, B., Maurer, U. E., Cyrklaff, M., Baumeister, W., & Lučić, V. (2010). Quantitative analysis of the native presynaptic cytomatrix by cryoelectron tomography. Journal of Cell Biology, 188(1), 145–156. http://doi.org/10.1083/jcb.200908082

Fouquet, W., Owald, D., Wichmann, C., Mertel, S., Depner, H., Dyba, M., … Sigrist, S. J. (2009). Maturation of active zone assembly by Drosophila Bruchpilot. Journal of Cell Biology, 186(1), 129–145. http://doi.org/10.1083/jcb.200812150

Gracheva, E. O., Hadwiger, G., Nonet, M. L., & Richmond, J. E. (2008). Direct interactions between C. elegans RAB-3 and Rim provide a mechanism to target vesicles to the presynaptic density. Neuroscience Letters, 444(2), 137–142. http://doi.org/10.1016/j.neulet.2008.08.026

Hallam, S. J., Goncharov, A., McEwen, J., Baran, R., & Jin, Y. (2002). SYD-1, a presynaptic protein with PDZ, C2 and rhoGAP-like domains, specifies axon identity in C. elegans. Nature Neuroscience, 5(11), 1137–1146. http://doi.org/10.1038/nn959

Hammarlund, M., Palfreyman, M. T., Watanabe, S., Olsen, S., & Jorgensen, E. M. (2007). Open syntaxin docks synaptic vesicles. PLoS Biology, 5(8), 1695–1711. http://doi.org/10.1371/journal.pbio.0050198

Han, Y., Kaeser, P. S., Südhof, T. C., & Schneggenburger, R. (2011). RIM determines Ca(2+) channel density and vesicle docking at the presynaptic active zone. Neuron, 69(2), 304–316. http://doi.org/10.1016/j.neuron.2010.12.014

Jang, S. R., Nelson, J. C., Bend, E. G., Rodríguez-Laureano, L., Tueros, F. G., Cartagenova, L., … Colón-Ramos, D. A. (2016). Glycolytic Enzymes Localize to Synapses under Energy Stress to Support Synaptic Function. Neuron, 90(2), 278–291. http://doi.org/10.1016/j.neuron.2016.03.011

Kaeser, P. S., Deng, L., Wang, Y., Dulubova, I., Liu, X., Rizo, J., & Südhof, T. C. (2011). RIM proteins tether Ca2+ channels to presynaptic active zones via a direct PDZ-domain interaction. Cell, 144(2), 282–295. http://doi.org/10.1016/j.cell.2010.12.029

Kaeser, P. S., & Regehr, W. G. (2014). Molecular Mechanisms for Synchronous, Asynchronous, and Spontaneous Neurotransmitter Release. Annual Review of Physiology, 76(1), 333–363. http://doi.org/10.1146/annurev-physiol-021113-170338

Kittel, R. J., Wichmann, C., Rasse, T. M., Fouquet, W., Schmidt, M., Schmid, A., … Sigrist, S. J. (2006). Clustering, Ca Channel, and Vesicle Release. Science, 312(May), 1051–1054. http://doi.org/10.1126/science.1126308

Kittelmann, M., Hegermann, J., Goncharov, A., Taru, H., Ellisman, M. H., Richmond, J. E., … Eimer, S. (2013). Liprin-α/SYD-2 determines the size of dense projections in presynaptic active zones in C. elegans. Journal of Cell Biology, 203(5), 849–863. http://doi.org/10.1083/jcb.201302022

Langnaese, K., Seidenbecher, C., Heike, W., Seidel, B., Hartung, K., Appeltauer, U., … Gundelfinger, E. D. (1996). Protein components of a rat brain synaptic junctional protein preparation. Molecular Brain Research, 42(1), 118–122. http://doi.org/10.1016/S0169-328X(96)00147-7

Leal-Ortiz, S., Waites, C. L., Terry-Lorenzo, R., Zamorano, P., Gundelfinger, E. D., & Garner, C. C. (2008). Piccolo modulation of Synapsin1a dynamics regulates synaptic vesicle exocytosis. Journal of Cell Biology, 181(5), 831–846. http://doi.org/10.1083/jcb.200711167

Letunic, I., Doerks, T., & Bork, P. (2012). SMART 7: Recent updates to the protein domain annotation resource. Nucleic Acids Research, 40(D1), 302–305. http://doi.org/10.1093/nar/gkr931

Limbach, C., Laue, M. M., Wang, X., Hu, B., Thiede, N., Hultqvist, G., & Kilimann, M. W. (2011). Molecular in situ topology of Aczonin/Piccolo and associated proteins at the mammalian neurotransmitter release site. Proceedings of the National Academy of Sciences, 108(31), E392–E401. http://doi.org/10.1073/pnas.1101707108

Mains, P. E., Sulston, I. A., & Wood, W. B. (1990). Dominant maternal-effect mutations causing embryonic lethality in Caenorhabditis elegans. Genetics, 125(2), 351–369. http://doi.org/10.1091/mbc.E05

Matkovic, T., Siebert, M., Knoche, E., Depner, H., Mertel, S., Owald, D., … Sigrist, S. J. (2013). The bruchpilot cytomatrix determines the size of the readily releasable pool of synaptic vesicles. Journal of Cell Biology, 202(4), 667–683. http://doi.org/10.1083/jcb.201301072

Mukherjee, K., Yang, X., Gerber, S. H., Kwon, H.-B., Ho, A., Castillo, P. E., … Sudhof, T. C. (2010). Piccolo and bassoon maintain synaptic vesicle clustering without directly participating in vesicle exocytosis. Proceedings of the National Academy of Sciences, 107(14), 6504–6509. http://doi.org/10.1073/pnas.1002307107

Nelson, J. C., & Colon-Ramos, D. A. (2013). Serotonergic Neurosecretory Synapse Targeting Is Controlled by Netrin-Releasing Guidepost Neurons in Caenorhabditis elegans. Journal of Neuroscience, 33(4), 1366–1376. http://doi.org/10.1523/JNEUROSCI.3471-12.2012

Notredame, C. 2010. Computing multiple sequence/structure alignments with the T-coffee package. Curr.Protoc.Bioinformatics. Chapter 3:Unit 3.8.1-25. doi: 10.1002/0471250953.bi0308s29.

Paix, A., Wang, Y., Smith, H. E., Lee, C. Y. S., Calidas, D., Lu, T., … Seydoux, G. (2014). Scalable and versatile genome editing using linear DNAs with microhomology to Cas9 sites in Caenorhabditis elegans. Genetics, 198(4), 1347–1356. http://doi.org/10.1534/genetics.114.170423

Paradis, E., Claude, J., & Strimmer, K. (2004). APE: Analyses of phylogenetics and evolution in R language. Bioinformatics, 20(2), 289–290. http://doi.org/10.1093/bioinformatics/btg412

Patel, M. R., & Shen, K. (2009). RSY-1 Is a Local Inhibitor of Presynaptic Assembly in C. elegans. Science, 323(5920), 1500–1503. http://doi.org/10.1126/science.1169025

Patel, M. R., Lehrman, E. K., Poon, V. Y., Crump, J. G., Zhen, M., Bargmann, C. I., & Shen, K. (2006). Hierarchical assembly of presynaptic components in defined C. elegans synapses. Nature Neuroscience, 9(12), 1488–1498. http://doi.org/10.1038/nn1806

Pechstein, A., & Shupliakov, O. (2010). Taking a back seat: Synaptic vesicle clustering in presynaptic terminals. Frontiers in Synaptic Neuroscience, 2(SEP), 1–7. http://doi.org/10.3389/fnsyn.2010.00143

Richmond, J. (2009). Dissecting and recording from the C. Elegans neuromuscular junction. Journal of Visualized Experiments : JoVE, (24), 1–4. http://doi.org/10.3791/1165

Schultz, J., Milpetz, F., Bork, P., & Ponting, C. P. (1998). SMART, a simple modular architecture research tool: Identification of signaling domains. Proceedings of the National Academy of Sciences, 95(11), 5857–5864. http://doi.org/10.1073/pnas.95.11.5857

Schwartz, M. L., & Jorgensen, E. M. (2016). SapTrap, a Toolkit for High-Throughput CRISPR/Cas9 Gene Modification in Caenorhabditis elegans. Genetics, 202(4), 1277–1288. http://doi.org/10.1534/genetics.115.184275

Shen, K., & Bargmann, C. I. (2003). The immunoglobulin superfamily protein SYG-1 determines the location of specific synapses in C. elegans. Cell, 112(5), 619–630. http://doi.org/10.1016/S0092-8674(03)00113-2

Shupliakov, O., Haucke, V., & Pechstein, A. (2011). How synapsin I may cluster synaptic vesicles. Seminars in Cell and Developmental Biology, 22(4), 393–399. http://doi.org/10.1016/j.semcdb.2011.07.006

Siksou, L., Rostaing, P., Lechaire, J.-P., Boudier, T., Ohtsuka, T., Fejtova, A., … Marty, S. (2007). Three-Dimensional Architecture of Presynaptic Terminal Cytomatrix. Journal of Neuroscience, 27(26), 6868–6877. http://doi.org/10.1523/JNEUROSCI.1773-07.2007

Stavoe, A. K. H., & Colón-Ramos, D. A. (2012). Netrin instructs synaptic vesicle clustering through Rac GTPase, MIG-10, and the actin cytoskeleton. Journal of Cell Biology, 197(1), 75–88. http://doi.org/10.1083/jcb.201110127

Stavoe, A. K. H., Nelson, J. C., Martínez-Velázquez, L. A., Klein, M., Samuel, A. D. T., & Colón-Ramos, D. A. (2012). Synaptic vesicle clustering requires a distinct MIG-10/lamellipodin isoform and ABI-1 downstream from Netrin. Genes and Development, 26(19), 2206–2221. http://doi.org/10.1101/gad.193409.112

Stigloher, C., Zhan, H., Zhen, M., Richmond, J., & Bessereau, J.-L. (2011). The presynaptic dense projection of the Caenorhabiditis elegans cholinergic neuromuscular junction localizes synaptic vesicles at the active zone through SYD-2/liprin and UNC-10/RIM-dependent interactions. The Journal of Neuroscience : The Official Journal of the Society for Neuroscience, 31(12), 4388–4396. http://doi.org/10.1523/JNEUROSCI.6164-10.2011

Südhof, T. C. (2012). The presynaptic active zone. Neuron, 75(1), 11–25. http://doi.org/10.1016/j.neuron.2012.06.012

Van Vactor, D., & Sigrist, S. J. (2017). Presynaptic morphogenesis, active zone organization and structural plasticity in Drosophila. Current Opinion in Neurobiology, 43(Figure 2), 119–129. http://doi.org/10.1016/j.conb.2017.03.003

Wagh, D. A., Rasse, T. M., Asan, E., Hofbauer, A., Schwenkert, I., Dürrbeck, H., … Buchner, E. (2006). Bruchpilot, a protein with homology to ELKS/CAST, is required for structural integrity and function of synaptic active zones in Drosophila. Neuron, 49(6), 833–844. http://doi.org/10.1016/j.neuron.2006.02.008

Waites, C. L., Leal-Ortiz, S. A., Andlauer, T. F. M., Sigrist, S. J., & Garner, C. C. (2011). Piccolo Regulates the Dynamic Assembly of Presynaptic F-Actin. Journal of Neuroscience, 31(40), 14250–14263. http://doi.org/10.1523/JNEUROSCI.1835-11.2011

Weimer, R. M., Gracheva, E. O., Meyrignac, O., Miller, K. G., Richmond, J. E., & Bessereau, J.-L. (2006). UNC-13 and UNC-10/Rim Localize Synaptic Vesicles to Specific Membrane Domains. The Journal of Neuroscience , 26(31), 8040–8047. http://doi.org/10.1523/JNEUROSCI.2350-06.2006

White, J.G., Southgate, E., Thomson, J.N., Brenner, S. (1986). The Structure of the Nervous System of the Nematode Caenorhabditis elegans. Philosophical Transactions of the Royal Society of London. Series B, Biological Sciences, 314(1165), 1–340.

Yu, G., Smith, D. K., Zhu, H., Guan, Y., & Lam, T. T. Y. (2017). Ggtree: an R Package for Visualization and Annotation of Phylogenetic Trees With Their Covariates and Other Associated Data. Methods in Ecology and Evolution, 8(1), 28–36. http://doi.org/10.1111/2041-210X.12628

Zhen, M., & Jin, Y. (1999). The liprin protein SYD-2 regulates the differentiation of presynaptic termini in C. elegans. Nature, 401(6751), 371–375. http://doi.org/10.1038/43886

III. SENTRYN ACTS WITH A SUBSET OF ACTIVE ZONE PROTEINS TO LINK THE GUIDED TRANSPORT AND CAPTURE OF SYNAPTIC AND DENSE CORE VESICLES

This chapter has been modified from two manuscripts in preparation, listed below. All figures have been copied or modified from these manuscripts with permission from the authors.

Sentryn and SAD Kinase Link Dense Core Vesicle Axonal Transport and Synaptic Capture
Logan M. Morrison[1], Stacey L. Edwards[1], Laura Manning[2], Natalia Stec[1], Janet E. Richmond[2], and Kenneth G. Miller[1]

Sentryn Acts with a Subset of Active Zone Proteins to Link the Guided Transport and Capture of Synaptic Vesicles
Stacey L. Edwards[1], Logan M. Morrison[1], Laura Manning[2], Natalia Stec[1], Janet E. Richmond[2], and Kenneth G. Miller[1]

[1]Genetic Models of Disease Laboratory
Oklahoma Medical Research Foundation

[2]Department of Biological Sciences
University of Illinois at Chicago

A. Introduction

Neurons must receive and send signals using specialized processes that emanate from their cell bodies. The processes that receive signals are called dendrites, and those that send signals are synaptic terminals. Signaling vesicles are created in the cell body and must be transported, often distances, down axons to release sites. These vesicles must also be clustered near active zones in the synaptic region to ensure efficient communication.

Signaling vesicles can be grouped into two classes (Richmond and Broadie, 2002; Sudhof, 2004). Synaptic vesicles (SVs) release in response to electrical signals and execute much of the rapid neuronal signaling at synapses. Dense core vesicles (DCVs) release neuropeptides in

response to electrical signals (Levitan, 2008; Sossin and Scheller, 1991) that can influence neuronal circuit activity (Banerjee et al., 2017; Bhattacharya and Francis, 2015; Bhattacharya et al., 2014; Chen et al., 2016; Choi et al., 2015; Hu et al., 2011; Lim et al., 2016; Liu et al., 2007) often by modulating pre/postsynaptic responsivity (Hu et al., 2015). Compared to SVs, DCVs are usually present in lower numbers in most neurons and are not as closely associated with AZs (Hammarlund et al., 2008; Hoover et al., 2014; Weimer et al., 2006).

Despite these differences in localization, both SVs and DCVs use similar components to arrive at synapses. Both vesicle classes, and other cargo, are transported using a network of microtubule tracks and motors. Axonal microtubules are polarized, with the plus-end pointing out towards axon terminals and the minus-end pointing in towards somas and dendrites (Burton and Paige, 1981; Heidemann et al., 1981; Baas and Lin, 2011). In *C. elegans*, UNC-104/KIF1A is the plus-end motor that directs forward transport of SVs and DCVs from the soma to synaptic regions (Edwards et al., 2015b; Hall and Hedgecock, 1991; Pack-Chung et al., 2007). Dynein is the minus-end motor that mediates reverse transport in the opposite direction (Cavolo et al., 2015; Edwards et al., 2015b; Goodwin et al., 2012; Ou et al., 2010; Wong et al., 2012). While cargo is transported from soma to synapse, both forward and reverse motors act on it, resulting in bidirectional movement in which cargo changes direction several times before arriving at the synaptic region (Edwards et al., 2015b). The implications of bidirectional transport are poorly understood, but suggest that for proper levels of SVs and DCVs to reach the synaptic region, KIF1A-directed forward movement must outcompete dynein-directed reverse movement. This process is known as guided axonal transport.

Previous work has uncovered several important regulators of guided axonal transport. The first was UNC-16/JIP3, a unique member of the JNK-interacting protein family thought to execute two functions. First, it serves as an adaptor protein between Kinesin-1 and small transport vesicles, promoting their transport to the plus-end of neurons. Second, UNC-16/JIP3 promotes endosomal organelle clearance. Thus, in an *unc-16/JIP3* mutant, lysosomes and early endosomes accumulate in the synaptic region of axons (Edwards et al., 2015a; Miller et al., 2016). In a screen for suppressors of this axonal accumulation phenotype, a second class of proteins was identified, including **C**DK-5, **S**AD-1, **S**YD-2/Liprin-α, as well as SYD-1 and SAD-1-interacting protein STRADα. This group of proteins, named the CSS system, prevents axonal retention of lysosomes and early endosomes in an *unc-16/JIP3* mutant background. Together, CSS components limit the effectiveness of dynein, allowing plus-end transport to dominate. In mutants lacking these proteins, SVs and endosomal organelles accumulate at minus-ends of neurons in somas and dendrites (Edwards et al., 2015a; Edwards et al., 2015b; Miller et al., 2005). Furthermore, CSS proteins are known to regulate SV clustering at synapses (Zhen and Jin, 1999; Crump et al., 2001; Hallam et al., 2002; Patel et al., 2006; Dai et al., 2006; Stigloher et al., 2011; Wu et al., 2013; Edwards et al., 2015b). These results reveal two separate functions of the CSS system: 1) to promote plus-end directed transport to the synaptic region, and 2) to prevent cargo from moving past the synapse (in a plus or minus-end direction). The mechanisms behind this functional switch between cargo transport and cargo capture are poorly understood.

While SVs and DCVs are transported by the same molecular motors, less is known about the specific mechanisms involved in DCV transport. We therefore sought to identify regulators of DCV localization and understand how CSS system proteins can influence both transport and capture of synaptic cargo. Using a forward genetic screen for DCV localization, we identified two proteins involved in DCV transport and capture: SAD-1 and STRN-1. These are the first proteins identified in DCV capture, the latter representing a novel but highly conserved protein found in all animals. We named this novel protein Sentryn, from the word "sentry," because we believe it captures SVs and DCVs near active zones and protects them from motor transport activity. Sentryn is one of very few novel active zone proteins reported in the last 11 years, and it provides a mechanistic link between vesicle transport and capture. We propose a model in which Sentryn is a core component of the CSS system that operates with SAD Kinase to enable SYD-2/Liprin-α function, and we redefine the CSS system based on the active zone-enrichment of SAD-1, SYD-2, SYD-1, and Sentryn, but not CDK-5.

B. Results

1. SAD Kinase and Sentryn influence DCV transport and capture

To identify proteins involved in trafficking DCVs to synapses, we conducted a forward genetic screen using a fluorescent marker for DCV cargo expressed in cholinergic motor neurons (Figure 3.1A). These neurons co-release ACh from SVs and neuropeptides from DCVs. Following EMS mutagenesis, we screened for mutant animals with increased fluorescence in cell bodies (located in the ventral cord) and reduced fluorescence in axons (located in the dorsal cord). This specific pattern of mislocalized cargo implies increased minus-end transport or decreased plus-

end transport. We screened 23,300 grand-progeny to complete 3.6-fold coverage for a gene of average size. (see Materials and Methods).

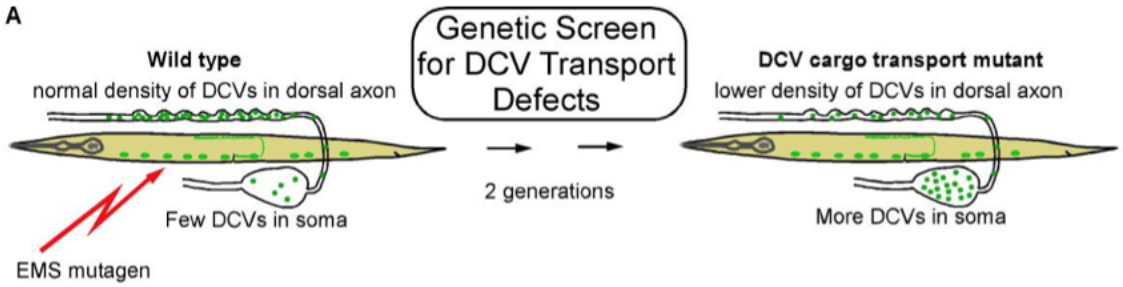

B

New Mutants Isolated in Genetic Screen for DCV Transport Defects			
Gene	Allele	Protein	Mutation
sad-1	*ce776*	SAD-1 Kinase	E280stop nonsense
sad-1	*ce784*	SAD-1 Kinase	Splice site mutation in intron 8
strn-1	*ce793*	STRN-1 (Sentryn)	Q175stop nonsense

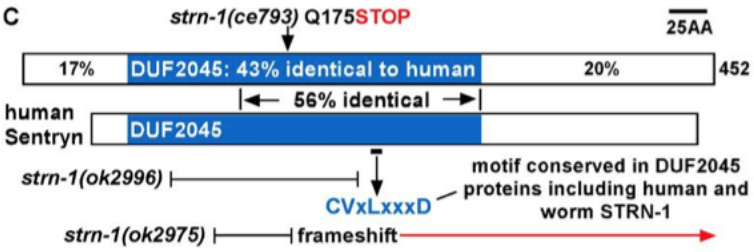

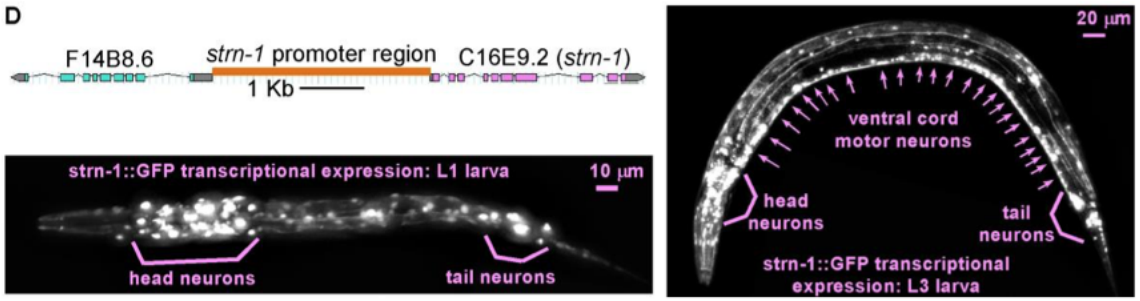

Figure III.1 Forward genetic screen for DCV transport mutants identifies SAD Kinase and a novel, conserved protein. A. Drawings illustrate the forward genetic screen. The screen used EMS to mutagenize wild type animals carrying the integrated transgene ceIs201, which co-expresses the neuropeptide INS-22-Venus (to mark dense core vesicles) and mCherry (as an expression control) in the ventral cord cholinergic motor neurons. We screened the F2 grand-progeny of mutagenized animals on 96-well glass bottom Mat-Tek plates using an inverted microscope and selected animals with lower densities of DCVs in their axons and/ or higher densities in somas. **B.**

Summary of mutants isolated in the genetic screen. **C.** Comparison of human and worm Sentryn proteins and mutation locations. Sentryn's human ortholog is similar in length. Percents indicate percent identities between corresponding regions of the human and worm proteins. The conserved motif "CVLxxxD" is found in both human and worm Sentryn in a large region that is 56% identical between the two proteins. Three allele lesions disrupting the conserved DUF2045 region (Domain of Unknown Function) are shown. The two proteins were aligned using the Align X module of Vector NTI. **D.** Scale drawing of strn-1 promoter region and images of larvae expressing GFP from the strn-1 promoter in the ceEx461 extrachromosomal transgenic array. Sentryn is highly expressed throughout the nervous system. Data collected by Miller lab.

From this screen, we identified four mutants that affect DCV cargo localization. The first, *unc-104(kif1a)*, is a temperature-sensitive mutant in the plus-end (forward) motor for SVs and DCVs that we have previously studied (Edwards et al., 2015b). Two of the mutant lines were identified as loss-of-function mutations in *sad-1 (SAD Kinase)* through complementation testing, mapping, and whole-genome sequencing. The fourth mutant contains a loss-of-function mutation in a novel protein with domains of unknown function (DUF) (Figure 3.1B).

We named this novel protein STRN-1 (Sentryn), given its function of keeping DCVs and SVs at the synapse (see Discussion). STRN-1 is predicted to be a ~53 kDA, medium-sized cytosolic protein and is conserved in all animals. Human Sentryn shares 29% overall amino acid identity with worm Sentryn. A DUF comprises about half the protein in either species, and within that DUF, human and worm Sentryn share 43% amino acid identity. In a region within two-thirds of the DUF, they share 56% identity (Figure 3.1C).

To observe the expression pattern of *strn-1*, we created a transgenic transcriptional GFP reporter. *strn-1*::GFP was highly expressed in the nervous system and was expressed at lower levels in non-neuronal cells (Figure 3.1D). This pattern supports previous microarray data that

found Sentryn (previously named C16E9.2) transcripts expressed pan-neuronally in embryos and larvae (Von Stetina et al., 2007).

2. Sentryn and SAD Kinase regulate DCV distribution cell-autonomously in cholinergic motor neuron synapses

We found that null mutations for both *strn-1* and *sad-1* resulted in dramatic reductions of DCV cargo fluorescence in axons of cholinergic motor neurons in the dorsal cord. We also observed drastic increases in fluorescence at somas in these mutants (Figure 3.2). In null mutant *strn-1(ok2975)* axons, we could rescue DCV fluorescence to wild-type levels by transgenically expressing *strn-1* cDNA in cholinergic motor neurons. This effect was also observed by rescue with human Sentryn. Interestingly, neither worm nor human Sentryn could fully rescue DCV levels in the soma, although *strn-1* cDNA partially reduced the DCV accumulation phenotype.

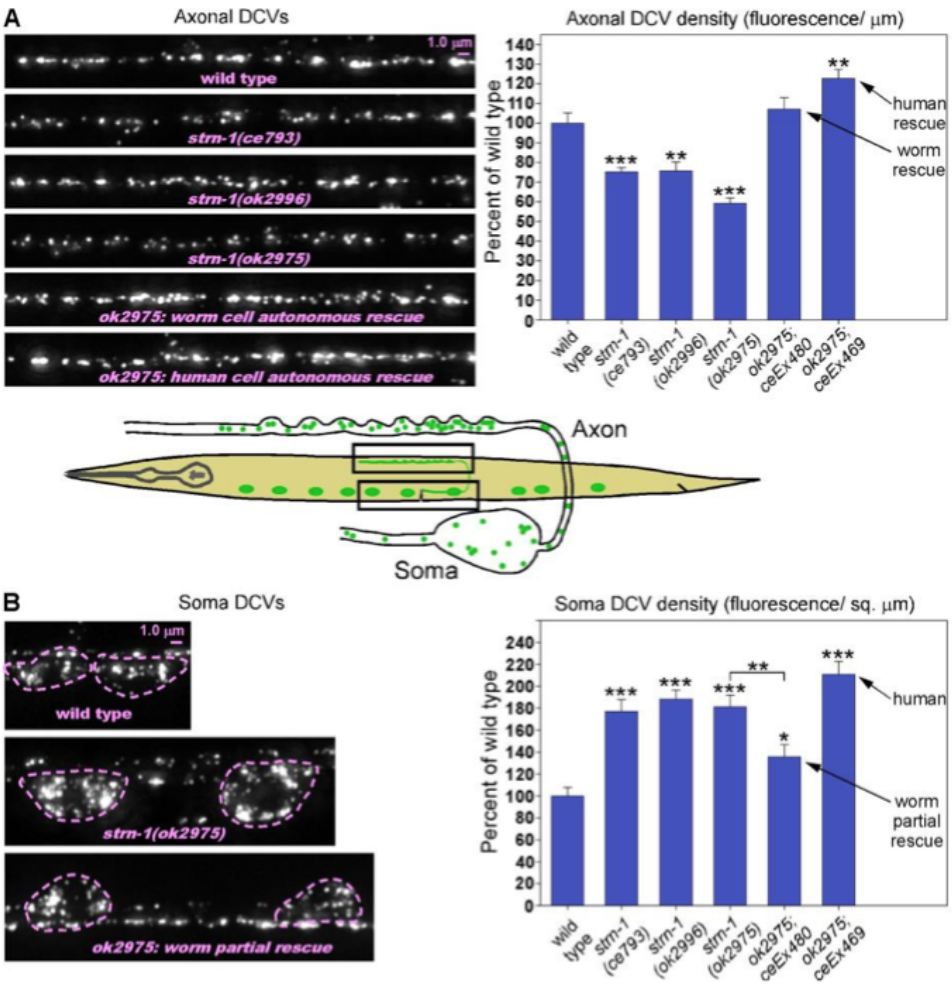

Figure III.2 Sentryn acts cell-autonomously to control the distribution of DCVs in ventral cord cholinergic motor neurons. A-B. Rectangles in drawing indicate regions imaged. Representative images and quantification of DCV fluorescence in axons and somas in the indicated genotypes. The DCV marker INS-22-Venus (a tagged neuropeptide) is expressed from the integrated transgene *ceIs201*. Images are identically-scaled. Dashed lines in (B) outline cell somas. Graph data are means and standard errors from 14-15 animals each. Unmarked bars are not significantly different from wild type. *, **, and *** indicate P-values that are <.05, <.01, or <.001, respectively. Asterisks that are not above relationship bars compare the indicated bar to wild type. Data collected by Miller lab.

We found similar effects in *sad-1(ce749)* null mutant animals (Edwards et al., 2015a), in which *sad-1* cDNA expression in cholinergic motor neurons rescued axonal DCV fluorescence loss, but only partially rescued accumulation at the soma (Figure 3.3). Together, these results suggest that *strn-1* and *sad-1* function cell-autonomously to regulate DCV localization at synapses.

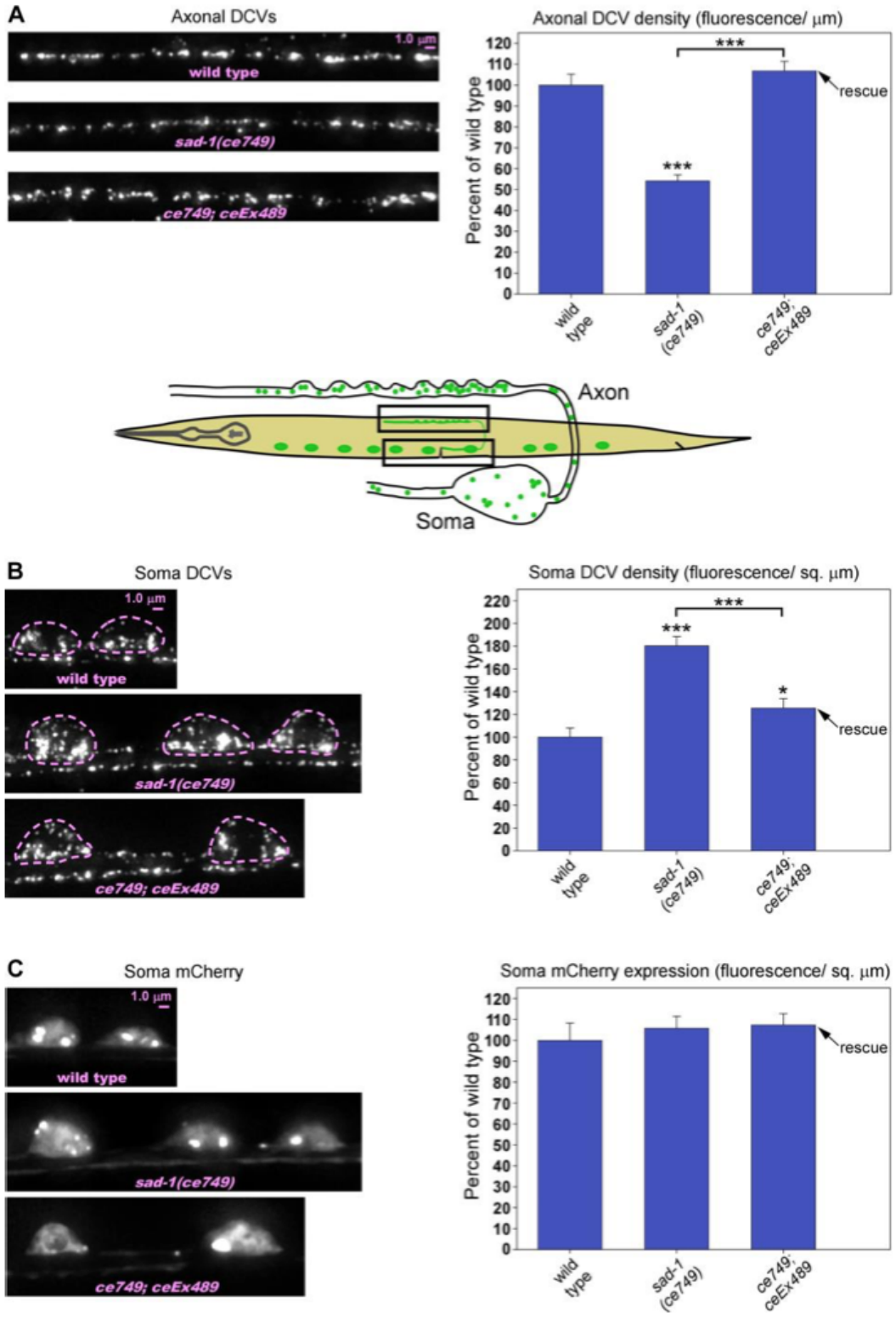

Figure III.3 SAD-1 regulates DCV trafficking cell autonomously in ventral cord cholinergic neurons. A-C. Rectangles in drawing indicate regions imaged. Representative images and quantification of DCV or soluble mCherry fluorescence in axons and somas in the indicated

genotypes. The DCV marker INS-22-Venus (a tagged neuropeptide) and mCherry are expressed from the integrated transgene *ceIs201* using the same promoter. mCherry thus provides an internal control for changes in expression. Images are identically-scaled. Dashed lines in (B) outline cell somas. Graph data are means and standard errors from 13-15 animals each. Unmarked bars are not significantly different from wild type. * and *** indicate P-values that are <.05 or <.001, respectively. Asterisks that are not above relationship bars compare the indicated bar to wild type.

3. Sentryn and SAD Kinase antagonize dynein function during DCV trafficking

Previous work suggests that *sad-1* opposes dynein activity during cargo transport. In a *sad*-1 null mutant, we observed that lysosomes and SVs accumulate at dendrites and somas, presumably because *sad-1* inhibition of dynein was disturbed (Edwards et al., 2015a, b). Because *strn-1* mutants show a similar DCV trafficking defect as *sad-1* mutants, we hypothesized that dynein could be involved in *strn-1*-regulated DCV localization. Specifically, we predicted that the DCV mislocalization phenotype observed in *strn-1* null animals resulted from excess dynein-dependent, minus-end-directed transport.

To test this claim, we observed DCV levels in axons and somas in dynein-deficient animals. Since a dynein neuronal null is sterile lethal in *C. elegans*, we used *nud-2*, a null mutant for a dynein regulator that severely reduced dynein activity in motor neurons (Ou et al., 2010). As predicted, *nud-2* mutant animals exhibited excess DCV levels in axons and corresponding losses in somas, presumably due to plus-end transport dominating in a dynein-deficient animal (Figure 3.4). In the *strn-1;nud-2* mutant animal, axonal DCV levels were rescued to wild type. Soma levels were only partially rescued.

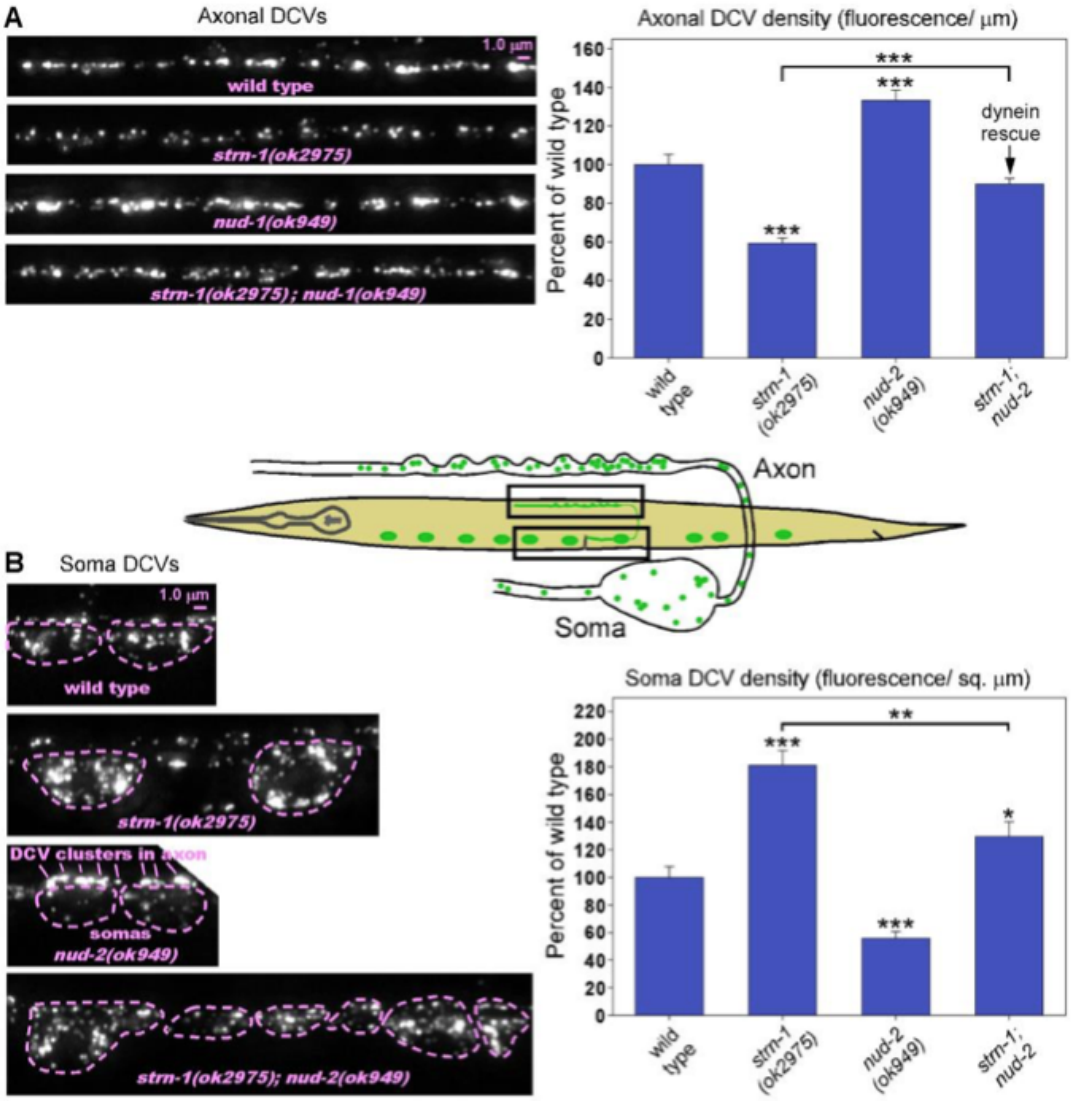

Figure III.4 Sentryn reduces the effectiveness of dynein during DCV transport and/ or capture. A-B. Rectangles in drawing indicate regions imaged. Representative images and quantification of DCV fluorescence in axons (A) and somas (B) in the indicated genotypes. The DCV marker INS-22-Venus (a tagged neuropeptide) is expressed from the integrated transgene ceIs201. Images are identically-scaled. Dashed lines in (B) outline cell somas. Graph data are means and standard errors from 14-15 animals each. Bars without asterisks are not significantly different from wild type. *, **, and *** indicate P-values that are <.05, <.01, or <.001, respectively. Asterisks that are not above relationship bars compare the indicated bar to wild type. Data collected by Miller lab.

We observed a similar phenomenon when comparing *sad-1* null mutants and *sad-1;nud-2* double mutants (Figure 3.5). These findings indicate that Sentryn and SAD-Kinase regulate DCV transport in a dynein-dependent manner.

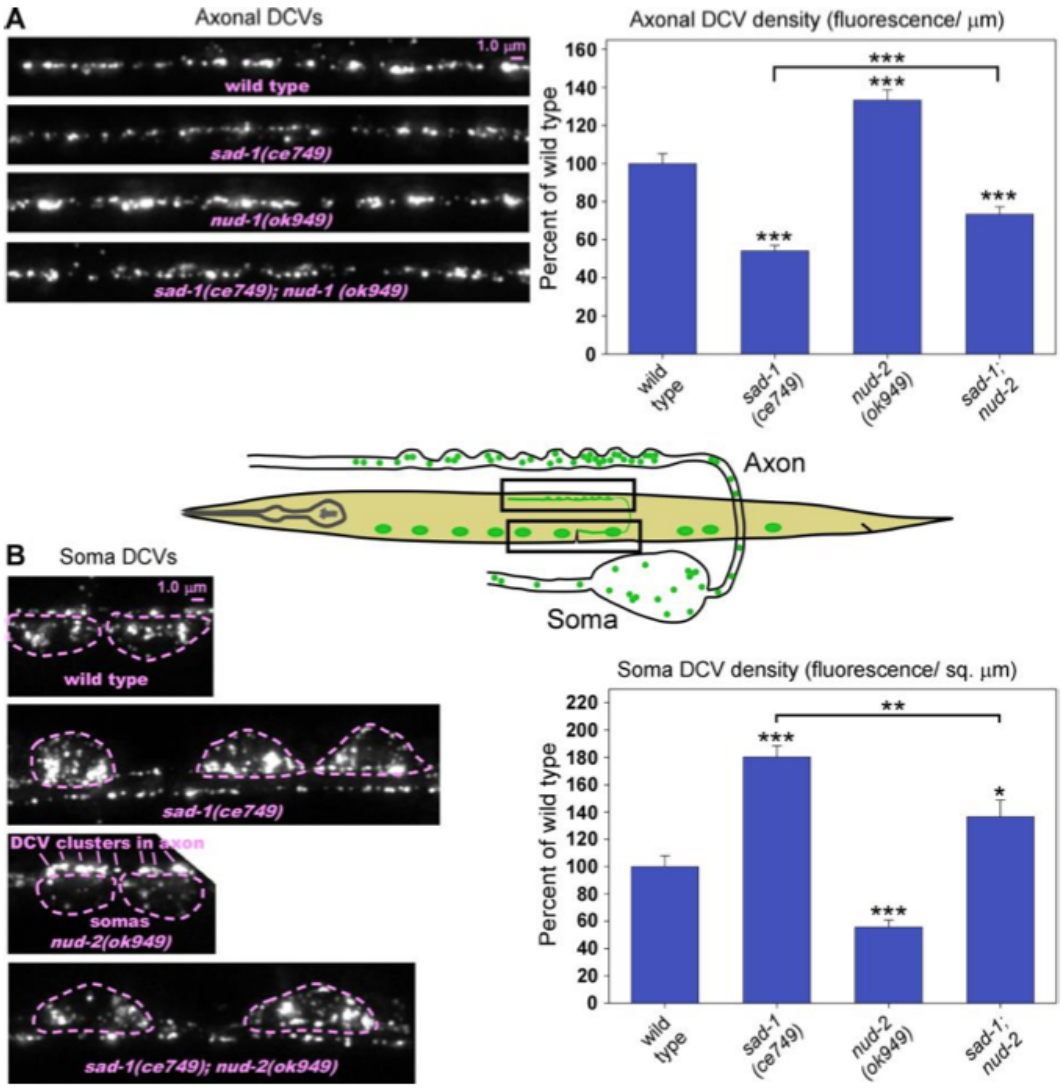

Figure III.5 SAD Kinase reduces the effectiveness of dynein during DCV transport and/ or capture. **A-B.** Rectangles in drawing indicate regions imaged. Representative images and quantification of DCV fluorescence in axons (A) and somas (B) in the indicated genotypes. The DCV marker INS-22-Venus (a tagged neuropeptide) is expressed from the integrated transgene ceIs201. Images are identically-scaled. Dashed lines in (B) outline cell somas. Graph data are means and standard errors from 13-17 animals each. Bars without asterisks are not significantly different from wild type. *, **, and *** indicate P-values that are <.05, <.01, or <.001, respectively. Asterisks that

are not above relationship bars compare the indicated bar to wild type. Data collected by Miller lab.

4. Sentryn and SAD Kinase promote KIF1A-directed DCV transport at the axon initial segment.

Previous studies of the CSS system support a model in which SAD Kinase regulates SV transport through interactions between cargo and motor (Edwards et al., 2015a; Edwards et al., 2015b; Miller 2016). Both *sad-1* and *strn-1* mutants show dynein-dependent DCV accumulation in somas and/or dendrites. Based on these results, we hypothesize that *sad-1* and *strn-1* mutants experience a transport defect in which dynein outcompetes KIF1A. To test this idea, we examined the DCV cargo levels at the axon initial segment (AIS) of DA9. The AIS is located more than 60 um away from the synaptic region where SAD-1 and Sentryn are enriched. We found that in multiple alleles of both *sad-1* and *strn-1* mutants, DCVs accumulated in the AIS (Figure 3.6A). In *strn*-1 mutants, we rescued this accumulation phenotype with cell-autonomous STRN-1 expression (Figure 3.6A). Interestingly, *nud-2* (dynein loss-of-function) animals did not exhibit this DCV build up in the AIS, and did not rescue buildup in a *strn-1;nud-2* double mutant (Figure 3.6B). Based on these findings, we concluded that dynein does not regulate DCV accumulation in the AIS.

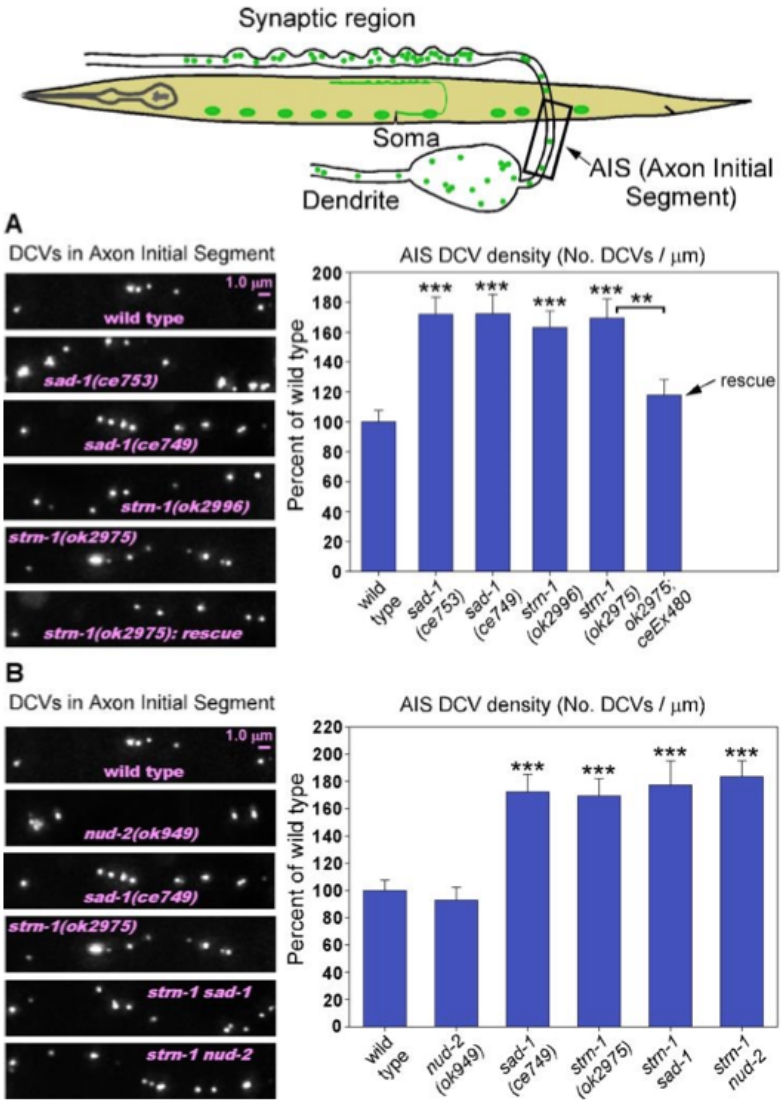

Figure III.6 Mutants lacking Sentryn or SAD-1 accumulate DCVs in the axon initial segment in a dynein independent manner. A-B. Representative images and quantification of DCV number/um asynaptic region (B) in the indicated genotypes. The DCV marker INS-22-Venus is expressed from the integrated transgene array *ceIs201*. Graph data are means and standard errors from 14-15 animals each. Bars without asterisks are not significantly different from wild type. *, **, and *** indicate P-values that are <.05, <.01, or <.001, respectively. Asterisks that are not above relationship bars compare the indicated bar to wild type. Data collected by Miller lab.

We next used time lapse imaging to track DCV movements in live animals. We recorded ~2000 DCV movements per strain and ~6000 images of DCV pausing in each strain. From these recordings, we measured length and velocity of anterograde (forward) and retrograde

(backward) movement, as well as time spent pausing. We found that DCVs spent more time paused in *strn-1*, *sad-1*, and *strn-1;sad-1* mutants (Figure 3.7A, B). This pausing could contribute to DCV build-up in the AIS, especially since loss of dynein could not rescue this phenotype. All strains exhibited bidirectional DCV movement, with more time spent moving in the anterograde direction (~60-65%) than retrogradely (Figure 3.7D). These strains also exhibited similar retrograde velocity and run length as wild type, although *strn-1;sad-1* mutants showed slightly faster retrograde movements (Figure 3.7D, E). Interestingly, although DCVs in each of the mutant strains spent a normal amount of time in anterograde movement, that movement had a lower velocity and run length than in wild type (Figure 3.7D, E). Since these defective anterograde movements are mediated by KIF1A, this evidence suggests that Sentryn and SAD Kinase normally reduce dynein activity, allowing KIF1A to outcompete dynein during transport in the AIS.

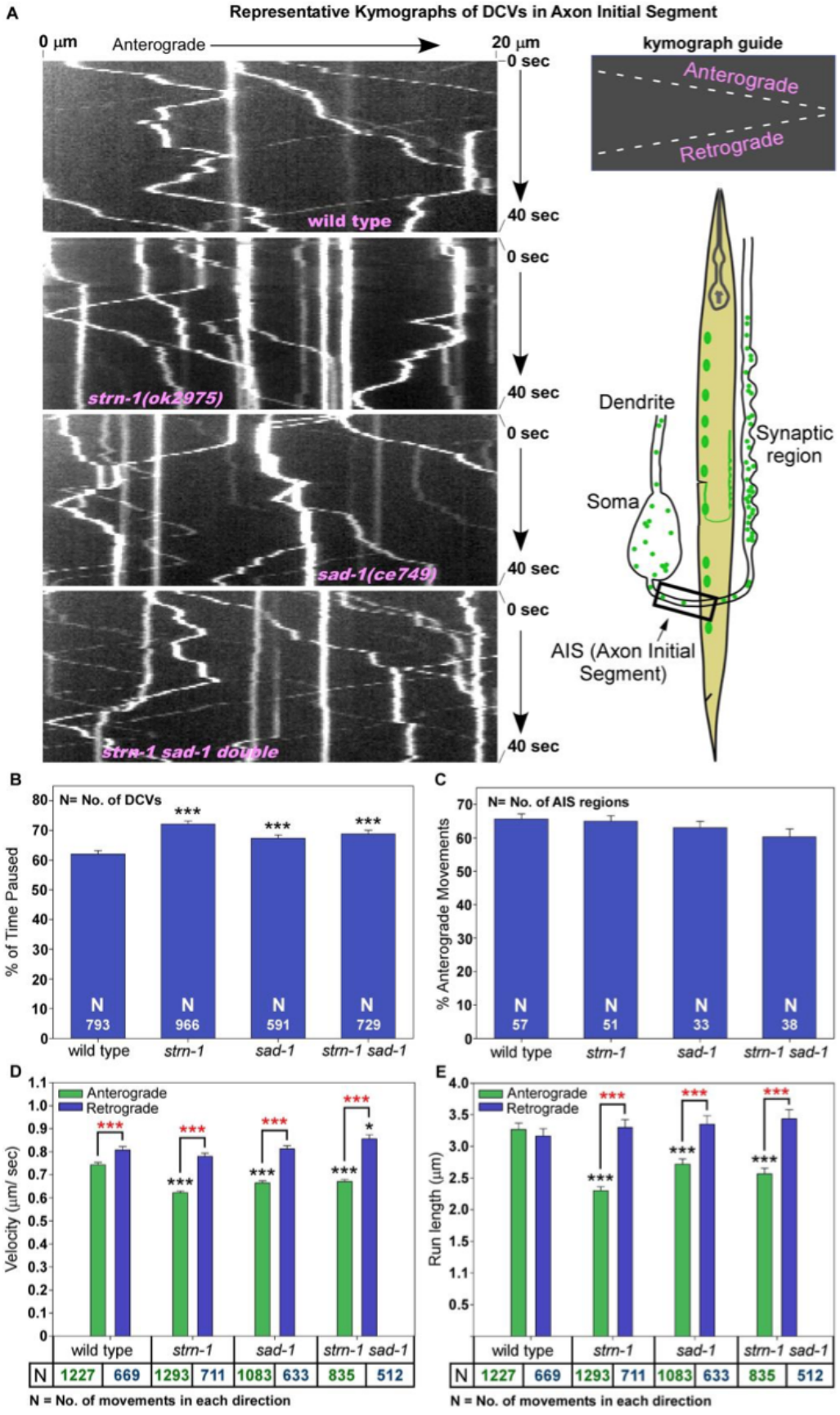
A
Representative Kymographs of DCVs in Axon Initial Segment
0 µm
Anterograde
20 µm
0 sec
40 sec
wild type
strn-1(ok2975)
sad-1(ce749)
strn-1 sad-1 double
kymograph guide
Anterograde
Retrograde
Dendrite
Soma
Synaptic region
AIS (Axon Initial Segment)
B
N= No. of DCVs
% of Time Paused
N 793
N 966
N 591
N 729
wild type
strn-1
sad-1
strn-1 sad-1
C
N= No. of AIS regions
% Anterograde Movements
N 57
N 51
N 33
N 38
D
Anterograde
Retrograde
Velocity (µm/ sec)
E
Run length (µm)
N 1227 669 1293 711 1083 633 835 512
N = No. of movements in each direction

Figure III.7 Reduced anterograde motor activity in the Axon Initial Segment in mutants lacking Sentryn or SAD-1. A. Representative kymographs of INS-22-Venus – loaded DCVs in the axon initial segment of DA and DB type cholinergic motor neurons. Worm drawing indicates region imaged. INS-22-Venus is expressed from the integrated transgene ceIs201. B–E. Graphs plotting various indicated parameters extracted from the time lapse analyses. Error bars are standard errors of the means. Bars without asterisks are not significantly different from wild type. *, **, and *** indicate P-values that are <.05, <.01, or <.001, respectively. Black asterisks compare the marked bar to the wild type value. Red asterisks compare the indicated two bars in a group. Unmarked bars are not significantly different from wild type or the other group member. Total recorded time lapse time (minutes: seconds in order of strains as shown): 42:45, 38:15, 24:45, and 28:30. Data collected by Miller lab.

5. Sentryn functions cell autonomously with CSS system proteins to prevent dynein-dependent lysosome accumulation at dendrites

In addition to SV and DCV transport, the CSS system clears lysosomes and early endosomes from axons. To determine if Sentryn functions with other CSS system proteins to transport these organelles, we experimented with an *unc-16/JIP3* null mutant background. UNC-16/JIP3 normally blocks CSS function, allowing minus-end directed dynein transport to dominate. Thus, in *unc-16/JIP3* mutants, CSS proteins can retain lysosomes and early endosomes at axons and prevent them from accumulating in dendrites and somas. In double mutants of *unc-16/JIP3* and other CSS system proteins, axonal retention is reduced and accumulation at dendrites and somas is greater (Edwards et al., 2015a).

To observe how Sentryn interacts with UNC-16/JIP3, we measured transgenic expression of lysosomal cysteine transporter CTNS-1::RFP in nine cholinergic motor neurons that contain discrete regions of dendrites, axons, and cell somas (Edwards et al., 2015a). We found that *unc-*

16;strn-1 double mutants accumulate ~3.5 times more dendritic lysosomes than *unc-16* single mutants, similar to other CSS protein/*unc-16* double mutants (Figure 3.8A).

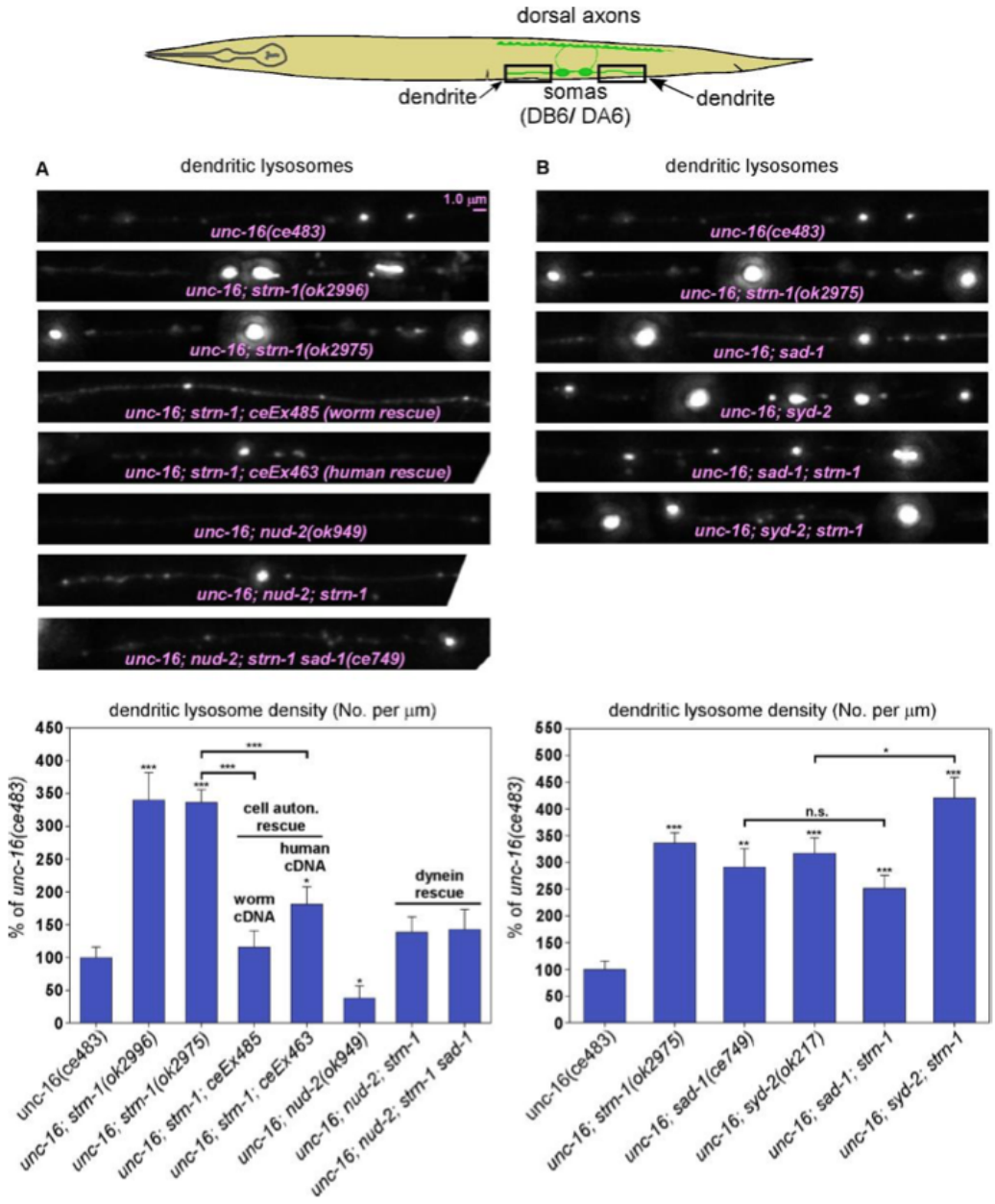

Figure III.8 In unc-16 mutant dendrites, Sentryn acts cell autonomously with the CSS proteins SAD-1 and SYD-2 to inhibit the dynein-dependent accumulation of lysosomes. A-B. Rectangles in drawing indicate regions imaged. Representative images and quantification of lysosome density in DB6/ DA9 dendrites in the indicated genotypes. The lysosome marker CTNS-1-RFP is expressed from the integrated transgene *ceIs56*. Representative images are identically-scaled. We

quantified lysosome density by both number per um and fluorescence intensity per um and obtained similar results. Representative images were chosen based on intensity per, and the graph data depicts number per um. Graph data are means and standard errors from 14-15 animals each. Unmarked bars are not significantly different from wild type. *, **, and *** indicate P-values that are <.05, <.01, or <.001, respectively. Asterisks that are not above relationship bars compare the indicated bar to wild type. Data collected by Miller lab.

This result held for another distinct *strn-1* loss-of-function mutant allele, and was rescued by cell-specific expression of wildtype *strn-1* cDNA. Cell-specific expression of human Sentryn cDNA could also rescue the lysosome accumulation, suggesting that Sentryn's role in dendritic lysosome accumulation is conserved in humans. We observed slightly reduced levels of lysosomes in cell somas in *unc-16;strn-1* double mutants. This phenotype was also rescued with cell-specific expression of wildtype *strn-1* cDNA (Figure 3.9A).

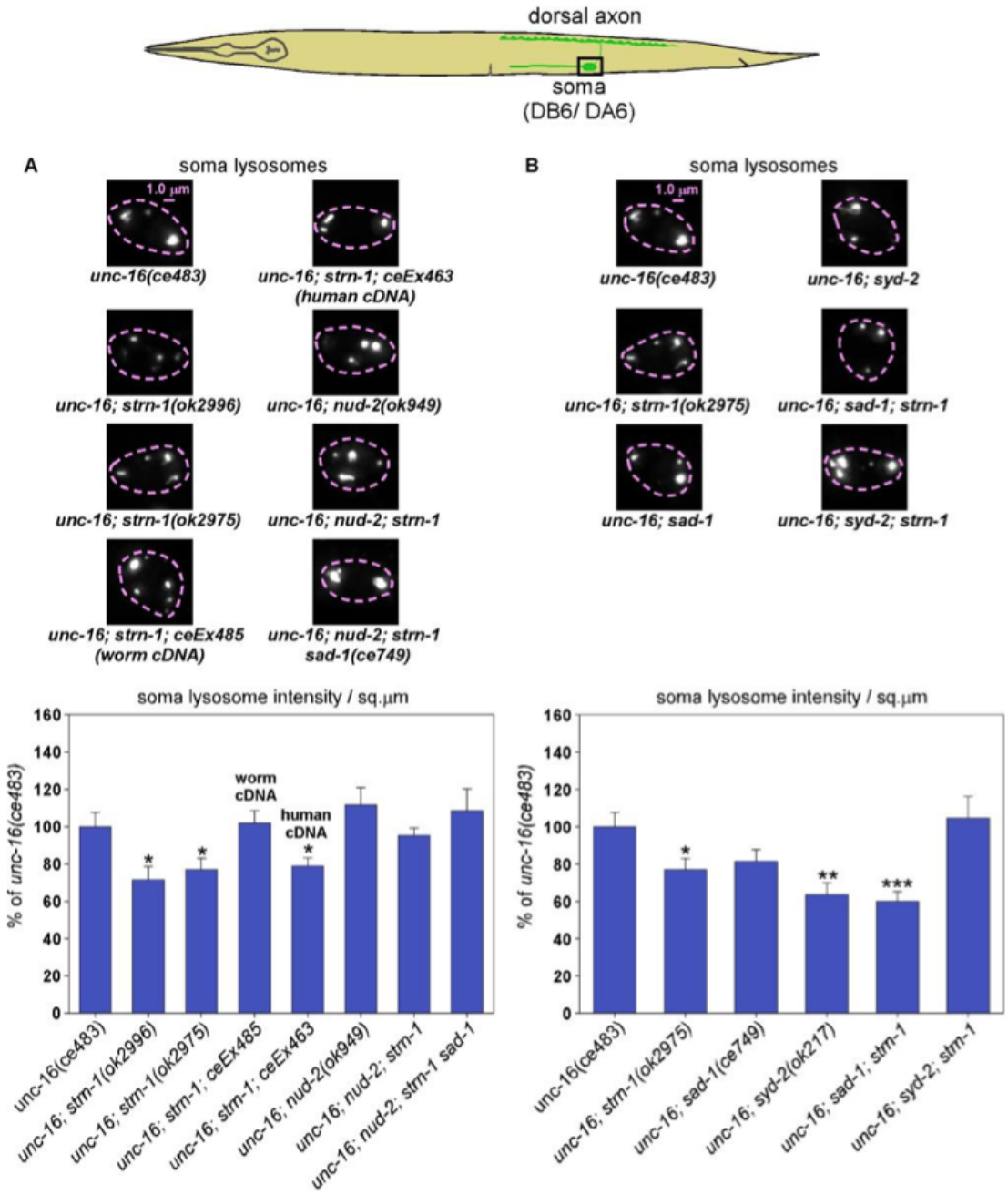

Figure III.9 In an unc-16(-) background, strn-1 null mutations are associated with a significant dynein-dependent depletion of lysosome density in cell somas. A-B. Rectangle in drawing indicates region imaged. Representative, identically-scaled images of lysosome intensity in DB6/ DA9 somas in the indicated genotypes. The lysosome marker CTNS-1-RFP is expressed from the integrated transgene ceIs56. Graph data are means and standard errors from 13-18 animals each. Unmarked bars are not significantly different from wild type. *, **, and *** indicate P-values that are <.05, <.01, or <.001, respectively.

If Sentryn operates within the CSS system, dendritic lysosome accumulation in these mutants should be dynein-dependent. Indeed, we observed reduced dendritic lysosome accumulation in *unc-16;nud-2* mutant animals. The loss of dynein function in both *unc-16;nud-2;strn-1* and *unc-16;nud-2;strn-1;sad*-1 animals reduced dendritic lysosome accumulation to *unc-16* mutant levels, confirming the role for dynein in this mechanism (Figure 3.8A, Figure 3.9A).

Finally, we expected that if Sentryn functioned with CSS proteins, *strn-1* mutants would not display additive phenotypes in mutant backgrounds for these proteins. Indeed, we observed similar levels of dendritic lysosome accumulation in *unc-16;strn-1* as *unc-16;sad-1*, and *unc-16;sad-1;strn-1*, (Figure 3.8B). Lysosome levels in *unc-16;syd-2;strn-1* were slightly higher than in *unc-16;syd-2* alone. These results suggest that Sentryn functions largely overlap with the CSS proteins SAD Kinase and Liprin-α to regulate lysosome trafficking in dendrites.

6. Sentryn promotes removal of endosomes from axons and prevents their accumulation in dendrites

We next examined early endosome distribution in *unc-16/JIP3* mutants. As with lysosomes, UNC-16/JIP3 promotes minus-end transport of early endosomes from axon terminals to dendrites. Using a mCherry::SYN-13 early endosome marker, we found that *unc-16;strn-1* double mutant animals displayed a similar “rescue” effect on early endosome distribution. Dendrites showed an almost 5-fold increase in early endosomes compared to *unc*-16 alone, and *unc-16;strn-1* axons showed a slight reduction of accumulated endosomes (Figure 3.11A,B).

These results suggest that Sentryn plays a similar role as other CSS proteins in regulating UNC-16/JIP3 interaction with early endosome transport. Interestingly, in a *strn-1* single mutant background, early endosomes were reduced ~70% in axons compared to wild-type (Figure 3.11A). Dendritic levels were unchanged (Figure 3.11B). These results suggest that Sentryn plays an important role in clearing early endosomes from axons.

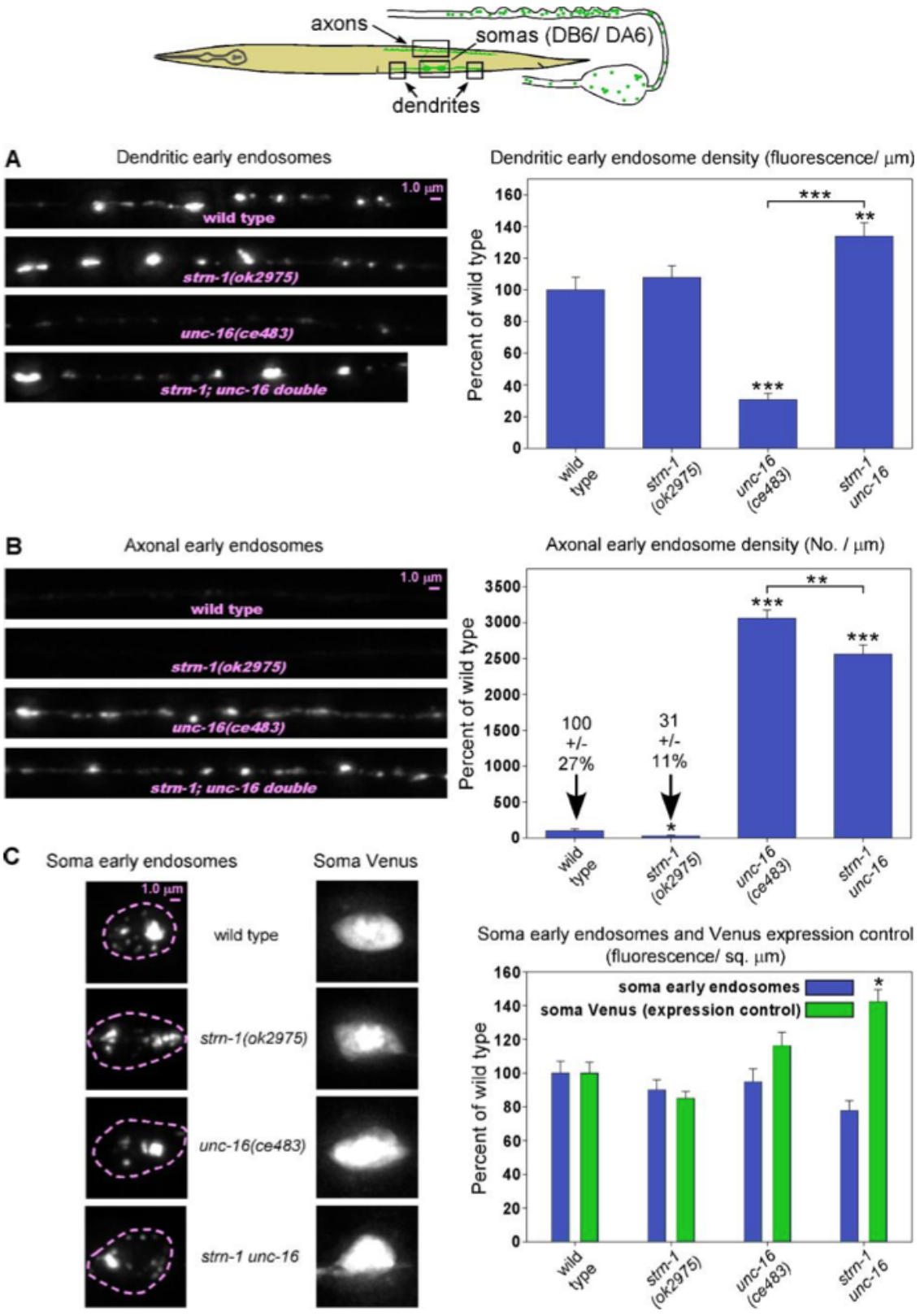

Figure III.10 In *unc-16* mutant neurons, Sentryn inhibits the minus-end accumulation of early endosomes. A-C. Rectangles in the drawing indicate regions imaged. Representative images and

quantification of early endosome density in the indicated regions of DA6/ DB6 cholinergic motor neurons in the indicated genotypes. The early endosomes marker mCherry-SYN-13 is expressed from the integrated transgene ceIs259. Representative images are identically scaled. We quantified endosome density by fluorescence intensity per um in the dendrite and soma (where puncta were more concentrated) and by number per um in the axon. Graph data are means and standard errors from 14-15 animals each. Unmarked bars in (A) and (B) are not significantly different from wild type. Unmarked bars in (C) are not significantly different from their corresponding color bar in an unc-16(+) background (left 2 strains) or an unc-16(-) background (right 2 strains). *, **, and *** indicate P-values that are <.05, <.01, or <.001, respectively. Asterisks that are not above relationship bars compare the indicated bar to wild type in (A) and (B). The asterisk in (C) compares the indicated bar to its corresponding color in the unc-16(ce483) single mutant group. Data collected by Miller lab.

To confirm that *unc-16* or *strn-1* mutation did not affect expression of the early endosomal marker, we co-expressed soluble YFP with this marker. We quantified fluorescence in both channels at the soma and found no significant changes in fluorescence that would impact our interpretation of these results (Figure 3.10C).

7. Sentryn functions with CSS system SAD Kinase and Liprin-α to regulate SV distribution at synapses

We next sought to examine Sentryn's role in regulating SVs at synapses. We examined the SV marker GFP::RAB-3 expressed in cholinergic motor neuron DA9. Two separate mutant alleles of *strn-1* showed reduced SV density in the synaptic region of this neuron (Figure 3.11A, Figure 3.12A). These phenotypes were each rescued to wild-type levels with cell autonomous expression of Sentryn cDNA (Figure 3.12D). These results are consistent with our model of Sentryn antagonizing dynein-dependent transport. We observed all combinations of single, double, and triple mutants of Sentryn, SAD Kinase, and Liprin-α. *sad-1* mutants showed reduced

SV density at the synaptic region that was similar to *strn*-1 levels. *syd-2* mutants showed a more severe reduction of SVs than either *strn-1* or *sad-1* (Figure 3.11). A double mutant of *strn-1;sad-1* had a steeper reduction of synaptic SV density than either single mutant, but reached the same level as *syd-2* alone (Figure 3.11A). In fact, each combination of *strn-1;syd-2, sad-1;syd-2,* and *strn-1;sad-1;syd-2* resulted in SV density reductions similar to *syd-2* alone (Figure 3.11A). These results indicate that Sentryn, SAD Kinase, and Liprin-α all operate in the same system. While Sentryn and SAD Kinase likely have one or more independent functions, their combined functions enable that of Liprin-α.

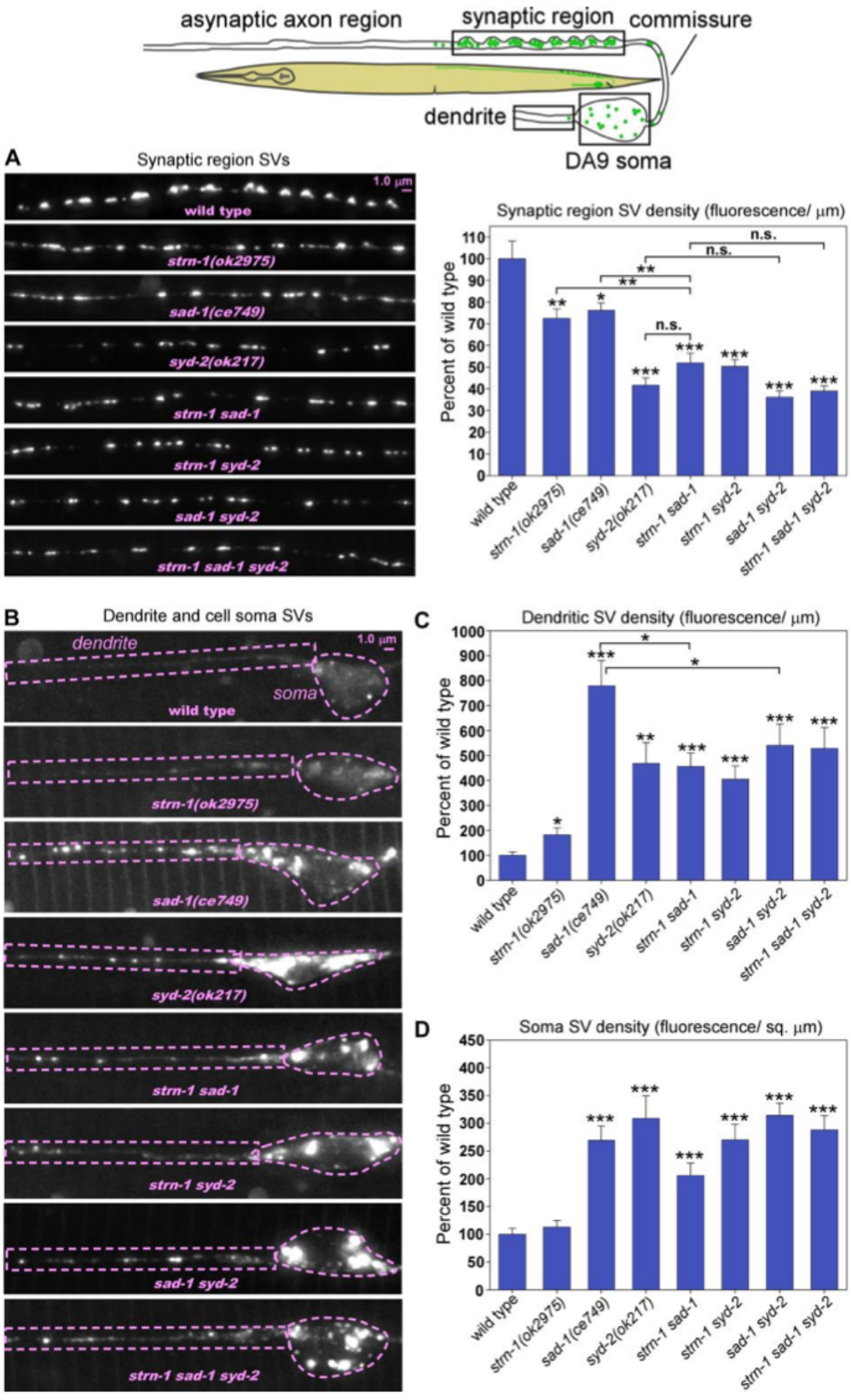
asynaptic axon region
synaptic region
commissure
dendrite
DA9 soma
A
Synaptic region SVs
1.0 µm
wild type
strn-1(ok2975)
sad-1(ce749)
syd-2(ok217)
strn-1 sad-1
strn-1 syd-2
sad-1 syd-2
strn-1 sad-1 syd-2
Synaptic region SV density (fluorescence/ µm)
Percent of wild type
n.s.
B
Dendrite and cell soma SVs
dendrite
soma
C
Dendritic SV density (fluorescence/ µm)
D
Soma SV density (fluorescence/ sq. µm)

Figure III.11 Sentryn acts with the CSS proteins SAD-1 and SYD-2 to ensure that optimal levels of SVs accumulate in the synaptic region. A-D. Rectangles in the drawing indicate regions imaged. Representative images and quantification of SV density in the indicated regions of the DA9 cholinergic motor neuron in the indicated genotypes. The SV marker GFP-RAB-3 is expressed from the integrated transgene wyIs85. Representative images are identically scaled for each region. Dashed lines outline the dendrite and soma regions. Graph data are means and standard errors from 14-15 animals each. Unmarked bars are not significantly different from wild type. *, **, and *** indicate P-values that are <.05, <.01, or <.001, respectively. Asterisks that are not above relationship bars compare the indicated bar to wild type. We also quantified SV levels in the strn-1 null mutant the synaptic region of a different motor neuron (DB7) using a different integrated transgene (ceIs263) (Edwards et al., 2015b) and got a value similar to that of DA9 (69 +/- 5% of wild type; N=13; P=.001). Data collected by Miller lab.

When we measured GFP::RAB-3 signal at the soma and dendrites, we found mostly similar results. Wild type animals contain a small number of SVs in these areas compared to the synaptic region. In *strn-1* mutants, dendritic SVs were slightly higher than wild type, though they did not change at the soma (Figure 3.11B-D). Mutant *sad-1* and *syd*-2 each resulted in dramatic increases in SVs at both dendrites and somas (Figure 3.11B-D; Figure 3.12B-D). Interestingly, dendritic SV density in *strn-1;sad-1* and *sad-1;syd-2* mutants was lower than *sad-1* alone. We do not know the reason for this phenotype. Still, no other genetic combinations showed additivity. We therefore conclude that Sentryn, SAD Kinase, and Liprin-α each operate in the same system to regulate SV distribution at somas and dendrites, although Sentryn seems to play a minor role here.

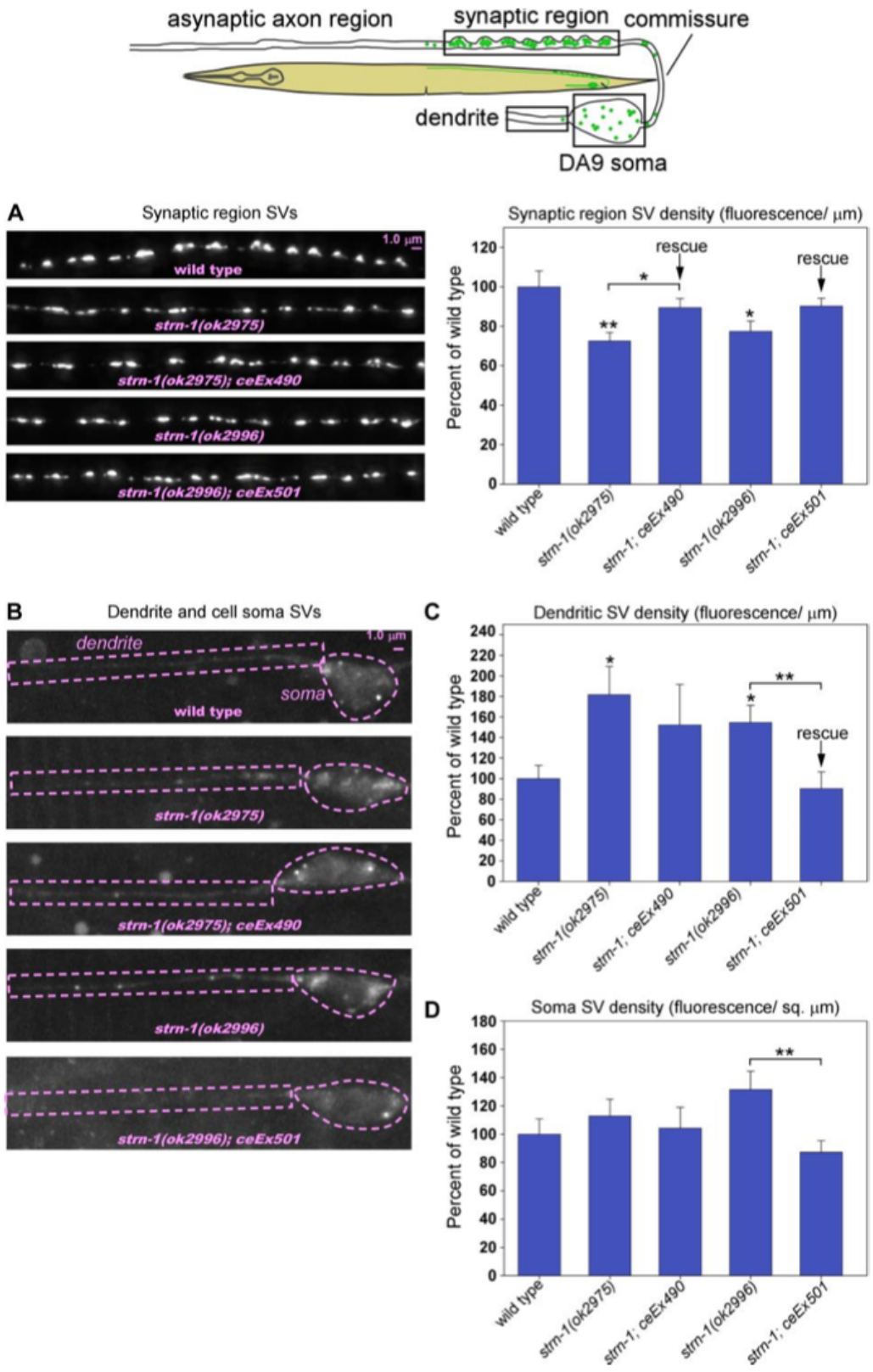

Figure III.12 Sentryn acts cell-autonomously in DA9 to optimize the transport of SVs to clusters and to keep SVs out of dendrites. A-D. Rectangles in the drawing indicate regions imaged.

Representative images and quantification of SV density in the indicated regions of the DA9 cholinergic motor neuron in the indicated genotypes. The SV marker GFP-RAB-3 is expressed from the integrated transgene wyIs85. Representative images are identically scaled for each region. Dashed lines outline the dendrite and soma regions. Graph data are means and standard errors from 12-16 animals each. Unmarked bars are not significantly different from wild type. * and ** indicate P-values that are <.05 or <.01, respectively. Asterisks that are not above relationship bars compare the indicated bar to wild type.

8. Sentryn functions with CSS system proteins SAD-1, and SYD-2 to promote SV capture in the synaptic region

While Sentryn, SAD Kinase, and Liprin-α seem to influence DCV and SV levels at axons, somas, and dendrites, the details of this function are still unclear. It is likely that Sentryn and CSS proteins regulate transport motors for SVs and other organelles. It is also possible that these proteins assist in capturing SVs at synapses. Reduced SV density in these mutants could therefore result from either a transport defect or a failure to capture SVs in the synaptic region.

To distinguish between a transport and capture role for Sentryn, SAD-1, and SYD-2, we examined the entire .05 mm axon of DA9. This neuron contains a short proximal asynaptic region near the cell body, followed by a short synaptic region, and a long distal asynaptic region (White et al., 1986; Klassen and Shen, 2007). In DA9, a capture defect could manifest as lower SV density in the synaptic region, with more SVs in the flanking asynaptic regions. We used a large field-of-view camera with multiple, overlapping images to create high-resolution images of fluorescently tagged SVs in the entire DA9 axon. We created plot profiles of these fluorescence patterns and found that in wild-type animals, SVs were enriched in a 100um synaptic region of the axon and absent from flanking regions (Figure 3. 13). We set a threshold for fluorescence

that indicated synaptic levels of enrichment. We then measured the length of region above that threshold in mutant worms, such that a longer region would indicate a capture defect, as SVs were transported away from synapses.

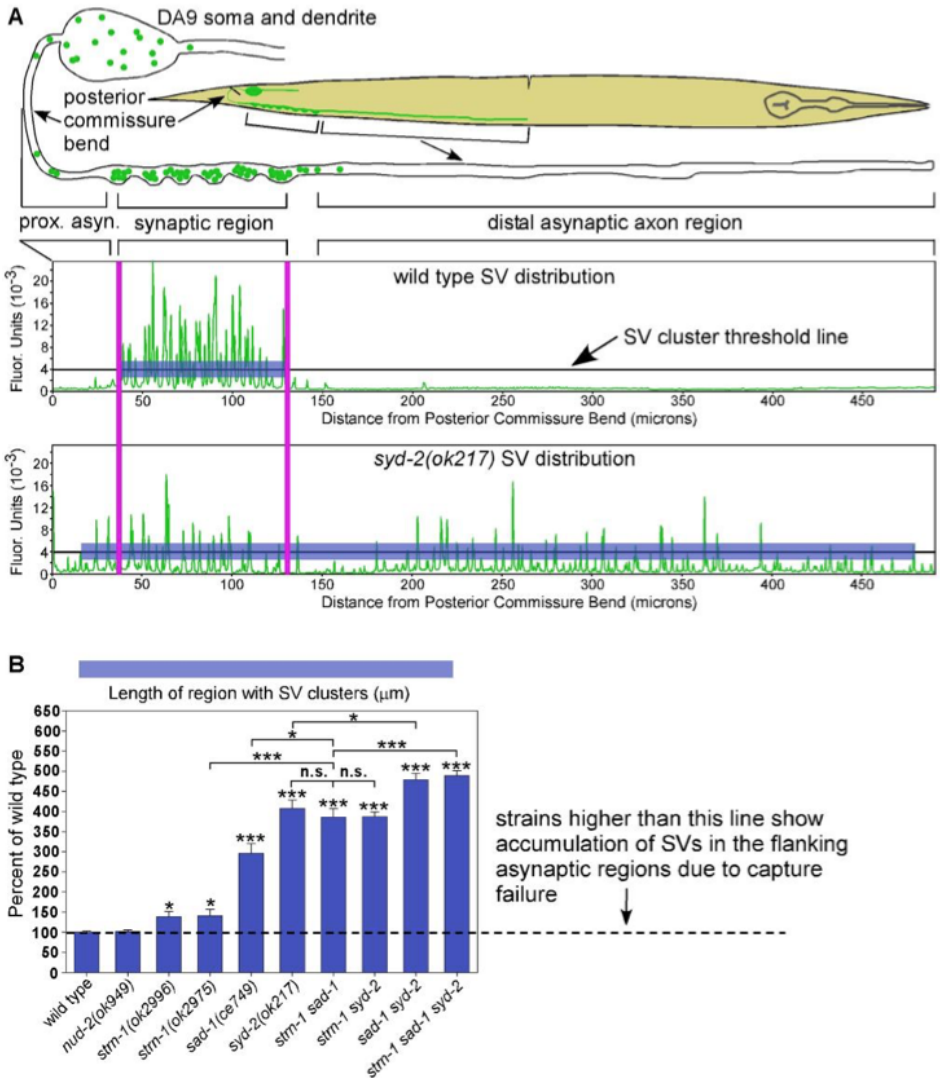

Figure III.13. Sentryn acts with the CSS proteins SAD-1 and SYD-2 to promote the capture of SVs in the synaptic region. A. Drawing indicates regions of the DA9 motor neuron. Graphs plot fluorescence intensity of the SV marker GFP-RAB-3 as a function of distance from the posterior commissure bend. A threshold line indicates the intensity cut-off used for defining SV clusters. Blue highlighted segments indicate regions exceeding the threshold in wild type and a syd-2 null mutant. Pink vertical lines connect identical locations in wild type and the syd-2 mutant to show that SVs mislocalize both proximal and distal to the synaptic region in syd-2 mutants. High

resolution images acquired with a large field-of view Flash 4.0 camera were used to reconstruct the dorsal axon from multiple images. GFP-RAB-3 is expressed from the integrated transgene array wyIs85. **B.** Graph quantifies SV capture efficiency in the indicated genotypes by measuring the length of the region with SV clusters exceeding the threshold line (shown in (A)). This quantifies the extent to which SVs have overshot the synaptic region and have moved toward microtubule plus ends in the long asynaptic region. Graph data are means and standard errors from 14-15 animals each. * and *** indicate P-values that are <.05 or <.001, respectively. Asterisks that are not associated with relationship bars compare the indicated strain to wild type. Data collected by Miller lab.

In each of the single mutants *strn-1*, *sad-1,* and *syd-2*, the region containing SVs was expanded. *strn-1* mutants showed the mildest effect, with an SV-containing region only slightly longer than wild-type. *sad-1* mutants showed a more severe effect, and *syd-2* mutants showed the most striking expansion, with a SV-enriched region four times longer than wild type (Figure 3.13B). As predicted, these results suggest that Sentryn, SAD Kinase, and SYD-2 regulate SV capture at synapses. While *strn-1;sad-1* double mutants showed some additivity, their expanded SV-containing regions were no longer than that seen in *syd-2* mutants or *strn-1;syd-2* double mutants. These results indicate that Sentryn operates in the same pathway as SYD-2. Interestingly, *sad-1;syd-2* double mutants showed a more expanded region than *syd-2* single mutants. Moreover, *strn-1;sad-2;syd-2* mutants showed a longer SV-enriched region than *strn-1;sad-1* mutants (Figure 3.13B). Thus, it appears that SAD Kinase and SYD-2 can function independently to promote SV capture at synapses. Sentryn and SAD Kinase likely have at least one non-overlapping function, but their combined actions enable most of SYD-2 function to capture SVs at synapses.

9. Sentryn and SAD Kinase capture DCVs at the synaptic region of axons

We next examined DCV capture in these animals using a similar experimental design. We created a transgenic animal expressing DCV cargo solely in the DA9 neuron. DCVs display a looser spatial relationship to synapses as compared to SVs which cluster tightly near active zones (Hammarlund et al., 2008; Hoover et al., 2014). Therefore, we first sought to determine whether DCVs, like SVs, are in fact captured at synapses. We reconstructed images of the DA9 axon as describe above and observed that DCVs are in fact enriched at the synaptic region and excluded from the asynaptic region in wild type animals (Figure 3.14A). This distribution pattern is similar to that observed for SVs and provides evidence that DCVs are captured at synapses.

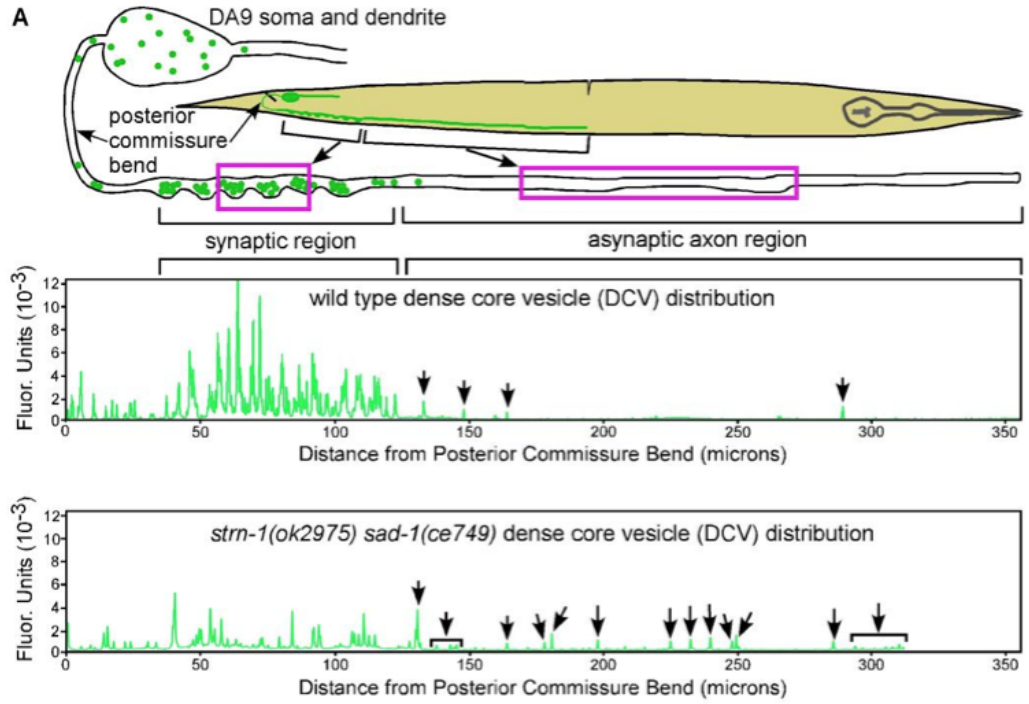
A
DA9 soma and dendrite
posterior commissure bend
synaptic region
asynaptic axon region
wild type dense core vesicle (DCV) distribution
Fluor. Units (10-3)
Distance from Posterior Commissure Bend (microns)
strn-1(ok2975) sad-1(ce749) dense core vesicle (DCV) distribution
Fluor. Units (10-3)
Distance from Posterior Commissure Bend (microns)

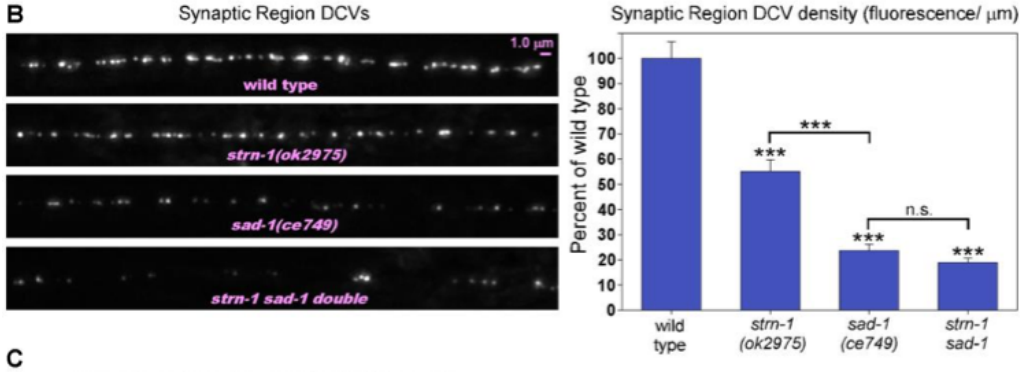
B
Synaptic Region DCVs
1.0 µm
wild type
strn-1(ok2975)
sad-1(ce749)
strn-1 sad-1 double
Synaptic Region DCV density (fluorescence/ µm)
Percent of wild type
***
***
n.s.
***
wild type
strn-1 (ok2975)
sad-1 (ce749)
strn-1 sad-1

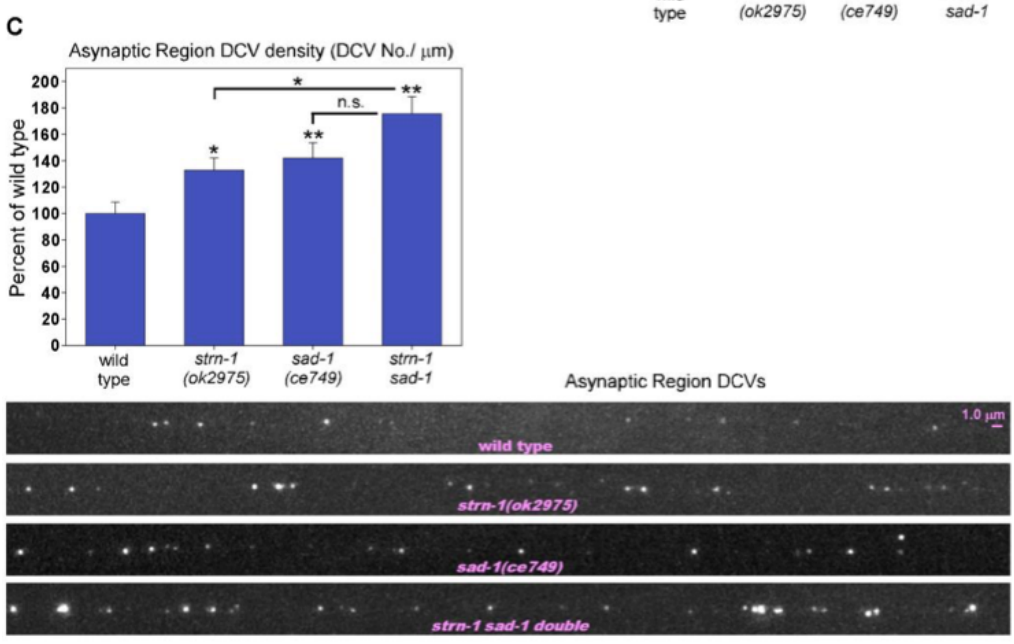
C
Asynaptic Region DCV density (DCV No./ µm)
Percent of wild type
*
n.s.
**
*
**
wild type
strn-1 (ok2975)
sad-1 (ce749)
strn-1 sad-1
Asynaptic Region DCVs
1.0 µm
wild type
strn-1(ok2975)
sad-1(ce749)
strn-1 sad-1 double

Figure III.14. Sentryn and SAD-1 inhibit the plus-end accumulation of DCVs in distal asynaptic region to keep them captured in the synaptic region. A. Rectangles in drawing indicate regions of the DA9 motor neuron that were imaged. Graphs plot fluorescence intensity of the DCV marker INS- 22-Emerald as a function of distance from the posterior commissure bend. High resolution images acquired with a large field-of-view Flash 4.0 camera were used to reconstruct the dorsal axon from multiple images. Arrows indicate DCVs in the asynaptic region. In wildtype, DCVs are tightly captured in a small region of the axon and do not significantly accumulate in the long asynaptic region, whereas, in strn-1 sad-1 double mutants, DCVs do accumulate in this region (arrows). INS-22- Emerald is expressed from the genomically-integrated transgene array ceIs308. See Figure S7 for mCherry expression controls showing that the observed differences are not caused by changes in expression from the transgene. B-C. Representative images and quantification of DCV fluorescence/ um in the synaptic region (B) or DCV number/ um in the asynaptic region (C) in the indicated genotypes. Note that only the center part of each region was imaged as indicated in the drawing in (A). The DCV marker INS-22-Emerald is expressed from the integrated transgene array ceIs308. Graph data are means and standard errors from 14-15 animals each. n.s., *, **, and *** indicate P values that are not significant, <.05, <.01, or <.001, respectively. Data collected by Miller lab.

We next compared DCV density (fluorescence/um) at synaptic regions where DCVs should be captured versus the asynaptic region distal to synapses, where uncaptured DCVs might escape. DCV density in the synaptic region was reduced in *strn-1, sad-1,* and *strn-1;sad-1* animals. This phenotype was most severe in *strn-1;sad-1* mutants. We observed a corresponding increase in DCV density in the asynaptic region of each of these mutants, and again observed the strongest effect in *strn-1;sad-1* mutants. We found similar results in a *syd-2(ok217)* null mutant "(synaptic region DCV density reduced to 17.5+/- 1.5% of wild type, P<.0001; asynaptic region DCV density increased to 136.1 +/- 9.5% of wild type, P=.0094; N=14 animals)." The levels of DCVs in the synaptic region in both the *strn-1;sad-1* and *syd-2* mutant animals represented a nearly random distribution between synaptic and asynaptic regions. These results suggest that Sentryn, SAD Kinase, and SYD-2 operate as DCV capture proteins, but that additional proteins may play a role in capturing DCVs at the synapse.

10. Sentryn and SAD Kinase operate in the same pathway to regulate DCV trafficking

As an additional test of our transgenetic experiments, and to confirm that our findings were not an artifact of overexpressed fluorescent markers, we used immunostaining to examine endogenous DCV localization. First, we performed immunostaining on non-transgenic animals using an antibody against EGL-21 (Carboxypeptidase E), a neuropeptide processing enzyme that is co-packaged with neuropeptides in DCVs (Cool et al., 1997; Fricker 1988; Rindler, 1998, Hoover et al., 2014). Examining synapses in the dorsal cord, where cell somas and dendrites are absent, we found that both *strn-1* and *sad-1* null mutants displayed a loss of DCV signal in axons. A similar loss of axonal DCVs was observed in the *strn-1;sad-1* double mutant, suggesting that these proteins operate in the same pathway to regulate DCV trafficking (Figure 3.15A). We did not image somas in this experiment because they are tightly packed with axons and dendrites in the ventral cord, thus making it difficult to image them specifically.

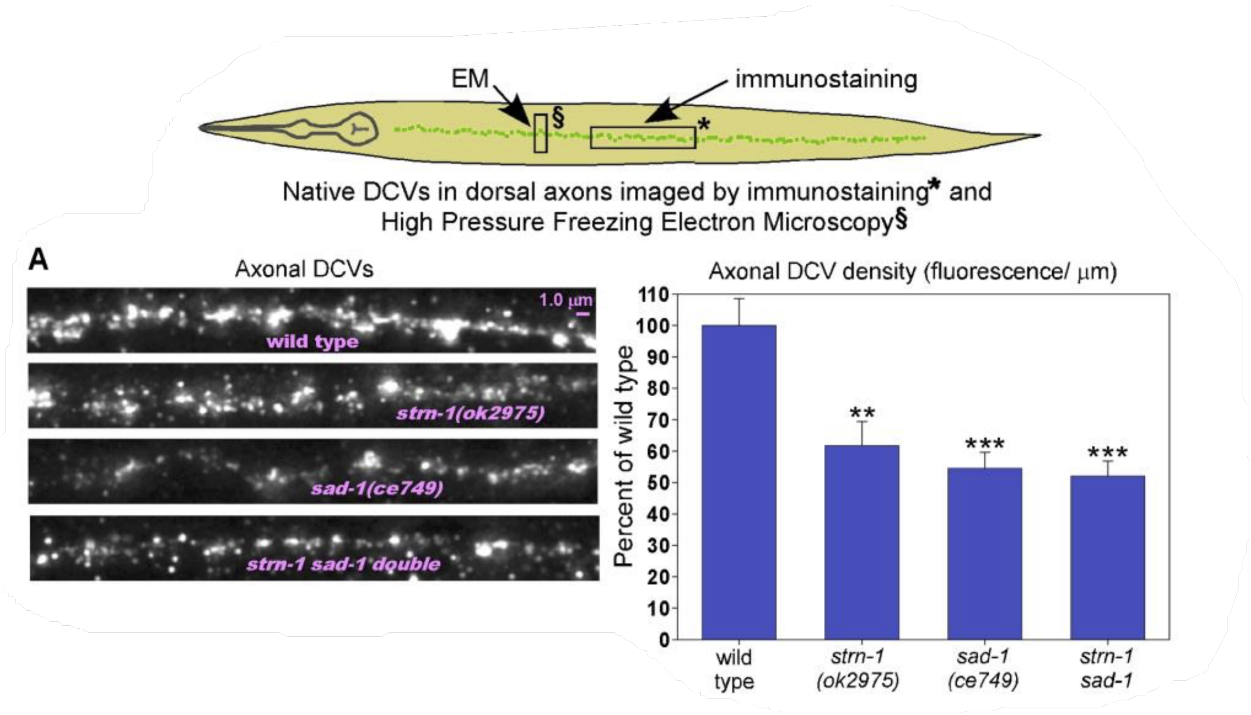

Figure III.15. DCV transport/ capture defects in mutants lacking Sentryn and/ or SAD Kinase imaged by immunostaining. Rectangles in drawing show regions imaged in (A) Immunostaining and (B) HPF EM (Figure 3.16). Representative images and quantification of native EGL-21 (Carboxypeptidase E) immunostaining in dorsal cord axons of animals with the indicated genotypes. Graph data are means and standard errors from 18 animals each. ** and *** indicate P-values that are <.01 or <.001, respectively. Data collected by Miller lab.

To confirm that these results reflect DCV localization specifically at synapses, we employed high pressure freeze electron microscopy (HPF EM) to examine well-preserved ultrastructure at these synapses. We reconstructed serial sections of 40nm thickness in wild type, *strn-1*, *sad-1*, and *strn-1;sad-1* double mutants. We scored an average of 15 cholinergic motor neuron synapses in the dorsal cord for each strain while blinded to genotype. Each synapse spanned an average of 13 sections (Figure 3.16).

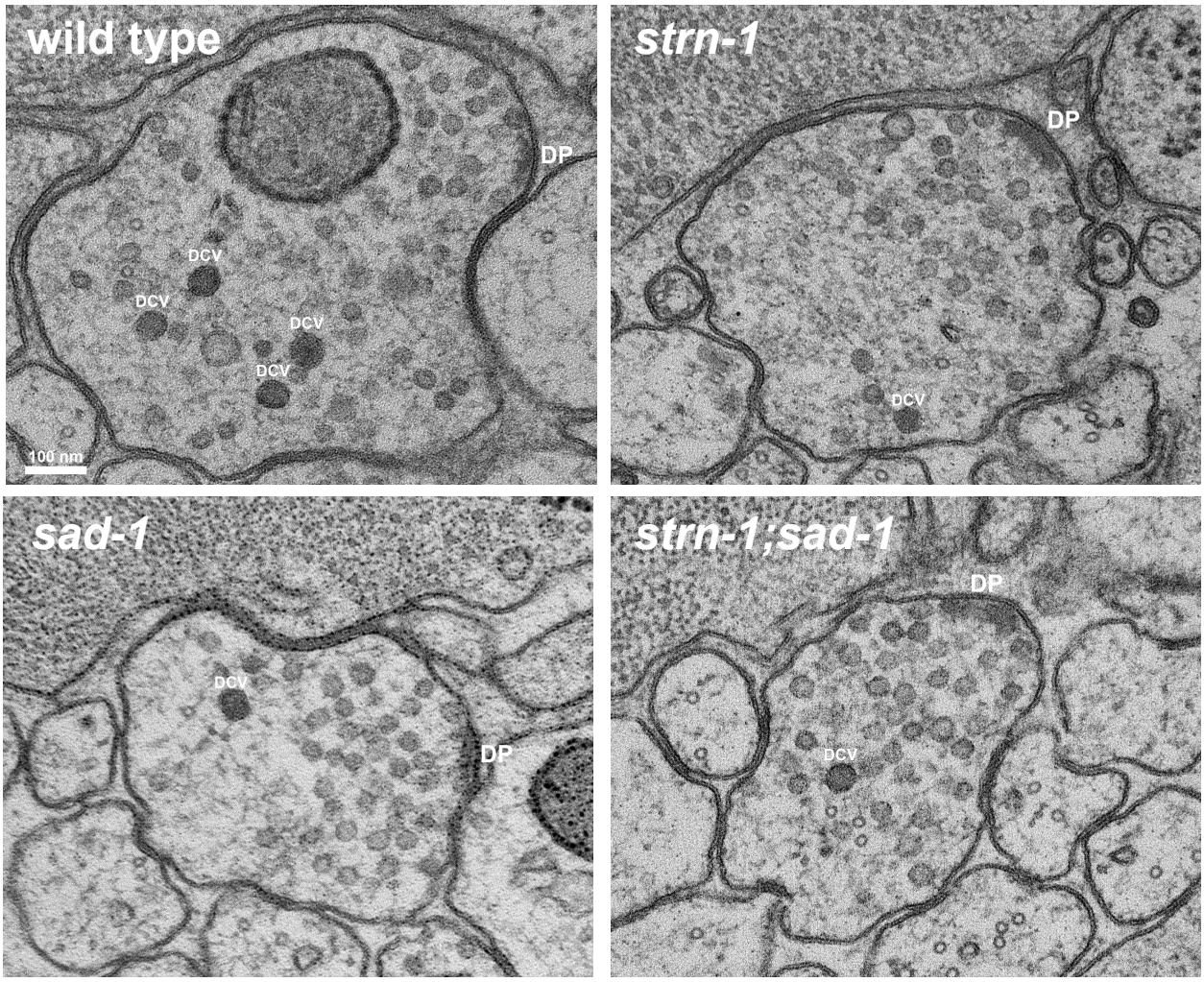

Figure III.16. Representative single-section EM images and quantification of cholinergic motor neuron synapses visualized by High Pressure Freezing Electron Microscopy (HPF EM). Labels in the representative images are as follows: DCV (dense core vesicle), DP (dense projection). Note that each single 40 nm section shown in the representative images is only 7 – 10% of a synapse. Data collected by Laura Manning.

Wild-type synapses contained an average of 29 DCVs across those synaptic sections. This number was reduced to 38% of wild-type in *strn-1* synapses, 48% in *sad-1* synapses, and 22% in *strn-1;sad-1* synapses (Figure 3.17A). Overall, these observations support our findings using genetic tags as well as immunostaining. We measured the distribution of each DCV to the DP, which is located at the center of the synapse. As observed in previous studies, we noted that

DCVs did not localize tightly to the DP (Figure 3.17B-D). The loss of DCVs in both *strn-1* and *strn-1;sad-1* double mutants appeared evenly distributed throughout the synapse (Figure 3.17B,C). In *strn-1;sad-1* synapses, DCVs were completely absent between 495 and 693 nm from the dense projection (Figure 3.17D).

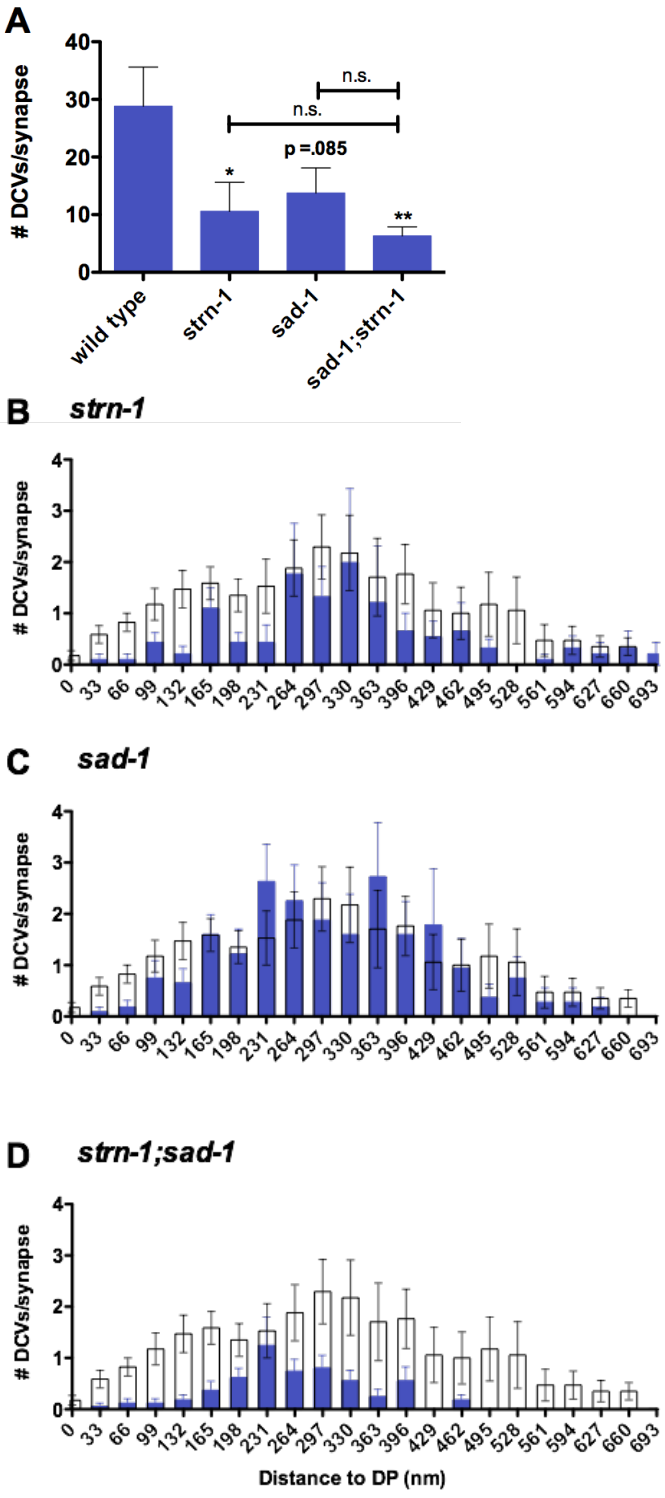

Figure III.17. DCV transport/ capture defects in mutants lacking Sentryn and/ or SAD Kinase imaged by HPF/FS EM. A. Total number of DCVs present in each synapse. Graph data are means and standard errors of total DCVs from 17, 12, 17, and 16 synapses reconstructed from 220, 115, 150, and 134 40 nm sections for wild type, strn-1, sad-1, and strn-1 sad-1 double mutants, respectively. * and ** indicate P-values that are <.05 or <.01, respectively. **B-D.** The distance from each dense core vesicle to the dense projection, per synapse, was measured and plotted as a frequency distribution. Wild type measurements are shown as white/clear bars with a black outline. (B) strn-1, (C), sad-1 and (D) sad-1;strn-1 are shown overlaid in blue. Data collected by Laura Manning.

11. Sentryn and SAD Kinase contribute to presynaptic ultrastructure

We also observed SV capture defects at the EM level. While wild-type animals contained an average of ~412 SVs at each synapse, this number was reduced in *strn-1* and *sad-1* mutants to 63% and 72% of wild-type, respectively (Figure 3.18A). Although these reductions did not reach statistical significance, the pattern was similar to those obtained looking at our transgenic SV tags. In the *strn-1;sad-1* double mutant however, SVs were further and significantly reduced to 52% of wild-type (Figure 3.18A).

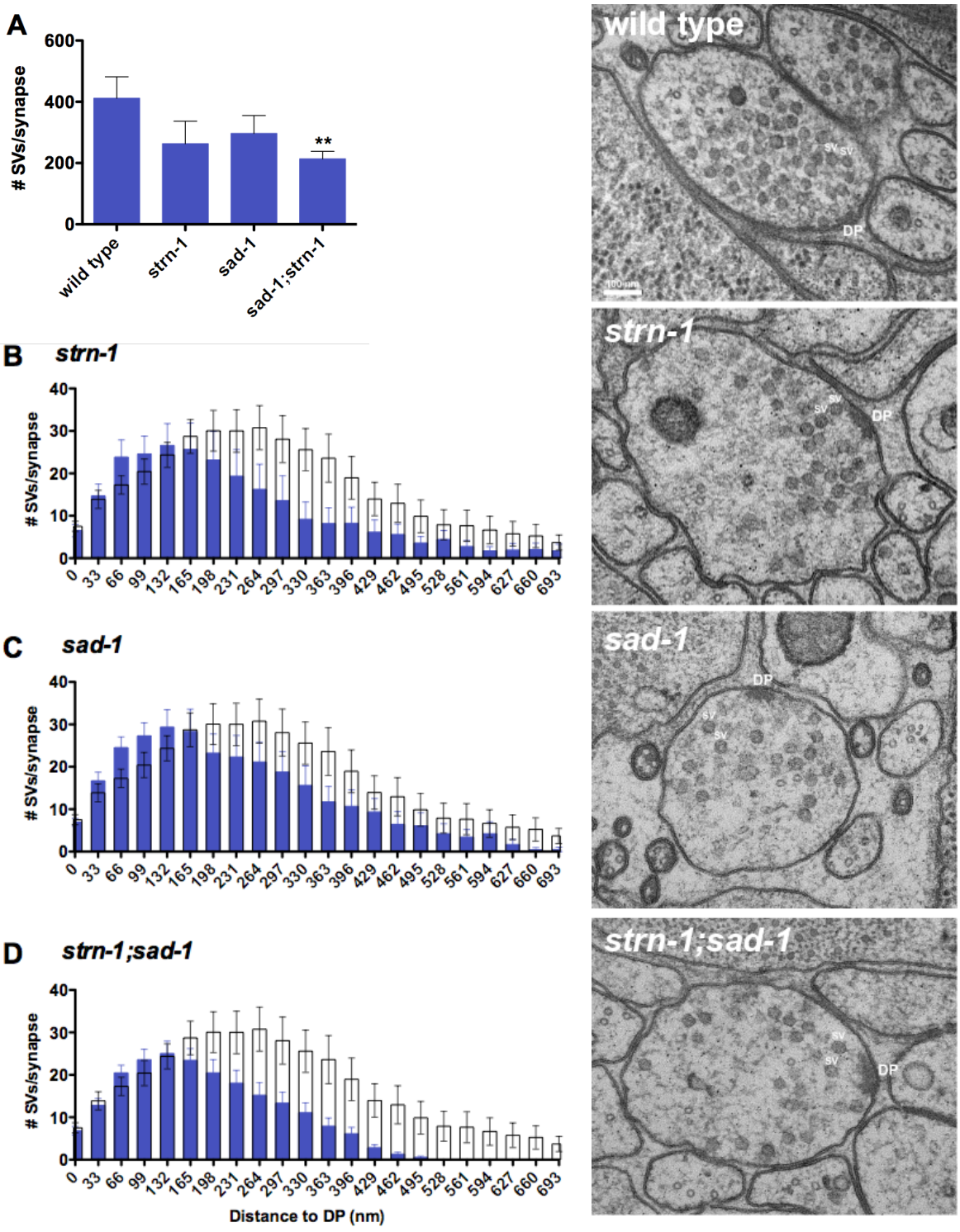

Figure III.18. Synaptic vesicle distribution is altered in CSS system mutants. A. Graph plotting number of SVs, both docked and undocked, in cholinergic motor neuron synapses visualized by High Pressure Freezing Electron Microscopy (HPF EM). **B-D.** The distance from each synaptic

vesicle, including docked and undocked vesicles, to the dense projection, was measured per synapse. Wild type measurements are shown as white or clear bars with a black outline in each graph. (B/F) strn-1, (C/G), sad-1 and (D/H) sad-1;strn-1 are shown overlaid in blue. To the right of each graph is a representative 40 nm single-section images of synapses from the indicated genotype, taken near the center of the dense projection. Two of many SVs in each image are labeled "SV", along with the dense projection ("DP"). Note that each single 40 nm section is only 7 – 10% of a synapse. Graph data are means and standard errors from 17, 12, 17, and 16 synapses reconstructed from 220, 115, 150, and 134 thin (40 nm) sections for wild type, strn-1, sad-1, and strn-1 sad-1 double mutants, respectively. ** indicates P-values that are <=.01. Data collected by Laura Manning.

Synaptic vesicles exhibit a stereotyped distribution to the DP, and most vesicles that fuse are located within ~300 nm of the DP (Figure 3.18B-D; Watanabe et al., 2013; Hammarlund et al., 2008). In *strn-1* mutants, the prevalence of vesicles within this 300 nm area matched wild type levels closely, but was reduced at areas further from the active zone (Figure 3.18B). *sad-1* mutant synapses showed a similar, though slightly less exaggerated pattern. This phenotype was most pronounced in *sad-1;strn-1* mutants, which showed dramatic loss of SVs at >200 nm from the DP (Figure 3.18D). This effect suggests that STRN-1 and SAD-1 may help to capture SVs that are located at the periphery of the synapse. Without these proteins, SVs that have been recruited closer the DP remain intact, but distal SVs may be more susceptible to transport.

strn-1 mutants experienced no significant reduction in docked SVs, while *sad-1* mutant synapses contained docked SVs at 66% of wild-type and *strn-1;sad-1* mutants at 53% of wild-type (Figure3.19A). This is similar to previous results in *syd-2* null animals (Kittelmann et al., 2013). We also examined docked SV distribution to the DP (Figure 3.19B-D). Although docking was slightly reduced in each mutant, we did not observe significant loss at either proximal or distal locations in the synapse.

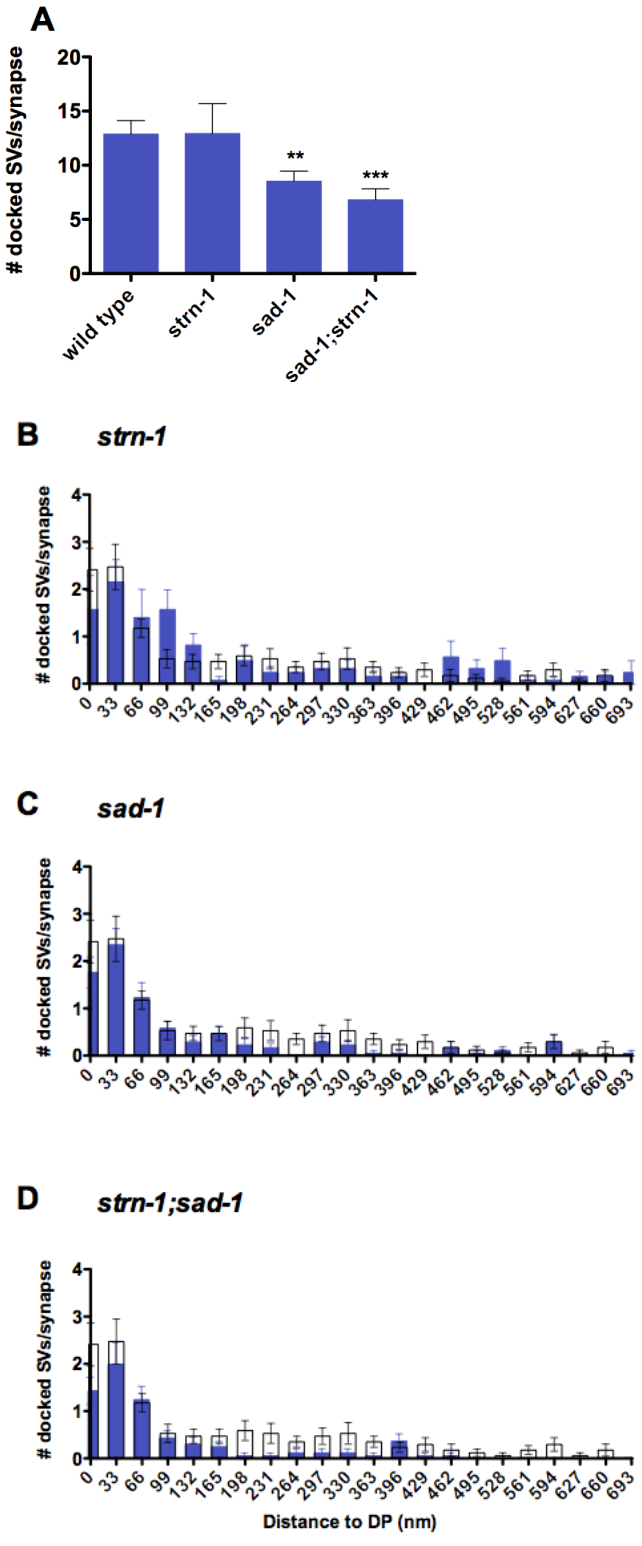

Figure III.19. sad-1 and strn-1;sad-1 mutants show mild docking defects. A. Graph plotting number of docked SVs in cholinergic motor neuron synapses visualized by High Pressure Freezing Electron Microscopy (HPF EM). **B-D.** The distance from each docked synaptic vesicle to the dense projection, was measured per synapse. Wild type measurements are shown as white or clear bars with a black outline in each graph. (B) strn-1, (C), sad-1 and (D) sad-1;strn-1 are shown overlaid in blue. Graph data are means and standard errors from 17, 12, 17, and 16 synapses reconstructed from 220, 115, 150, and 134 thin (40 nm) sections for wild type, strn-1, sad-1, and strn-1 sad-1 double mutants, respectively. ** and ** indicate P-values that are <=.01 or <.001, respectively. Data collected by Laura Manning.

Interestingly, we found that the length of the dense projection, an electron dense structure at the center of the active zone, was reduced in all three mutants, despite normal terminal area (Figure 3.20A; data not shown). This change was most striking in *strn-1;sad-1* mutants, whose dense projection spanned an average of 50% fewer sections than wild type. Previous work has shown that dense projections in *syd-2* mutant synapses show a similar reduction in length. *syd-2* mutants also showed a reduction in the number of docked and undocked SVs contacting the DP (Stigloher et al., 2011). We did not observe these affects in any of the mutants we examined (Figure 3.20B,C). There was a slight but highly variable increase in undocked SVs contacting the DP in *strn*-1 mutants. Together, these findings are consistent with our model that Sentryn and SAD Kinase function with Liprin-α to regulate the synapse.

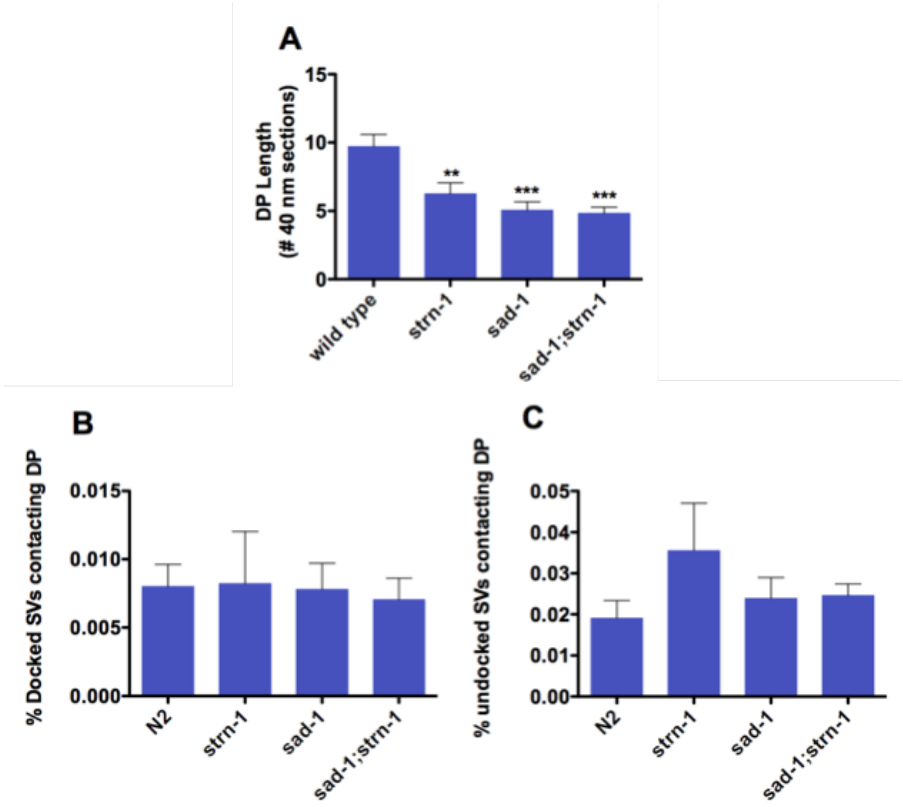

Figure III.20. Presynaptic ultrastructure is significantly altered in mutants lacking Sentryn and/or SAD Kinase. Graph data are means and standard errors from 17, 12, 17, and 16 synapses reconstructed from 220, 115, 150, and 134 thin (40 nm) sections for wild type, strn-1, sad-1, and strn-1 sad-1 double mutants, respectively. ** and ** indicate P-values that are <=.01 or <.001, respectively. **A.** "Dense Projection Length" represents the number of 40 nm cross-sections containing a dense projection that comprise each synapse. **B/C.** The number of docked (B) or undocked (C) synaptic vesicles contacting the

dense projection (distance of 0 nm) as a percentage of total vesicles (docked and undocked) at the synapse.

12. Sentryn is a novel active zone protein that requires SYD-2/Liprin-α to localize to synapses

The CSS proteins SYD-2/Liprin-α and SAD Kinase are both enriched at active zones, which are sites of localized SV capture and exocytosis (Weimer et al., 2006; Hoover et al., 2014; Stigloher et al., 2011; Ackley et al., 2005; Yeh et al., 2005; Fouquet et al., 2009). Since Sentryn appears to operate with these CSS proteins and affect ultrastructure, we imaged fluorescently tagged Sentryn. We found that Sentryn is enriched at synapses and colocalizes tightly with both SAD-1 and UNC-10/RIM (Figure 3.21A). We also imaged a full length, GFP-tagged Sentryn expressed at low levels in the cholinergic motor neuron, DB7. Sentryn::GFP appeared at the ventral tip of synaptic boutons, where active zones organize. In a *syd-2* mutant, Sentryn::GFP was still present in the neuron, but its localization pattern was highly disrupted. A *sad-1* mutation had no effect on Sentryn::GFP localization. These results support a model in which Sentryn is an active zone protein that requires SYD-2/Liprin-α to localize specifically to active zones.

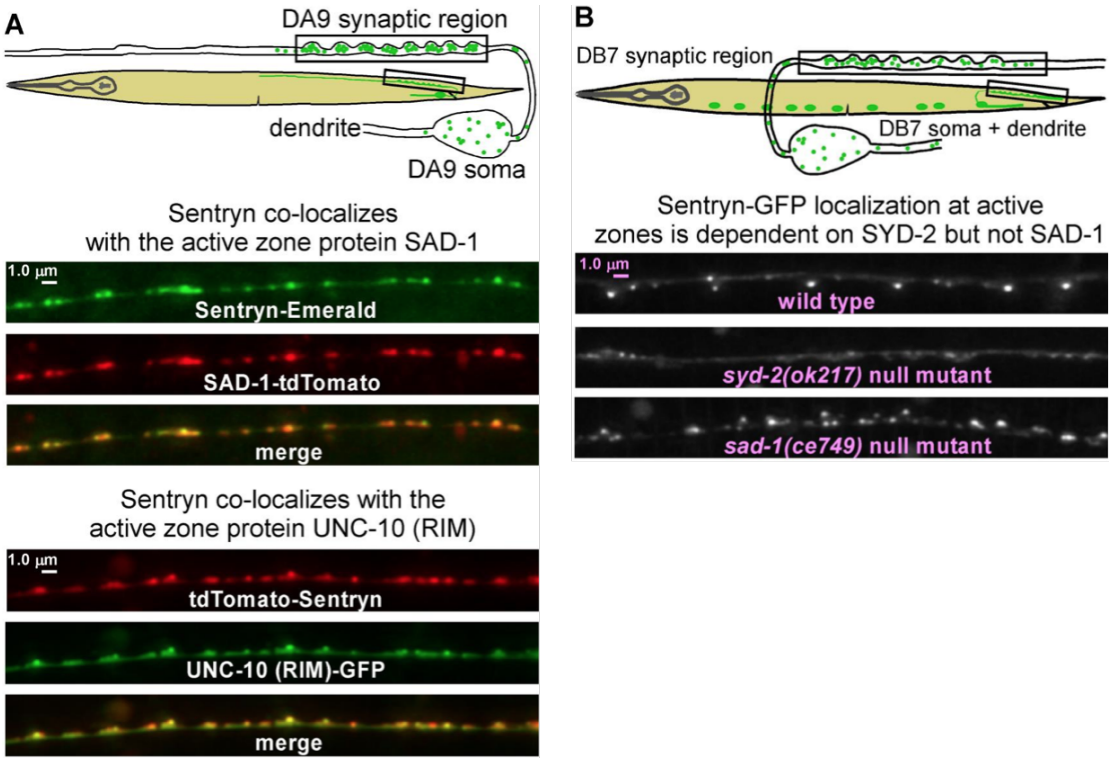

Figure III.21. Sentryn shows a SYD-2–dependent enrichment at active zones. A. Rectangle in drawing shows region imaged. Representative images showing co-localization of Sentryn with the active zone proteins SAD-1 and UNC-10 (RIM) in the DA9 motor neuron synaptic region. Sentryn-Emerald and SAD-1-tdTomato are co-expressed from the ceEx510 transgenic array. tdTomato-Sentryn and UNC-10 [627-974]-GFP are co-expressed from the ceEx503 transgenic array. **B.** Rectangle in drawing shows region imaged. Representative, identically-scaled images showing localization of Sentryn-GFP in the DB7 motor neuron synaptic region in wild type and in the indicated mutant backgrounds. Note that the highly focal localization of Sentryn-GFP is greatly disrupted in the syd-2 null mutant, but that similar amounts of Sentryn are present in the synaptic region in wild type and in the syd-2 null mutant. Data collected by Miller lab.

13. Sentryn, SAD Kinase, and Liprin-α comprise a specialized class of active zone proteins

Since Liprin-α and SAD Kinase seem to regulate SV and DCV transport and are known to be highly enriched near active zones (Ackley et al., 2005; Fouquet et al., 2009; Weimer et al., 2006; Yeh et al., 2005; Inoue et a., 2006), we wondered if additional active zone proteins also contributed to regulating DCV distribution. We examined null mutant backgrounds of seven active zone proteins: *syd-1*, *ELK/ERC/Bruchpilot elks-1, RIM/unc-10, RIM-binding protein rimb-1,*

LAR/ptp-3, git-1, and *CASK/lin-2*. Of these mutant strains, none showed the combined phenotype of lower axonal DCV levels with higher cell soma DCVs. Interestingly, *syd-1* mutants exhibited higher DCV fluorescence in cell somas, but only exhibited a slight, statistically insignificant, reduction in axonal DCV levels. Thus, it is possible that while SYD-1 is important for regulating DCV trafficking at the soma, its function is redundant or non-essential at the synapse. *lin-2* animals showed a slightly lower axonal DCV level with no corresponding change at somas, so we did not pursue this weak phenotype.

We also tested these mutants using the capture failure assay described in Figure 3.13. We examined the length of the synaptic region in DA9 axons in the mutants listed above (Figure 3.22A).

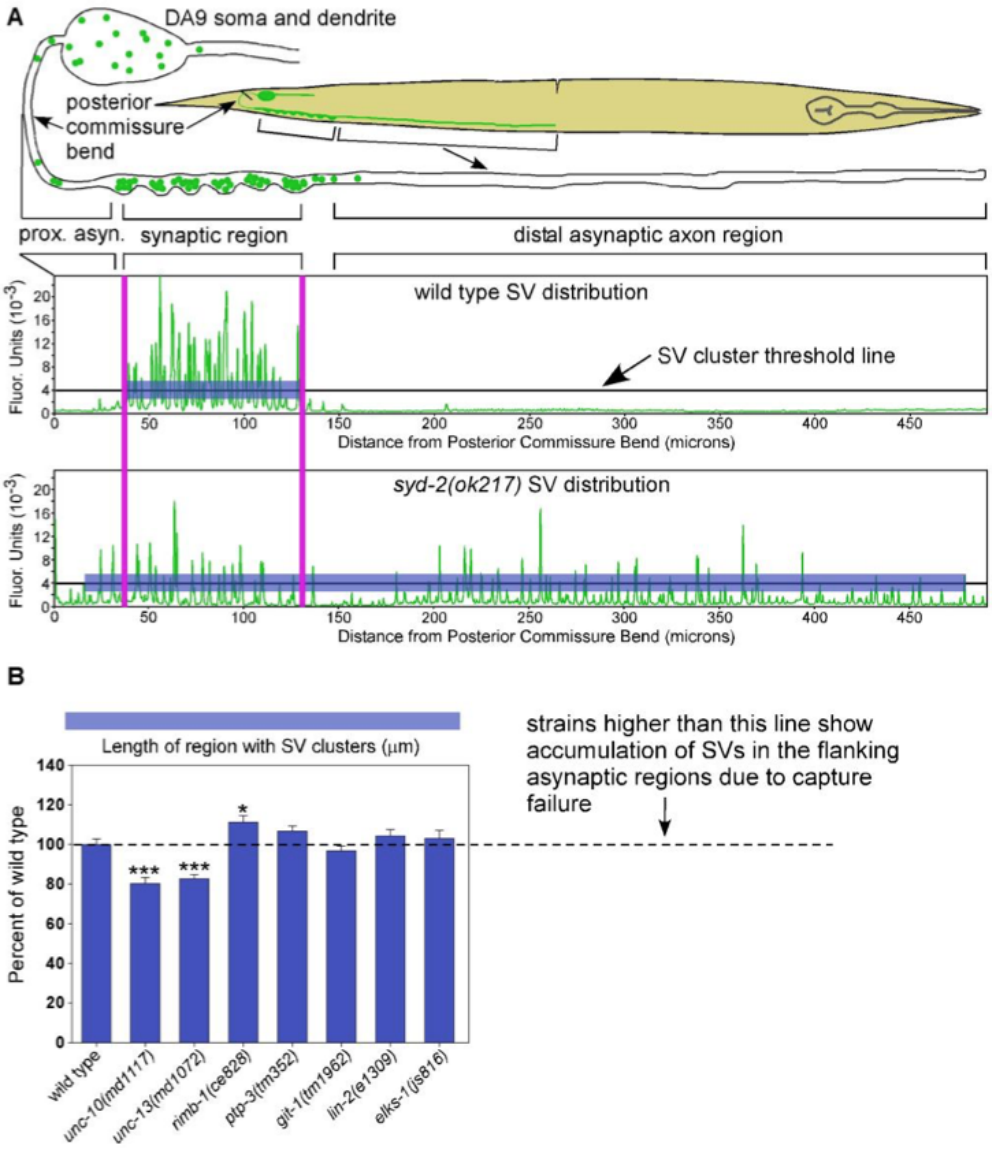

Figure 22. Null mutations in most non-CSS active zone-enriched proteins do not impair SV capture. A. Drawing indicates regions of the DA9 motor neuron. Graphs plot fluorescence intensity of the SV marker GFP-RAB-3 as a function of distance from the posterior commissure bend. A threshold line indicates the intensity cut-off used for defining SV clusters. Blue highlighted segments indicate regions exceeding the threshold in wild type and a syd-2 null mutant. Note that SVs are tightly captured in a small region of the axon in wild type animals, but SVs accumulate in the long distal asynaptic region in the syd-2 null mutant. High resolution images acquired with a large field-of-view Flash 4.0 camera were used to reconstruct the dorsal axon from multiple images. GFP-RAB-3 is expressed from the integrated transgene array wyIs85. B. Graph quantifies SV capture efficiency in the indicated genotypes by measuring the length of the region with SV clusters exceeding the threshold line (shown in (A)). This quantifies the extent to which SVs have overshot the synaptic region and have moved toward microtubule plus ends in the long asynaptic region. Graph data are means and standard errors from 14-15

animals each. Unmarked bars are not significantly different from wild type. * and *** indicate P-values that are <.05 or <.001, respectively, and compare the indicated bar to wild type. The C. elegans gene names and the common names of each protein are as follows, along with one or more references demonstrating that the protein is enriched at active zones: UNC-10 (RIM: Rab3 Interacting Molecule), UNC-13; RIMB-1 (RIM-Binding Protein), PTP-3 (LAR: Leukocyte-common Antigen Related), GIT-1 (GIT: G protein coupled receptor kinase 2 Interacting protein), LIN-2 (CASK: name ontology unknown), ELKS-1 (ELKS/ ERC/ Bruchpilot). Evidence that 5 of these active zone enriched proteins interact with SYD-2 (Liprin-α) in C. elegans or other animals is as follows: in C. elegans and/ or other animals: ELKS, RIM, CASK, LAR, and GIT. Data collected by Miller lab.

Of these, only *rmb-1* (RIM-Binding Protein), showed an expansion of SV signal into the asynaptic region. Though mild, this expansion was significant compared to wild-type. We also found that SVs accumulated at minus-end dendrites in *rmb*-1 mutant animals (192 +/- 32% wt; N=15; P=.015), although SV density at the synaptic region was normal (103+/-4% WT, N=15). Thus, it appears that RIMB-1 may play a small but redundant role in CSS regulation of SV capture. None of the other AZ-enriched proteins we tested showed this phenotype, although both *unc-10/RIM* and *unc-13* mutants displayed a slight reduction of SV density in the synaptic region (Figure 3.20B). We therefore conclude that CSS proteins make up a specialized class of active-zone enriched proteins that are critical for SV capture at synapses.

C. Discussion

We used a forward genetic screen to identify proteins that regulate DCV localization at synapses. We found that SAD Kinase and the novel protein, Sentryn, function together in guided axonal transport of DCVs, SVs, and other cargo. We also describe the novel protein, Sentryn, which is conserved in all animals and is a core component of the CSS protein system. Our results indicate that CSS system proteins are a specialized subset of active-zone enriched proteins that provide a link between guided vesicle transport and synaptic capture.

Sentryn functions with CSS system proteins SAD Kinase and SYD-2 in guided axonal transport and capture.

SAD-1/SAD Kinase was first discovered in *C. elegans*, where *sad-1* mutants exhibited diffuse SV localization (Crump et al., 2001). Subsequent studies demonstrated that SAD-1 regulates SV distribution and synaptic clusters (Chia et al., 2012; Hung et al., 2007; Kim et al., 2010; Kim et al., 2008; Klassen et al., 2010). Here we reveal an additional role for SAD Kinase in regulating DCV transport and capture, and we characterize the novel protein Sentryn. In both *sad-1* and *strn-1* mutants, DCVs were reduced in axons and accumulated in cell somas and dendrites. This phenotype indicates that minus-end transport of vesicles toward somas and dendrites prevailed over plus-end transport toward synapses. Interestingly, we found that we could rescue this phenotype by adding a mutation that reduced dynein activity. Using genetic experiments, we determined that Sentryn operates with other CSS system proteins to regulate DCV and SV transport and synaptic capture in a dynein-dependent manner.

It well studied that SAD Kinase operates with SYD-2 in synapse assembly and SV capture (Patel et al., 2006). SV clustering defects in *syd-2* mutants appear to be more severe than in *SAD Kinase* mutants, which led us to believe there may be additional proteins involved in this process (Edwards et al., 2015b; Patel et al., 2006). Indeed, we believe Sentryn is the missing link that, together with SAD Kinase, enables SYD-2 function. Our evidence suggests that Sentryn and SAD Kinase have at least one distinct, non-overlapping role, as well as some overlapping roles in the CSS system. Regarding the synaptic region specifically, we believe that Sentryn, as part of the CSS

system, enables KIF1A to outcompete dynein-mediate transport. This action results in overall preference for plus-end directed transport that ensures SVs and DCVs arrive at the synapse.

How can the CSS system reduce dynein-mediated transport? It is possible that these proteins inhibit dynein-mediated movement, promote kinesin-mediated movement, or both. Our work provides evidence for both mechanisms. Time lapse imaging of lysosomes in dendrites showed that CSS proteins inhibit dynein-mediated movements without affecting kinesin-directed movement (Edwards 2015a). On the other hand, imaging DCVs at the AIS showed that Sentryn and SAD Kinase promote forward movement but not dynein-mediated reverse movement. We also found that SYD-2, Sentryn, and SAD Kinase reduce pausing during DCV transport here. Previous work in *C. elegans* has shown that SYD-2 promotes plus-end directed transport mediated by KIF1A and reduces minus-end directed transport (Wagner et al., 2009). Similar results were observed by time lapse imaging in *Drosophila* motor axons (Miller et al., 2005). Thus, it appears that the exact mechanisms for CSS regulation of plus or minus-end transport may be unique for different cargo and at different locations of the neuron.

Sentryn, SAD Kinase, and SYD-2 have varying functions at different parts of the neuron

It is important to note that the functional hierarchy of Sentryn, SAD Kinase, and SYD-2 is slightly different in different parts of the neuron and for different cargo. For example, when we imaged SVs and DCVs at the synaptic region of DA9, we found that Sentryn and SAD Kinase were additive, with at least one non-overlapping function. However, when we observed lysosomes and SVs at dendrites, we did not find additivity between SAD Kinase and Sentryn. We found that

strn-1 and other CSS mutants could also affect transport of lysosomes and early endosomes. Our previous work suggests that UNC-16/JIP3 blocks the physical interaction between CSS proteins and kinesin (Edwards et al., 2015a). When we combined *strn-1*, *sad-1*, or *syd-2* mutants with an *unc-16* mutant background, we observed a dynein-dependent accumulation of lysosomes and early endosomes in dendrites and cell somas. In support of our previous work, this effect was not present in animals with wild-type UNC-16/JIP3 (Edwards et al., 2015a). Thus, in the absence of UNC-16, CSS system proteins can gain access to lysosomes and early endosomes and promote plus-end directed transport. To our knowledge, these are the only mutants that show the combined phenotype of minus-end accumulation and plus-end loss of cargo. These subtle differences suggest that CSS proteins operate differently in different parts of the neuron.

CSS system proteins link vesicle transport and capture and are enriched at active zones.

Synaptic vesicles are known to cluster tightly at synapses near active zones, which contain a specialized set of proteins and a dense projection. (Hammarlund et al., 2008; Weimer et al., 2006). Using electron tomography, experimenters have observed filamentous connections among SVs in a cluster and physical contact with the DP (Stigloher et al., 2011). On the other hand, DCVs have a looser spatial relationship with active zones, most commonly located more than 100 nm from the DP (Hammarlund et al., 2008; Hoover et al., 2014; Weimer et al., 2006). Physical connectors contacting DCVs are less common, though they have been observed (Stigloher et al., 2011). Due to these distinct patterns, we were surprised to find that DCVs do in fact localize to the specialized synaptic region where SVs cluster, and they are captured by the same proteins: Sentryn, SAD Kinase, and SYD-2/Liprin-α. Interestingly, we observed that in *strn-*

1;sad-1 double mutants, the reduction in SVs was primarily from SVs distal to the active zone (>300 nm to DP). DCVs were depleted from the same area, in addition to loss near the DP. Previous work has proposed that vesicles located on the edge of the cluster may have fewer physical connectors to other vesicles and/or the DP, and thus may be more susceptible to motor transport out of the synapse. Specifically, after heat-induced impairment of *unc-104/KIF1A*, SV clusters were reduced by ~50%, and remained at that level despite further exposure to the restrictive temperature (Edwards et al., 2015b). The results presented here may provide ultrastructural support for this theory, although HPF/FS EM analysis should be conducted specifically in the experimental paradigm that was used.

We took advantage of the unique architecture of DA9, whose short synaptic region is flanked by two long asynaptic regions, to characterize clustering defects which manifested as a longer region enriched with SVs. That is, in CSS system mutants, DCVs and SVs localized more diffusely from the synaptic region than in wild-type **(**Edwards et al., 2015b**)**. Because SVs tend to cluster, even during transport, the SV signal was not evenly spaced throughout the axon (Klassen et al., 2010).

Varying instances of SV clustering defects have been observed in *C. elegans* as "expansion," "diffusion," and "overlapping" clusters in both *sad-1* and *syd-2* mutants (Crump et al., 2001; Zhen and Jin, 1999). Analogous defects have also been reported in autonomic ganglion synapses of SAD Kinase mutant mice (Lilley et al., 2014). In these neurons, synapses are located at boutons near the end of a terminal axon branch. SVs normally cluster near the AZ. In SAD

Kinase mutants, SVs mislocalize away from the bouton and AZ, towards the distal region of the axon itself. Thus, varying neuronal anatomy may result in different clustering patterns. Studies in *Drosophila* have also demonstrated evidence for DCV capture at synapses (Shakiryanova et al., 2006; Wong et al., 2012), and this capture may even be altered under different physiological conditions (Bulgari et al., 2017; Cavolo et al., 2015). To our knowledge, the proteins involved in capture have remained unidentified prior to this study, with the exception of *Drosophila* Huntington, which was recently identified as an inhibitor of DCV capture (Bulgari et al., 2017).

Having observed the mechanisms of guided active transport of SVs and DCVs and their subsequent capture in the synaptic region, we believe these two processes are linked through the CSS system proteins Sentryn, SAD Kinase, and Liprin-α (Edwards et al., 2015b; Patel et al., 2006; Dai et al., 2006). This dual role poses an interesting problem. For DCVs and SVs to be transported from cell body to synapse, plus-end, kinesin-directed transport must outcompete reverse transport by dynein. In fact, we believe that the CSS system promotes transport to synapses in a dynein-dependent manner, either by inhibiting dynein, promoting kinesin, or both. Then, when cargo arrives at the synaptic region, CSS system proteins must stop transport in either direction. For example, SYD-2 prevents SVs from dissociating from clusters (Wu et al., 2013), which requires SVs to stop moving in either forward or reverse directions. In *syd-2* (and other CSS system) mutants, SVs and DCVs accumulate distally past the synapse. Thus, during capture, the CSS system should ultimately stop both forward and reverse transport.

How do these proteins switch function? First, CSS proteins are enriched at the AZ, and a greater copy number of protein may change the way they can interact with motors there. SYD-2/Liprin-α is well-known to be enriched at the active zone and promotes SV contact with the DP (Stigloher et al., 2011). Is it possible that SYD-2 physically connects SVs to the DP with tethers or filaments? There are several lines of evidence to refute this idea. First, most SVs in the synaptic population do not contact the DP (Stigloher et al., 2011). Second, DCVs must also rely on SYD-2 and CSS proteins to be captured. DCVs are less likely to be present, let alone docked or physically connected to the DP, near active zones compared to SVs (Weimer et al., 2006; Hammarlund et al., 2008; Hoover et al., 2014). Third, some mutant mice have displayed a disappearance of active zones and/or DP's but can still capture SVs at normal levels at the synapse (Wang et al., 2016; Acuna et al., 2016). Finally, while connections or tethers to the DP may help prevent SV diffusion from synapses, it is unlikely that they are strong enough to prevent the activity of transport motors. Thus, we believe that rather than physically anchoring SVs and DCVs to the DP, SYD-2 and other CSS system proteins regulate motor activity to allow for capture.

CSS system proteins make up a specialized group of active-zone enriched proteins

While all CSS proteins are enriched at active zones, not all active zone proteins participate in the CSS system. This finding supports a growing body of evidence that suggests there are at least two functional groups of AZ proteins. The first group is made of structural components that affect release (Sudhof et al., 2012; Ackermann et al., 2015). For example, a combination of *RIM/unc-10* and *RIM-BP* mutants or *RIM/unc-10* and *ELKS* mutants result in a disassembled active zone and DP, as well as eliminated SV tethering and docking. However, SYD-

2 localization and SV clustering remain normal in these mutants (Wang et al., 2016; Acuna et al., 2016). SYD-2 is part of a second group of AZ proteins, the CSS system, whose main function is to capture SVs and DCVs by modulating motors. These proteins can also influence dense projection length in *C. elegans*, as seen in *syd*-2 mutants and described here (Kittelmann et al., 2013;). It is important to note that early studies of *syd-2* and *syd-1* mutants reported normal looking, or even elongated DPs (Zhen and Jin, 1999; Hallam et al., 2002). However, these studies were performed using conventional fixation methods that provide inferior preservation of cellular structures.

The CSS system was first named for CDK-5, SAD-1, and SYD-2, which were all involved in preventing dynein-mediated lysosome clearance in *unc-16* axons (Edwards et al., 2015a). Based on the findings presented here, we believe the CSS system specializes in vesicle transport and capture. Active zone enrichment is thus a requirement for the two different processes of promoting plus-end movement during transport versus preventing movement during capture. Since CDK-5 is not enriched at AZ's and does not capture SVs (95+/-15% of wt; N=14), it no longer fits into this definition of CSS proteins. We therefore propose a new definition for CSS, Core Synapse Stability System, based on its primary role in maintaining SV and DCVs captured at the synaptic region.

D. Materials and Methods

C. elegans culture and strains

Worm culture and manipulation essentially followed previously described methods [Stiernagle, 2006 #1571;Brenner, 1974 #3;Sulston, 1988 #61]. Briefly, culture media was modified NGM (referred to as NGM-LOB) [Hoover, 2014 #1436]. Prior studies defined the culture plate types "spread plates", "streak plates", "locomotion plates", "24-well plates", and "96-well solid media culture plates" [Miller, 1999 #1563;Edwards, 2008 #1554;Edwards, 2015 #1661]. The wild type strain was N2 except when the strain CB4856 was used for mapping the ce793 mutation and the insertion sites of integrated transgenes. Non-wild type strains that were used in this study are listed in Table S1. The relevant mutations present in the worm strains, along with the methods we used for genotyping them in crosses, are listed Table S2. Some strains contained one or more transgenic arrays. Transgenic arrays are listed in Table S3 along with their plasmid contents, injection concentrations, and genomic form (extrachromosomal or integrated).

We mutagenized 9000 L4's of the strain KG4247 ceIs201 with 27.6 mM EMS in M9 [Sulston, 1988 #61] supplemented with OP-50 bacteria for 4 hr at 20°. Subsequent manipulation and growth procedures to produce F2 grand-progeny of mutagenized animals were essentially the same as we reported for previous genetic screens [Edwards, 2015 #1660]. At 20 min intervals, we pipetted 50 ul (~12 worms) of L4-stage F2's from a stirring suspension into each of 18 wells of a 96-well Mat-Tek glass bottom plates (MatTek Corporation, Ashland, MA; P96G-1.5-F-F). Before animal distribution, each well was pre-loaded with 50 ul of 300 uM Levamisole (Sigma L-9756) in water per well. We screened animals in each well for decreased INS-22-Venus fluorescence in the dorsal cord axons and increased INS-22-Venus fluorescence in the ventral cord somas. At the end of each 20 min screening session, after noting wells containing mutants,

we pipetted the contents of each mutant-bearing well onto a pre-dried streak plate using a Pasteur pipet, rinsed the well with 100 ul of M9, and then, immediately after the liquid dried in, clonally distributed the animals to a 96-well solid-media culture plate (see "C. elegans culture and strains"). After 4 d at 20° C, we used a sterile toothpick to pick ~6 L4-stage animals from each well into Mat-Tek wells containing 150 uM Levamisole. After re-screening on the inverted microscope, we noted wells with 100% mutant phenotype and used the corresponding well on the 96-well plate to score behavioral and other phenotypes and to set up stocks. We repeated this screen for 3 weekly cycles, for a total of 23,328 F2's. This computes to ~4.67-fold genomic coverage for an average size gene [Greenwald, 1980 #143]. However, taking into account an experimentally-determined 23% loss of animals during recovery of the mutants, the actual fold-coverage was ~3.6.

Complementation tests and mapping

We determined that ce784 and ce776 are allelic using a complementation test similar to previously described methods [Edwards, 2015 #1660]. ce776 and ce784 were not further mapped, but were subjected to whole genome sequencing (see below). ce793 was roughly mapped relative to left arm, center, and right arm markers on X using methods similar to those previously described [Edwards, 2015 #1660]. By this method, we mapped ce793 a region of X between -11.1 cM and 2.13 cM.

Whole genome sequencing

We produced genomic DNA and libraries for whole genome sequencing as described [Edwards, 2015 #1660]. Whole genome sequencing and analysis was performed as described [Edwards, 2015 #1660].

Targeted knockout of rimb-1 by CRISPR

We inserted the sequence GC TAG C TAA A TGA after codon 16 of the rimb-1 gene (out of 1276 codons total). The underlined sequence is a Nhe I site for snip-PCR screening [Paix, 2014 #1487]. The insert contains 3 stop codons, each in a different reading frame [Paix, 2014 #1487]. We used the oligonucleotide-templated co-conversion strategy [Arribere, 2014 #1484], using dpy-10(cn64) as a co-conversion marker and screened for conversion by PCR followed by restriction digest.

We cloned the Cas9 target sequence CATGCCATAGGAGGATGCGG into the pJP118 gRNA expression cassette as previously described for cloning targeting sequences into pRB1017 [Arribere, 2014 #1484]. pJP118 is a modified version of the published pRB1017 plasmid [Arribere, 2014 #1484]. It contains a modified sgRNA (F+E), with an extended Cas9 binding structure and removes a potential PolIII terminator by an A-U basepair flip. The oligo template contained 50 bases of homology on each side of this insertion for 113 bases total. The oligo was ordered from Sigma at the 0.2 umole scale with PAGE purification. The injection mixture was pDD162 (Cas9 plasmid; 50 ng/ ul) [Dickinson, 2013 #1482], pJA58 (dpy-10 gRNA plasmid; 25 ng/ ul) [Arribere, 2014 #1484], KG#843 (rimb-1 gRNA plasmid; 25 ng/ ul), and the dpy-10(cn64) and rimb-1(ce828) oligo templates (500 nM and 2400 nM, respectively). We injected 36 wild type animals with this mixture and cloned 48 F1 rollers, 47 of which yielded progeny. 34 of the 47

rollers (72%) showed successful edits, as indicated by Nhe I cleavage of a PCR product containing the insertion site.

DNA Constructs

The plasmids used in this study, along with sources and/ or key construction details, are listed in Table S4. For Gibson Assembly plasmid construction using NEBuilder, we followed the manufacturer's instructions with the following options and modifications: 1) we designed primers with 30 bp of overlap, with all of the overlap on one of the 2 fragments to be combined; 2) we used 15 ng/ ul as a starting template concentration for all PCR reactions, rather than the much lower concentration recommended by the manufacturer; 3) we performed the optional Dpn I digestions, gel-purified the PCR fragments, and quantified them with a Nanodrop; 4) the assembly reaction contained 200 ng of the vector fragment and a 3-fold molar excess of each remaining fragment; 5) each reaction was performed in 10 ul total volume, starting with 5 ul frozen aliquots of 2X NEBuilder master mix; and 6) we directly transformed 2 ul of the reaction using electroporation. In all constructs involving the cloning of PCR fragments, we sequenced the inserts and used clones containing no mutations in the fragment of interest to make the final stock.

Production and integration of transgenes

We prepared plasmids for microinjection using the Qiagen Tip-20 system according to the manufacturer's instructions, except that we added a 0.1M potassium acetate/ 2 volumes ethanol precipitation step after resuspending the isopropanol – precipitated pellet. We produced

transgenic strains bearing extrachromosomal arrays by the method of Mello et al. [Mello, 1991 #68]. For the strn-1 rescue experiments, the host was KG4786 strn-1(ok2975); ceIs201. For all other injection experiments, N2 was the host. We used pBluescript carrier DNA to bring the final concentration of DNA in each injection mixture to 165-175 ng/ ul. We integrated transgenes into the genome using 9100 Rads of gamma rays as described [Reynolds, 2005 #1559]. We mapped the insertion site of ceIs308 by crossing the integrant through CB4856, re-isolating and cloning homozygous animals in the F2 generation, and using the resulting mapping lines to map the integration sites relative to SNPs as described [Schade, 2005 #1560].

Strain constructions

We constructed strains containing multiple mutations or transgenes using standard genetic methods [Edwards, 2015 #1660;Edwards, 2015 #1661]. After making a strain composed of two or more mutations, or one or more mutations plus an integrated transgenic array insertion or an extrachromosomal array, we confirmed the homozygosity of each mutation using the genotyping methods in the above “Mutation Lesions” table.

Growth and mounting of strains for imaging

Strain growth: Young adult progeny that had not previously been starved were grown for imaging as described [Edwards, 2015 #1660]. Growth times and plating numbers were modified for slow growing or lower fertility strains, such as strains containing syd-2(ok217) or nud-2(ok949). ~55 young adults were selected and transferred to an unseeded plate immediately prior to mounting as described below.

Agarose pad slide production: Clean glass slides were produced as described [Edwards, 2015 #1660]. We produced ~18-19 mm diameter agarose pads, except we standardized the agarose concentration at 4% in M9 buffer as follows. After melting 0.4 g of agarose in 10 mls of M9 in a 50 ml Pyrex bottle (Thermofisher, No. 1395) with the lid screwed as tight as possible, we cooled the bottle on a folded paper towel for 2 min, slowly unscrewed the cap to prevent boiling, and poured 0.5 ml of the molten agarose into up to 10 X 1.5 ml microcentrifuge tubes in a 100° Isotemp block (Fisher) for distribution to clean slides as described, using a method described for standardizing agarose pad slides for time lapse video microscopy [Edwards, 2015 #1660].

Mounting animals on agarose pad slides: We applied a 30 ul drop of 30 mg/ ml BDM (2, 3-Butanedione monoxime; Sigma B0753) in M9 buffer onto a 24 X 30 mm coverslip. We then transferred the 157tyrofoam animals in one pick-full to the drop on the coverslip and incubated them for 10 min, placing the coverslip on a 1.5 cm square pad of folded paper towel tissue under a Petri plate lid. After the incubation, we removed ~19 ul of the solution using a P20 microinjection tip (Eppendorf 5242 956.003), leaving the worms behind in the remaining anesthetic, and inverted the coverslip onto a ~18-19 mm diameter 4% agarose pad that had been dried without its protective coverslip for the final 4 min of the incubation. We imaged animals over the next 35 – 55 min.

Image acquisition and processing

We viewed animals using a Nikon Eclipse Ti-E inverted microscope equipped with a Nikon CFI Apo TIRF 100X/ 1.49 N.A. objective, a Nikon motorized high resolution z-drive, and a motorized filter turret containing GFP, YFP, and Texas Red filter cubes (Semrock). Our illumination source

was a SOLA Light Engine LED source (Lumencor). We acquired images with an ORCA Flash 4.0 16-bit camera (Hamamatsu, Bridgewater, NJ) controlled by Metamorph v. 7.7. We controlled exposure times by using Metamorph to turn the LEDs on and off rather than using a shutter. We only collected images from animals with their ventral or dorsal surfaces facing the objective and "center quad" (center quadrant) mode of the camera. Z-series interval sizes (0.312 um) and plane numbers (16) were the same for all strains and transgenes. Exposure times were identical for different strains in each experiment and chosen to collect at sub-saturating levels. Before imaging each strain, we measured the light power of the peak emission wavelength at the objective using an XR2100 power meter (Lumen Dynamics) and an XP750 objective plane light sensor (Lumen Dynamics) with the stage position set at a standard distance (z-position) from the objective. We then adjusted the percent power of the SOLA Light Engine to produce the targeted mW power for the experiment. We used AutoDeblur Gold CWF (Media Cybernetics) to deconvolve the image stacks using the Adaptive PSF blind method and 10 iterations at the low noise setting. After deconvolving, we used Metamorph to make maximum intensity projections of each image stack.

Quantitative image analysis

We used Metamorph 7.7 for most analysis and quantification. To quantify fluorescence intensities per micron, we used the Trace Region tool to trace the region and used the Multiline tool to obtain the length of the traced region. We then copied and moved the region to a similar "on animal" background region for use in background subtraction. For dorsal axons in ceIs201 strains, we traced the entire axon length across the image. To trace the dendrite regions around

DA6 and DB6 in ceIs255 strains, we started each of the two dendrite regions at the outer edge of each soma, proceeding outward toward each edge of the image and combining the data from the two dendrite regions. Axonal and dendritic data were logged to a spreadsheet, which subtracted the background and computed the total fluorescence per micron of length. To quantify cell soma intensity per square micron in ceIs201 strains, we chose the 2 most average brightness somas in the image. We traced the somas individually unless they were adjacent, in which case we traced them as a single region. In some cases, axons from the ventral nerve cord ran over part of one or both somas. If this was the case, we excluded this section of the soma from the traced region. After quantifying an image set, we produced representative images for display by saving an 8-bit version of an image that was close to mean +/- standard error for the set. All representative images within an experiment were scaled identically.

Special modifications of imaging methods

Imaging strn-1::GFP transcriptional reporter expression (ceEx461 transgene): To image whole L1 or L3 larvae, animals were immobilized as described above under "Mounting animals…." and imaged using the above-described microscope and camera in full-frame mode (not center quad). For L1s, we used a 40X oil, 1.3 Numerical Aperture objective, acquiring 20 z-planes at 0.7 um intervals using 7 mS exposure times through the GFP filter set. Images were processed by deconvolution as described above in "Processing Images". For L3s, we used a 20X dry, 0.75 Numerical Aperature objective, acquiring 18 z-planes at 1.0 um intervals using 10 mS exposure times through the GFP filter set. Images were processed by deconvolution as described above in "Processing Images".

Imaging DCVs in the DA9 synaptic and distal asynaptic regions: To obtain high resolution images of DCVs in the entire DA9 dorsal axon (~500 microns in length), we acquired ~3 overlapping full-frame images (designated a, b, and c) spanning from the posterior bend of the axon through to the first commissure that intersects with the DA9 asynaptic region (which ends just posterior to the vulva). DCVs were marked in DA9 with the neuropeptide cargo INS-22-Emerald using the ceIs308 genomically-integrated transgenic array. We used exposure times of 20 mS (GFP filter) and 2 mS (Texas Red filter). Images were processed by deconvolution as described above. To quantify the synaptic region, we used the trace region tool in Metamorph to trace the brightest 40 micron part of the synaptic region (and a corresponding "on animal" background region). In ventrally oriented animals, we traced the DA9 soma, avoiding the nearby VA12 soma. To determine the start of the asynaptic region, we first determined the longest synaptic region length in 15 wild type image sets. To do this, we opened the first (most posterior) "a" wild type image in the first set of overlapping images. We used the multi-line tool to trace the DA9 axon from the center of the posterior commissure bend in the tail through the synaptic region to last DCV punctum that precedes a gap of >= 6 um. If there was no such gap in the "a" image in the set, we traced to the edge of the image, opened the overlapping "b" image, identified the region of overlap, and continued tracing until we reached a gap of >= 6 um between DCV puncta, adding the 2 lengths from the "a" and "b" images. We repeated this for all 15 wild type image sets and noted the longest wild type synaptic region length. This length was the starting point for counting DCVs in the asynaptic region in both wild type and mutants. To count DCVs in the asynaptic region, we counted all DCVs detectable above background, from the start of the asynaptic region through to the point at which the first fluorescently-labeled

commissure intersects with the DA9 axon, proceeded through all 3 overlapping images in each set and tracking the axon length and number of DCVs in each image. Overlapping images were aligned using landmarks in the axon and animal. Scaling was adjusted as necessary to detect all DCV puncta above background. An Excel workbook accepted the a, b, and c lengths and DCV numbers, added them together for total length and total number and then determine DCV number/ micron and the mean, standard deviation, and standard error of the mean.

Profile plots of DCV fluorescence in the DA9 axon: To plot the DCV fluorescence distribution in DA9, we used the Plot Profile module of Image J. We used the segmented line tool with a line width of 20 pixels to trace along the length of the axon in each of 3 overlapping images comprising the DA9 axon (see above). We started at the posterior bend and ended at the point where the first fluorescently labeled commissure intersects with the DA9 axon. We created profile plots from each of the 3 overlapping images in the set. The Y-axis maximum was set to the highest Y value in the 3 overlapping images of the set. We then copied the plot values into a SigmaPlot workbook. We saved the SigmaPlot graphs (one for each of the 3 overlapping images of the set) as JPEGs, imported them into Canvas and cropped them. We then used Object > Scale to shrink the vertical dimension and expand the horizontal dimension. The 3 graphs were further cropped and merged together at their points of overlap to make a single high resolution profile plot comprising the entire DA9 dorsal axon.

Counting DCVs in the axon initial segment: We used ventral soma images acquired from strains containing ceIs201. These images contained multiple somas with commissures (axon initial segments) extending toward the dorsal cord. We counted DCVs in any commissures that were in the field of view and in focus from the edge of the soma to the point where it crosses one of the

sublateral axon tracks running longitudinally down the animal. We used the line tool to click along the commissure and determine its length. We then simply counted all of the DCV puncta in each commissure. Any puncta that were distinguishable above background were considered countable. Puncta positioned close to each other were counted as multiple if cleavage between the puncta could be distinguished. From previous time lapse studies, and the time lapse experiments in the current study, we have determined that most such puncta in the axon initial segment represent individual DCVs since DCVs are not known to be transported in clusters.

Immunostaining of formaldehyde-fixed animals

Freeze cracking and fixing animals: We prepared freeze-cracked 4% paraformaldehyde fixed, young adult worms for immunostaining as described [Charlie, 2006 #1558;Charlie, 2006 #1558], with the exception that we modified the freeze cracking procedure as follows to prevent the fixative from freezing during freeze cracking. Steps before and after freeze cracking were identical to the above published procedures. To freeze crack worms, we filled one 50 ml conical per strain with 40 mls of 4% formaldehyde in 1X PBS, pH 7.4. The fixative was made fresh by breaking a 10 ml ampule of 16% formaldehyde (Ted Pella EM grade #NC9658705) and mixing its contents with 26 mls of ddH2O and 4 mls of 10X PBS in a 50 ml conical. The 50 ml conical with fixative was immersed in ice for at least 45 min. Freshly frozen slide sandwiches containing ~1500 young and mature adults sandwiched between two overlapping glass slides were prepared as described [Charlie, 2006 #1558;Charlie, 2006 #1557]. Then, up to 12 such sandwiches were successively cracked and combined with cold fixative as follows. At time 0 sec, a count-up timer was started. The first slide sandwich was removed from its dry ice block, and

the two slides of the first sandwich were vigorously separated and laid, worm-side-up on a 163Styrofoam surface at room temperature for 1:30 min. At 1:20 – 1:30 min, the second slide sandwich was cracked and laid next to the first two halves on the 163Styrofoam surface. From 1:30 min – 2:45 min, the two halves of the first sandwich were placed back-to-back and immersed in the ice cold fixative in the 50 ml conical tube, using forceps to hold the slides. The worms were rinsed off of both slides forcefully using a P1000 pipet, and then the rinsed slides were discarded. The third sandwich was then cracked at 2:50 – 3:00 min, followed by rinsing worms from the second sandwich at 3:00 – 4:15, etc. until all the worms from 2 – 12 sandwiches have been rinsed into the cold fixative. The worms were then concentrated by pouring ~1/3rd of the suspension into a 15 ml conical, spinning 2000 rpm for 10 sec in a swinging bucket rotor in a Dynac clinical centrifuge at room temperature with the brake applied, removing the supernatant with vacuum suction, and repeating twice more. We left ~ 1 ml after the 3rd spin, and then used a Pasteur Pipet or P1000 to forcefully rinse off any animals stuck to the bottom of the tube and transfer the suspension into a 1.5 ml snap-cap tube. We then spun this tube at 6000 rpm for 12 sec in a microfuge, removed most of the cold fixative, and replaced it with 1 ml of previously reserved room temperature fixative. All subsequent steps (30 min fixation at room temperature, quenching in 1 ml of 0.1M glycine, pH 7.4 for 5 min, washing with Antibody Buffer B, blocking with 3% BSA block, and staining with primary and secondary antibodies, and post-staining washes) were performed as described [Charlie, 2006 #1558;Charlie, 2006 #1557]. For immunostaining of EGL-21 dense core vesicles we used Rabbit anti-EGL-21 primary antibody (1/200; KM39A-5.1) [Hoover, 2014 #1436]. The secondary antibody was Goat anti-Rabbit Dylight 550 (Pierce). We used a Semrock Cy3 filter set to view the Dylight 550 signal.

Imaging animals: We used the same microscope, objective, light power monitoring system, and acquisition software described above for live animal imaging. We imaged well-filleted animals that had their dorsal cords exposed and oriented toward the objective. Any such region of the dorsal cord except the first or last 15% was chosen for imaging. Z-stacks of 20 images separated by 0.2 um were collected.

Image processing and quantification: We processed, deconvolved, quantified, and chose representative images as described above for live animal imaging.

High Pressure Freezing Electron Microscopy

Worms were prepared using high-pressure freeze (HPF) fixation as described previously [Weimer, 2006 #1917]. Briefly, young adult hermaphrodites were placed in specimen chambers filled with Escherichia coli and frozen at -180°C and high pressure using a Leica SPF HPM 100. Freeze substitution was then performed on the frozen samples using a Leica Reichert AFS. Samples were held at -90°C for 107 h with 0.1% tannic acid and 2% OsO_4 in anhydrous acetone. The temperature was increased at 5°C/h to -20°C, kept at -20°C for 14h, and increased by 10°C/h to 20°C. After fixation, samples were infiltrated with 50% Epon/acetone for 4h, 90% Epon/acetone for 18h, and 100% Epon for 5 hours. Finally, samples were embedded in Epon and incubated for 48h at 65°C. All specimens were prepared in the same fixation and subsequently blinded for genotype. Ultra-thin (40 nm) serial sections were cut using a Leica Ultracut 6 and collected on formvar- covered, carbon-coated copper grids (EMS, FCF2010-Cu). Post-staining was performed using 2.5% aqueous uranyl acetate for 4 min, followed by Reynolds lead citrate for 2 min. Images were acquired starting at the anterior reflex of the gonad using a Jeol JEM-

1220 transmission electron microscope operating at 80 kV. Micrographs were collected using a Gatan digital camera at a magnification of 100,000X. Images were taken of cross sections of the dorsal cord of three animals for each strain. Cholinergic synapses were identified by morphology [White, 1986 #563]. A synapse was defined as a set of serial sections containing a dense projection and two flanking sections from both sides without dense projections. Dense core vesicles were identified as spherical structures with a dark gray center and an average diameter of ~40 nm. Images were analyzed using NIH ImageJ software and macros provided by the Jorgensen lab. Serial images were aligned using TrakEM2 before annotating organelle structures in ImageJ. Analysis of these structures was performed using MATLAB scripts written by the Jorgensen lab and Ricardo Fleury.

Time lapse video microscopy

Growth of strains: Animals were grown to the young adult stage as described above for quantitative fluorescence imaging, except we used as many as 30-40 locomotion plates to provide sufficient numbers of animals for the many time lapse mountings.

Agarose pad slide production: We prepared agarose pad slides as above. Slides were stored at 4° and used fresh the next day.

Mounting animals on slides: We first equilibrated the agarose pad slides at room temperature in their humidified container and prepared fresh 6 mM Levamisole in M9 from a powder stock of Levamisole (Acros Organics; AC187870100; <6 months old). To mount animals on a pad, we pre-picked 30-40 young adults to an unseeded plate, applied 30 ul of 6 mM levamisole to a 24 X 30 mm coverslip, picked the 30 young adults to the droplet in one pick-full, and incubated them for

6:10 min on a moist Kimwipe square under a Petri plate lid. Immediately after picking the worms to the drop, we removed the coverslip from one of the agarose pad slides and added 10 ul of M9 + 6 mM Levamisole to the coverslip, and then re-applied the coverslip to the pad, leaving it on the pad until ~40 sec remained on the count-down timer. When removing the coverslip we also removed as much of the 10 ul as possible along with the coverslip by tilting the coverslip up as soon as it slides off the pad and dragging the liquid away from the pad. We then blotted around the edge of the pad with a Kimwipe to remove excess liquid. When the 6:10 timer finished, we put the coverslip back on the Petri plate lid (wiping the moisture off of the part that contacted the wet Kimwipe square first) and removed 23.5 — 25.5 ul of liquid (average 24.5, but adjusted as needed depending on pad size and wetness after removing the M9) by pipetting while viewing under the stereomicroscope. We used a gel loading tip inserted onto a P20 set on the desired volume to remove the liquid in one attempt. When applying the new coverslip with worms face down onto the pad, we used a pair of jeweler's forceps to gently lower it onto the pad. On properly mounted coverslips, a small amount of liquid should wick across in all directions and slightly overflow the pad.

Image acquisition: We acquired images using the same microscope, camera, and computer system described above. We adjusted the light power of a SOLA LED light engine to 25% (a good level for reducing bleaching without compromising signal when using the YFP filter and the ceIs201 transgene). We mounted the slide on the microscope and scanned the pad left to right, top to bottom using transmitted light and DIC optics to find the first animal oriented with its ventral cord facing the objective. Using the YFP filter, we then focused on the cholinergic motor neuron commissures ~halfway between the central and posterior part of the animal and

positioned the stage to allow viewing of the soma and 2-3 commissures. At 5:30 min after applying the coverslip, we started the first time lapse and continued collecting for 45 sec. Each time lapse consisted of 115 frames collected at 394 msec intervals, with an exposure time of 50 msec for each frame. We used the "center quad" mode of the camera. If possible, one additional time lapse was collected from a different animal, starting within 1:15 min of finishing the first time lapse. However, no more than 2 time lapses were collected per slide. During each time lapse, the focus was adjusted as needed to optimize the focus of the 1 – 3 visible commissures.

Processing time lapse images and converting them to kymographs: We used the Review Multidimensional Data Metamorph plug-in to convert the time lapse images into a multi-image TIFF file. We then used the Multi-line tool to trace along the center of the axon initial segment, starting at the cell soma boundary and proceeding outward. During tracing we moved back and forth between tracing and the slider such that we could visualize the precise path as INS-22-Venus DCV puncta moved through the axon (i.e. following the puncta by clicking as they move along the axon). After ending the trace, we used the Kymograph plug-in to set the line width at a value that included all of the puncta throughout the movie. If animal movement shifted the axon's position slightly during the movie, we adjusted the line width to the minimum width that allowed all puncta along the commissure to be included in the boundaries (up to ~30 pixels maximum). We then created, reviewed, and saved the Kymograph, used the Save Regions plug-in to save the line traces associated with the file, and noted the optimal line width for each trace.

Quantifying movements and percent of time spent paused from kymographs: After opening the multi-plane tiff file in Metamorph, using the Load Regions plug-in to re-load the line traces, and setting the line width at the above determined optimum, we re-created the kymograph

(previously saved kymographs can't be used to log data). Each punctum was analyzed separately and its movements traced with the line tool set on specific colors for each movement state as follows: anterograde (green), retrograde (red), and paused (yellow). Then, if the punctum was not visible for the entire kymograph, we drew a light blue line covering the total time that the punctum was visible. Pauses were analyzed on all time lapses having at least 58 frames. The key to pause analysis is to create a separate region file for each punctum in the commissure. To start, we chose one punctum to analyze and traced each movement and pause using the line tool and the above color code. We always traced the punctum's pauses last, after tracing anterograde and retrograde movements. In crowded commissures it was helpful to switch between the kymograph and the original multi-plane tiff file to follow movements. If 2 puncta merge and then split off again, we assumed that each punctum maintained its original direction. We then saved this region as a .rgn file appended with "-pause-xx", where xx denotes a sequential number for each puncta in the commissure. We then logged the pause data, selecting Time as the only outputted measurement. We deleted each yellow pause line as we logged it, and then logged the blue "total time visible" line last. The red and green lines were not logged or deleted at this point. We then repeated this procedure for the rest of the puncta in the commissure, successively building a new region file for each new punctum. Each new region file started with the anterograde and retrograde movements of all previous puncta in the commissure. We then added the movements and pauses for the next puncta as above, logged and deleted the next puncta's pauses, etc. until the region file for the last punctum in the commissure was created. The final region file will thus contain all of the anterograde and retrograde movements for all puncta in the commissure, with all of the yellow pause lines

deleted because they have been logged. Our Excel Workbook calculated mean, standard deviation, and standard error of the % of time each puncta spent in a paused state. Calculations were performed in a "combined" fashion (grouped by commissure) and in an "uncombined" fashion (all puncta measurements pooled together). We then logged all anterograde data for the commissure by successively logging and deleting each green line. We finished by logging all retrograde data for the commissure by successively logging and deleting each red line. Our Excel spreadsheet then calculated the average run lengths and velocities in each direction in a "combined" fashion (grouped by commissure) and in an "uncombined" fashion (all puncta measurements pooled together). The above steps were repeated for each commissure's kymograph.

Definition of a movement: A "movement" was defined as occurring when a punctum moves at a velocity of >= 0.35 microns/ sec for a time of >= 0.90 sec (for short movements that last 0.90 – 3.0 seconds) or a velocity of >= 0.075 microns/ sec for a time of >= 3.0 seconds. A movement continues until it pauses for >= 1 seconds or until it reverses direction, or until it reaches the end of the time course, or until it merges with another punctum and does not reappear out the other side. Movements that changed their velocity without pausing or changing direction were treated as single point-to-point straight line movements, with one end of the line at the beginning of the movement and the other end at the end of the movement (thus creating an average distance and time from point A to point B).

Quantification and Statistical Analysis

We performed all statistical comparisons using the unpaired t test, Welch corrected (for comparisons between two selected groups) or ANOVA followed by the Tukey Kramer post-test (for comparisons involving 3 or more groups) using Graphpad Instat 3 (Graphpad Software). All statistical parameters, including the exact value of n, what n represents, and what error bars represent are reported in the figure legends or in the text for data presented in text form.

Non-wild type C. elegans strains

Strain name	Genotype (origin and/ or first use cited if not produced in this study)
KG4789	ceEx461 [strn-1::GFP]
KG2882	ceIs123 [unc-129::GFP] (Hoover et al., 2014)
KG4247	ceIs201 [unc-17::INS-22-Venus, unc-17::RFP, unc-17::ssmCherry] (Hoover et al., 2014)
KG4664	ceIs255 [unc-129::INS-22-Venus, unc-129::mCherry, unc-129::ssmCherry] (Edwards et al., 2015b)
KG5082	ceIs308 [mig-13::INS-22-Em, mig-13::RFPA]
KG4845	elks-1(js816); ceIs201 [unc-17::INS-22-Venus, unc-17::RFP, unc-17::ssmCherry]
KG5033	git-1(tm1962); ceIs201 [unc-17::INS-22-Venus, unc-17::RFP, unc-17::ssmCherry]
KG5012	lin-2(e1309); ceIs201 [unc-17::INS-22-Venus, unc-17::RFP, unc-17::ssmCherry]
KG4585	nud-2(ok949) ceIs201 [unc-17::INS-22-Venus, unc-17::RFP, unc-17::ssmCherry]
KG5016	ptp-3(tm352); ceIs201 [unc-17::INS-22-Venus, unc-17::RFP, unc-17::ssmCherry]
KG5028	rimb-1(ce828); ceIs201 [unc-17::INS-22-Venus, unc-17::RFP, unc-17::ssmCherry]
KG4400	sad-1(ce749) [2X outcrossed] (Edwards et al., 2015a)

KG4941 sad-1(ce749); ceIs123 [unc-129::GFP]

KG4414 sad-1(ce749); ceIs201 [unc-17::INS-22-Venus, unc-17::RFP, unc-17::ssmCherry]

KG4991 sad-1(ce749); ceIs201 [unc-17::INS-22-Venus, unc-17::RFP, unc-17::ssmCherry]; ceEx489 [unc-17::sad-1 cDNA]

KG4824 sad-1(ce749); ceIs255 [unc-129::INS-22-Venus, unc-129::mCherry, unc-129::ssmCherry]

KG5111 sad-1(ce749); ceIs308 [mig-13::INS-22-Em, mig-13::RFPA]

KG5240 sad-1(ce749); nud-2(ok949); ceIs201 [unc-17::INS-22-Venus, unc-17::RFP, unc-17::ssmCherry]

KG4947 sad-1(ce753); ceIs201 [unc-17::INS-22-Venus, unc-17::RFP, unc-17::ssmCherry]

KG4319 sad-1(ce776); ceIs201 [unc-17::INS-22-Venus, unc-17::RFP, unc-17::ssmCherry]

KG4382 sad-1(ce776); dpy-11(e224); ceIs201 [unc-17::INS-22-Venus, unc-17::RFP, unc-17::ssmCherry]

KG4357 sad-1(ce784); ceIs201 [unc-17::INS-22-Venus, unc-17::RFP, unc-17::ssmCherry]

KG4896 strn-1(ce793); ceIs201 [unc-17::INS-22-Venus, unc-17::RFP, unc-17::ssmCherry] [2X outcrossed]

KG4932 strn-1(ok2975) [4X outcrossed]

KG4887 strn-1(ok2975); ceIs123 [unc-129::GFP]

KG4786 strn-1(ok2975); ceIs201 [unc-17::INS-22-Venus, unc-17::RFP, unc-17::ssmCherry]

KG4820 strn-1(ok2975); ceIs201 [unc-17::INS-22-Venus, unc-17::RFP, unc-17::ssmCherry]; ceEx469 [unc-17::STRN-1-Hs]

KG4899 strn-1(ok2975); ceIs201 [unc-17::INS-22-Venus, unc-17::RFP, unc-17::ssmCherry]; ceEx480 [unc-17::STRN-1]

KG4794 strn-1(ok2975); ceIs255 [unc-129::INS-22-Venus, unc-129::mCherry, unc-129::ssmCherry]

KG5110 strn-1(ok2975); ceIs308 [mig-13::INS-22-Em, mig-13::RFPA]

KG4904 strn-1(ok2975); nud-2(ok949) ceIs201 [unc-17::INS-22-Venus, unc-17::RFP, unc-17::ssmCherry]

KG4833 strn-1(ok2975) sad-1(ce749)

KG4945 strn-1(ok2975) sad-1(ce749); ceIs123 [unc-129::GFP]

KG4847 strn-1(ok2975) sad-1(ce749); ceIs201 [unc-17::INS-22-Venus, unc-17::RFP, unc-17::ssmCherry]

KG5112 strn-1(ok2975) sad-1(ce749); ceIs308 [mig-13::INS-22-Em, mig-13::RFPA]

KG4848 strn-1(ok2975) syd-2(ok217); ceIs201 [unc-17::INS-22-Venus, unc-17::RFP, unc-17::ssmCherry]

KG4988 strn-1(ok2975) syd-2(ok217) sad-1(ce749); ceIs201 [unc-17::INS-22-Venus, unc-17::RFP, unc-17::ssmCherry]

KG4430 strn-1(ok2996); ceIs201 [unc-17::INS-22-Venus, unc-17::RFP, unc-17::ssmCherry]

KG4978 strn-1(ok2996) sad-1(ce753); ceIs201 [unc-17::INS-22-Venus, unc-17::RFP, unc-17::ssmCherry]

KG5006 syd-1(tm6234); ceIs201 [unc-17::INS-22-Venus, unc-17::RFP, unc-17::ssmCherry]

KG4828 syd-2(ok217); ceIs201 [unc-17::INS-22-Venus, unc-17::RFP, unc-17::ssmCherry]

KG4725	syd-2(ok217); ceIs255 [unc-129::INS-22-Venus, unc-129::mCherry, unc-129::ssmCherry] (Edwards et al., 2015b)
KG4977	syd-2(ok217) sad-1(ce749); ceIs201 [unc-17::INS-22-Venus, unc-17::RFP, unc-17::ssmCherry]
KG4979	unc-10(md1117); ceIs201 [unc-17::INS-22-Venus, unc-17::RFP, unc-17::ssmCherry]

Table 2. Mutation lesions and methods used for genotyping in strain constructions

Mutation	Description of Molecular Lesion	Method(s) used for genotyping	References
elks-1(js816)	494 bp deletion within exon 6. Splicing of remaining exon creates a frameshift that results in a stop codon at amino acid 292 (out of 837 amino acids).	PCR with primers inside deleted region	(Deken et al., 2005)
git-1(tm1962)	483 bp deletion and 23 bp insertion beginning in intron 7, including all of exons 8 and 9, and ending in intron 9. Splicing of exon 7 to exon 10 creates a frameshift that results in a stop at amino acid 318 (out of 670 amino acids).	PCR with primers inside deleted region	Japanese National Bioresource Project for the Experimental Animal "Nematode C.

			elegans" and (Patel et al., 2006)
lin-2(e1309)	Not published.	Vulvaless and Egl-D phenotypes	(Ferguson and Horvitz, 1985)
nud-2(ok949)	1109 bp deletion and a 1 bp insertion. Starts at the predicted ATG of nud-2 and deletes the entire open reading frame except the last part of the last exon.	PCR with primers inside deleted region	C. elegans Gene Knockout Consortium and (Fridolfsson et al., 2010)
ptp-3(tm352)	506 bp deletion beginning in exon 7, including all of exons 8 and 9, and ending in exon 10 of the "a" isoform. Splicing of the remaining portions of exons 7 and 10 creates a frameshift that results in a stop at amino acid 357 (out of 2180 amino acids). Changes/ eliminates 83.7% of the total protein.	PCR with primers inside deleted region	Japanese National Bioresource Project for the Experimental Animal "Nematode C. elegans" and (Ackley et al., 2005)

rimb-1(ce828)	13 bp insertion after AA16 (out of 1276 AA total) introduced through oligo templated Cas9 homologous recombination. Insert contains 3 stop codons, each in a different reading frame as well as an Nhe I site for screening.	Make 542 bp PCR product centered on the insertion, followed by restriction digest with Nhe I (the insertion creates an Nhe I site). Confirm using PCR followed by sequencing.	This study
sad-1(ce749)	Q57Stop (out of 835 or 914 amino acids, depending on the isoform). Mutation position is the same in both isoforms.	Make 250 bp PCR product centered on the mutation, followed by restriction digest with Mse I (the mutation creates an Mse I site).	(Edwards et al., 2015a)
sad-1(ce753)	R147Stop nonsense mutation	Make 500 bp PCR product centered on the mutation,	(Edwards et al., 2015a)

		followed by restriction digest with Bst UI (site is only present in wild type).	
sad-1(ce776)	E280Stop nonsense mutation	Not used in crosses	This study
sad-1(ce784)	Putative splicing mutation. Mutates the 8th intron of the "a" isoform near the splice. In wild type, it is gtgggataaaatgcatttt, which is not a great consensus after the gt (G-24%; G-9%) (Blumenthal). In the mutant it is gtgggatctgctgcatttt (changed from aaaa in wild type). The "C" at position +8 has a consensus of 9% (Blumenthal and Steward, 1997). GC (at positions 10-11 of the mutant) is sometimes rarely used as a 5' splice donor site and the att at positions 4-6 after that might enhance the site to cause mis-	Not used in crosses	This study

	splicing (Blumenthal and Steward, 1997).		
strn-1(ok2975)	558 bp deletion and 49 bp insertion that causes a frameshift resulting in R178Stop (out of 457 amino acids). Changes/ eliminates approximately 72.5% of the protein.	PCR with primers inside deleted region	C. elegans Gene Knockout Consortium and this study
strn-1(ok2996)	699 bp deletion with single bp (A) insertion. A97D and amino acids 98-222 (out of 457) are deleted; then the same reading frame resumes. Affects approximately 27.5% of the protein.	PCR with primers inside deleted region	C. elegans Gene Knockout Consortium and this study
syd-1(tm6234)	1266 bp deletion starting in the intron between exons 7 and 8 and ends in the middle of exon 11 of the "b" isoform. The deletion eliminates R249 – Y471 (out of 942 amino acids total) and results in a frame shift predicted to prevent translation of the remaining protein.	Behavioral phenotypes and PCR with primers inside deleted region	Japanese National Bioresource Project for the Experimental Animal "Nematode C. elegans" and (Edwards et al., 2015a)

syd-2(ok217)	~2 Kb deletion covering most of the N-terminal coiled coil domains. Results in a frame shift and stop codon at amino acid 200 (out of 1139 amino acids total).	Behavioral phenotypes and PCR with primers inside deleted region	C. elegans Gene Knockout Consortium and (Kittelmann et al., 2013; Wagner et al., 2009)
unc-10(md1117)	Deletion of entire unc-10 coding region.	PCR with primers inside deleted region	(Koushika et al., 2001)

Table S3. Transgenic arrays

Array name	Insertion location in the genome	Experimental contents and injection concentrations	Co-transformation markers and injection concentrations	References for transgene or integrated insertion

ceEx461	extrachromosomal array	KG#796 [strn-1::GFP] (25 ng/ ul)	None	This study
ceEx469	extrachromosomal array	KG#802 [unc-17::STRN-1-Hs cDNA] (4 ng/ ul)	pPD118.33 [myo-2::GFP] (0.75 ng/ ul)	This study
ceEx480	extrachromosomal array	KG#817 [unc-17::STRN-1 cDNA] (4 ng/ ul)	pPD118.33 [myo-2::GFP] (0.75 ng/ ul)	This study
ceEx489	extrachromosomal array	KG#838 [unc-17::SAD-1a cDNA] (4 ng/ ul)	pPD118.33 [myo-2::GFP] (0.75 ng/ ul)	This study
ceIs123	I: ~13.31	KG#367 [unc-129::GFP] (5 ng/ ul)	KG#255 [ttx-3::RFP] (25 ng/ ul)	(Hoover et al., 2014)
ceIs201	I: ~1.0	KG#686 [unc-17::INS-22-Venus] (6 ng/ ul) KG#654 [unc-17::ssmCherry] (4 ng/ ul) KG#248 [unc-17::mCherry] (4 ng/ ul)	KG#381 [myo-2::RFP] (1.5 ng/ ul)	(Hoover et al., 2014)
ceIs255	I: -23 or +21	KG#691 [unc-129::INS-22-Venus] (1.5 ng/ ul) KG#687 [unc-129::ssmCherry] (2.5 ng/	KG#255 [ttx-3::RFP] (15 ng/ ul)	(Edwards et al., 2015b)

		ul) KG#240 [unc-129::mCherry] (2.5 ng/ ul)		
ceIs308	IV: ~3.4	KG#859 [mig-13::INS-22-Emerald] (5 ng/ ul) KG#500 [mig-13::RFPA] (5 ng/ ul)	KS#4 [odr-1::RFP] (20 ng/ ul)	This study

Table S4. Plasmids

Plasmid name	Brief Description	Cloning details or reference giving cloning details
KG#59	rab-3:: expression vector	(Schade et al., 2005)
KG#94	unc-17:: expression vector	(Edwards et al., 2008)
KG#230	unc-129:: expression vector	(Edwards et al., 2009)
KG#240	unc-129::mCherry	(Edwards et al., 2009)
KG#248	unc-17::mCherry	(Hoover et al., 2014)
KG#255	ttx-3::RFP	(Edwards et al., 2009)
KG#367	unc-129::GFP	(Edwards et al., 2013)
KG#381	myo-2::-RFP	(Hoover et al., 2014)

KG#471	mig-13:: expression vector	(Edwards et al., 2015b)
KG#497	myo-3::mcs-RFPA	(Hoover et al., 2014)
KG#500	mig-13::mcs-RFPA	Used Kpn I/ Apa I to cut out the ~1.0 Kb unc-54 3' control region from KG#230, leaving the 6.1 Kb vector fragment containing the mig-13 promoter. To this vector fragment, we ligated the 1.8 Kb Kpn I/ Apa I fragment (containing RFPA + unc-54 3' control region) cut from KG#497 myo-3::mcs-RFPA.
KG#654	unc-17::ssmCherry	(Hoover et al., 2014)
KG#686	unc-17::INS-22-Venus	(Hoover et al., 2014)
KG#687	unc-129::ssmCherry	(Edwards et al., 2015b)
KG#691	unc-129::INS-22-Venus	(Edwards et al., 2015b)
KG#696	unc-17β::sad-1a cDNA	(Edwards et al., 2015a)
KG#720	rab-3::STRN-1-FLAG cDNA	Used AffinityScript Multiple Temperature Reverse Transcriptase and a primer engineered with a restriction site and FLAG tag to make the strn-1-FLAG cDNA (1470 bp). Used Herculase II polymerase and primers engineered with restriction sites to amplify and clone the cDNA into Nhe I/ Kpn I cut KG#59 (rab-3::___ expression vector; 4.9 Kb).

KG#796	strn-1::GFP	Used Herculase II polymerase and primers engineered with restriction sites to amplify and clone the 3.4 Kb strn-1 (C16E9.2) promoter region from N2 genomic DNA into Pst I/ Sac I cut pPD95.67 (4.5 Kb). The promoter region included the entire intergenic region between the 5' UTR of F14B8.6 (which is in opposite orientation upstream of strn-1) and the 5' UTR of C16E9.2 and also includes the 1st 10 bp of C16E9.2's 5' UTR.
KG#802	unc-17::STRN-1-Hs (Homo sapiens)	Used Herculase II DNA polymerase and primers engineered with restriction sites to amplify and clone the 1.2 Kb strn-1-Hs cDNA (conserved protein KIAA0390) from the Genscript ORF clone ID Ohu03925 into Nhe I/ Kpn I cut KG#94 unc-17:: expression vector (6.9 Kb).
KG#817	unc-17::STRN-1cDNA	Used Herculase II DNA polymerase and primers engineered with restriction sites to amplify and clone the 1470 bp strn-1 cDNA from KG#720 rab-3::strn-1-FLAG cDNA into Nhe I/ Kpn I cut KG#94 (unc-17::___; 6.9 Kb).
KG#838	unc-17::sad-1a cDNA	Use Nhe I/ Kpn I to cut out the 2.7 Kb sad-1a cDNA from KG#696 (unc-17::sad-1a cDNA) and clone it into the like-digested unc-17:: expression vector KG#94 (6.9 Kb).

KG#843	gRNA F&E plasmid for targeting rimb-1 knockout	Designed forward and reverse primers bearing the gRNA site and complimentary overhangs (forward: 5'-TCTTGN_{20}-3' and reverse 5'-AAACN*$_{20}$C-3', where N*$_{20}$ denotes the reverse complement of N_{20}). We began by annealing forward and reverse oligonucleotides and then ligated them into the BsaI – cut vector pJP118. We did a Qiagen Tip-20 prep on 1 clone, confirmed the size by restriction digest, and submitted it for sequence with the M13 primer to sequence across the insertion site.
KG#858	ANF-Emerald	Gift of Edwin Levitan, University of Pittsburgh
KG#859	mig-13::INS-22-Emerald	Used Q5 Polymerase and engineered primers to produce overlapping PCR fragments followed by NEBuilder Master Mix to insert the 331 bp INS-22 gene coding region (from N2 genomic DNA) and the 720 bp Emerald fragment (PCRed from KG#858) into the mig-13:: expression vector KG#471 (7.1 Kb).
KS#4	odr-1::RFP	Gift of Kang Shen, Stanford University (Klassen and Shen, 2007)
pDD162	eft-3::Cas9	AddGene
pPD95.67	Promoterless GFP vector with SV40	Gift of Andrew Fire, Stanford University

	nuclear localization signal	
pPD118.33	myo-2::GFP	Gift of Andrew Fire, Stanford University
pJP118	U6::sgRNA (F+E) (gRNA F+E plasmid)	Gift of Andrew Fire and Joshua Arribere, Stanford University

Table S1. C. elegans non-wild type Strains.

Strain name	Genotype (origin and/ or first use cited if not produced in this study)
KG4790	ceEx462 [unc-129::STRN-1-GFP]
KG5131	ceEx503 [mig-13::UNC-10-GFP, Td Tomato-STRN-1]
KG5203	ceEx510 [mig-13::STRN-1-Emerald, SAD-1-tdTomato]
KG2882	ceIs123 [unc-129::GFP, ttx-3::mCherry] (Hoover, 2014)
KG4671	ceIs259 [unc-129::RFP-SYN-13, -Venus] (Edwards, 2015)
KG2430	ceIs56 [unc-129::CTNS-1-RFP, unc-129::nlp-21-Venus] (Edwards, 2009)
KG4846	elks-1(js816); wyIs85 [itr-1::GFP-RAB-3, odr-1::RFP]
KG5030	git-1(tm1962); wyIs85 [itr-1::GFP-RAB-3, odr-1::RFP]
KG5011	lin-2(e1309); wyIs85 [itr-1::GFP-RAB-3, odr-1::RFP]
KG4506	nud-2(ok949); wyIs85 [itr-1::GFP-RAB-3, odr-1::RFP]
KG5021	ptp-3(tm352); wyIs85 [itr-1::GFP-RAB-3, odr-1::RFP]
KG5029	rimb-1(ce828); wyIs85 [itr-1::GFP-RAB-3, odr-1::RFP]

KG4400	sad-1(ce749)
KG4822	sad-1(ce749); ceEx462 [unc-129::STRN-1-GFP]
KG4941	sad-1(ce749); ceIs123 [unc-129::GFP, ttx-3::mCherry]
KG4610	sad-1(ce749); wyIs85 [itr-1::GFP-RAB-3, odr-1::RFP]
KG4932	strn-1(ok2975) [4x O.C.]
KG4740	strn-1(ok2975) ceIs56 [unc-129::CTNS-1-RFP, unc-129::nlp-21-Venus]
KG4833	strn-1(ok2975) sad-1(ce749)
KG4945	strn-1(ok2975) sad-1(ce749); ceIs123 [unc-129::GFP, ttx-3::mCherry]
KG4849	strn-1(ok2975) sad-1(ce749); wyIs85 [itr-1::GFP-RAB-3, odr-1::RFP]
KG5013	strn-1(ok2975) syd-2(ok217) sad-1(ce749); wyIs85 [itr-1::GFP-RAB-3, odr-1::RFP]
KG4812	strn-1(ok2975) syd-2(ok217); wyIs85 [itr-1::GFP-RAB-3, odr-1::RFP]
KG4887	strn-1(ok2975); ceIs123 [unc-129::GFP, ttx-3::mCherry]
KG4886	strn-1(ok2975); ceIs259 [unc-129::RFP-SYN-13, -Venus]
KG4787	strn-1(ok2975); wyIs85 [itr-1::GFP-RAB-3, odr-1::RFP]
KG4992	strn-1(ok2975); wyIs85 [itr-1::GFP-RAB-3, odr-1::RFP]; ceEx490 [itr-1::STRN-1 cDNA]
KG4490	strn-1(ok2996)
KG4933	strn-1(ok2996) sad-1(ce749)
KG4943	strn-1(ok2996); wyIs85 [itr-1::GFP-RAB-3, odr-1::RFP]
KG5126	strn-1(ok2996); wyIs85 [itr-1::GFP-RAB-3, odr-1::RFP]; ceEx501 [itr-1::STRN-1 cDNA]

KG4987	syd-2(ok217) sad-1(ce749); wyIs85 [itr-1::GFP-RAB-3, odr-1::RFP]
KG4821	syd-2(ok217); ceEx462 [unc-129::STRN-1-GFP]
KG4526	syd-2(ok217); wyIs85 [itr-1::GFP-RAB-3, odr-1::RFP]
KG4981	unc-10(md1117); wyIs85 [itr-1::GFP-RAB-3, odr-1::RFP]
KG5001	unc-13(md1072); wyIs85 [itr-1::GFP-RAB-3, odr-1::RFP]
KG4673	unc-16(ce483); ceIs259 [unc-129::RFP-SYN-13, -Venus]
KG4192	unc-16(ce483); ceIs56 [unc-129::CTNS-1-RFP, unc-129::nlp-21-Venus]
KG4573	unc-16(ce483); nud-2(ok949); ceIs56 [unc-129::CTNS-1-RFP, unc-129::nlp-21-Venus]
KG4931	unc-16(ce483); nud-2(ok949); sad-1(ce749) strn-1(ok2975) ceIs56 [unc-129::CTNS-1-RFP, unc-129::nlp-21-Venus]
KG4892	unc-16(ce483); nud-2(ok949); strn-1(ok2975) ceIs56 [unc-129::CTNS-1-RFP, unc-129::nlp-21-Venus]
KG4893	unc-16(ce483); nud-2(ok949); syd-2(ok217) strn-1(ok2975) ceIs56 [unc-129::CTNS-1-RFP, unc-129::nlp-21-Venus]
KG4498	unc-16(ce483); sad-1(ce749) ceIs56 [unc-129::CTNS-1-RFP, unc-129::nlp-21-Venus]
KG4811	unc-16(ce483); sad-1(ce749) strn-1(ok2975) ceIs56 [unc-129::CTNS-1-RFP, unc-129::nlp-21-Venus]
KG4750	unc-16(ce483); strn-1(ok2975) ceIs56 [unc-129::CTNS-1-RFP, unc-129::nlp-21-Venus]

KG4805	unc-16(ce483); strn-1(ok2975) ceIs56 [unc-129::CTNS-1-RFP, unc-129::nlp-21-Venus]; ceEx463 [unc-129::STRN-1-Hs]
KG4958	unc-16(ce483); strn-1(ok2975) ceIs56 [unc-129::CTNS-1-RFP, unc-129::nlp-21-Venus]; ceEx485 [unc-129::STRN-1]
KG4791	unc-16(ce483); strn-1(ok2975) ceIs56; ceEx462 [unc-129::STRN-1—GFP]
KG4905	unc-16(ce483); strn-1(ok2975); ceIs259 [unc-129::RFP-SYN-13, -Venus]
KG4520	unc-16(ce483); strn-1(ok2996) ceIs56 [unc-129::CTNS-1-RFP, unc-129::nlp-21-Venus]
KG4563	unc-16(ce483); syd-2(ok217) ceIs56 [unc-129::CTNS-1-RFP, unc-129::nlp-21-Venus]
KG4814	unc-16(ce483); syd-2(ok217) strn-1(ok2975) ceIs56 [unc-129::CTNS-1-RFP, unc-129::nlp-21-Venus]
TV1229	wyIs85 [itr-1::GFP-RAB-3, odr-1::RFP] [Klassen, 2007]

Table S2. Mutation lesions and methods used for genotyping in strain constructions.

Mutation	Description of Molecular Lesion	Effect on Protein	Method(s) used for genotyping	References

elks-1(js816)	494 bp deletion within exon 6. Splicing of remaining exon creates a frameshift that results in a stop codon at amino acid 292 (out of 837 amino acids).	Putative null	PCR with primers inside deleted region	(Deken et al., 2005)
git-1(tm1962)	483 bp deletion and 23 bp insertion beginning in intron 7, including all of exons 8 and 9, and ending in intron 9. Splicing of exon 7 to exon 10 creates a frameshift that results in a stop at amino acid 318 (out of 670 amino acids).	Putative null	PCR with primers inside deleted region	Japanese National Bioresource Project for the Experimental Animal “Nematode C. elegans” and (Patel et al., 2006)
lin-2(e1309)	Not published.	Putative null	Vulvaless and Egl-D phenotypes	(Ferguson and Horvitz, 1985)

nud-2(ok949)	1109 bp deletion and a 1 bp insertion. Starts at the predicted ATG of nud-2 and deletes the entire open reading frame except the last part of the last exon.	Putative null	PCR with primers inside deleted region	C. elegans Gene Knockout Consortium and (Fridolfsson et al., 2010)
ptp-3(tm352)	506 bp deletion in ptp-3a (bp# 1462-1967). Mutation eliminates exons 8 and 9. The subsequent splicing of exons 7 and 10 creates a frameshift at AA355 that results in a stop at AA357. This changes/eliminates 83.7% of the total protein.		PCR with primers inside deleted region	Japanese National Bioresource Project for the Experimental Animal “Nematode C. elegans” and (Ackley et al., 2005)
rimb-1(ce828)	13 bp insertion after AA16 (out of 1276 AA	Putative null	Make 542 bp PCR product	This study

	total) introduced through oligo templated Cas9 homologous recombination. Insert contains 3 stop codons, each in a different reading frame as well as an Nhe I site for screening.		centered on the insertion, followed by restriction digest with Nhe I (the insertion creates an Nhe I site). Confirm using PCR followed by sequencing.	
sad-1(ce749)	Q57Stop (out of 835 or 914 amino acids, depending on the isoform). Mutation position is the same in both isoforms.	Putative null	Make 250 bp PCR product centered on the mutation, followed by restriction digest with Mse I (the mutation creates an Mse I site).	(Edwards et al., 2015)

strn-1(ok2975)	558 bp deletion and 49 bp insertion that causes a frameshift resulting in R178Stop (out of 457 amino acids). Changes/ eliminates approximately 72.5% of the protein.		PCR with primers inside deleted region	C. elegans Gene Knockout Consortium
strn-1(ok2996)	699 bp deletion with single bp (A) insertion. A97D and amino acids 98-222 (out of 457) are deleted; then the same reading frame resumes. Affects approximately 27.5% of the protein.		PCR with primers inside deleted region	C. elegans Gene Knockout Consortium
syd-2(ok217)	~2 Kb deletion covering most of the N-terminal coiled coil domains. Results in a frame shift and stop codon at amino acid 200 (out of 1139 amino acids total).	Putative null	Behavioral phenotypes and PCR with primers inside deleted region	C. elegans Gene Knockout Consortium and (Kittelmann et al., 2013; Wagner et al., 2009)

unc-10(md1117)	Deletion of entire unc-10 coding region.	Null	PCR with primers inside deleted region	(Koushika et al., 2001)
unc-13(md1072)	26- to 38-kb deletion that eliminates all of the L coding region		Behavioral phenotypes and PCR with primers inside deleted region	(Kohn et al., 2000)
unc-16(ce483)	Q304Stop (out of1157 amino acids of the ZK1098.10b isoform)	Putative null	Behavioral phenotypes and PCR followed by sequencing	(Edwards et al., 2013)

Table 3. Transgenic arrays.

Array name	Insertion location in genome	Experimental contents and injection concentrations	Co-transformation markers and injection concentrations	References for transgene or integrated insertion (if

				not made in this study)
ceEx462	extrachromosomal array	KG#797 (unc-129::STRN-1-GFP) (0.7 ng/ ul)	KG#67 (ttx-3::GFP) (25 ng/ ul)	this study
ceEx463	extrachromosomal array	KG#799 (unc-129::STRN-1-Hs cDNA) (5 ng/ ul)	KG#67 (ttx-3::GFP) (25 ng/ ul)	this study
ceEx485	extrachromosomal array	KG#818 (unc-129::STRN-1 cDNA) (2.5 ng/ ul)	KG#67 (ttx-3::GFP) (25 ng/ ul)	this study
ceEx490	extrachromosomal array	KG#819 (itr-1::STRN-1) (1 ng/ ul)	KS#5 (odr-1::GFP) (20 ng/ ul)	this study
ceEx501	extrachromosomal array	KG#819 (itr-1::STRN-1 cDNA) (4 ng/ ul)	KS#5 (odr-1::GFP) (20 ng/ ul)	this study
ceEx503	extrachromosomal array	KG#840 (mig-13::UNC-10 [627-974]-GFP) (1.5 ng/ ul) KG#899 (mig-13::tdTomato-STRN-1) (1.5 ng/ul)	KS#4 (odr-1::RFP) (20 ng/ ul)	this study

ceEx510	extrachromosomal array	KG#917 (mig-13::STRN-1-Emerald) (1.0 ng/ ul) KG#921 (mig-13::SAD-1-tdTomato) (1.0 ng/ ul)	KS#4 (odr-1::RFP) (20 ng/ ul)	this study
ceIs123	I: ~13.31	KG#367 [unc-129::GFP] (5 ng/ ul)	KG#255 [ttx-3::RFP] (25 ng/ ul)	(Hoover et al., 2014)
ceIs259	IV: ~3.4	KG#414 [unc-129::RFP-SYN-13] (1.0 ng/ ul) KG#374 [unc-129::mCherry] (1.0 ng/ ul)	KG#255 (ttx-3::RFP) (15 ng/ ul)	this study
ceIs56	X: ~9.0	KG#371 [unc-129::CTNS-1a-RFP] (5 ng/ ul)	KG#255 [ttx-3::RFP] (15 ng/ ul) KP#1383 unc-129::NLP-21-Venus (15 ng/ ul)	(Edwards et al., 2009; Edwards et al., 2013)
wyIs85	V: near 4.63	itr-1::GFP-RAB-3 – 10 ng/ ul	odr-1::dsRed — 20 ng/ ul	(Klassen and Shen, 2007)

Table S4. Plasmids.

Plasmid name	Brief Description	Cloning details or reference giving cloning details
KG#67	ttx-3::GFP	Gift of Oliver Hobert, Columbia University

KG#230	unc-129:: expression vector	[Edwards, 2009]
KG#255	ttx-3::RFP	(Edwards et al., 2009)
KG#367	unc-129:___-GFP	(Edwards et al., 2013)
KG#371	unc-129::ctns-1a-RFP (mCherry)	(Edwards et al., 2013)
KG#374	unc-129::___-Venus expression vector	(Edwards et al., 2009)
KG#414	unc-129::RFP-SYN-13	(Edwards et al., 2013)
KG#471	mig-13:: expression vector	[Edwards, 2015]
KG#473	mig-13::___-GFP	Used Kpn I/ Apa I to cut out the ~1000 bp unc-54 3' control region from KG#471, leaving the 6.0 kb vector fragment containing the mig-13 promoter. To this vector fragment, we will ligate the 1800 bp Kpn I/ Apa I fragment (containing GFP + unc-54 3' control region) cut from pPD94.81.
KG#695	unc-129::SAD-1-GFP cDNA	[Edwards, 2015]
KG#720	rab-3::STRN-1-FLAG cDNA	Used AffinityScript Multiple Temperature Reverse Transcriptase and a primer engineered with a restriction site and FLAG tag to make the strn-1-FLAG cDNA (1470

		bp). Used Herculase II polymerase and primers engineered with restriction sites to amplify and clone the cDNA into Nhe I/ Kpn I cut KG#59 (rab-3::___ expression vector; 4.9 Kb).
KG#730	itr-1::expression vector	[Edwards, 2015]
KG#797	unc-129::STRN-1-GFP	Used Herculase II DNA polymerase and primers engineered with restriction sites to amplify and clone the 1.4 Kb strn-1 (C16E9.2) cDNA (minus its stop codon) from KG#720 rab-3::strn-1-FLAG into Nhe I/ Kpn I cut KG#367 (unc-129::___-GFP; 7.2 Kb) such that it is in-frame with the GFP.
KG#799	unc-129::STRN-1-Hs (Homo sapiens)	Used Herculase II DNA polymerase and primers engineered with restriction sites to amplify and clone the 1.2 Kb strn-1-Hs cDNA (conserved protein KIAA0390) from the Genscript ORF clone ID Ohu03925 into Nhe I/ Kpn I cut KG#230 (unc-129::___; 6.4 Kb).
KG#818	unc-129::STRN-1cDNA	Used Herculase II DNA polymerase and primers engineered with restriction sites to amplify and clone the 1470 bp strn-1 cDNA from KG#720 rab-3::strn-1-FLAG cDNA into Nhe I/ Kpn I cut KG#230 (unc-129::___; 6.4 Kb).
KG#819	itr-1::STRN-1cDNA	Used Herculase II DNA polymerase and primers engineered with restriction sites to amplify and clone the

		1470 bp strn-1 cDNA from KG#720 rab-3::strn-1-FLAG cDNA into Nhe I/ Kpn I cut KG#730 (itr-1::___; 6.0 Kb).
KG#840	mig-13::UNC-10 [627-974]-GFP cDNA	Used AffinityScript Multiple Temperature Reverse Transcriptase and a primer engineered with a restriction site to make the unc-10 first strand cDNA starting at codon 974. Then used Herculase II polymerase and primers engineered with restriction sites and an artificial Met start codon to amplify and clone the 1044 bp UNC-10 [H627-R974] cDNA into Sbf I/ Kpn I cut KG#473 (mig-13::___ GFP expression vector; 7.8 Kb).
KG#859	mig-13::INS-22-Emerald	Used ApE to digitally construct the plasmid, then design the primers necessary to assemble INS-22-Emerald in the mig-13:: vector background. Then used Q5 Polymerase to produce the fragments and the NEBuilder Master Mix to make the new plasmid.
KG#899	mig-13::tdTomato—STRN-1	Used ApE to digitally construct the plasmid, then designed the primers necessary to assemble tdTomato + a 2XGGSG linker onto the N-terminus of the strn-1 cDNA (PCRed from KG#818 unc-129::strn-1 cDNA) in the KG#471 mig-13::___ expression vector to make mig-13::tdTomato-strn-1 cDNA. Then used Q5 Polymerase to produce the

		fragments and the NEBuilder Master Mix to make the new plasmid.
KG#906	mig-13::__-tdTomato	Used Q5 DNA polymerase and primers engineered with restriction sites to amplify the 1.4 Kb tdTomato cDNA plasmid (gift of Dean Dawson, OMRF) and cloned it into Kpn I/ Xho I cut KG#471 (7.1 kb; mig-13::___ expression vector).
KG#917	mig-13::STRN-1—Emerald	Used Q5 polymerase and primers engineered with restriction sites to amplify the 1.4 Kb strn-1 cDNA and C-terminal linker from KG#797 unc-129::strn-1—GFP and cloned it into Not I/ Kpn I cut KG#920 (mig-13::INS-22-Emerald), removing INS-22 to leave the 7.8 Kb vector fragment).
KG#918	mig-13::SAD-1—Emerald	Used Q5 polymerase and primers engineered with restriction sites to amplify the 2.7 Kb sad-1 cDNA (adding the same C-terminal linker) from KG#695 unc-129::sad-1-GFP and cloned it into Not I/ Kpn I cut KG#920 (mig-13::INS-22-Emerald), removing INS-22 to leave the 7.8 Kb vector fragment).
KG#919	mig-13::__-tdTomato with NotI site	Used the Q5 Site-Directed Mutagenesis Kit to insert a Not I site in KG#906 plasmid. Digested with Not I to verify that the modification was successful.

KG#920	13::INS-22-Emerald with Not I site	Used the Q5 Site-Directed Mutagenesis Kit to insert a Not I site in KG#859 plasmid. Digested with Not I to verify that the modification was successful.
KG#921	mig-13::SAD-1—tdTomato	Used Q5 polymerase and primers engineered with restriction sites to amplify the 2.7 Kb sad-1 cDNA (including the C-terminal linker) from KG#918 mig-13::SAD-1-Emerald and cloned it into Not I/ Kpn I cut KG#919 (mig-13::___-tdTomato; 8.1 Kb).
KP#1383	unc-129::NLP-21-Venus	Gift of Joshua Kaplan and Derek Sieburth, Massachusetts General Hospital/ Harvard University (Sieburth et al., 2007)
KS#5	odr-1::GFP	Gift of Kang Shen, Stanford University (Klassen and Shen, 2007)
pPD94.81	unc-54::GFP	Gift of Andrew Fire, Stanford University
pJP118	U6::sgRNA (F+E) (gRNA F+E plasmid)	Gift of Andrew Fire and Joshua Arribere, Stanford University

E. Cited Literature

Ackley, B. D. (2005). The Two Isoforms of the Caenorhabditis elegans Leukocyte-Common Antigen Related Receptor Tyrosine Phosphatase PTP-3 Function Independently in Axon Guidance and Synapse Formation. Journal of Neuroscience, 25(33), 7517–7528. http://doi.org/10.1523/JNEUROSCI.2010-05.2005

Arribere, J. A., Bell, R. T., Fu, B. X. H., Artiles, K. L., Hartman, P. S., & Fire, A. Z. (2014). Efficient marker-free recovery of custom genetic modifications with CRISPR/Cas9 in Caenorhabditis elegans. Genetics, 198(3), 837–846. http://doi.org/10.1534/genetics.114.169730

Baas, & Lin. (2012). Orientation in the Neuron, 71(6), 403–418. http://doi.org/10.1002/dneu.20818.Hooks

Banerjee, N., Bhattacharya, R., Gorczyca, M., Collins, K. M., & Francis, M. M. (2017). Local neuropeptide signaling modulates serotonergic transmission to shape the temporal organization of C. elegans egg-laying behavior. PLoS Genetics, 13(4). http://doi.org/10.1371/journal.pgen.1006697

Bhattacharya, R., & Francis, M. M. (2015). during food searching, (September), 1–5.

Bhattacharya, R., Touroutine, D., Barbagallo, B., Climer, J., Lambert, C. M., Clark, C. M., … Francis, M. M. (2014). A Conserved Dopamine-Cholecystokinin Signaling Pathway Shapes Context???Dependent Caenorhabditis elegans Behavior. PLoS Genetics, 10(8). http://doi.org/10.1371/journal.pgen.1004584

Bulgari, D., Deitcher, D. L., & Levitan, E. S. (2016). Loss of Huntingtin stimulates capture of retrograde dense-core vesicles to increase synaptic neuropeptide stores. European Journal of Cell Biology, (March). http://doi.org/10.1016/j.ejcb.2017.01.001

Burton, P. R., & Paige, J. L. (1981). Polarity of axoplasmic microtubules in the olfactory nerve of the frog. Neurobiology, 78(5), 3269–3273. http://doi.org/10.1073/pnas.78.5.3269

Cavolo, S. L., Zhou, C., Ketcham, S. A., Suzuki, M. M., Ukalovic, K., Silverman, M. A., … Levitan, E. S. (2015). Mycalolide B dissociates dynactin and abolishes retrograde axonal transport of dense-core vesicles. Molecular Biology of the Cell, 26(14), 2664–2672. http://doi.org/10.1091/mbc.E14-11-1564

Chen, D., Taylor, K. P., Hall, Q., & Kaplan, J. M. (2016). The neuropeptides FLP-2 and PDF-1 act in concert to arouse Caenorhabditis elegans locomotion. Genetics, 204(3), 1151–1159. http://doi.org/10.1534/genetics.116.192898

Chia, P. H., Patel, M. R., & Shen, K. (2012). NAB-1 instructs synapse assembly by linking adhesion molecules and F-actin to active zone proteins. Nature Neuroscience, 15(2), 234–242. http://doi.org/10.1038/nn.2991

Choi, S., Taylor, K. P., Chatzigeorgiou, M., Hu, Z., Schafer, W. R., & Kaplan, J. M. (2015). Sensory Neurons Arouse C. elegans Locomotion via Both Glutamate and Neuropeptide Release. PLoS Genetics, 11(7), 1–20. http://doi.org/10.1371/journal.pgen.1005359

Cool, D. R., Normant, E., Shen, F., Chen, H. C., Pannell, L., Zhang, Y., & Loh, Y. P. (1997). Carboxypeptidase E is a regulated secretory pathway sorting receptor: genetic obliteration leads to endocrine disorders in Cpe(fat) mice. Cell, 88(1), 73–83. http://doi.org/10.1016/S0092-8674(00)81860-7

Crump, J. G., Zhen, M., Jin, Y., & Bargmann, C. I. (2001). The SAD-1 kinase regulates presynaptic vesicle clustering and axon termination. Neuron, 29(1), 115–129. http://doi.org/10.1016/S0896-6273(01)00184-2

Dai, Y., Taru, H., Deken, S. L., Grill, B., Ackley, B., Nonet, M. L., & Jin, Y. (2006). SYD-2 Liprin-alpha organizes presynaptic active zone formation through ELKS. Nat Neurosci, 9(12), 1479–1487. http://doi.org/nn1808 [pii]\r10.1038/nn1808

Edwards, S. L., Morrison, L. M., Yorks, R. M., Hoover, C. M., Boominathan, S., & Miller, K. G. (2015). UNC-16 (JIP3) acts through synapse-assembly proteins to inhibit the active transport of cell soma organelles to Caenorhabditis elegans motor neuron axons. Genetics, 201(1), 117–141. http://doi.org/10.1534/genetics.115.177345

Edwards, S. L., Yorks, R. M., Morrison, L. M., Hoover, C. M., & Miller, K. G. (2015). Synapse-assembly proteins maintain synaptic vesicle cluster stability and regulate synaptic vesicle transport in Caenorhabditis elegans. Genetics, 2011. Edwa(1), 91–116. http://doi.org/10.1534/genetics.115.177337

Fouquet, W., Owald, D., Wichmann, C., Mertel, S., Depner, H., Dyba, M., … Sigrist, S. J. (2009). Maturation of active zone assembly by Drosophila Bruchpilot. Journal of Cell Biology, 186(1), 129–145. http://doi.org/10.1083/jcb.200812150

Fricker, L. D. (1988). Carboxypeptidase E. Ann. Rev. Physiol, 50(7), 309–21. Retrieved from http://www.annualreviews.org/doi/pdf/10.1146/annurev.ph.50.030188.001521

Goodwin, P. R., Sasaki, J. M., & Juo, P. (2012). Cyclin-Dependent Kinase 5 Regulates the Polarized Trafficking of Neuropeptide-Containing Dense-Core Vesicles in Caenorhabditis elegans Motor Neurons. Journal of Neuroscience, 32(24), 8158–8172. http://doi.org/10.1523/JNEUROSCI.0251-12.2012

Hall, D. H., & Hedgecock, E. M. (1991). Kinesin-related gene unc-104 is required for axonal transport of synaptic vesicles in C. elegans. Cell, 65(5), 837–847. http://doi.org/10.1016/0092-8674(91)90391-B

Hallam, S. J., Goncharov, A., McEwen, J., Baran, R., & Jin, Y. (2002). SYD-1, a presynaptic protein with PDZ, C2 and rhoGAP-like domains, specifies axon identity in C. elegans. Nature Neuroscience, 5(11), 1137–1146. http://doi.org/10.1038/nn959

Hammarlund, M., Watanabe, S., Schuske, K., & Jorgensen, E. M. (2008). CAPS and syntaxin dock dense core vesicles to the plasma membrane in neurons. Journal of Cell Biology, 180(3), 483–491. http://doi.org/10.1083/jcb.200708018

Heidemann, S. R., Landers, J. M., & Hamborg, M. A. (1981). Polarity orientation of axonal microtubules. Journal of Cell Biology, 91(3 I), 661–665. http://doi.org/10.1083/jcb.91.3.661

Hoover, C. M., Edwards, S. L., Yu, S. C., Kittelmann, M., Richmond, J. E., Eimer, S., … Miller, K. G. (2014). A novel CaM kinase II pathway controls the location of neuropeptide release from Caenorhabditis elegans motor neurons. Genetics, 196(3), 745–765. http://doi.org/10.1534/genetics.113.158568

Hu, Z., Vashlishan-Murray, a. B., & Kaplan, J. M. (2015). NLP-12 Engages Different UNC-13 Proteins to Potentiate Tonic and Evoked Release. Journal of Neuroscience, 35(3), 1038–1042. http://doi.org/10.1523/JNEUROSCI.2825-14.2015

Hu, Z., Pym, E. C. G., Babu, K., Vashlishan Murray, A. B., & Kaplan, J. M. (2011). A Neuropeptide-Mediated Stretch Response Links Muscle Contraction to Changes in Neurotransmitter Release. Neuron, 71(1), 92–102. http://doi.org/10.1016/j.neuron.2011.04.021

Hung, W., Hwang, C., Po, M. D., & Zhen, M. (2007). Neuronal polarity is regulated by a direct interaction between a scaffolding protein, Neurabin, and a presynaptic SAD-1 kinase in Caenorhabditis elegans. Development (Cambridge, England), 134(2), 237–49. http://doi.org/10.1242/dev.02725

Inoue, E., Mochida, S., Takagi, H., Higa, S., Deguchi-Tawarada, M., Takao-Rikitsu, E., … Takai, Y. (2006). SAD: A Presynaptic Kinase Associated with Synaptic Vesicles and the Active Zone Cytomatrix that Regulates Neurotransmitter Release. Neuron, 50(2), 261–275. http://doi.org/10.1016/j.neuron.2006.03.018

Kim, J. S. M., Hung, W., Narbonne, P., Roy, R., & Zhen, M. (2010). C. elegans STRADalpha and SAD cooperatively regulate neuronal polarity and synaptic organization. Development (Cambridge, England), 137(1), 93–102. http://doi.org/10.1242/dev.041459

Kim, J. S., Lilley, B. N., Zhang, C., Shokat, K. M., Sanes, J. R., & Zhen, M. (2008). A chemical-genetic strategy reveals distinct temporal requirements for SAD-1 kinase in neuronal polarization and synapse formation. Neural Development, 3(1), 23. http://doi.org/10.1186/1749-8104-3-23

Kittelmann, M., Hegermann, J., Goncharov, A., Taru, H., Ellisman, M. H., Richmond, J. E., … Eimer, S. (2013). Liprin-α/SYD-2 determines the size of dense projections in presynaptic active zones in C. elegans. Journal of Cell Biology, 203(5), 849–863. http://doi.org/10.1083/jcb.201302022

Klassen, M. P., & Shen, K. (2007). Wnt Signaling Positions Neuromuscular Connectivity by Inhibiting Synapse Formation in C. elegans. Cell, 130(4), 704–716. http://doi.org/10.1016/j.cell.2007.06.046

Klassen, M. P., Wu, Y. E., Maeder, C. I., Nakae, I., Cueva, J. G., Lehrman, E. K., … Shen, K. (2010). An Arf-like Small G Protein, ARL-8, Promotes the Axonal Transport of Presynaptic Cargoes by Suppressing Vesicle Aggregation. Neuron, 66(5), 710–723. http://doi.org/10.1016/j.neuron.2010.04.033

Levitan, E. S. (2008). Signaling for vesicle mobilization and synaptic plasticity. Molecular Neurobiology, 37(1), 39–43. http://doi.org/10.1007/s12035-008-8014-3

Lilley, B. N., Krishnaswamy, A., Wang, Z., Kishi, M., Frank, E., & Sanes, J. R. (2014). SAD kinases control the maturation of nerve terminals in the mammalian peripheral and central nervous systems. Proceedings of the National Academy of Sciences, 111(3), 1138–1143. http://doi.org/10.1073/pnas.1321990111

Lim, M. A., Chitturi, J., Laskova, V., Meng, J., Findeis, D., Wiekenberg, A., … Zhen, M. (2016). Neuroendocrine modulation sustains the C. elegans forward motor state. eLife, 5(NOVEMBER2016), 1–33. http://doi.org/10.7554/eLife.19887

Liu, T., Kim, K., Li, C., & Barr, M. M. (2007). FMRFamide-like neuropeptides and mechanosensory touch receptor neurons regulate male sexual turning behavior in Caenorhabditis elegans. J Neurosci, 27(27), 7174–7182. http://doi.org/10.1523/JNEUROSCI.1405-07.2007

Miller, K. G. (2016). Keeping Neuronal Cargoes on the Right Track: New Insights into Regulators of Axonal Transport. The Neuroscientist, 1–22. http://doi.org/10.1177/1073858416648307

Miller, K. E., Deproto, J., Kaufmann, N., Patel, B. N., Duckworth, A., & Vactor, D. Van. (2005). Direct Observation Demonstrates that Liprin- ⎵ Is Required for Trafficking of Synaptic Vesicles, 15, 684–689. http://doi.org/10.1016/j.cub.2005.02.061

Ou, C., Poon, V. Y., Maeder, C. I., Watanabe, S., Lehrman, E. K., Fu, A. K. Y., … Shen, K. (2010). Two Cyclin-Dependent Kinase Pathways Are Essential for Polarized Trafficking of Presynaptic Components. Cell, 141(5), 846–858. http://doi.org/10.1016/j.cell.2010.04.011

Pack-Chung, E., Kurshan, P. T., Dickman, D. K., & Schwarz, T. L. (2007). A Drosophila kinesin required for synaptic bouton formation and synaptic vesicle transport. Nature Neuroscience, 10(8), 980–989. http://doi.org/10.1038/nn1936

Patel, M. R., Lehrman, E. K., Poon, V. Y., Crump, J. G., Zhen, M., Bargmann, C. I., & Shen, K. (2006). Hierarchical assembly of presynaptic components in defined C. elegans synapses. Nature Neuroscience, 9(12), 1488–1498. http://doi.org/10.1038/nn1806

Richmond, J. E., & Broadie, K. S. (2002). The synaptic vesicle cycle: Exocytosis and endocytosis in Drosophila and C. elegans. Current Opinion in Neurobiology, 12(5), 499–507. http://doi.org/10.1016/S0959-4388(02)00360-4

Rindler, M. J. (1998). Carboxypeptidase E, a peripheral membrane protein implicated in the targeting of hormones to secretory granules, Co-aggregates with granule content proteins at acidic pH. Journal of Biological Chemistry, 273(47), 31180–31185. http://doi.org/10.1074/jbc.273.47.31180

Shakiryanova, D., Tully, A., & Levitan, E. S. (2006). Activity-dependent synaptic capture of transiting peptidergic vesicles. Nature Neuroscience, 9(7), 896–900. http://doi.org/10.1038/nn1719

Sossin, W. S., & Scheller, R. H. (1991). Biosynthesis and sorting of neuropeptides. Current Opinion in Neurobiology, 1(1), 79–83. http://doi.org/10.1016/0959-4388(91)90013-W

Stigloher, C., Zhan, H., Zhen, M., Richmond, J., & Bessereau, J.-L. (2011). The presynaptic dense projection of the Caenorhabiditis elegans cholinergic neuromuscular junction localizes synaptic vesicles at the active zone through SYD-2/liprin and UNC-10/RIM-dependent interactions. The Journal of Neuroscience : The Official Journal of the Society for Neuroscience, 31(12), 4388–4396. http://doi.org/10.1523/JNEUROSCI.6164-10.2011

Südhof, T. C. (2004). The Synaptic Vesicle Cycle. Annual Review of Neuroscience, 27(1), 509–547. http://doi.org/10.1146/annurev.neuro.26.041002.131412

Von Stetina, S. E., Watson, J. D., Fox, R. M., Olszewski, K. L., Spencer, W. C., Roy, P. J., & Miller, D. M. (2007). Cell-specific microarray profiling experiments reveal a comprehensive picture of gene expression in the C. elegans nervous system. Genome Biology, 8(7), R135. http://doi.org/10.1186/gb-2007-8-7-r135

Wagner, O. I., Esposito, A., Köhler, B., Chen, C.-W., Shen, C.-P., Wu, G.-H., … Klopfenstein, D. R. (2009). Synaptic scaffolding protein SYD-2 clusters and activates kinesin-3 UNC-104 in C. elegans. Proceedings of the National Academy of Sciences of the United States of America, 106(46), 19605–19610. http://doi.org/10.1073/pnas.0902949106

Watanabe, S., Rost, B. R., Camacho-Pérez, M., Davis, M. W., Söhl-Kielczynski, B., Rosenmund, C., & Jorgensen, E. M. (2013). Ultrafast endocytosis at mouse hippocampal synapses. Nature, 504(7479), 242–247. http://doi.org/10.1038/nature12809

Weimer, R. M., Gracheva, E. O., Meyrignac, O., Miller, K. G., Richmond, J. E., & Bessereau, J.-L. (2006). UNC-13 and UNC-10/Rim Localize Synaptic Vesicles to Specific Membrane Domains. The Journal of Neuroscience , 26(31), 8040–8047. http://doi.org/10.1523/JNEUROSCI.2350-06.2006

White, J.G., Southgate, E., Thomson, J.N., Brenner, S. (1986). The Structure of the Nervous System of the Nematode Caenorhabditis elegans. Philosophical Transactions of the Royal Society of London. Series B, Biological Sciences, 314(1165), 1–340.

Wong, M. Y., Zhou, C., Shakiryanova, D., Lloyd, T. E., Deitcher, D. L., & Levitan, E. S. (2012). Neuropeptide delivery to synapses by long-range vesicle circulation and sporadic capture. Cell, 148(5), 1029–1038. http://doi.org/10.1016/j.cell.2011.12.036

Wu, Y. E., Huo, L., Maeder, C. I., Feng, W., & Shen, K. (2013). The Balance between Capture and Dissociation of Presynaptic Proteins Controls the Spatial Distribution of Synapses. Neuron, 78(6), 994–1011. http://doi.org/10.1016/j.neuron.2013.04.035

Wu, Y., Huo, L., Maeder, C., Feng, W., & Shen, K. (2013). The Balance between Capture and Dissociation of Presynaptic Proteins Controls the Spatial Distribution of Synapses. Neuron, 78(6), 994–1011. http://doi.org/10.1016/j.neuron.2013.04.035

Yeh, E. (2005). Identification of Genes Involved in Synaptogenesis Using a Fluorescent Active Zone Marker in Caenorhabditis elegans. Journal of Neuroscience, 25(15), 3833–3841. http://doi.org/10.1523/JNEUROSCI.4978-04.2005

Zhen, M., & Jin, Y. (1999). The liprin protein SYD-2 regulates the differentiation of presynaptic termini in C. elegans. Nature, 401(6751), 371–375. http://doi.org/10.1038/43886

IV. THE DEG/ENAC CATION CHANNEL PROTEIN UNC-8 DRIVES ACTIVITY-DEPENDENT SYNAPSE REMOVAL IN REMODELING GABAERGIC NEURONS

Tyne W Miller-Fleming[1†], Sarah C Petersen[2†‡], Laura Manning[3], Cristina Matthewman[4], Megan Gornet[2], Allison Beers[2], Sayaka Hori[5], Shohei Mitani[5], Laura Bianchi[4], Janet Richmond[3], David M Miller III[1,2*]

[1]Neuroscience Program, Vanderbilt University, Nashville, United States;
[2]Department of Cell and Developmental Biology, Vanderbilt University, Nashville, United States;
[3]Department of Biological Sciences, University of Illinois at Chicago, Chicago, United States;
[4]Department of Physiology and Biophysics, University of Miami, Miami, United States;
[5]Department of Physiology, Tokyo Women's Medical University, Tokyo, Japan

This chapter has been modified from a previous publication in *eLife* 2016;5. All figures have been copied or modified from the published work. The publisher's statement is included in Appendix B.

A. Introduction

During development, neural circuits often undergo a dramatic change in architecture before they reach their mature state. This remodeling process usually occurs during a specific timeframe in which the circuit is particularly sensitive to synaptic activity. While this activity strengthens some synapses, other synapses are weakened and eventually removed. For example, the mammalian brain establishes binocular vision during a critical period of development. This period of plasticity is regulated by GABA signaling, although the specific molecular mechanisms underlying this rewiring are poorly understood (Deidda et al., 2015; Hensch, 1998).

A known modulator of synaptic strength that is linked to synaptic activity is intracellular calcium. Active neurons experience an influx of calcium through voltage-gated calcium channels (VGCCs) that enable synaptic vesicle (SV) fusion and neurotransmitter release (Catterall et al.,

2008). The resulting elevated intracellular calcium can regulate gene expression and protein function to modulate the synapse (Flavell and Greenberg, 2008; Baumgärtel and Mansuy, 2012). One such mediator of calcium-dependent modulation is the calcium-sensitive phosphatase, calcineurin. Calcineurin can reverse LTP by phosphorylating AMPA receptor subunits, resulting in their endocytosis (Baumgärtel and Mansuy, 2012; Winder et al., 1998). Recent evidence in *C. elegans* implicates a role for an additional molecule, the canonical apoptotic protease CED-3/Caspase, in synapse removal. CED-3 and its upstream regulator, CED-4/Apaf1, are calcium sensitive proteins that destabilize the synapse by activating gelsolin, an F-actin severing protein. This pathway promotes disassembly of synaptic machinery and underscores the role for calcium in remodeling mechanisms (Ertürk et al., 2014; Wang et al., 2014).

An additional family of proteins known to influence synaptic activity are Degenerin/Epithelial Sodium Channels (DEG/ENaCs). These voltage-insensitive trimeric cation channels are named degenerins because constitutively active forms of the channels cause neurodegeneration (Bianchi and Driscoll, 2002). DEG/ENaC proteins are expressed in mammalian epithelial tissue where they mediate sodium reabsorption (Wemmie et al., 2002). Additional research indicates that DEG/ENaCs can modulate synapses (Wemmie et al., 2002, 2003; Krepple et al., 2014). The acid-sensing DEG/ENaC ASIC1a, for example, is expressed in specific brain regions and is linked to learning and memory (Wemmie et al., 2003, 2004; Zha et al., 2006; Ziemann et al., 2009). Cation flow through ASIC1a can activate voltage-gated channels on the postsynaptic cell and influence receptor signaling (Wemmie et al., 2006). Alternatively, ASIC1a can also enhance neurotransmitter release by activating presynaptic VGCCs (Cho and Askwith, 2008; Voglis and Tavernarakis, 2008; Younger et al., 2013). In this study, we examine a new

remodeling mechanism that relies on elevated intracellular calcium to regulate synapse strength. Rather than stabilize the synapse, however, this pathway results in synapse removal during development.

To understand alternative mechanisms of synapse modulation, we examined the GABAergic motor neuron circuit in *C. elegans*, which remodels in an activity-dependent manner during development (White et al., 1978; Hallam and Jin, 1998; Park et al., 2011; Thompson-Peer et al., 201). GABAergic D-type motor neurons are comprised of ventrally innervating VD class motor neurons and dorsally innervating DD class motor neurons. DD cell bodies and synapses appear in the ventral cord in the embryo (Figure 4.1A). Between larval stages L1 and L2 of development, these neurons relocate their synapses from the ventral to the dorsal cord of the animal. Meanwhile, during L2, VD cell bodies emerge and form synapses in the ventral nerve cord, where they remain throughout adulthood (Figure 4.1B). How do these two classes of neurons reach opposite fates in synapse localization? One clue is that the transcription factor UNC-55, which is expressed exclusively in VD neurons, inhibits the endogenous synaptic remodeling program, thus maintaining VD synapses in the ventral cord (Walthall and Plunkett, 1995; Zhou and Walthall, 1998; Shan et al., 2005) (Figure 4.1E). Previous work has demonstrated strong evidence for this model. First, ectopic expression of UNC-55 in DD's prevents remodeling to the dorsal cord (Shan et al., 2005). In an *unc-55* mutant, however, ventral VD synapses are ectopically relocated to the dorsal cord, leaving virtually no GABA synapses on the ventral cord (Petersen et al., 2011; Meng et al., 2015). This is the expected fate of DD neurons. The ectopically remodeled synapses in an *unc-55* mutant are functional on dorsal muscles

(Thompson-Peer et al., 2012). Finally, two targets inhibited by UNC-55, Iroquois homeobox (*irx-1)* and hunchback-like (*hbl-1)*, are normally expressed in DDs and mediate remodeling (Petersen et al., 2011; Thompson-Peer et al., 2012).

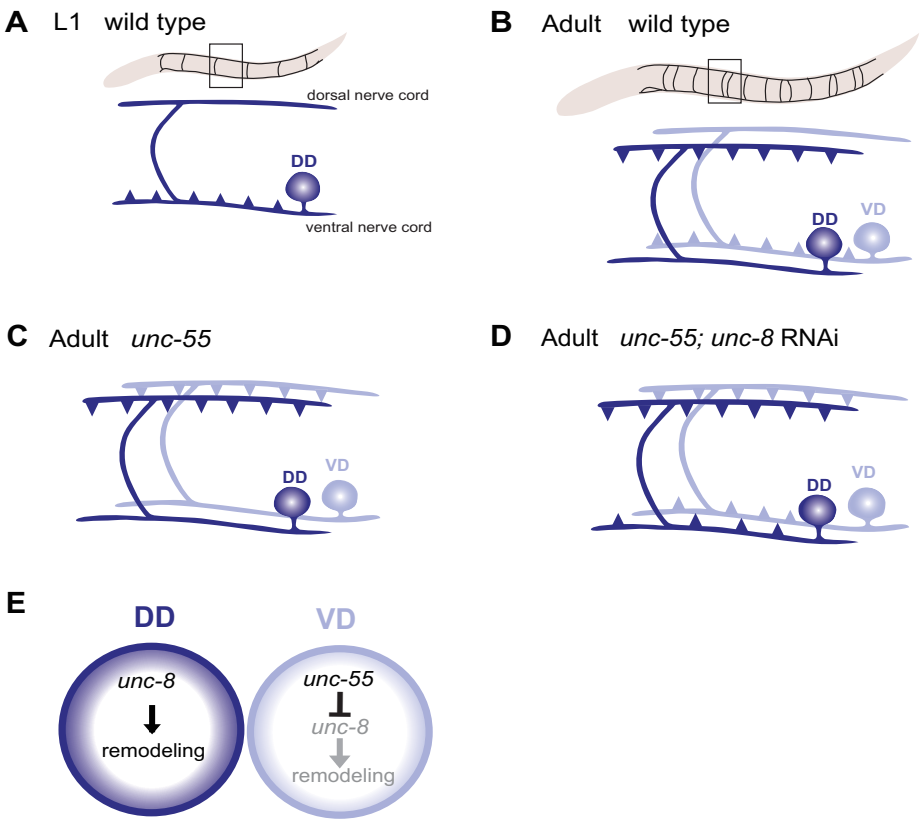

Figure IV.1 GABAergic neuron synaptic remodeling is transcriptionally controlled and depends on UNC-8. A. Dorsal D (DD) GABAergic motor neurons (dark blue) synapse with ventral muscles during embryonic development. **B.** DD synapses are relocated to dorsal muscles at the end of the first larval stage (L1). Ventral D (VD) GABAergic motor neurons (light blue) are generated in the late L1 and innervate ventral muscles. **C.** The COUP/TF transcription factor UNC-55 is expressed in VD neurons and blocks remodeling; VD neurons relocate synapses to the dorsal side in loss-of-function unc-55 mutants. **D/E.** UNC-8/DEG/ENaC expression is negatively regulated by UNC-55 and RNAi knockdown of unc-8 suppresses ectopic VD remodeling in unc-55 mutants. These results suggest that UNC-8 may also promote DD remodeling. Schematics modified from Petersen et al. (2011).

The mutant phenotype of *unc-55* provides an excellent background in which to identify other downstream targets of UNC-55 involved in remodeling. We used cell-specific profiling and

an RNAi screen to identify downstream effectors in the remodeling program that prevent ectopic remodeling in *unc-55* mutants (Petersen et al., 2011). One candidate gene target was the DEG/ENaC *unc-8*. In this study, we found that UNC-8 promotes synapse removal in remodeling GABA neurons (Figure 4.1D,E). UNC-2/VGCC and TAX-6/Calcineurin are also required in this pathway and indicate a role for elevated intracellular calcium. Since UNC-8 appears to function downstream of TAX-6, it is possible that TAX-6 activates UNC-8. Depolarization through UNC-8 may stimulate VGCC activity, resulting in calcium influx and a positive feedback loop between TAX-6, UNC-8, and UNC-2. This loop could raise intracellular calcium levels past a critical threshold upon which the caspase-dependent cell death pathway is activated and the synapse is dismantled (Meng et al., 2015). We therefore propose a model in which UNC-8 promotes synaptic removal in an activity-dependent manner and is regulated both genetically and through intracellular calcium signaling.

B. Results

1. UNC-8 is expressed in GABAergic D-class motor neurons.

Previous microarray assays showed that *unc-8* expression was enhanced in GABA neurons of *unc-55* mutants, indicating that UNC-8 may be an important target in the UNC-55 regulated remodeling system (Peterson et al., 2011). To further probe this finding, we created a reporter gene to examine UNC-8 expression in VD and DD neurons. The reporter gene, *punc-8::GFP*, includes 1.6 kb of genomic region upstream of the *unc-8* coding sequence (Etchberger et al., 2007). As predicted, *punc-8::GFP* was visible in adult wild type worms in DD, but not VD, cell bodies (Figure 4.2A,B).

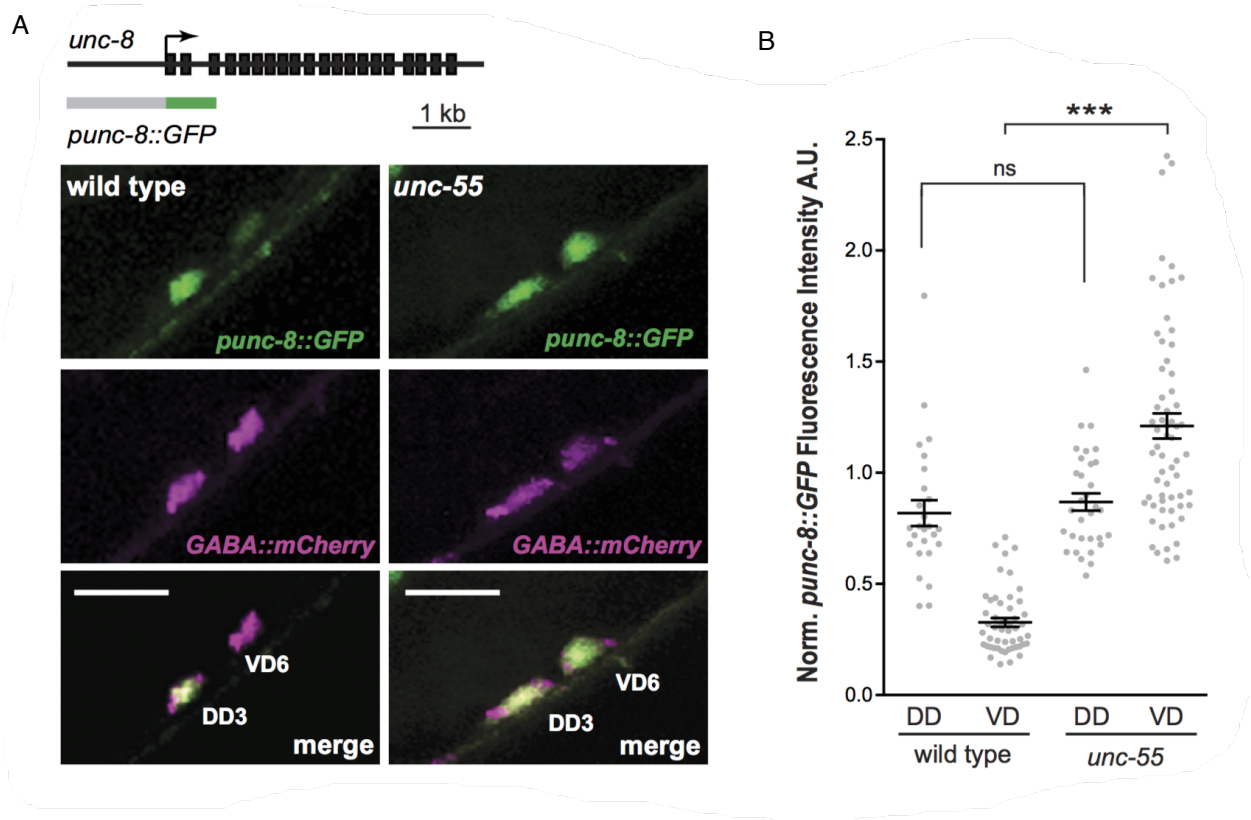

Figure IV.2. UNC-8 is expressed in remodeling GABA neurons. A. *unc-8* expression in remodeling neurons is visualized with a punc-8::GFP reporter gene. Strong punc-8::GFP (green) expression was observed in DD motor neurons in wild type, but was also detected in VD motor neurons in *unc-55* animals. GABAergic motor neurons are labeled with pttr-39::mCherry (magenta). Scale bar is 10 mm. **B.** Normalized fluorescence intensity is plotted on the Y-axis in arbitrary units (A.U.). punc-8::GFP expression is enhanced in VDs, but not DDs, in *unc-55* mutants (***p<0.001, ns is not significant, One-Way ANOVA with Bonferroni correction). n ≥ 26 DDs and n ≥ 51 VDs per genotype, data are mean ± SEM. Data collected by Miller lab.

In contrast, *unc-55* adult worms displayed *punc-8::GFP* in both DD and VDs. These results support our findings that UNC-55 normally inhibits UNC-8 expression in VD neurons. An additional test of this idea was to create a fosmid reporter gene, UNC-8::GFP, that includes the entire UNC-8 locus and flanking regions, with a C-terminally fused GFP (Figure 4.3). In early L1 and L2 wildtype worms, UNC-8::GFP was expressed in DD neurons. Interestingly, expression was also observed in cholinergic DA and DB neurons in these animals. This expression pattern is

predicted by a previous study which showed that overexpression of a constitutively active UNC-8 protein resulted in selective cell death of certain classes of neurons, including DA and DBs (Wang et al., 2013). In adult *unc-55* animals, UNC-8::GFP was observed in DD and VD neurons. The UNC-8::GFP fosmid also appears to be functional. When we examined GABA::mCherrry::RAB-3, a presynaptic marker, in the ventral cord of adult animals, we found that both *unc-55* and *unc-55;unc-8* mutant animals showed similar levels of synapse loss compared to wild type animals. The UNC-8::GFP fosmid partially rescued ventral synapses in *unc-55;unc-8* mutant animals, indicating it is likely functional and reflects some level of endogenous expression of *unc-8* **(**Figure 4.3A-C). Overall, these results support a role for UNC-8 in the genetically driven DD remodeling program.

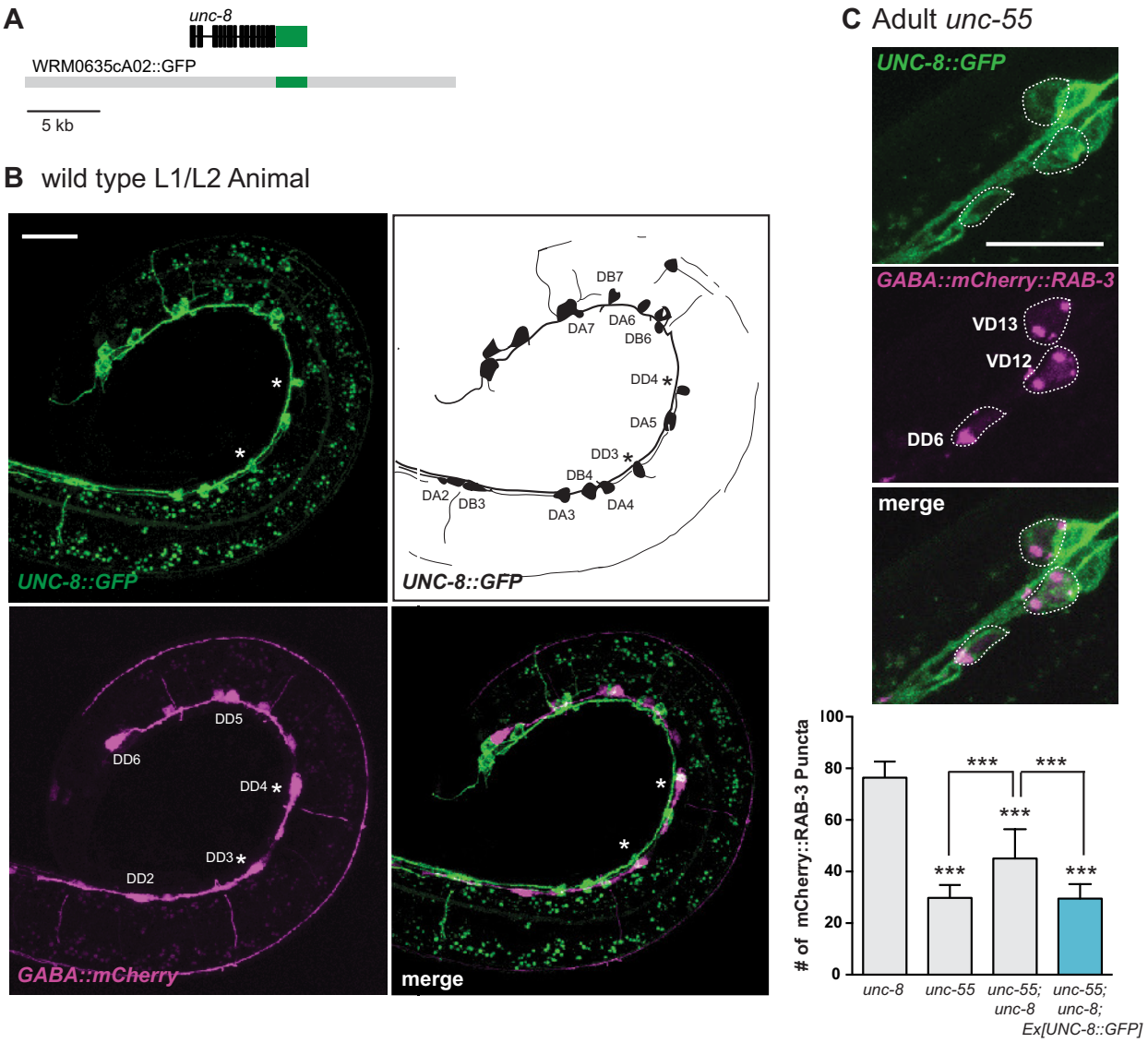

Figure IV.3. UNC-8::GFP colocalizes with DD neurons. A. A GFP C-terminal fusion with the intact UNC-8 protein was generated by recombineering (see Materials and Methods). **B.** UNC-8::GFP shows mosaic expression in the ventral nerve cord (VNC) of early L2 animals in GABAergic DD neurons (asterisks) and in cholinergic DA and DB neurons (upper left). Schematic denotes VNC neurons that express UNC-8::GFP (upper right). The six DD neurons are labeled with punc-25::mCherry. mCherry-labeled cell bodies between the DD neurons are the newly born VD neurons (lower left). Merged image of UNC-8::GFP fosmid and punc-25::mCherry-labeled GABA neurons (lower right). Asterisks denote an expression of UNC-8::GFP in DD3 and DD4. Scale bar is 20 mm. **C.** UNC-8::GFP is expressed in DD and VD neurons in *unc-55* mutants. GABA neurons are labeled with wdIs90 [punc-25::mCherry::RAB-3]. UNC-8::GFP-expressing GABA neurons are outlined. Scale bar is 10 mm. UNC-8::GFP rescues the *unc-55* remodeling phenotype in *unc-55;unc-8 animals* (***p<0.001, n ≥ 20 animals, One-Way ANOVA with Bonferroni correction, data are mean ± SD). Data collected by Miller lab.

2. UNC-8 promotes ventral DD synapse removal

To understand a more precise role for UNC-8 in the remodeling program, we turned to RNAi results that showed UNC-8 appears to promote synapse removal from the ventral cord (Petersen et al., 2011). Building on these results, we specifically examined DD synapses during the ventral removal phase of remodeling that begins at late L1. Using a DD-specific promoter (*pflp-13*), we observed presynaptic vesicle markers GFP::RAB-3 and SNB-1::GFP/synaptobrevin. We generated a loss of function mutant allele, *unc-8(tm5052)*, which deletes 197 nucleotides of the first transmembrane domain and shifts the reading frame to create a premature stop codon. This allele is predicted to create an unstable *unc-8* mRNA and a probable null (Figure 4.4A). Between late L1 and adulthood, we observed wild-type DD:GFP::RAB-3 puncta decrease in the ventral cord. This phenomenon is expected because at this time in remodeling, synapses are removed from the ventral cord and transported to the dorsal cord (Hallam and Jin, 1998; Petersen et al., 2011). In the *unc-8* mutant, however, synapse removal was delayed at all time points, including adulthood (Figure 4.4B-C). Additionally, residual ventral DD:SNB-1::GFP puncta were increased in the *unc-8* adult, suggesting that ventral DD synapse removal cannot be completed without UNC-8. When we examined the dorsal cord in *unc-8* animals, we observed no changes in synapse assembly between wild type and *unc-8* (Figure 4.4D,E).

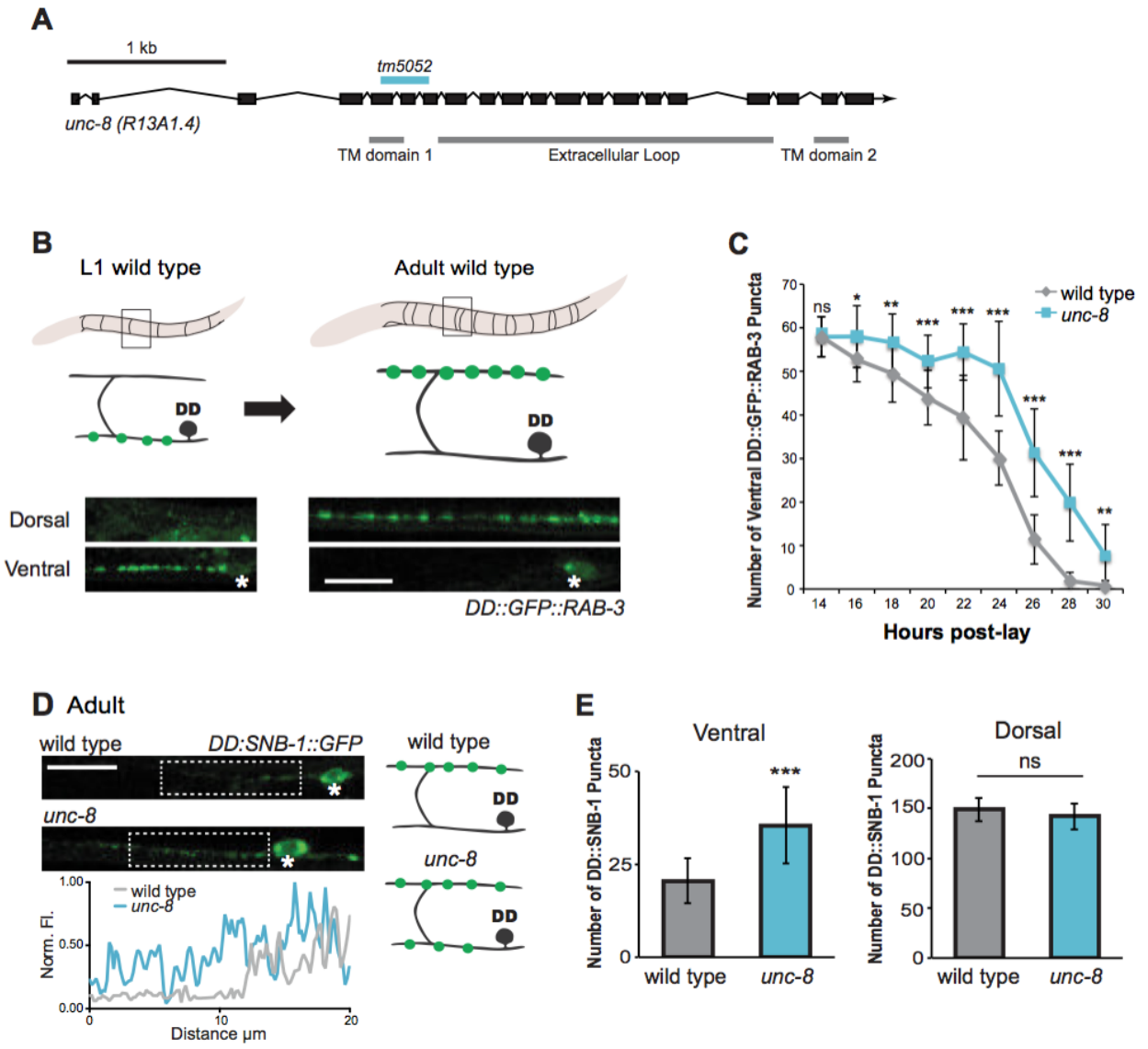

Figure IV.4. The DEG/ENaC subunit UNC-8 promotes removal of ventral DD synapses. A. Schematic of the *unc-8* gene and predicted UNC-8 protein. DEG/ENaC channel subunits contain two transmembrane domains (TM domains) and a large extracellular loop (gray bars). The *unc-8* deletion allele *tm5052* is indicated (blue bar). **B.** DD GABA neuron synapses (green) with ventral muscles are relocated to the dorsal side during development. DD-specific GFP-tagged RAB-3 (pflp-13::GFP::RAB-3) labels synapses in the ventral nerve cord of early L1 larvae and the dorsal nerve cord of adults. Asterisk denotes DD4 soma. Scale bar is 10 mm. **C.** DD remodeling was quantified by counting GFP::RAB-3 puncta during larval stages. Removal of ventral DD synapses is significantly delayed in unc-8 animals (*p<0.05, **p<0.01, ***p<0.001, ns is not significant, Student's t-test, data are mean ± SD). **D.** Representative images of wild-type and unc-8 adult ventral nerve cords (asterisk denotes DD5 soma). Ventral DD synapses labeled with GFP-tagged synaptobrevin (pflp-13::SNB-1::GFP) are retained in *unc-8* mutant adult animals. Scale bar is 10 mm. Inset shows pixel intensity over a 20 mm region (indicated by dashed boxes) of the ventral nerve cord in wild-type and *unc-8* animals. **E.** Removal of DD::SNB-1::GFP puncta is defective in

unc-8 mutant adults; however, dorsal DD synaptic assembly is not affected (***p<0.001, n ≥ 20, ns is not significant, Student's t-test, data are mean ± SD). Data collected by Miller lab.

These findings were not likely due to overall delayed development in the mutant, as the birth of VD neurons was not delayed in *unc-8(tm5052)* (Figure 4.5A-D). These results suggest that UNC-8 promotes the ventral removal of DD synapses but does not affect their dorsal assembly (Figure 4.5F). Finally, we drove expression of UNC-8::GFP in GABAergic neurons and found that UNC-8::GFP puncta localized in the ventral cord, with no signal observed in the dorsal cord. This finding reinforces our conclusion that UNC-8 operates ventrally.

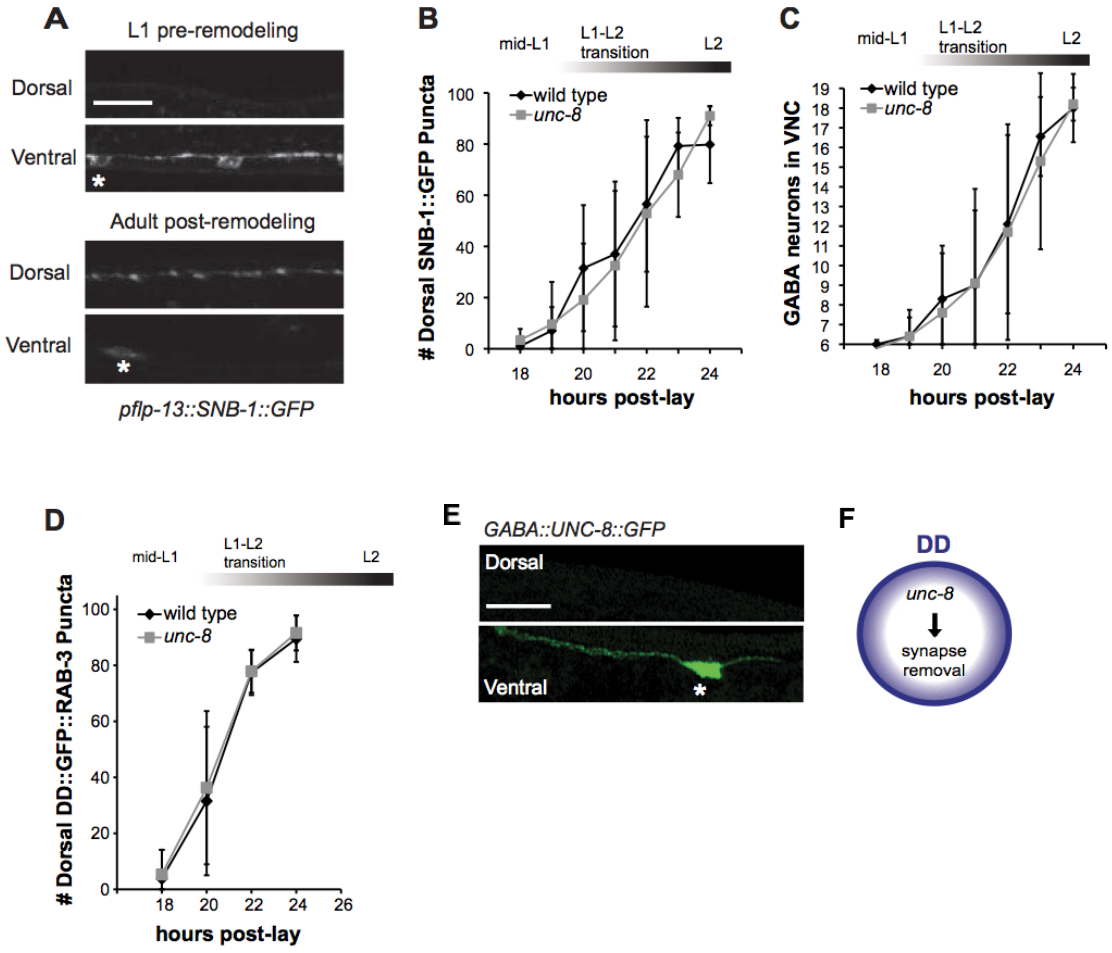

Figure IV.5. UNC-8 removes ventral synapses, but is not required for assembly of dorsal synapses. A. DD-specific expression of SNB-1::GFP (pflp-13::SNB-1::GFP) labels DD synapses. In the wild type, all SNB-1::GFP puncta are ventrally localized in early L1 larvae, but are strictly dorsal in adults after DD remodeling. Scale bar is 10 mm. Asterisk denotes DD4 cell soma. **B.** Loss

of *unc-8* function does not delay dorsal DD synapse formation. Dorsal SNB-1::GFP puncta were counted in developing wild-type and *unc-8* mutant L1/L2 larvae. **C.** GABA neuron development is not delayed in *unc-8*. GABA neurons (DD + VD) in the ventral cord, marked with SNB-1::GFP, were counted in developing wild-type and *unc-8* mutant L1/L2 larvae. **D.** DD remodeling was quantified by counting GFP::RAB-3 puncta during the L1-L2 larval stages. Assembly of dorsal DD synapses is not significantly different between wild-type and *unc-8* animals (Student's t-test, data are mean ± SD). Results for (B–D) were pooled from 3 independent experiments. **E.** Ventral localization of GFP-tagged UNC-8 in GABA neurons. Asterisk denotes DD5 soma. Scale bar is 10 mm. **F.** UNC-8 promotes removal of ventral presynaptic components in DD neurons, but is not required for dorsal synapse formation. Data collected by Miller lab.

3. UNC-8 can function in both DD and VD remodeling programs

If UNC-8 promotes ventral synapse removal in remodeling DD neurons, and UNC-8 expression is normally inhibited in VD neurons, could DDs and VDs share a subset of molecules involved in remodeling? Previous work has demonstrated that VD synapses remodel ectopically in *unc-55* mutants (Shan et al., 2005; Petersen et al., 2011). Therefore, we predicted that UNC-8 may also promote synapse removal in ectopically remodeling VDs. We measured GABA::SNB-1::GFP puncta count and fluorescence intensity to examine remodeling in both VDs and DDs. In wild-type adults, ventral puncta were observed. As shown previously, these puncta are nearly eliminated in *unc-55* mutants. In an *unc-55;unc-8* double mutant, some of the ventral puncta were preserved (Figure 4.6).

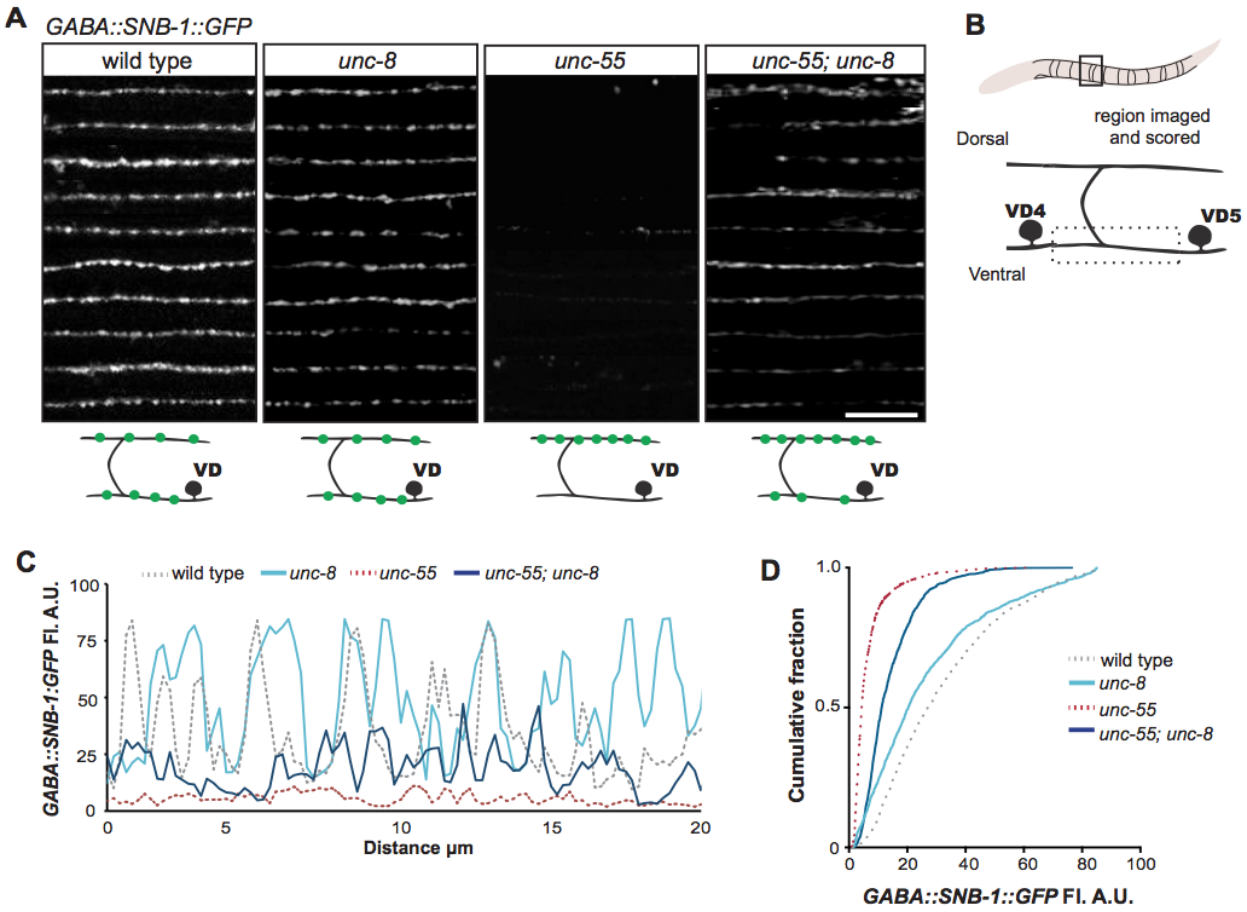

Figure IV.6 UNC-8 drives removal of ventral GABAergic synapses. A. Ventral GABA synapses labeled with GFP-tagged synaptobrevin (punc-25::SNB-1::GFP) for 10 adult animals. Wild-type and *unc-8(tm5052)* show similar distributions of SNB-1::GFP puncta. Ventral SNB-1::GFP is depleted from *unc-55* due to VD remodeling, but partially restored in *unc-55;unc-8* animals. **B.** Data for Figure panels A, C, D were collected from the ventral nerve cord between VD4 and VD5. **C.** SNB-1::GFP fluorescent intensity measurements from each genotype. Each line represents the pixel intensity over a 20 mm region of the VNC from a single representative animal. **D.** Cumulative frequency curves for SNB-1::GFP fluorescence intensity for each genotype (n > 10 animals). *unc-55* animals show a significant loss of ventral SNB-1::GFP fluorescence ($p < 0.0001$ vs wild type). SNB-1::GFP fluorescence is partially restored in *unc-55;unc-8* animals, demonstrating the role of UNC-8 for synapse removal ($p<0.0001$ vs *unc-55*). p values calculated with Kruskal-Wallis and Dunn's post test.

Using time course assays, we saw that these changes persisted throughout adulthood (Figure 4.7B). To identify whether the residual ventral synapses in the *unc-55;unc-8* mutant resided in DD or VD neurons, we coexpressed the DD-specific *flp-13::mCherry::RAB-3* with

GABA:SNB-1::GFP. We found that DD neurons housed ~40% of the remaining ventral synapses, and 60% were located in VD neurons (Figure 4.7C). These findings demonstrate that UNC-8 can promote ventral removal of both classes of GABA neurons and indicate that both classes share a common branch of the remodeling pathway (Shan et al., 2005, Peterson et al., 2011).

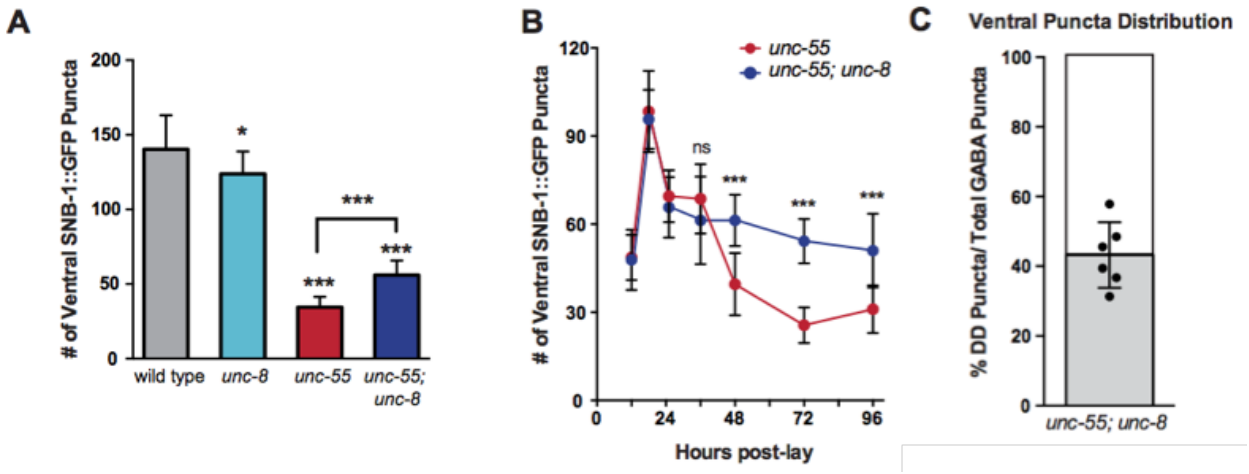

Figure IV.7 UNC-8 promotes synapse disassembly in remodeling GABAergic neurons. Fluorescent puncta for the presynaptic protein SNB-1::GFP were counted in the ventral nerve cord from VD3 to VD11. **A.** SNB-1::GFP puncta are removed from ventral synapses in *unc-55*, and this effect partially depends on *unc-8* (***p<0.001, *p<0.05, n ≥ 10). One-Way ANOVA with Bonferroni correction, data are mean ± SD. B. Time course experiments with *unc-55* and *unc-55;unc-8* animals show the removal of ventral GABAergic synapses (punc-25::SNB-1::GFP) over time. Ventral VD synapses are initially established at 24-hr post lay in both *unc-55* and *unc-55;unc-8* and these synapses are largely removed in *unc-55* animals. Loss of *unc-8* function disrupts ventral synapse removal in *unc-55* animals and results in the retention of significantly more ventral synapses. (***p<0.001, ns is not significant, Student's t-test). n ≥ 78 animals per genotype, data are mean ± SD. **C.** Ventral GABA synapses in *unc-55;unc-8* animals were colabeled with punc-25::SNB-1::GFP, which marks all synapses (DD and VD) and pflp-13::mCherry::RAB-3, which labels DD synapses only. The proportion of ventral DD synapses (labeled with pflp-13::mCherry::RAB-3) in *unc-55;unc-8* adults are shown in gray as a percentage of total ventral synapses. Data collected by Miller lab.

4. UNC-8 expression in GABAergic neurons is sufficient for synapse removal

Next, we wanted to know if UNC-8 acts cell-autonomously in remodeling D class neurons. We created a cell-specific RNAi (csRNAi) to knockdown *unc-8* expression in GABA neurons. Using

an empty vector RNAi, *unc-55* mutants showed the expected loss of ventral synapses. When we expressed *unc-8(csRNAi)* in an *unc-55* mutant, we found a significant retention of ventral GABA::SNB-1::GFP puncta (Figure 4.3E, F), confirming that UNC-8 operates in GABA neurons to promote ventral synapse removal.

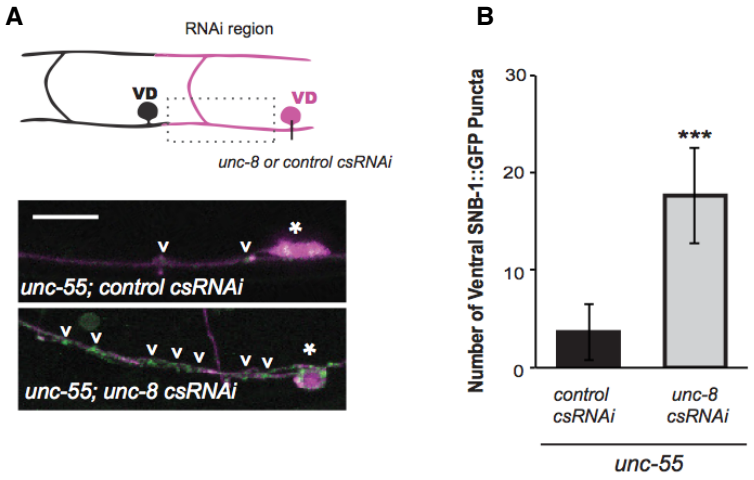

Figure IV.8 UNC-8 promotes remodeling cell autonomously. A. Knockdown of *unc-8* by GABA-neuron-specific RNAi (*unc-8 csRNAi*) restored SNB-1::GFP puncta to the VNC of unc-55; juIs1 animals vs control animals expressing the empty vector RNAi (control csRNAi). GABAergic neurons are labeled with punc-25::mCherry (magenta). Asterisks denote GABA neuron cell bodies and arrowheads point to SNB-1::GFP-labeled ventral synapses. **B.** Quantification of ventral synapses in the region anterior to each cell body expressing the RNAi construct (n > 60 animals). RNAi knockdown of *unc-8;in unc-55* mutant GABA neurons significantly suppresses synapse removal (***p<0.001, Student's t-test. Data are mean ± SD). Scale bars are 10 mm. Data collected by Miller lab.

We then forced expression of *unc-8* cDNA in GABA neurons. Where ventral synapses are restored in an *unc-55;unc-8* double mutant, addition of *unc-8* cDNA eliminated these synapses (Figure 4.9A). Furthermore, expression of *unc-8* cDNA in GABA neurons in the wild type adult resulted in reduced ventral synapses (Figure 4.6, Figure 4.8, Figure 4.9B). Therefore, we conclude that UNC-8 is sufficient to promote synapse removal in remodeling GABAergic neurons.

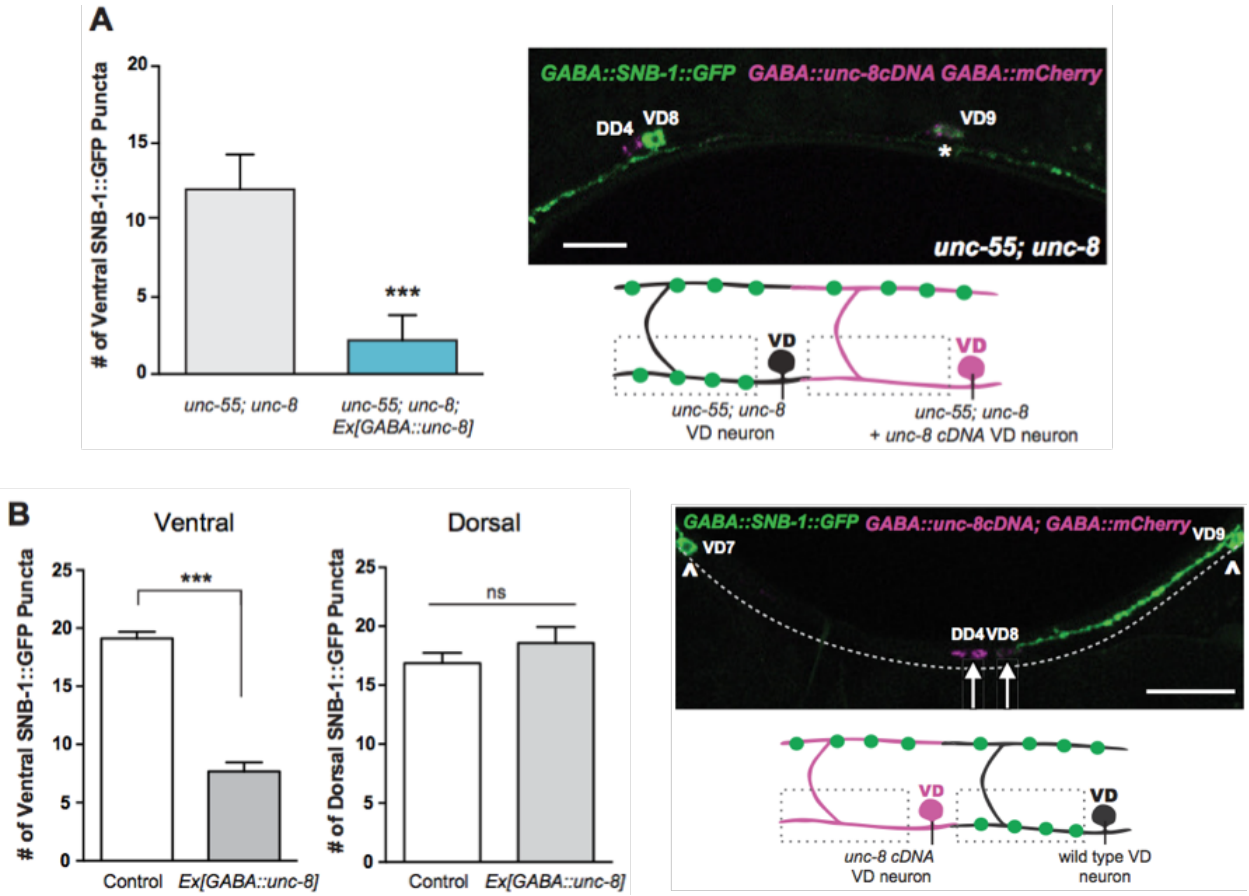

Figure IV.9 UNC-8 functions cell autonomously and is sufficient to promote ventral synapse elimination in GABA neurons. A. UNC-8 function is cell-autonomous. Ventral synapses were counted in *unc-55;unc-8* animals injected with GABA::unc-8 cDNA and the GABA marker punc-25::mCherry (left). Asterisk denotes cell expressing *unc-8* cDNA and punc-25::mCherry. Scale bar is 10 mm, anterior to left. GABA neurons expressing *unc-8* cDNA showed fewer ventral puncta than neighboring *unc-55;unc-8* neurons that do not express the *unc-8* cDNA transgene, indicating that UNC-8 functions in GABA neurons to promote synapse removal (***$p<0.001$, $n \geq 15$ animals, Student's t-test, data are mean ± SD). **B.** Forced expression of *unc-8* cDNA in GABA neurons induces disassembly of ventral synapses. VD neurons expressing *unc-8* cDNA (co-labeled with GABA::mCherry, VD8 denoted with arrow) show significantly fewer ventral SNB-1::GFP (punc-25::SNB-1::GFP) puncta than neighboring VD neurons that do not express *unc-8* cDNA which are unaffected (e.g., VD9 denoted with arrowhead). Anterior to left. Ectopic expression of *unc-8* cDNA in VD neurons has no effect on dorsal synapses (***$p<0.001$, ns is not significant, Student's t-test, $n \geq 51$ VDs (ventral) and $n = 7$ VDs (dorsal), data are mean ± SEM). Data collected by Miller lab.

5. UNC-8 stimulates removal of the presynaptic complex in remodeling GABAergic neurons

Having observed *unc-8*-driven removal of synaptic vesicle markers SNB-1::GFP and GFP::RAB-3 in remodeling GABAergic neurons, we next looked to see if *unc-8* promotes removal of other presynaptic components. We examined fluorescent markers for the membrane-associated endocytic protein, endophilin/UNC-57, and the presynaptic density protein α-liprin/SYD-2. Similar to SNB-1::GFP, each of the additional markers displayed ventral puncta in wild-type animals that were nearly depleted in *unc-55* mutant animals. In the *unc-55;unc-8* double mutants, a significant number of ventral puncta were retained, indicating that UNC-8 may contribute to removal of the entire presynaptic complex (Figure 4.6, Figure 4.8, Figure 4.9A, Figure 4.10A-E).

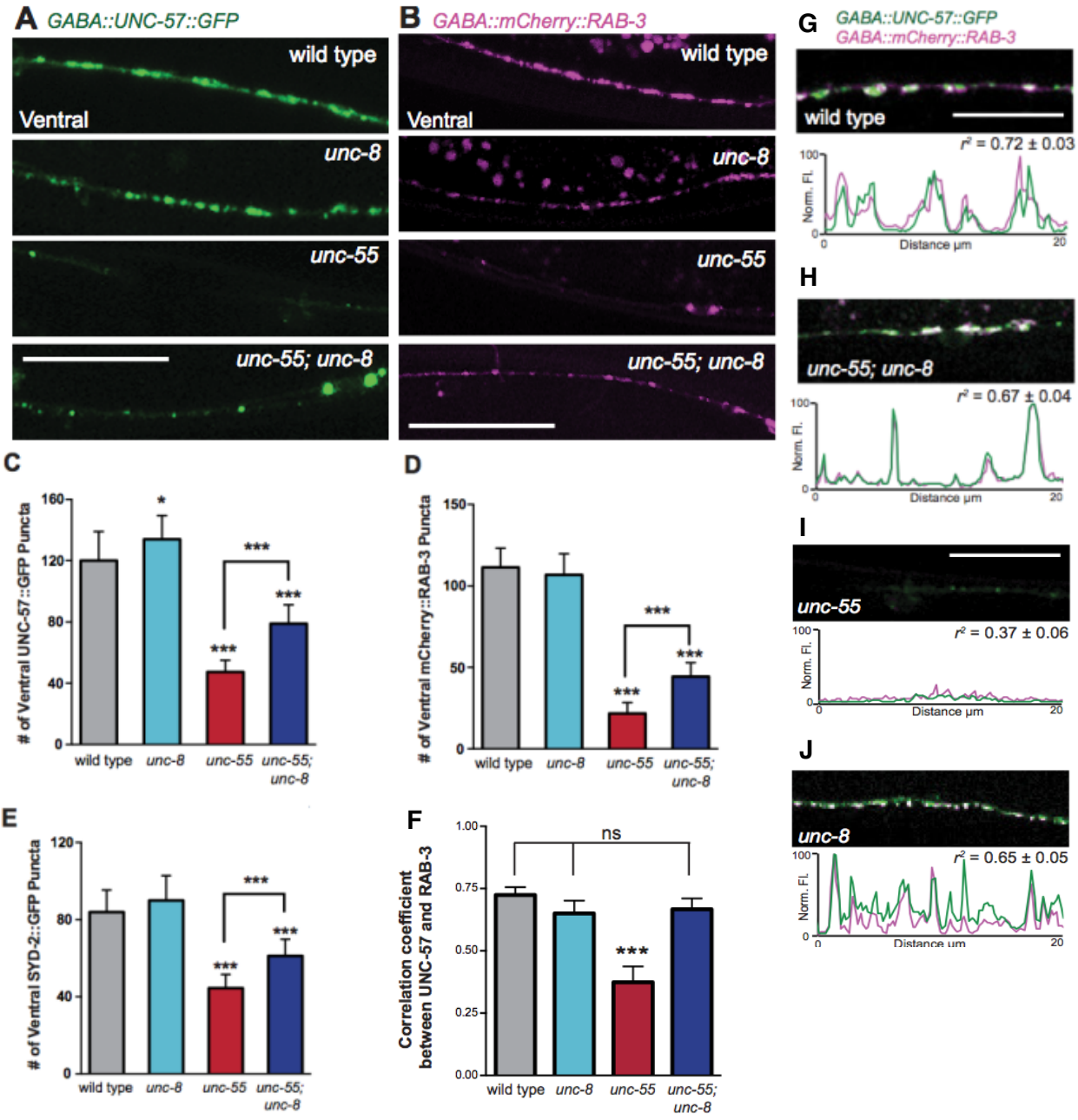

Figure IV.10 UNC-8 promotes disassembly of the presynaptic apparatus in GABAergic motor neurons. Fluorescent puncta for presynaptic proteins (UNC-57::GFP, mCherry::RAB-3, and SYD-2::GFP) were counted in the ventral nerve cord from VD3 to VD11. **A/C**. Representative images (A) and quantification (C) of endophilin/UNC-57 indicate that *unc-8* promotes removal of UNC-57::GFP from ventral synapses in remodeling neurons (*p<0.05, ***p<0.001, n ≥ 25). **B/D**. Representative images (B) and quantification (D) show reduced removal of the presynaptic G protein RAB-3 in *unc-55;unc-8* animals (***p<0.001, n ≥ 21). Scale bars are 10 mM. E. Efficient removal of the presynaptic density protein a-liprin/SYD-2 from ventral synapses in *unc-55* requires *unc-8* (***p<0.001, n ≥ 21, One-Way ANOVA with Bonferroni correction, data are mean

± SD). **F.** Average coefficient of determination for UNC-57::GFP and mCherry::RAB-3. Wildtype, *unc-8*, and *unc-55;unc-8* animals show no significant differences; whereas, *unc-55* animals show much lower r^2 values (n ≥ 11, data are mean ± SEM, Mann-Whitney test, ***p<0.001, ns is not significant). **G/H.** GFP-tagged endophilin (punc-25::UNC-57::GFP) and mCherry::RAB-3 (punc-25::mCherry::RAB-3) are co-localized in GABA neurons of wild-type and *unc-55;unc-8* animals. Representative images and normalized fluorescence intensity plots for a 20 mm region of the ventral nerve cord are shown. Scale bar is 10 mm. r^2 is Pearson's correlation coefficient (n > 10, mean ± SEM). Presynaptic components are co-localized in wild type (r^2 = 0.72 ± 0.03) and unc-55;unc-8 (r^2 = 0.67 ± 0.04). Average r^2 value for *unc-55;unc-8* is not statistically different from the average r^2 value for wild type (p<0.001, Mann-Whitney test). **I–J.** *unc-55* and *unc-8* animals expressing GFP-tagged endophilin (punc-25::UNC-57::GFP) and mCherry::RAB-3 (punc-25::mCherry::RAB-3) were examined for co-localization. Representative images and normalized fluorescence intensity plots for a 20 mm ventral cord region of *unc-55* and *unc-8* animals are shown. Scale bar is 10 mm. r^2 is the coefficient of determination (n > 10, mean ± SEM). UNC-57::GFP and mCherry::RAB-3 puncta are co-localized in *unc-8* (r2 = 0.65 ± 0.05); but not in *unc-55* mutants which show few residual ventral VD synapses (r2 = 0.37 ± 0.06). Data collected by Miller lab.

Further supporting this hypothesis is the finding that mCherry::RAB-3 and UNC-57::GFP are highly colocalized in ventral synapses. UNC-57 recycles between the presynaptic membrane and SVs, and RAB-3 cycles on and off SVs in a GTP/GDP-dependent fashion. Therefore, these markers provide information about additional components of the synapse. Even in the *unc-55;unc-8* ventral cord, although synapse number was reduced compared to wild-type, RAB-3 and UNC-57 remain tightly colocalized in the remaining synapses (Figure 4.10).

In order to examine these synapses at a higher resolution, we used electron microscopy (EM) to view GABAergic synapses in *unc-55;unc-8*. Ventral GABAergic motor neuron synapses can be distinguished at the EM level by morphological criteria such as anatomical position in the cord and orientation to the muscle (see Materials and methods). We observed GABAergic synapses in wildtype, *unc-8,* and *unc-55; unc-8* animals with normal levels of SVs present in synaptic profiles (wild type = 6 synapses/20.08 µm, n = 3 animals, *unc-8* = 5 synapses/12.88 µm,

n = 2 animals, *unc-55; unc-8* = 2 synapses/12.16 µm, n = 2 animals, Figure 4.11A-C). As expected, GABAergic synapses were not detected in the ventral cord of *unc-55* mutants (0 synapses/9.84 µm, n = 2 animals). Ventral cholinergic motor neuron synapses, on the other hand, were present in all genotypes (data not shown). The presence of GABAergic synapses in *unc-55;unc-8* double mutants is consistent with the partial rescue of fluorescently-labeled presynaptic markers to ventral GABA synapses in *unc-55; unc-8* worms (Figure 4.6A, Figure 4.7, Figure 4.10). These results support our findings that the wild-type *unc-8* gene promotes disassembly of multiple components of the presynaptic apparatus.

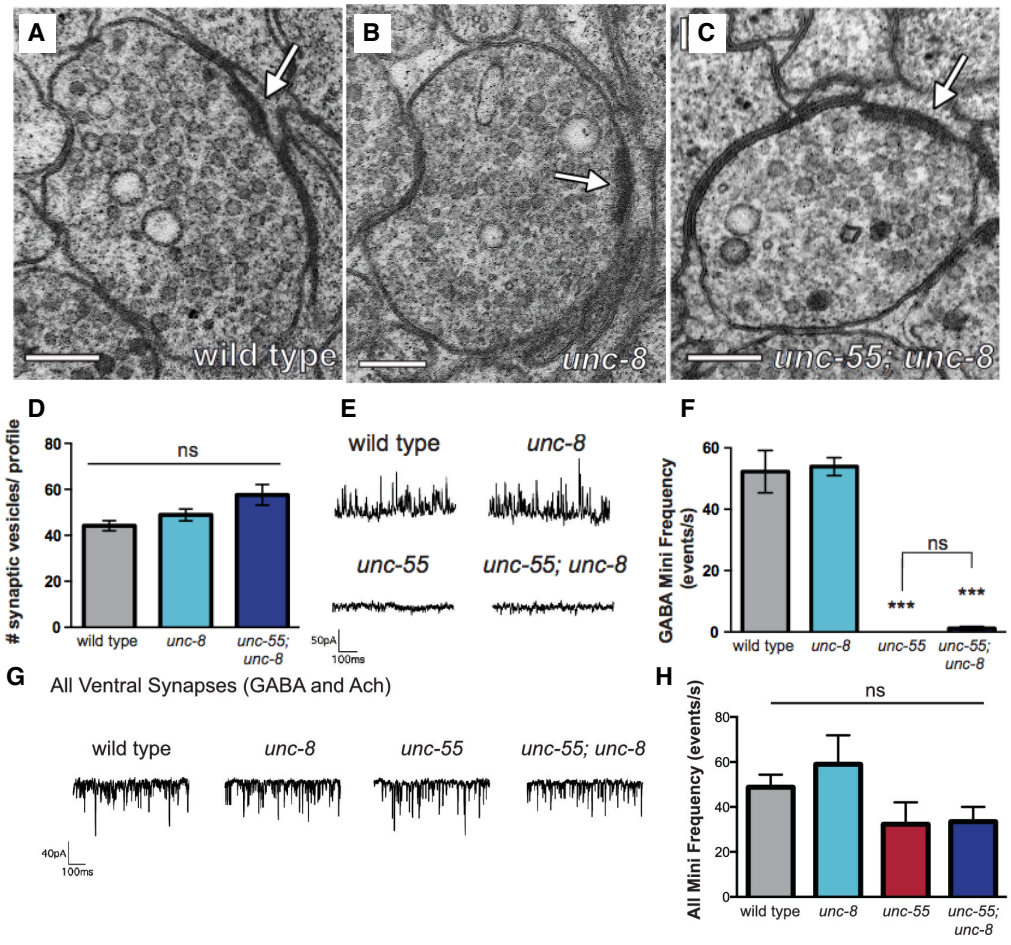

Figure IV.11. Ventral GABAergic synapses are present but not functional in *unc-55;unc-8* mutants. A-C. Electron micrographs of GABA synapses with ventral muscles in (A) wild type, (B) *unc-8*, and (C) *unc-55;unc-8* animals. No ventral GABA presynaptic densities were detected in

unc-55. Arrows point to presynaptic density; scale bars are 200 nm. **D.** Synaptic vesicles were quantified in ventral GABAergic synapses. Synapses in wild-type, *unc-8* and *unc-55;unc-8* animals contain comparable numbers of synaptic vesicles (N > 5 for each genotype, ns is not significant). **E.** Representative traces of ventral mini-iPSCs from each genotype. **F.** The high frequency of ventral mini-iPSCs in wildtype and in unc-8 animals were not observed in unc-55 or unc-55;unc-8. **G/H.** Frequency of ventral spontaneous events (GABAergic and cholinergic) demonstrate that the loss of GABA activity in *unc-55* and *unc-55;unc-8* animals is not due to defects in neurotransmission to ventral muscles (***p<0.001, ns is not significant, n ≥ 5, data are mean ± SEM, One-Way ANOVA with Bonferroni correction). Data collected by Laura Manning and Janet Richmond.

Since ventral synapses are partially restored in *unc-55;unc-8* mutants, we tested whether these synapses are functional. We recorded spontaneous inhibitory postsynaptic currents (iPSCs) caused by GABA release from motor neurons onto ventral body wall muscles. Both wild-type and *unc-8* animals showed normal release rates. As observed previously, *unc-55* mutant animals showed almost no release events (Petersen et al., 2011). To our surprise, ventral iPSCs in *unc-55;unc-8* animals were not recovered, despite restoration of synaptic elements described previously (Figure 4.12E,F). This effect was specific to GABAergic synapses, as total ventral activity (cholinergic and GABAergic) was not significantly reduced in *unc-55;unc-8* compared to wild-type. To rule out postsynaptic defects in *unc-55;unc-8* animals, we first measured postsynaptic $GABA_A$ responses by pressure-ejecting GABA onto voltage-clamped muscles. The GABA-response was unaffected in *unc-55*, *unc-8* or double mutants, indicating that GABA receptors are fully functional in these mutant backgrounds. To test the possibility that *unc-8* mutants impact GABA receptor synaptic clustering an UNC-49::GFP marker was crossed into the *unc-8*, *unc-55* and double mutant strains and colocalization with presynaptic GABA::mCherry::RAB-3 was examined. These markers exhibited a wild-type pattern in both *unc-8* and *unc-55;unc-8* strains, both before and after remodeling (Gally and Bessereau, 2003; Petersen et al., 2011). These experiments suggest that the functional defect in *unc-55;unc-8*

synapses is likely due to presynaptic dysfunction. Thus, while *unc-8* mutants partially suppress ectopic remodeling of VD synapses in the absence of UNC-55, the retained ventral synapses appear to lack functionality. The missing components appear to be regulated by an additional and parallel pathway that is independent of UNC-8, that requires the homeodomain transcription factor, *irx-1*, previously described and discussed further below (Petersen et al., 2011).

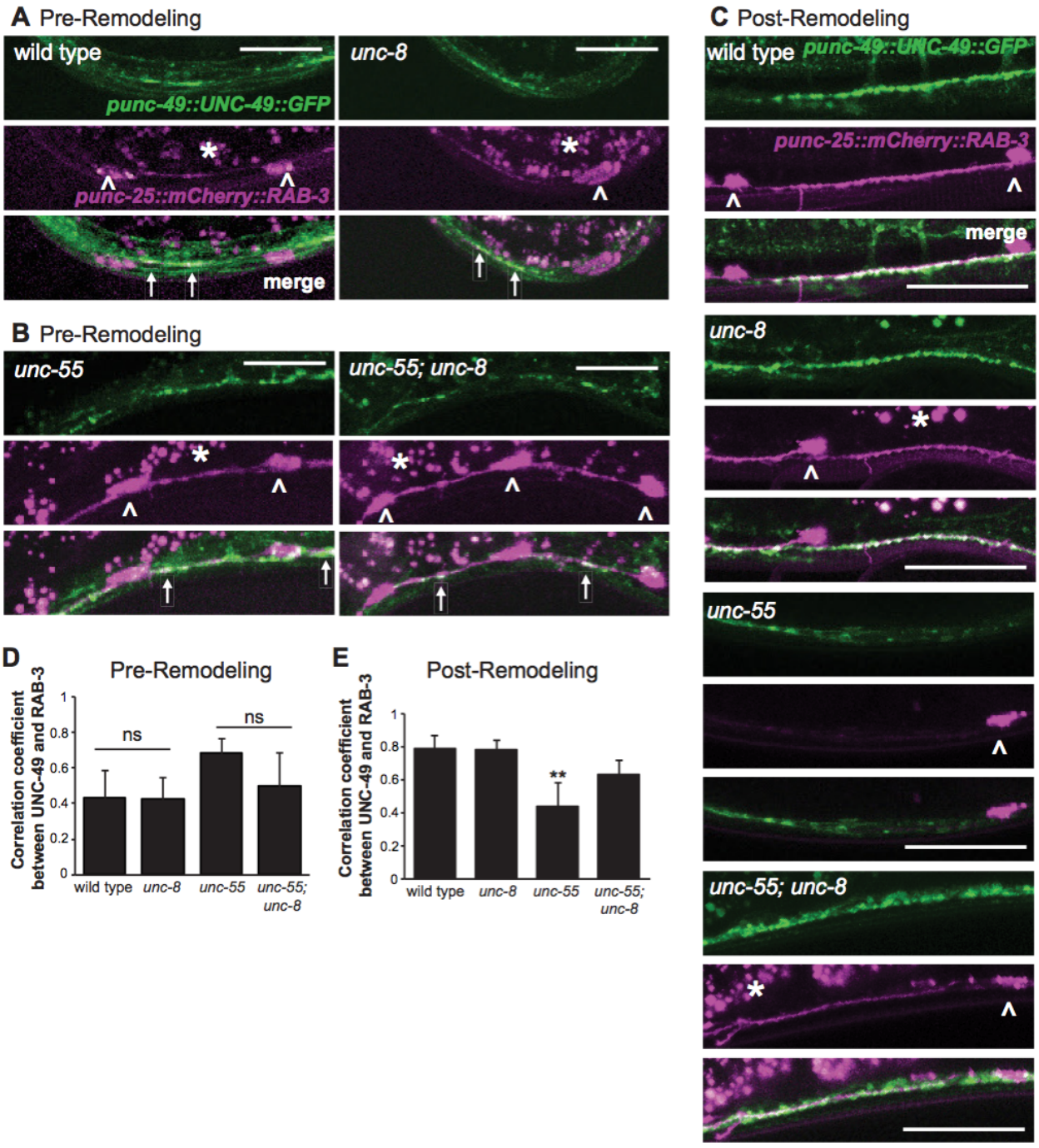

Figure IV.12. The postsynaptic UNC-49 GABAA receptor co-localizes with the presynaptic domains of remodeling GABAergic neurons. Presynaptic regions (GABAergic neurons) are labeled with mCherry::RAB-3 (magenta) and the postsynaptic compartment (body muscle) is marked with UNC-49::GFP (green); arrows denote regions of co-localization. Arrowheads point to GABA neuron cell soma. Asterisks mark intestinal autofluorescent granules. **A.** Pre-remodeling DD synapses with ventral muscles (early L1 larva, 2 hr post hatch). **B.** Pre-remodeling VD synapses with ventral muscles (L2 larva, 18 hr post hatch). Note co-localization of mCherry::RAB-3 and

UNC-49::GFP in both *unc-55* and *unc-55; unc-8* animals before remodeling. Scale bars are 10 mm. **C.** Ventral GABAergic synapses in young adults. Few ventral mCherry::RAB-3-marked presynaptic domains are detected in the unc-55 mutant background due to ectopic remodeling but are abundant in both *unc-8* and *unc-55;unc-8*. Scale bars are 25 mm. **D**. Average correlation coefficient for ventral UNC-49::GFP and mCherry::RAB-3 puncta before remodeling. *unc-8* is not significantly different from wild type ($p>0.05$, $n \geq 3$ L1 larvae, ns is not significant) and unc-55;unc-8 is not significantly different from unc-55 ($p>0.05$, $n \geq 5$ L2 larvae, ns is not significant, data are mean ± SD, Mann-Whitney test). **E.** Average coefficients of determination for ventral UNC-49::GFP and mCherry::RAB-3 puncta after remodeling are not significantly different among wild-type, *unc-8* and *unc-55;unc-8* animals. *unc-55* shows significantly lower values likely due to the relative depletion of mCherry::RAB-3 vs UNC-49::GFP (**$p<0.01$, ns is not significant, $n \geq 5$ young adults, data are mean ± SD, Kruskal-Wallis with Dunn's multiple comparisons test). Mutant strains were *unc-55(e1170)* and *unc-8(tm5052)*. Data collected by Miller lab.

6. Sodium transport through UNC-8 mediates ventral synapse removal in remodeling GABAergic neurons

Having established that *unc-8* is sufficient to cause removal of ventral synapses in remodeling GABA motor neurons, we next tested whether UNC-8 channel activity itself is responsible for this effect. We previously showed that UNC-8 preferentially passes sodium when expressed in *Xenopus* ooctyes (Wang et al., 2013). To test whether this ion flow could promote synapse removal, we exposed developing worms to Benzamil, a known DEG/ENaC channel inhibitor, and quantified ventral GABA::SNB-1::GFP in adulthood as a measure of residual synapses (Figure 4.13). We grew *unc-55* mutant worms on 3 mM Benzamil and found that compared to those grown on control media, the Benzamil-treated *unc-55* mutant worms had retained a significant number of ventral synapses (Figure 4.13A, B). The synapse retention was similar to that seen in an *unc-55;unc-8* double mutant. When we exposed the *unc-55;unc-8* double mutant worms to Benzamil, however, no change in ventral synapse number was observed. This indicated that Benzamil-mediated synapse retention required UNC-8 activity. To confirm that Benzamil specifically acts on UNC-8, we measured currents through the

constitutively active UNC-8(G387E) expressed in the *Xenopus* oocyte system (Figure 4.13C,D). We found that Benzamil treatment sharply reduced sodium transport through UNC-8(G387E) in Ca^{2+} and divalent cation-free solution (K_i ~ 119 μm). This effect was enhanced in a physiological solution that contained Ca^{2+} and divalent cations (K_i = 47 μm), suggesting that the presence of Ca^{2+} may increase Benzamil binding to UNC-8. We performed similar scoring experiments with the drug Amiloride, which is also known to inhibit DEG/ENaC channels in a divalent cation-dependent manner.

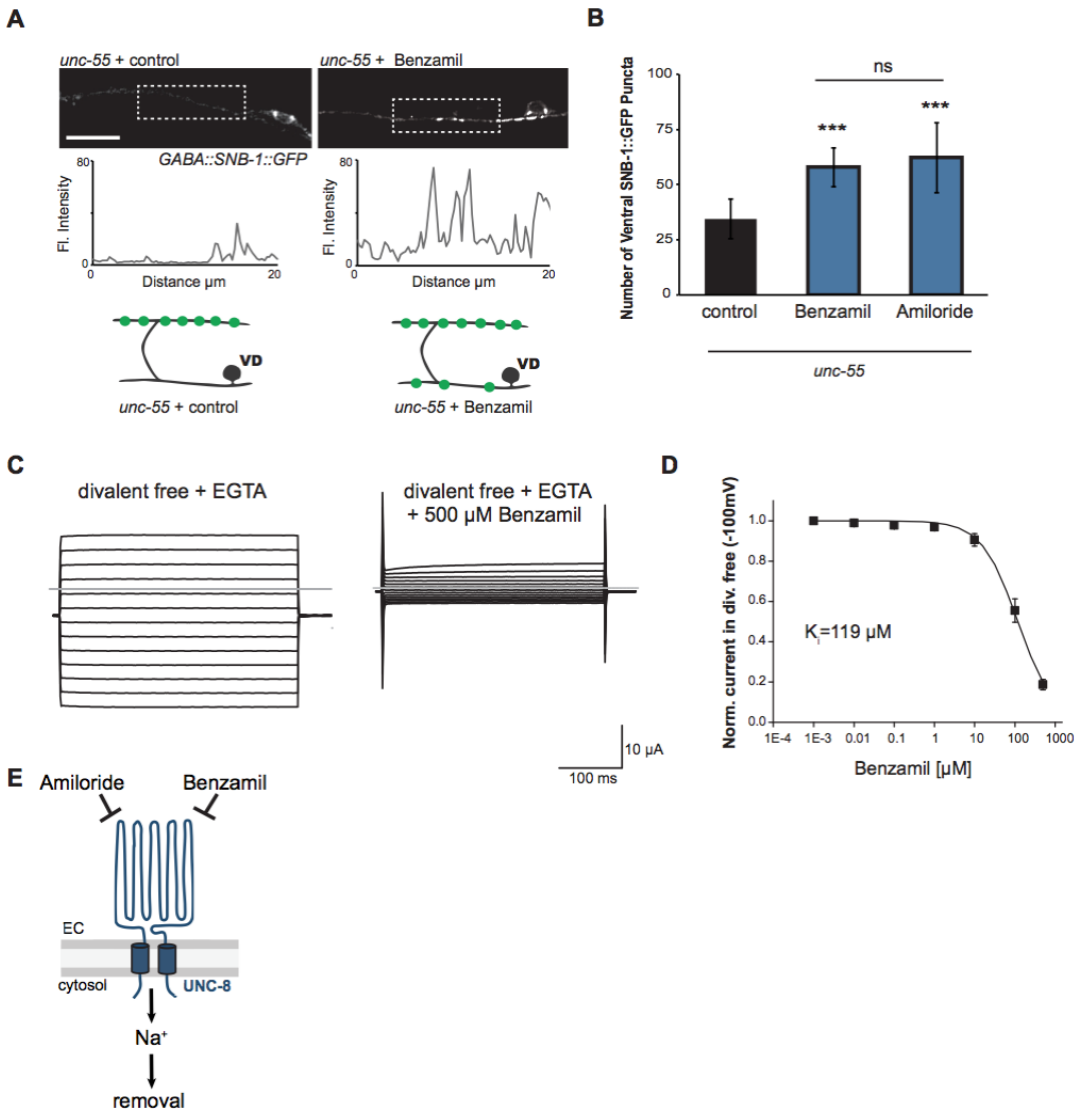

Figure IV.13. UNC-8 cation channel activity promotes the removal of ventral synapses in remodeling GABA neurons. A. Representative images and fluorescence intensity plots (generated from 20 mm dashed region) of SNB-1::GFP-marked ventral GABA neuron synapses in *unc-55* animals treated with either 3 mM Benzamil or water (control). Scale bar is 10 mm. B. Benzamil and Amiloride antagonize the removal of ventral GABA synapses in *unc-55* mutant animals. Ventral GABA neuron synapses were quantified by counting SNB-1::GFP puncta (***p<0.001, ns is not significant, n ≥ 25 animals, data are mean ± SD, One-Way ANOVA with Bonferroni correction). C. Benzamil blocks UNC-8(G387E) current in Xenopus oocytes. Representative currents from oocyte expressing UNC-8(G387E) in a bath of divalent cation-free solution plus EGTA. Currents elicited by 20mV voltage steps from -160mV to +100mV. The holding potential was -30mV. The gray line represents the zero current level (left). The same oocyte exposed to 500mM Benzamil (right). D. Benzamil dose-response curve in divalent cation-free bath solution. Currents recorded with Benzamil were normalized against recordings in divalent cation-free bath solution plus EGTA at -100mV. Data were fitted to the Boltzmann's equation to derive Ki = 119

mM (n = 10 oocytes). Data are mean ± SEM. **E.** Pharmacological inhibition of UNC-8 channel activity with either Benzamil or Amiloride blocks removal of ventral synapses in remodeling GABA neurons synaptic remodeling (EC is extracellular). Data collected by Miller lab and Bianchi lab.

Indeed, when we exposed animals to 3 mM Amiloride, we saw similar effects as with Benzamil (Figure 4.14). Drug-treated *unc-55* mutant animals showed partial restoration of ventral GABA::SNB-1::GFP puncta, and no effect was observed in treated *unc-55;unc-8* animals. These results demonstrate that UNC-8 channel activity is necessary to promote ventral synapse removal in remodeling DD and VD neurons.

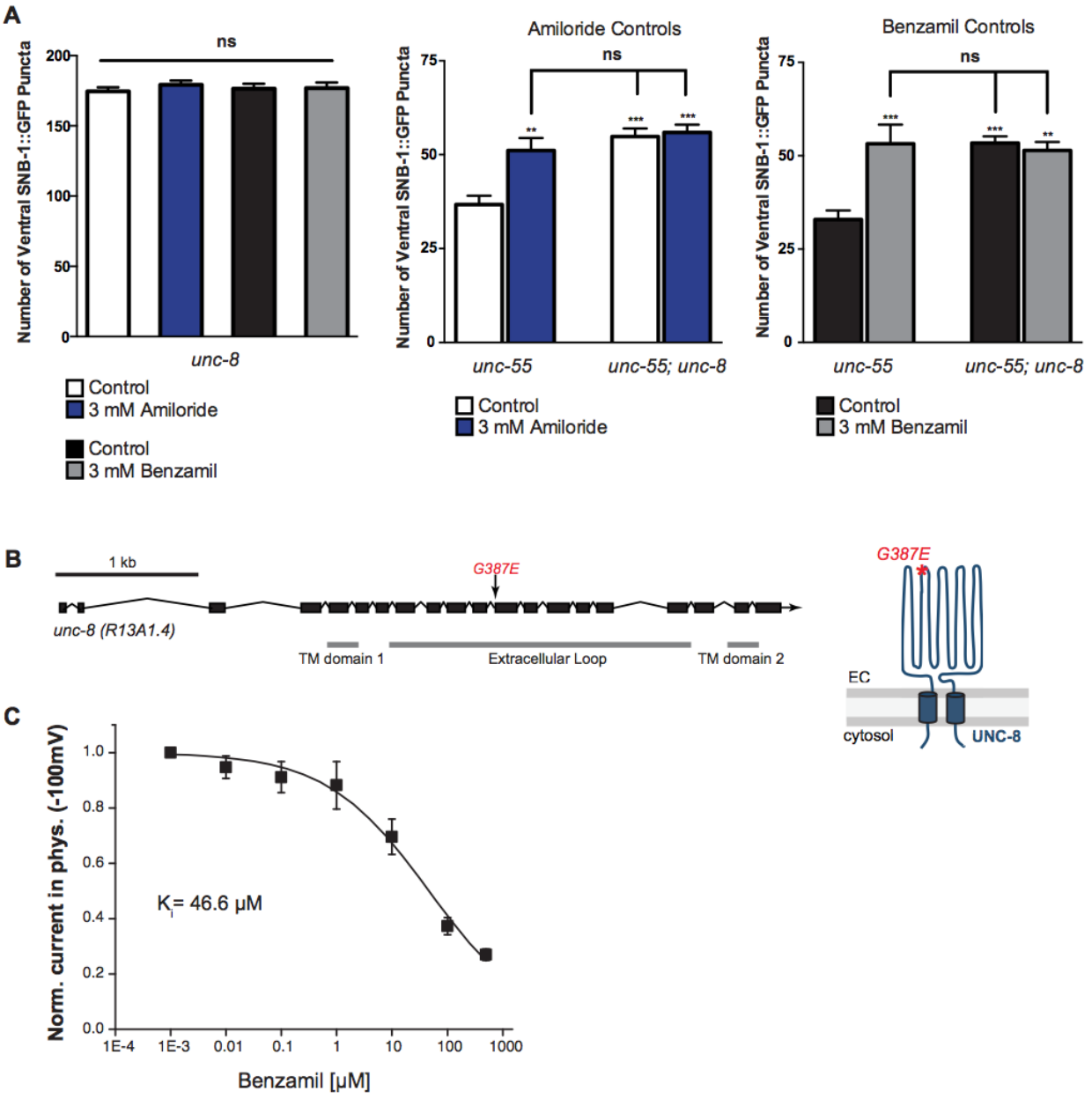

Figure IV.14. UNC-8 is required for the inhibitory effect of Benzamil and Amiloride on synaptic removal. A. Treatment of *unc-8* and *unc-55;unc-8* animals with either 3 mM Amiloride or 3 mM Benzamil does not limit removal of ventral synapses. Vehicle control for Amiloride and Benzamil treatment is water ($n \geq 10$, **p<0.01, ***p<0.001, ns is not significant, mean ± SEM, One-Way ANOVA with Bonferroni correction). **B.** The point mutant G387E renders the UNC-8 channel constitutively active and was used for in vitro oocyte experiments. Schematic shows the *unc-8* genomic region and denotes the locations of transmembrane domains TM1 and TM2 and the predicted extracellular loop region. **C.** UNC-8(G387E) currents recorded in physiological solution plus the DEG/ENaC inhibitor Benzamil at -100mV were normalized against currents recorded in physiological solution at -100mV. Data were fitted with the Boltzmann's equation for Ki = 46.6 mM (n = 10 oocytes). Data are mean ± SEM. Data collected by Miller lab and Bianchi lab.

7. Neuronal activity promotes UNC-8-mediated removal of remodeling synapses.

While UNC-8 activity influences ventral synapse elimination, it has been shown that synaptic activity can drive dorsal DD synapse assembly. Mutant worms with enhanced synaptic activity exhibit faster rates of dorsal synapse formation, and these synapses develop more slowly in mutant worms with reduced transmission (Thompson-Peer et al., 2012). If synaptic activity influences dorsal DD synapse assembly, we infer it may play a role in ventral synapse removal. To test this hypothesis, we measured residual ventral GABA::SNB-1::GFP in mutants that increase or reduce synaptic transmission (Figure 4.15). VGCC's allow intracellular calcium to enter the presynaptic terminal and trigger SV fusion (Catterall et al., 2008). In *C. elegans*, *unc-2* encodes the CaV2 α1 subunit of the P/Q-type voltage-gated calcium channel (Mathews et al., 2003). It localizes to the presynaptic active zone and is required for Ca^{2+}-dependent neurotransmitter release (Gracheva et al., 2008; Saheki and Bargmann, 2009). We found that a significant number of ventral puncta were restored in an *unc-55;unc-2* mutant compared to *unc-55* alone (Figure 4.15A, B). The extent of synapse retention was similar to the *unc-55;unc-8* mutant. Interestingly, we observed no additional rescue of ventral puncta in an *unc-55;unc-8;unc-2* triple mutant, indicating that *unc-2* and *unc-8* operate in the same pathway to mediate ventral synapse disassembly. Next, we examined *tom-1* mutants. Tomosyn normally inhibits neurotransmitter release by blocking SV priming. In a *tom-1* mutant, SV release is enhanced (Gracheva et al., 2006; McEwen et al., 2006). Previous work has shown that *tom-1* mutants exhibit faster rates of dorsal DD synapse assembly (Thompson-Peer et al., 2012). We found similar results by imaging DD-

specific SNB-1::GFP in the dorsal cord of *tom-1* mutants. In a *tom-1;unc-8* double mutant, this precocious remodeling effect was reduced, though still faster than in wild-type worms (Figure 4.15C). These results indicate that *unc-8* is involved in precocious dorsal DD synaptic assembly in worms lacking Tomosyn. It should be noted that we previously found *unc-8* affects only ventral DD synapse removal in wild-type animals (Petersen et al., 2011). Based on the current observations, it is possible that precocious remodeling in *tom-1* mutants is caused by an indirect effect of UNC-8. Dorsal DD synapse assembly may require recycling of presynaptic components that are affected by UNC-8 activity.

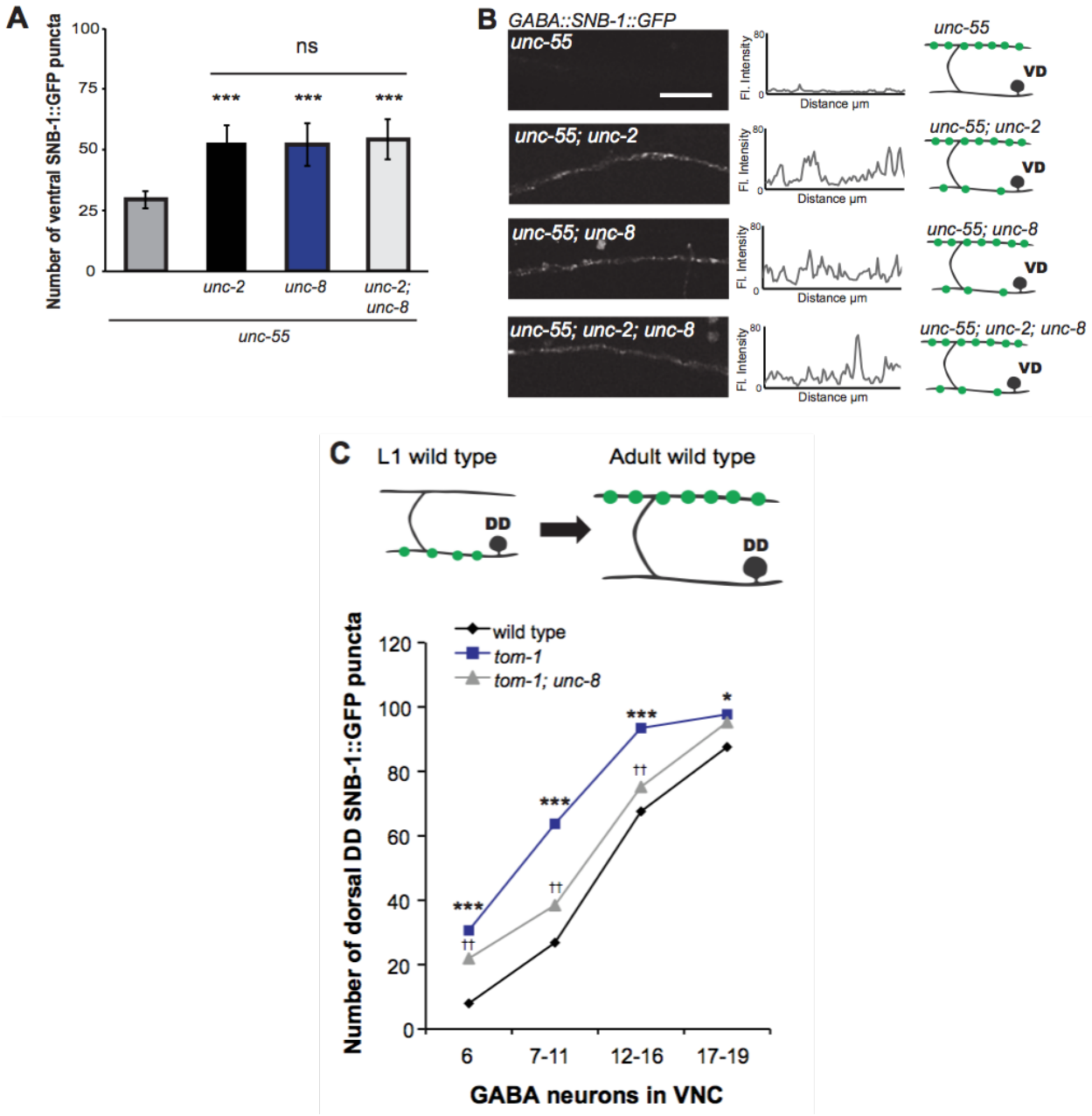

Figure IV.15. UNC-8 drives synaptic remodeling in an activity-dependent pathway that requires neurotransmitter release. A. Loss-of-function mutations in either *unc-2* (VGCC) or *unc-8* impairs removal of ventral SNB-1::GFP in *unc-55* animals. The *unc-8* mutation does not enhance the *unc-55;unc-2* remodeling defect, demonstrating that UNC-2/VGCC and UNC-8/DEG/ENaC function in a common pathway to promote GABA synapse removal (***p<0.001 vs unc-55, One-Way ANOVA with Bonferroni correction, data are mean ± SD, n ≥ 17). B. Representative images and insets show fluorescence intensity plots over a 20 mm region of the ventral nerve cord for each genotype. Scale bar is 5 mm. **C.** DD synapses are precociously remodeled in *tom-1* mutants. This effect is suppressed in *unc-8;tom-1* animals (*p<0.05, ***p<0.001 vs wild type, ††p<0.01 vs *tom-1* Student's t-test, results pooled from > 3 independent experiments per genotype) Plots are

normalized for the total number of GABA neurons labeled with SNB-1::GFP in the ventral cord to account for developmental delay in tom-1 mutants. Data collected by Miller lab.

While these genetic experiments confirm the activity-dependence of ventral synapse removal, they are based on mutations that could affect other properties in the worm. To further test our model, we induced activity specifically in GABA neurons using channel-rhodopsin (Liu et al., 2009). Blue light stimulation in GABA::ChR2 worms causes activation of GABA motor neurons and relaxation of muscle (Schuske et al., 2004). We exposed animals to blue light at 0.5 Hz for 13 hours and then scored dorsal DD::SNB-1::GFP (Figure 4.16). Exposure to light, and presumably enhanced GABA activity, resulted in greatly increased puncta in the dorsal cord. This effect was not observed in animals that lacked exposure to blue light or to ATR. Taken together, these results indicate that neurotransmission in DD's is sufficient to promote synaptic remodeling. Synaptic activity may be linked to *unc-8* function in this pathway in a cell-autonomous manner.

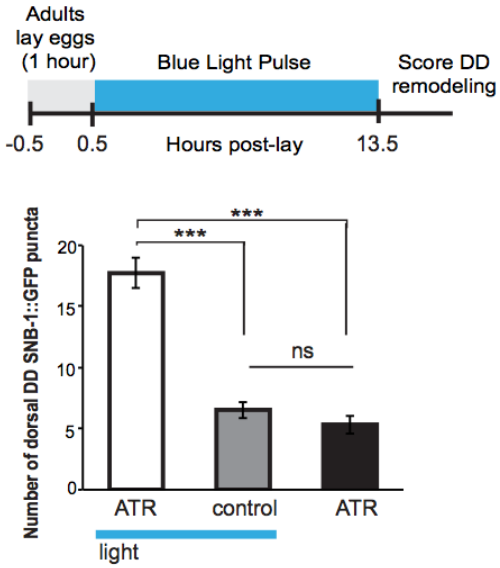

Figure IV.16. DD synapses remodeling is activity-dependent. Optogenetic stimulation of channelrhodopsin (ChR2)-induced activity in GABA neurons for 13 hr (0.5 Hz) results in precocious appearance of SNB-1::GFP marked DD synapses in the dorsal nerve cord ($n \geq 18$ animals, ***$p<0.001$, data are mean ± SEM, One-Way ANOVA with Bonferroni correction), ATR is all-trans retinal. Data collected by Miller lab.

8. UNC-8 operates downstream of the calcium/calmodulin-dependent phosphatase Calcineurin to promote ventral synapse disassembly

Given that UNC-2 and UNC-8 appear to function together to trigger ventral synapse removal, we turned our focus to potential mechanisms for this process. One possible target of elevated intracellular calcium through VGCCs is the calcium/calmodulin-activated phosphatase, calcineurin. This protein is highly expressed in the nervous system and has been previously studied as part of activity-dependent mechanisms for maintaining synapses (Baumgärtel and Mansuy, 2012; Winder et al., 1998). Calcineurin is comprised of a catalytic subunit calcineurin A and regulatory subunit calcineurin B (Figure 4.17A). We created a translational reporter gene for the *C. elegans* homolog of calcineurin A, TAX-6. *Ptax-6::TAX-6::GFP* colocalized with

GABA::mCherry and therefore is likely present in GABA neurons (Figure 4.17C). Using ventral UNC-57::GFP puncta as a measure of residual synapses, we found that *unc-55;tax-6* animals showed reduced ventral puncta compared to wild type, with some rescue of ventral synapses (Figure 4.17B). This finding suggests that Calcineurin A contributes to ventral synapse removal in remodeling GABA neurons. We observed a similar phenotype caused by the Calcineurin B homolog, *cnb-1*. The ectopic synapse removal in *unc-55* animals was partially restored in the *unc-55;cnb-1* double mutant. Levels of synapse retention were similar in *unc-55;cnb-1, unc-55;unc-8, and unc-55;unc-8;cnb-1* mutants, suggesting that these proteins operate in the same pathway to promote ventral synapse removal (Figure 4.17D). To further test this idea, we tracked synapse numbers using DD::GFP::RAB-3::in the dorsal and ventral cords from L1 to adulthood. This time, we tested a constitutively active TAX-6, *tax-6(d)*. We found that indeed, overactive TAX-6 resulted in precocious remodeling. Furthermore, this effect was reduced by the application of the DEG/ENaC channel blocker Benzamil (Figure 4.17E). This set of results provides solid evidence that TAX-6 likely functions upstream of UNC-8 to mediate ventral synapse removal in remodeling GABAergic neurons. Because UNC-2 and UNC-8 likely operate in the same pathway in synapse elimination, we propose that activity-induced intracellular calcium through UNC-2 and UNC-8 activates TAX-6/Calcineurin.

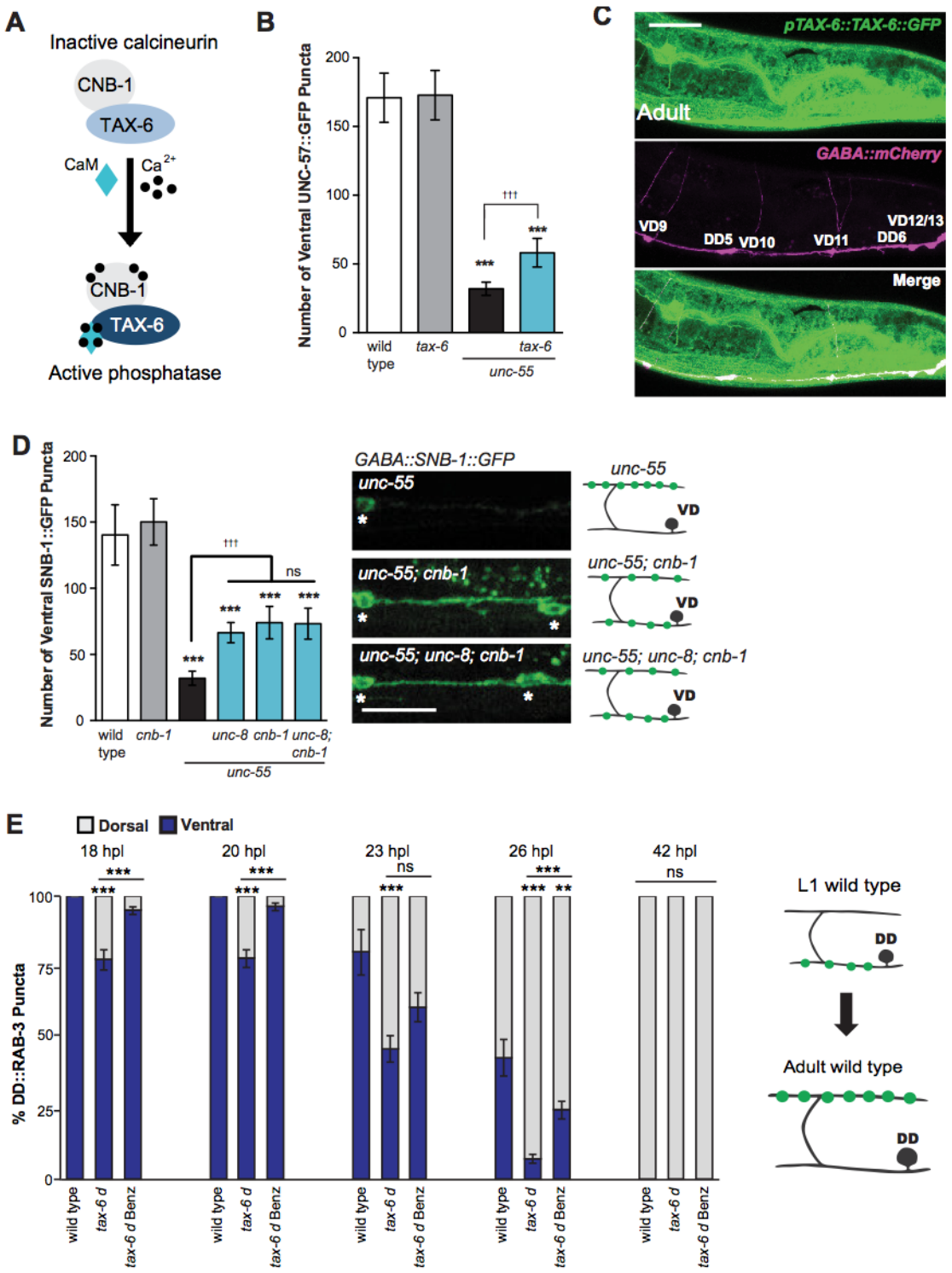

Figure IV.17. The calcium/calmodulin-dependent phosphatase calcineurin promotes GABA synapse removal in the UNC-8 pathway. **A.** Calcineurin A and B subunits (TAX-6 and CNB-1, respectively) require calcium and calmodulin (CaM) to activate phosphatase activity. **B.** Loss of tax-6 partially suppresses the **unc-55** remodeling phenotype in GABA neurons (***p<0.001, ns is not significant, One-Way ANOVA with Bonferroni correction, data are mean ± SD, n ≥ 25). **C.**

GFP-tagged TAX-6 under the control of the *tax-6* promoter region (ptax-6::TAX-6::GFP) is expressed in GABA neurons (punc-47::mCherry). Scale bar is 20 mm. **D.** CNB-1 is required for remodeling in *unc-55* animals. Loss of *cnb-1* function does not enhance the *unc-55;unc-8* remodeling defect, suggesting that calcineurin and UNC-8 promote synapse removal in a common genetic pathway (left, ***p<0.001 compared to wild type, tttp<0.001 compared to *unc-55*, ns is not significant, One-Way ANOVA with Bonferroni correction, data are mean ± SD, wild type n = 10, mutants n = 20). Representative images of ventral nerve cords in *unc-55, unc-55;cnb-1* and *unc-55;unc-8;cnb-1* animals. Asterisks denote GABA neuron soma; scale bar is 20 mm (right). **E.** Gain-of-function *tax-6 (tax-6d)* mutants remodel precociously and this effect is suppressed by Benzamil. Percentage of ventral (blue) vs dorsal (gray) DD synapses (pflp-13::GFP::RAB-3, **p<0.01, ***P<0.001, ns is not significant, One-Way ANOVA with Bonferroni correction, n ≥ 8 animals per time point, data are mean ± SEM). Results for *tax-6d* and for the *tax-6d* control for Benzamil treatment (see Materials and Methods) are combined because they were not significantly different. Benz denotes 3mM DEG/ENaC inhibitor Benzamil. Mutant alleles were *tax-6 (p675)*, *tax-6d(jh107)*, *cnb-1(ok276)*. Data collected by Miller lab.

9. UNC-8 operates in the same pathway as cell death gene, CED-4, to promote ventral synapse removal.

Knowing that calcium signaling and UNC-8 play a role in eliciting ventral synapse removal, we sought to understand the mechanism for disassembly. Previous work has shown that remodeling DD synapses rely on the canonical apoptotic pathway. Adaptor protein CED-4/Apaf1 and its downstream target, CED-3/caspase, activate gelsolin, an actin-severing protein that destabilizes the presynaptic F-actin network during the synapse removal process (Meng et al., 2015). Interestingly, both caspase and gelsolin are influenced by calcium (Pinan-Lucarre et al., 2012; Liu et al, 2011). We therefore tested whether UNC-8 and calcium signaling could be the trigger for this disassembly mechanism. We scored ventral SNB-1::GFP puncta in *unc-55;ced-4* double mutants and noticed rescue of a significant number of ventral synapses compared to the *unc-55* mutant alone (Figure 4.18). The level of rescue observed in *unc-55;ced-4* was similar to that seen in *unc-55;unc-8* animals. Moreover, we observed no additional rescue of ventral

synapses in the *unc-55;unc-8;ced-4* triple mutant. These results suggest that CED-4 is required to remove ventral GABA synapses. In the context of the results presented here, this synapse elimination mechanism is likely triggered by higher intracellular calcium levels and UNC-8 activity in active GABA synapses.

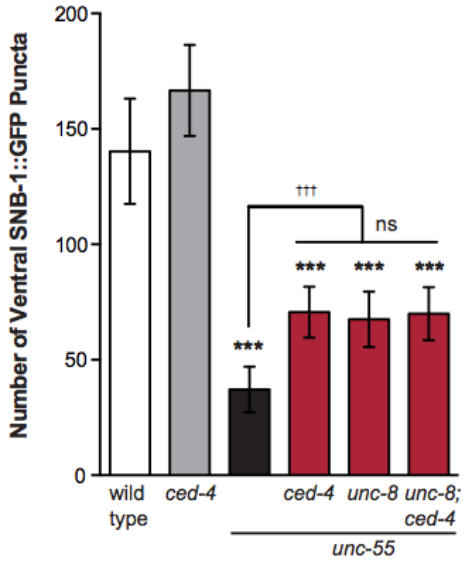

Figure IV.18. A loss-of-function mutation in the pro-apoptotic gene ced-4 partially suppresses GABA neuron remodeling in unc-55 animals. Genetic ablation of *unc-8* in the triple mutant *unc-55;ced-4;unc-8* mutants does not enhance the remodeling defect and thus suggests that UNC-8 and CED-4 promote synapse elimination in a common pathway (***p<0.001 compared to wild type, tttp<0.001 compared to unc-55, ns is not significant, One-Way ANOVA with Bonferroni correction, data are mean ± SD, wild type n = 10, mutants n = 20) Mutant allele is ced-4(n1162). Data collected by Miller lab.

C. Discussion

The maintenance and modulation of synapses and neuronal circuitry underlie development and learning. At a cellular level, this modulation often occurs through assembly or elimination of synapses during a 'critical period' in development, often in an activity-dependent

manner. Extensive work has examined these developmental periods, but less is known about the mechanisms that determine their transcriptional control and activity-dependence. Here, we show that the transcriptional target UNC-8, a cation channel in the conserved family of DEG/ENaC proteins, plays a key role in an activity-dependent pathway to trigger the removal of remodeling GABAergic synapses in *C. elegans*.

The UNC-8/DEG/ENaC channel promotes synapse removal in an activity-dependent process

DEG/ENaC channels are known to influence synaptic transmission and plasticity (Wemmie et al., 2002, 2004; Zha et al., 2006). One class of DEG/ENaCs, the acid-sensing ion channels known as ASICs, are linked to learning and memory through their ability to sense low pH. It is thought that neurotransmitter release, which acidifies the synaptic cleft, can trigger sodium influx through ASICs. This activity increases membrane depolarization and can activate voltage-gated channels and NMDA receptors in the postsynaptic membrane. In this way, ASIC activity can enhance postsynaptic signaling (Wemmie et al., 2013). Interestingly, UNC-8 does not appear to operate according to this mechanism. When reconstituted UNC-8 was expressed in the *Xenopus* oocyte system, its activity was inhibited by low pH. It is therefore unlikely that UNC-8 functions like an ASIC *in vivo* (Wang et al., 2013). This finding is important, because non-ASIC proteins are expressed in the brain and may influence synaptic function in a currently unknown fashion (Giraldez et al., 2013, Yamamura et al., 2004; Waldmann 1995).

Another member of the DEG/ENaC family, pickpocket, has recently been shown to mediate homeostatic balance of neurotransmitter release at the *Drosophila* neuromuscular junction. Sodium influx through pickpocket results in local depolarization that activates nearby

VGCCs, resulting in neurotransmitter release. This homeostatic process is regulated by transcription of pickpocket and its insertion into the membrane. It is also consistent with the finding that homeostasis at the synapse requires the $Ca_V2.1$ VGCC subunit (Muller and Davis, 2012). Based on our results, we think UNC-8 has a similar role for increasing intracellular calcium influx. Rather than maintain synapses, however, UNC-8 promotes synapse removal. Our findings are consistent with the different phenotypes observed for *unc-8* and pickpocket.

Our studies show that UNC-8 promotes removal of presynaptic components in remodeling GABAergic neurons. UNC-8 channel activity is required to drive synapse removal and likely results in sodium influx. UNC-8 expressed in the *Xenopus* oocyte system exhibited preferential sodium transport and could not transport calcium (Wang et al., 2013). Because UNC-8 localizes in puncta in the ventral nerve cord, sodium influx through these channels could in fact activate nearby VGCCs (Wemmie et al., 2013). In hippocampal neurons, VGCC activity is required for ASICs to mediate a rise in intracellular calcium (Zha et al., 2006). Just as this ASIC activity relies on VGCC function, UNC-8 requires UNC-2, the Ca_V2 channel subunit, to mediate synapse removal. In the *unc-2* mutant, remodeling was disrupted. Thus, we conclude that UNC-8 cation channel activity promotes a rise in intracellular calcium through UNC-2 in GABA neurons. Because *unc-2* and *unc-8* operate in a common genetic pathway, the rise in intracellular calcium may be required for full dismantling of presynaptic components in remodeling neurons (see below).

Calcium signaling and a caspase-dependent pathway elicit GABA synapse removal

Following the evidence that calcium plays a role in remodeling, we found that the calcineurin homolog TAX-6 is also involved in the *unc*-8-dependent synapse removal mechanism. Calcineurin/CaN is a serine-threonine phosphatase that is activated by calcium and Calmodulin. It has been shown to regulate neural plasticity by opposing LTP. In this mechanism, Calcineurin dephosphorylates the GluR1 subunit of AMPA receptors, prompting receptor removal from postsynaptic membrane (Winder et al.,1998; Sanderson et al., 2012; Lee et al., 1998). In the remodeling paradigm, constitutively active TAX-6 resulted in faster synapse removal. This phenotype was blocked by Benzamil, a potent DEG/ENaC inhibitor (Fig 7E). It is possible that TAX-6 somehow activates UNC-8 to promote synapse disassembly. UNC-8 activity could promote a positive feedback loop in which UNC-2, TAX-6/Calcineurin, and UNC-8 act to increase intracellular calcium levels. In a similar mechanism, CaMKII phosphorylates ASIC1a. ASIC1a activation promotes calcium influx through VGCCs which elicits further CamKII activity (Zha et al., 2006; Gao et al., 2005; Zha 2013). In our model, UNC-8 could be an amplifier that promotes the positive feedback loop to increase intracellular calcium.

Our finding that calcium signaling is a key component of the GABA synapse removal mechanism is consistent with studies that have examined the canonical apoptotic pathway in remodeling GABA synapses. Specifically, it has been found that CED-4/Apaf1 activates CED-3/Caspase, which then cleaves gelsolin, an actin-severing protein. Active gelsolin then destabilizes the F-actin network at the presynaptic membrane (Meng et al., 2015). Of note, CED-3 and gelsolin both show calcium dependence (Pinan-Lucarre et al., 2012; Liu et al., 2011). Furthermore, this pathway is localized to the presynaptic membrane and is conserved in synapse elimination pathways in other species (Erturk et al., 2014; Wang et al., 2014; Li et al., 2010). Our

genetic experiments suggest that *unc-8* and *ced-4* function in a common pathway. Therefore, we propose that UNC-8 activity enhances depolarization at the presynaptic membrane that drives VGCC activity. Calcium influx through VGCCs stimulates the UNC-8/UNC-2 positive feedback loop that can eventually trigger apoptosis through the TAX -6/calcineurin and CED-3/caspase-3 pathways. Because each of these molecules are tightly localized at the presynaptic domain, local calcium increase is enough to activate synapse elimination without triggering cell death. Still, it is possible that additional DEG/ENaC-mediated mechanisms could contribute to the synapse removal process.

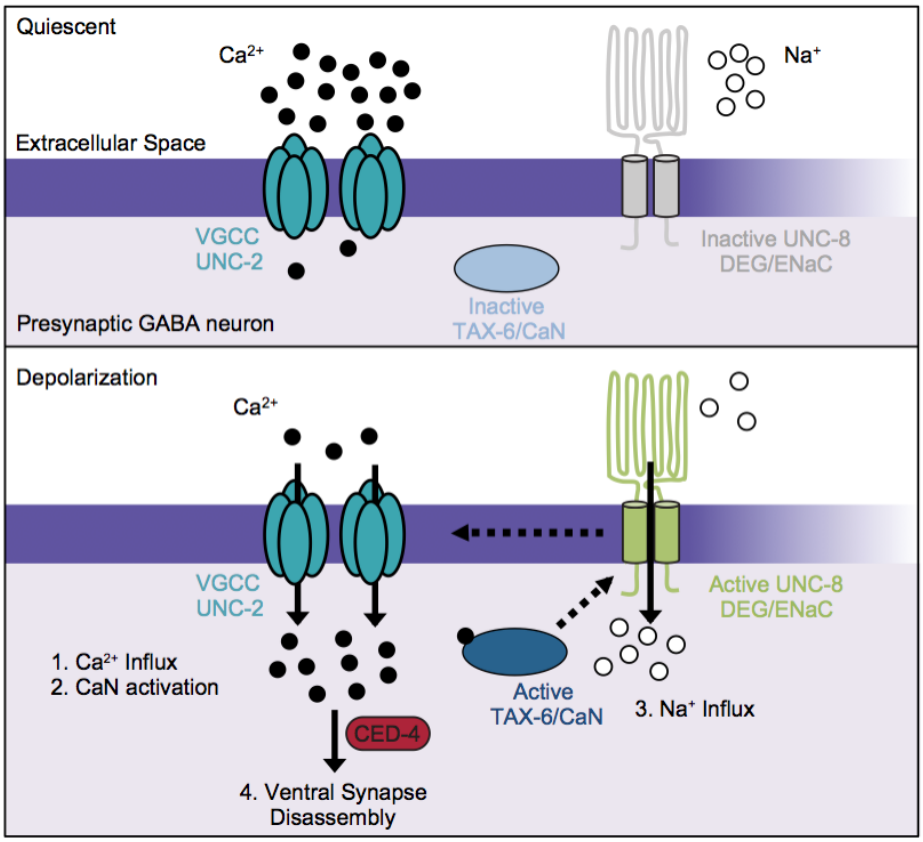

Figure IV.19. Model of UNC-8-driven synapse disassembly in the GABA neuron remodeling program. Model of a calcium-dependent mechanism for removal of the presynaptic apparatus. A DEG/ENaC channel containing UNC-8 is not active (gray) in quiescent GABA motor neurons (top

panel). (1) GABA neuron depolarization activates the voltage-gated calcium channel (VGCC), UNC-2, to allow calcium entry (black circles bottom panel). (2) Intracellular calcium activates the calcium/calmodulin-dependent phosphatase, calcineurin (CaN/TAX-6). (3) CaN phosphatase may activate UNC-8, which results in the movement of sodium ions (white circles) into the presynaptic GABA neuron, further depolarizing the presynaptic membrane and activating VGCCs. This positive feedback loop is predicted to further elevate intracellular calcium. (4) Our results show that UNC-8 drives the removal of presynaptic components and functions in a common genetic pathway with calcium signaling and with the apoptotic protein CED-4. Therefore, we hypothesize that selective expression of UNC-8 in remodeling GABA neurons effectively boosts the level of intracellular calcium to activate a CED-4-dependent pathway for removal of the presynaptic apparatus.

GABA synapse remodeling relies on multiple components

The results presented here demonstrate that *unc-8* promotes ventral GABA synapse removal, but is not required for dorsal synapse assembly. Similarly, the calcium/caspase dependent pathway also exclusively affects synapse removal (Meng et al., 2015). Because *unc-8* mediates only partial removal of synapses (Meng et al., 2015), there are likely other components that also contribute to remodeling (Howell et al., 2015; He et al., 2015). Indeed, it is known that cyclin box-containing protein CYY-1 influences synapse removal, while cyclin-dependent kinase CDK-5 specifically impacts synapse assembly (Park et al., 2011). Additionally, our previous work revealed that the Iroquois family homeodomain transcription factor IRX-1 promotes both DD ventral synapse removal and *de novo* dorsal synapse formation. While the exact function of this pathway is still unclear, *irx-1* likely coordinates multiple gene pathways to contribute to the removal and transport of synaptic components. Our evidence suggests that *irx-1* may be responsible for movement of release machinery. Specifically, in an *unc-55;irx-1* double mutant, residual ventral synapses are functional (Petersen et al., 2011). This is in contrast to residual synapses in an *unc-55;unc-8* mutant, which exhibit diminished GABA transmission. Future

experiments will examine the specific roles of *irx-1* and *unc-8* in the synapse removal pathway. While these genes likely operate in parallel pathways, UNC-8 alone is sufficient to trigger removal. Thus, *unc-8* expression is a genetic switch to drive synapse removal in remodeling GABA neurons.

D. Materials and Methods

C. elegans strains and genetics

Worm strains were maintained at 20°C on NGM plates seeded with OP50 (E. coli), unless otherwise stated (Brenner, 1974). The wild type strain is N2 and only hermaphrodite animals were analyzed. The *unc-55(e1170)* and *unc-8(tm5052)* alleles were used for these studies.

The *unc-8(tm5052)* allele was obtained from a UV/TMP mutagenized library, as described previously (Gengyo-Ando and Mitani, 2000) and was identified by PCR amplification with primers spanning the deleted region. *tm5052* likely corresponds to an *unc-8* null allele because it deletes a portion of the fifth and entire sixth exon (197 base pairs) with the insertion of CT resulting in a pre-mature stop codon prior to the first transmembrane domain. We used the following primers to detect the *tm5052* mutation: Forward 5'-TGGGGCCCTAATAATTTCGA-'3 and Reverse 5'-AGTGA- CAGTATGAAGCCAGG-'3.

C. elegans strains used in this study

Strain Name	Strain Description
NC2320	*wdIs74 [pttr-39::mCherry] V; otEx2876[punc-8::GFP; elt-2::GFP]*
NC2321	*unc-55(e1170) I; wdIs74 V; otEx2876[punc-8::GFP; elt-2::GFP]*
NC2585	*wyIs202[pflp-13::GFP::RAB-3; pflp-13::mCherry]* X
NC2480	*unc-8(tm5052)* IV; *wyIs202* X
NC2861	*juIs137[pflp-13::SNB-1::GFP]* II
NC2936	*unc-8(tm5052)* IV; *juIs137* II
NC2994	*unc-8 tm5052 IV*; wdEx960[*punc-25::UNC-8::GFP*]
CZ333	*juIs1[punc-25::SNB-1::GFP; lin-15+]* IV
CB1170	*unc-55(e1170)* I
NC1851	*unc-55(e1170)* I; *juIs1* IV
FX05052	*unc-8(tm5052)* IV
NC2387	*unc-8(tm5052) juIs1* IV
NC2388	*unc-55(e1170)* I*; unc-8(tm5052) juIs1* IV
KP5348	*nuIs279[punc-25::UNC-57::GFP;punc-25::mCherry::RAB-3]*
NC2984	*unc-55(e1170)* I; *nuIs279*
NC2870	*unc-8(tm5052)* IV; *nuIs279*
NC2873	*unc-55(e1170)* I; *unc-8(tm5052)* IV; *nuIs279*
ZM54	*hpIs3[punc-25::SYD-2::GFP; lin-15+]* X
NC1849	*unc-55(e1170)* I; *hpIs3* X

NC2875	*unc-8(tm5052)* IV; *hpIs3* X
NC2874	*unc-55(e1170)* I; *unc-8(tm5052)* IV; *hpIs3* X
NC2319	*unc-55(e1170)* I; *unc-119(ed3)* III; *juIs1* IV; *wdEx658* [*punc-25::mCherry, unc-119(+)*]
NC2601	*unc-55(e1170)* I; *unc-119(ed3)* III; *juIs1* IV; *wdIs86*[*pttr-39::unc-8; unc-119+; punc-25::mCherry; pttr-39::unc-8 antisense*]
IZ1607	*pflp-13::mCherry::RAB-3*
NC3063	*pflp-13::mCherry::RAB-3 ;unc-55; unc-8 juIs1 IV*
NC2894	*unc-8 tm5052* IV; *wpIs39 [punc-47::mCherry]* X; *wdEx944* [UNC-8::GFP fosmid; *punc-25::mCherry::RAB-3; pceh-22::GFP*]
NC3010	*unc-55 (e1170)* I; *unc-8 (tm5052)* IV; *wdIs90 [punc-25::mCherry::RAB-3; ceh-22::GFP]*; *wdEx962 [UNC-8::GFP fosmid; pmyo-2::mCherry]*
NC3064	*unc-55*; *unc-8 juIs1*; *wdEx*977[*pttr-39::UNC-8; punc-47::mCherry*]
EG5052	*oxIs351[punc-47:ChR2::mCherry; lin-15+ LITMUS 38i]* X
NC2211	*unc-55(e1170)* I; *oxIs351* X
NC2857	*unc-8(tm5052)* IV; *oxIs351* X
NC2807	*unc-55(e1170)* I; *unc-8(tm5052)* IV; *oxIs351* X
CB55	*unc-2 (e55)* X
NC2454	*unc-2(e55)* X; *juIs1* IV
NC2443	*unc-55(e1170)* I; *unc-2(e55)* X; *juIs1* IV
NC2834	*unc-55(e1170)* I; *unc-2(e55)* X; *unc-8(tm5052) juIs1* IV

RB1887	*tom-1(ok2437)* I
NC2616	*tom-1(ok2437)* I; *juIs1* IV
NC2709	*tom-1 (ok2437)* I; *unc-8(tm5052) juIs1* IV
NC2893	*juIs1* IV; *oxIs351* X
NC3065	*tax-6 p675 IV; nuIs279*
NC3066	*unc-55 e1170 I; tax-6 p675 IV; nuIs279*
MQD5	*hqIs5 [ptax-6::tax-6::GFP]*
NC3067	*hqIs5; punc-47::mCherry X*
NC3068	*tax-6 jh107 IV; wyIs202 X*
VC990	*cnb-1 ok276 V*
NC3069	*cnb-1 ok276 V; juIs1 IV*
NC3070	*unc-55 e1170 I; cnb-1 ok276 V; juIs1 IV*
NC3071	*unc-55 e1170 I; cnb-1 ok276 V; unc-8 tm5052 juIs1 IV*
NC3080	*ced-4 n1162 III; juIs1 IV*
NC3081	*ced-4 n1162 III; unc-55 e1170 I; juIs1 IV*
NC3082	*ced-4 n1162 III; unc-55 e1170 I; unc-8 tm5052 juIs1 IV*
NC3171	*juIs1; wdEx993[pttr-39::UNC-8cDNA; punc-25::mCherry::RAB-3; pmyo-2::dsRed]*
NC3167	*wdEx961 [punc-25::mCherry::RAB-3; ceh-22::GFP]; oxIs22 [punc-49::UNC-49::GFP; lin-15+] II*
NC3186	*unc-8 tm5052 IV; wdEx961; oxIs22*
NC3187	*unc-55 e1170 I; wdEx961; oxIs22 II*

NC3188	*unc-55 e1170 I; unc-8 tm5052 IV; wdEx961; oxIs22 II*

Molecular biology and transgenes

Construction of GABA csRNAi transgenic lines

RNAi plasmids used for GABA neuron-specific knock down of *unc-8* target the first 7 exons of the *unc-8* coding region. To clone the *unc-8* sense construct pSA76, a 2.3 kb region of *unc-8* cDNA was amplified with the following primers containing 5'AscI/3'SacII adaptors: Forward 5'-GGCGCGCCA TGTCACCTTTGCTGACGT-3' and Reverse 5'-GCCAGGAGGTGATATTCTAGCCGCGG-3'. This fragment was cloned into pCR2.1 via TOPO-TA reaction (Invitrogen, Waltham, MA) to yield pSA75. The 2.3 kb *unc-8* cDNA fragment was then subcloned into the existing GABAergic cell-specific RNAi (csRNAi) plasmid pSA47 via AscI/SacII to yield pSA76 (Petersen et al., 2011). pSA76 contains the DD/VD specific promoter, *pttr-39* and the *unc-119* wild-type mini gene (Maduro and Pilgrim, 1995). To construct the *unc-8* antisense plasmid pSA78, the 2.3 kb *unc-8* cDNA fragment was amplified with the following primers containing 5''SacII/3'AscI adaptors: Forward 5'-CCGCGGATGTCACC TTTGCTGACGTG-3' and Reverse 5'- CCAGGAGGTGATATTCTAGGGCGCGCC-3'. The *unc-8* anti-sense fragment was subcloned into pCR2.1 via TOPO-TA reaction (Invitrogen) to yield pSA73. The *unc-8* fragment from pSA73 was then inserted into the GABA neuron-specific RNAi (csRNAi) plasmid pSA47 via AscI/SacII to yield pSA77. The *unc-8*-containing region of pSA77 between ScaI and SacII was then inserted into plasmid pSA49 to yield pSA78. The *pttr-39* promoter in pSA78 drives expression of the 2.3 kb *unc-8* antisense fragment and mCherry. pSA76 (*unc-8* sense) and pSA78 (*unc-8* antisense) were linearized and ligated, then transformed into

unc-119 worms via microparticle bombardment to yield a spontaneous integrant (strain NC2601) as indicated by 100% transmission of rescued (*unc-119+*) movement (indicating *unc-8* sense) and mCherry expression in all GABAergic motor neurons (indicating *unc-8* antisense) (Praitis et al., 2001). A control plasmid was also created containing *pttr39*-driven mCherry and the *unc-119* rescuing gene, which was transformed into *unc-119* worms via microparticle bombardment.

Recombineering UNC-8::GFP fosmid

The UNC-8::GFP fosmid was recombineered as previously described (Tursun et al., 2009). Briefly, the 30 kb fosmid WRM0635cA02 containing the *unc-8* genetic locus was obtained from GeneService (Nottingham, UK) and purified. Fosmid DNA was transformed into electrocompetent SW105 cells and was verified by PCR. A GFP-galK recombineering cassette was amplified with 50 kb homology arms from pBALU1 and gel-purified. The GFP-galK PCR product was transformed into electrocompetent, lRed recombinase-activated, fosmid-containing SW105 cells. The cells containing the fosmid and GFP-galK were grown for more than 60 hr at 32°C and streaked on MacConkey and galactose plates with chloramphenicol to ensure the insertion of recombineering cassette. To excise galK from the GFP intron, colonies were incubated with 0.1% arabinose to create an *unc-8::GFP* expression fosmid. This *unc-8::GFP* fosmid was then purified and confirmed by sequencing. The fosmid was injected into *unc-8(tm5052)* animals at 25 ng/ml with co-injection marker *pceh-22::GFP* at 15 ng/ml.

Construction of punc-25::UNC-8::GFP plasmid

UNC-8 cDNA was PCR-amplified from pSGEM/pTWM60 (Wang et al., 2013) with primers that span the UNC-8 cDNA sequence and exclude the 3' stop codon. The primer sequences are: Forward 5'-A TGAGCGCAAGGAGTAGT-3' and Reverse 5'- TTTGCTCATTAACTCCTTTGT-3'. Primers include either 5'-AscI or 3'-SacII adaptors for inserting UNC-8 cDNA into pMLH260 (*punc-25::coq1cDNA:: GFP::unc-54*) in place of the coq-1 fragment. The resultant plasmid, pTWM62 (*punc-25:-8:: GFP*) was injected (10 ng/ml) with co-selectable marker *pmyo-2::mCherry::unc-54* (2.5 ng/ml) into *unc-8(tm5052)* animals.

Construction of *pttr-39::UNC-8* plasmid

UNC-8 cDNA was PCR-amplified from pSGEM/pTWM60 (Wang et al., 2013) with primers that span the UNC-8 cDNA sequence. The primer sequences are: Forward 5'-ATGAGCGCAAGGAGTAGT-3' and Reverse 5'- TTTGCTCATTAACTCCTTTGT-3'. Primers include either 5'-AscI or 3'-EcoRI adaptors for inserting UNC-8 cDNA into pTWM35 (pttr39::arx-5::GFP::unc-54) in place of the ARX-5::GFP fragment. The resultant plasmid, pTWM92 (pttr-39::UNC-8cDNA) was injected (25 ng/ml) with co- selectable markers pmyo-2::mCherry::unc-54 (2 ng/ml) and *punc-25::mCherry::RAB-3* (5 ng/ml) into *unc-55; unc-8(tm5052)* juIs1 or juIs1 animals.

Staging and synapse quantification

For time-course experiments, 100 adult hermaphrodites from each genotype were picked to fresh 60 mm plates and allowed to lay eggs for one hour. The mid-point at which the eggs were laid is considered T_0. All adults were removed from the plates after 1 hr. Plates were maintained

at 23°C until assayed. Puncta arising from localization of fluorescent presynaptic markers were counted with a Zeiss Axiovert microscope (63X oil objective) in immobilized animals. For timecourse experiments puncta were counted between DD1 and DD6 or from VD3 to VD11 in adults. Data were pooled from 3 separate experiments. In young adults, labeled puncta were counted in the ventral nerve cord region between VD3 and VD11. For experiments featuring mosaic expression of either *unc-8(csRNAi)* or *unc-8* cDNA, puncta were counted from individual DD and VD neurons. The examiner was blinded to genotype.

Confocal microscopy and image analysis

Animals were immobilized with 15 mM levamisole/0.05% tricaine and mounted on a 2% agarose pad in M9 buffer as previously described (Smith et al., 2010). Z-stack images were collected on a Leica TCS SP5 confocal microscope using a 63X oil objective (0.5 mm/step), spanning the focal depth of the ventral nerve cord GABA neurons and synapses. Leica Application Suite Advanced Fluorescence (LAS-AF) software was used to generate maximum intensity projections. Images in Figure 3A were collected from 10 animals of each genotype. Ventral nerve cord images between VD4 and VD5 were straightened using an ImageJ plug-in and aligned in rows. All fluorescence intensity plots were created by drawing a line through the ventral nerve cords of each animal and calculating the fluorescence intensity value in arbitrary units over the distance in micrometers with the ImageJ plot profile tool. For Figure 1, DD and VD neurons were identified by the GABA-specific marker *pttr-39::* mCherry. The cells were traced in ImageJ and the background was subtracted. The UNC-8::GFP fluorescence intensity was then normalized to the *pttr-39::*mCherry fluorescence intensity for each cell. Fluorescence intensity plots in Figure 4 and

Figure 4—figure supplement 1 were created with the ImageJ plot profile tool, analyzing the same region of the ventral nerve cord in both GFP and RFP channels. Fluorescence intensity values were normalized for each channel. The coefficient of determination (r2) was calculated in ImageJ using the Manders coefficients macro, from at least 10 animals for each genotype. r2 values were averaged and presented as mean ± SEM. An r2value of 0 represents no co-localization, whereas r2 = 1 represents complete co-localization.

Pharmacology

Amiloride hydrochloride hydrate (Sigma, #A7410) stock solution was prepared in sterile water (50 mg/ml) and stored at -20˚C. A final concentration of 3 mM Amiloride diluted in OP50 bacteria was seeded on NGM plates. Control NGM plates contained the same volume of sterile water added to OP50. Benzamil hydrochloride hydrate (Sigma, #B2417, St. Louis, MO) stock solution was prepared in sterile water (1 mg/ml) and stored at 4°C. A final concentration of 3 mM Benzamil diluted in OP50 bacteria was seeded on NGM plates. Control NGM plates contained the same volume of sterile water added to OP50. Plates were stored at 4°C for up to one week. Five adult *unc-55; juIs1* animals were placed on either Amiloride, Benzamil, or control plates at room temperature and progeny examined at the young adult stage. Adult *tax-6 (d); wyIs202* animals were grown on Benzamil or control plates and their larval progeny were collected on control or Benzamil plates for timecourse assays. The number of ventral puncta was counted using a Zeiss Axiovert microscope (63X oil objective) and Z-stack images were captured on a Leica TCS SP5 confocal microscope using a 63X oil objective (0.5 mm/step). The examiner was blinded to genotype and treatment condition.

Optogenetics

All-trans retinal (Sigma, #R2500) was dissolved in ethanol to prepare a 100 mM stock and stored at – 20°C. 300 mM of all-trans retinal stock solution (ATR plates) or ethanol (control plates) was added to OP50 bacteria and seeded onto NGM plates. Plates were protected from light and were stored at 4°C for up to one week. 100 adult hermaphrodites were placed on either ATR or control plates, allowed to lay eggs for 1 hr and then removed from the plate. The midpoint of this hour is considered T_0. Plates were exposed to blue light pulses with a 470-nm LED light (#M470L2, Thor Labs, Newton, NJ) for 13 hr (0.5 Hz, 2 mW/mm2 measured with Solartech Inc. Solar Meter 9.4 radiometer). Light stimulation was controlled using NI Max software through TTL signals generated by a digital function generator (National Instruments, Austin, TX). 13 hr after egg laying, animals were assayed for DD remodeling by counting the number of dorsal SNB-1::GFP puncta. The examiner was blinded to the treatment. Data were collected from three independent time course experiments with at least six animals per treatment.

Electrophysiology

The *C. elegans* dissection and electrophysiological methods were as previously described (Richmond and Jorgensen, 1999). Animals were immobilized along the dorsal axis with Histoacryl Blue glue, and a lateral cuticle incision was made with a hand-held glass needle, exposing ventral medial body wall muscles. Muscle recordings were obtained in the whole-cell voltage-clamp mode using an EPC-10 patch-clamp amplifier and digitized at 1 kHz. The extracellular solution consisted of 150 mM NaCl, 5 mM KCl, 5 mM $CaCl_2$, 4 mM $MgCl_2$, 10 mM glucose, 5 mM sucrose,

and 15 mM HEPES (pH 7.3, ~340 mOsm). The low Cl intracellular patch pipette solution used to isolate outward GABA minis at a 0 mV holding potential was composed of 115 mM KGluconate, 25 mM KCl, 0.1 mM $CaCl_2$, 1 mM BAPTA and 50 mM HEPES. Data were acquired using Pulse software (HEKA, Southboro, Massachusetts, United States) run on a Dell computer. Subsequent analysis and graphing was performed using Pulsefit (HEKA), Mini analysis (Synaptosoft Inc., Decatur, Georgia, United States) and Igor Pro (Wavemetrics, Lake Oswego, Oregon, United States).

Oocyte expression and electrophysiology

UNC-8(G387E) cRNA was synthesized using T7 mMESSAGE mMACHINE kit (Ambion, Waltham, MA). cRNA was purified and examined on a denaturating agarose gel to confirm correct size and integrity. cRNA quantification was performed spectroscopically. Stage VI defolliculated oocytes from Xenopus Laevis were purchased from Ecocyte Bioscience US LLC (Austin, Texas). Oocytes were injected with 10 ng/oocyte of cRNA and incubated in OR2 solution (82.5 mM NaCl, HPO 2.5 mM KCl, 1 mM $CaCl_2$, 1 mM $MgCl_2$, 1 mM Na_2HPO_4, 0.5 g/liter polyvinyl pyrolidone, and 5 mM HEPES, pH 7.2, supplemented with penicillin and streptomycin (0.1 mg/ml) and 2 mM Na-pyruvate) plus 500 mM amiloride (to prevent channel hyperactivation-dependent cell death) at 20°C for 2–3 d before recordings. Currents were measured using a two-electrode voltage-clamp amplifier (Gene- Clamp 500B; Axon Instruments, Sunnyvale, CA) at room temperature. Electrodes (0.2–0.5 MW) were filled with 3 M KCl, and oocytes were perfused with a physiological NaCl solution (100 mM NaCl, 2 mM KCl, 1 mM $CaCl_2$, 2 mM $MgCl_2$, and 10 mM HEPES, pH 7.2) and divalent cation free plus EGTA NaCl solution (110 mM NaCl, 2 mM KCl, 1 mM

EGTA, and 10 mM HEPES, pH 7.2). pH was adjusted at the indicated values using NaOH. The oocyte membrane was clamped at -30 mV and stepped from -160 to +100 mV. Benzamil was added to the solutions from a stock of 10 mM. A saturating concentration of benzamil (1mM) was added at the end of each experiment to confirm that endogenous/leak currents were similar in amplitude to non-injected oocytes within each oocyte batch. Oocytes that had larger endogenous/leak currents were not further analyzed. We used the pCLAMP suite of programs (Axon Instruments) for data acquisition and analysis. Currents were filtered at 200 Hz and sampled at 1 kHz. We used OriginPro 8 (OriginLab Corporation, Northampton, MA) to generate graphs, K_i, and for statistical analysis.

Electron microscopy

Young adult hermaphrodites of each strain were prepared for high-pressure freeze (HPF) fixation as described (Rostaing et al., 2004). 10–15 animals were loaded into a specimen chamber filled with *E. coli*. The specimens were frozen rapidly in a high-pressure freezer (Bal-Tec HPM010) at -180°C and high pressure. Freeze substitution was performed on frozen samples in a Reichert AFS machine (Leica, Oberkochen, Germany) with 0.1% tannic acid and 2% OsO_4 in anhydrous acetone. The temperature was kept at -90°C for 107 hr, increased at 5°C/hr to -20°C, and kept at -20°C for 14 hr. The temperature was then increased by 10°C/h to 20°C. Fixed specimens were embedded in Epon resin after infiltration in 50% Epon/acetone for 4 hr, 90% Epon/acetone for 18 hr, and 100% Epon for 5 hr. Embedded samples were incubated for 48 hr at 65°C. All specimens were prepared with the same fixation procedure and labeled with anonymous tags so that the examiner was blinded for genotype. Ultra-thin (40 nm) serial sections were cut using an

Ultracut 6 (Leica) and collected on formvar- covered, carbon-coated copper grids (EMS, FCF2010-Cu). Grids were counterstained in 2.5% aqueous uranyl acetate for 4 min, followed by Reynolds lead citrate for 2 min. Images were obtained on a Jeol JEM-1220 (Tokyo, Japan) transmission electron microscope operating at 80 kV. Micro-graphs were collected using a Gatan digital camera (Pleasanton, CA) at a magnification of 100k. Images were quantified using NIH ImageJ software. Dorsal and ventral cords were distinguished by size and morphology. GABAergic synapses were identified by previously established criteria, including position in the cord as well as the morphology of the synapse (White et al., 1986; Jin et al., 1999). GABAergic synapses are larger than their cholinergic motor neuron counterparts, and the active zones in these synapses form a direct, perpendicular angle with muscle arms. On the other hand, the presynaptic density in cholinergic synapses orient at an acute angle to the muscle, generally 30–45°, and are often dyadic. Some images were collected at 30k to aid in synaptic identification based on terminal position in the cord. Two colleagues with expertise in EM reconstruction of the *C. elegans* ventral nerve cord independently reviewed synapse images from each strain to verify identification. Each profile represents an image taken of a 40 nm section. A synapse was defined as a set of serial sections containing a presynaptic density and two flanking sections from both sides without presynaptic densities. Synaptic vesicles were identified as spherical, light gray structures with an average diameter of ~30 nm. At least two animals were analyzed for each genotype. Numbers of profiles analyzed for each genotype were: wild type = 502, *unc-8* = 322, *unc-55* = 246, *unc-55; unc-8* = 304 for ventral GABAergic synapse evaluation."

Miller-Fleming, T. W. *et al.* The DEG/ENaC cation channel protein UNC-8 drives activity-dependent synapse removal in remodeling GABAergic neurons. *Elife* **5,** 1–28 (2016).

E. Cited Literature

Baumgärtel, K., & Mansuy, I. M. (2012). Neural functions of calcineurin in synaptic plasticity and memory. Learning & Memory (Cold Spring Harbor, N.Y.), 19(9), 375–84. http://doi.org/10.1101/lm.027201.112

Bianchi, L., & Driscoll, M. (2002). Protons at the Gate: DEG/ENaC Ion Channels Help Us Feel and Remember. Neuron, 34(3), 337–340. http://doi.org/http://dx.doi.org/10.1016/S0896-6273(02)00687-6

Brenner, S. (1974). The genetics of Caenorhabditis elegans. Genetics, 77(1), 71–94. http://doi.org/10.1002/cbic.200300625

Catterall, W. A., & Few, A. P. (2008). Calcium Channel Regulation and Presynaptic Plasticity. Neuron, 59(6), 882–901. http://doi.org/10.1016/j.neuron.2008.09.005

Cho, J.-H., & Askwith, C. C. (2008). Presynaptic Release Probability Is Increased in Hippocampal Neurons From ASIC1 Knockout Mice. Journal of Neurophysiology, 99(2), 426–441. http://doi.org/10.1152/jn.00940.2007

Deidda, G., Allegra, M., Cerri, C., Naskar, S., Bony, G., Zunino, G., … Cancedda, L. (2014). Early depolarizing GABA controls critical-period plasticity in the rat visual cortex. Nature Neuroscience, 18(1), 87–96. http://doi.org/10.1038/nn.3890

Erturk, A., Wang, Y., & Sheng, M. (2014). Local Pruning of Dendrites and Spines by Caspase-3-Dependent and Proteasome-Limited Mechanisms. Journal of Neuroscience, 34(5), 1672–1688. http://doi.org/10.1523/JNEUROSCI.3121-13.2014

Etchberger, J. F., Lorch, A., Sleumer, M. C., Zapf, R., Jones, S. J., Marra, M. a, … Hobert, O. (2007). The molecular signature and cis -regulatory architecture of a C . elegans gustatory neuron. Genes & Development, 21, 1653–1674. http://doi.org/10.1101/gad.1560107.tatory

Flavell, S. W., & Greenberg, M. E. (2008). Signaling Mechanisms Linking Neuronal Activity to Gene Expression and Plasticity of the Nervous System. Annual Review of Neuroscience, 31(1), 563–590. http://doi.org/10.1146/annurev.neuro.31.060407.125631

Gally, C., & Bessereau, J.-L. (2003). GABA is dispensable for the formation of junctional GABA receptor clusters in Caenorhabditis elegans. The Journal of Neuroscience : The Official Journal of the Society for Neuroscience, 23(7), 2591–2599.

Gao, J., Duan, B., Wang, D. G., Deng, X. H., Zhang, G. Y., Xu, L., & Xu, T. Le. (2005). Coupling between NMDA receptor and acid-sensing ion channel contributes to ischemic neuronal death. Neuron, 48(4), 635–646. http://doi.org/10.1016/j.neuron.2005.10.011

Gengyo-Ando, K., & Mitani, S. (2000). Characterization of mutations induced by ethyl methanesulfonate, UV, and trimethylpsoralen in the nematode Caenorhabditis elegans. Biochemical and Biophysical Research Communications, 269(1), 64–69. http://doi.org/10.1006/bbrc.2000.2260

Giraldez, T., Domínguez, J., & Alvarez de la Rosa, D. (2013). ENaC in the brain--future perspectives and pharmacological implications. Current Molecular Pharmacology, 6(1), 44–9. Retrieved from http://www.ncbi.nlm.nih.gov/pubmed/23547934

Gracheva, E. O., Burdina, A. O., Holgado, A. M., Berthelot-Grosjean, M., Ackley, B. D., Hadwiger, G., … Richmond, J. E. (2006). Tomosyn inhibits synaptic vesicle priming in Caenorhabditis elegans. PLoS Biology, 4(8), e261. http://doi.org/10.1371/journal.pbio.0040261

Gracheva, E. O., Hadwiger, G., Nonet, M. L., & Richmond, J. E. (2008). Direct interactions between C. elegans RAB-3 and Rim provide a mechanism to target vesicles to the presynaptic density. Neuroscience Letters, 444(2), 137–142. http://doi.org/10.1016/j.neulet.2008.08.026

Hallam, S. J., & Jin, Y. (1998). lin-14 regulates the timing of synaptic remodeling in Caenorhabditis elegans. Nature, 395(6697), 78–82. http://doi.org/10.1038/25757

He, S., Philbrook, A., McWhirter, R., Gabel, C. V., Taub, D. G., Carter, M. H., … Miller, D. M. (2015). Transcriptional control of synaptic remodeling through regulated expression of an immunoglobulin superfamily protein. Current Biology, 25(19), 2541–2548. http://doi.org/10.1016/j.cub.2015.08.022

Hensch, T. K. (1998). Local GABA Circuit Control of Experience-Dependent Plasticity in Developing Visual Cortex. Science, 282(5393), 1504–1508. http://doi.org/10.1126/science.282.5393.1504

Howell, K., White, J. G., & Hobert, O. (2015). Spatiotemporal control of a novel synaptic organizer molecule. Nature, 523(7558), 83–87. http://doi.org/10.1038/nature14545

Jin, Y., Jorgensen, E., Hartwieg, E., & Horvitz, H. R. (1999). The Caenorhabditis elegans gene unc-25 encodes glutamic acid decarboxylase and is required for synaptic transmission but not synaptic development. The Journal of Neuroscience : The Official Journal of the Society for Neuroscience, 19(2), 539–548.

Kreple, C. J., Lu, Y., Taugher, R. J., Schwager-Gutman, A. L., Du, J., Stump, M., … Wemmie, J. A. (2014). Acid-sensing ion channels contribute to synaptic transmission and inhibit cocaine-evoked plasticity. Nature Neuroscience, 17(8), 1083–1091. http://doi.org/10.1038/nn.3750

Lee, H. K., Kameyama, K., Huganir, R. L., & Bear, M. F. (1998). NMDA induces long-term synaptic depression and dephosphorylation of the GluR1 subunit of AMPA receptors in hippocampus. Neuron, 21(5), 1151–1162. http://doi.org/10.1016/S0896-6273(00)80632-7

Li, Z., Jo, J., Jia, J. M., Lo, S. C., Whitcomb, D. J., Jiao, S., … Sheng, M. (2010). Caspase-3 activation via mitochondria is required for long-term depression and AMPA receptor internalization. Cell, 141(5), 859–871. http://doi.org/10.1016/j.cell.2010.03.053

Liu, Q., Hollopeter, G., & Jorgensen, E. M. (2009). Graded synaptic transmission at the Caenorhabditis elegans neuromuscular junction. Proceedings of the National Academy of Sciences of the United States of America, 106(26), 10823–10828. http://doi.org/10.1073/pnas.0903570106

Liu, Z., Kanzawa, N., & Ono, S. (2011). Calcium-sensitive activity and conformation of Caenorhabditis elegans gelsolin-like protein 1 are altered by mutations in the first gelsolin-like domain. Journal of Biological Chemistry, 286(39), 34051–34059. http://doi.org/10.1074/jbc.M111.237404

Mathews, E. A., Garcia, E., Santi, C. M., Mullen, G. P., Thacker, C., Moerman, D. G., & Snutch, T. P. (2003). Critical residues of the Caenorhabditis elegans unc-2 voltage-gated calcium channel that affect behavioral and physiological properties. J Neurosci, 23(16), 6537–6545. Retrieved from http://www.ncbi.nlm.nih.gov/pubmed/12878695

McEwen, J. M., Madison, J. M., Dybbs, M., & Kaplan, J. M. (2006). Antagonistic Regulation of Synaptic Vesicle Priming by Tomosyn and UNC-13. Neuron, 51(3), 303–315. http://doi.org/10.1016/j.neuron.2006.06.025

Meng, L., Mulcahy, B., Cook, S. J., Neubauer, M., Wan, A., Jin, Y., & Yan, D. (2015). The Cell Death Pathway Regulates Synapse Elimination through Cleavage of Gelsolin in Caenorhabditis elegans Neurons. Cell Reports, 11(11), 1737–1748. http://doi.org/10.1016/j.celrep.2015.05.031

Müller, M., & Davis, G. W. (2012). Transsynaptic control of presynaptic Ca 2+ influx achieves homeostatic potentiation of neurotransmitter release. Current Biology, 22(12), 1102–1108. http://doi.org/10.1016/j.cub.2012.04.018

Park, M., Watanabe, S., Poon, V. Y. N., Ou, C. Y., Jorgensen, E. M., & Shen, K. (2011). CYY-1/Cyclin Y and CDK-5 Differentially Regulate Synapse Elimination and Formation for Rewiring Neural Circuits. Neuron, 70(4), 742–757. http://doi.org/10.1016/j.neuron.2011.04.002

Petersen, S. C., Watson, J. D., Richmond, J. E., Sarov, M., Walthall, W. W., & Miller, D. M. (2011). A Transcriptional Program Promotes Remodeling of GABAergic Synapses in Caenorhabditis elegans. The Journal of Neuroscience , 31(43), 15362–15375. http://doi.org/10.1523/JNEUROSCI.3181-11.2011

Pinan-Lucarre, B., Gabel, C. V., Reina, C. P., Hulme, S. E., Shevkoplyas, S. S., Slone, R. D., … Driscoll, M. (2012). The core apoptotic executioner proteins CED-3 and CED-4 promote initiation of neuronal regeneration in Caenorhabditis elegans. PLoS Biology, 10(5). http://doi.org/10.1371/journal.pbio.1001331

Praitis, V., Casey, E., Collar, D., & Austin, J. (2001). Creation of low-copy integrated transgenic lines in Caenorhabditis elegans. Genetics, 157(3), 1217–1226.

Richmond, J. E., & Jorgensen, E. M. (1999). One GABA and two acetylcholine receptors function at the. America, 791–798.

Rostaing, P., Weimer, R. M., Jorgensen, E. M., Triller, A., & Bessereau, J.-L. (2004). Preservation of Immunoreactivity and Fine Structure of Adult C. elegans Tissues Using High-pressure Freezing. Journal of Histochemistry & Cytochemistry, 52(1), 1–12. http://doi.org/10.1177/002215540405200101

Saheki, Y., & Bargmann, C. I. (2009). Presynaptic CaV2 calcium channel traffic requires CALF-1 and the α2δ subunit UNC-36. Nature Neuroscience, 12(10), 1257–1265. http://doi.org/10.1038/nn.2383

Sanderson, J. L., Gorski, J. a., Gibson, E. S., Lam, P., Freund, R. K., Chick, W. S., & Dell'Acqua, M. L. (2012). AKAP150-Anchored Calcineurin Regulates Synaptic Plasticity by Limiting Synaptic Incorporation of Ca2+-Permeable AMPA Receptors. Journal of Neuroscience, 32(43), 15036–15052. http://doi.org/10.1523/JNEUROSCI.3326-12.2012

Schuske, K., Beg, A. A., & Jorgensen, E. M. (2004). The GABA nervous system in C. elegans. Trends in Neurosciences, 27(7), 407–414. http://doi.org/10.1016/j.tins.2004.05.005

Shan, G., Kim, K., Li, C., & Walthall, W. W. (2005). Convergent genetic programs regulate similarities and differences between related motor neuron classes in Caenorhabditis elegans. Developmental Biology, 280(2), 494–503. http://doi.org/http://dx.doi.org/10.1016/j.ydbio.2005.01.032

Smith, C. J., Watson, J. D., Spencer, W. C., Oapos; Brien, T., Cha, B., Albeg, A., … Miller, D. M. (2010). Time-lapse imaging and cell-specific expression profiling reveal dynamic branching and molecular determinants of a multi-dendritic nociceptor in C. elegans. Developmental Biology, 345(1), 18–33. http://doi.org/10.1016/j.ydbio.2010.05.502

Thompson-Peer, K. L., Bai, J., Hu, Z., & Kaplan, J. (2012). HBL-1 patterns synaptic remodeling in C. elegans. Neuron, 73(3), 453–465. http://doi.org/10.1016/j.neuron.2011.11.025

Tursun, B., Cochella, L., Carrera, I., & Hobert, O. (2009). A toolkit and robust pipeline for the generation of fosmid-based reporter genes in C. elegans. PLoS ONE, 4(3). http://doi.org/10.1371/journal.pone.0004625

Voglis, G., & Tavernarakis, N. (2008). A synaptic DEG/ENaC ion channel mediates learning in C. elegans by facilitating dopamine signaling. The EMBO Journal, 27(24), 3288–3299. http://doi.org/10.1038/emboj.2008.252

Waldmann, R., Champigny, G., Bassilana, F., Voilley, N., & Lazdunski, M. (1995). Molecular Cloning and Functional Expression of a Novel Amiloride-sensitive Na + Channel. Journal of Biological Chemistry, 270(46), 27411–27414. http://doi.org/10.1074/jbc.270.46.27411

Walthall, W. W., & Plunkett, J. A. (1995). Genetic transformation of the synaptic pattern of a motoneuron class in Caenorhabditis elegans. The Journal of Neuroscience : The Official Journal of the Society for Neuroscience, 15(2), 1035–1043.

Wang, H., & Sieburth, D. (2013). PKA controls calcium influx into motor neurons during a rhythmic behavior. PLoS Genetics, 9(9), e1003831. http://doi.org/10.1371/journal.pgen.1003831

Wang, J. Y., Chen, F., Fu, X. Q., Ding, C. S., Zhou, L., Zhang, X. H., & Luo, Z. G. (2014). Caspase-3 cleavage of dishevelled induces elimination of postsynaptic structures. Developmental Cell, 28(6), 670–684. http://doi.org/10.1016/j.devcel.2014.02.009

Wemmie, J. A., Askwith, C. C., Lamani, E., Cassell, M. D., Freeman, J. H., & Welsh, M. J. (2003). Acid-sensing ion channel 1 is localized in brain regions with high synaptic density and contributes to fear conditioning. The Journal of Neuroscience : The Official Journal of the Society for Neuroscience, 23(13), 5496–5502. http://doi.org/23/13/5496 [pii]

Wemmie, J. A., Coryell, M. W., Askwith, C. C., Lamani, E., Leonard, A. S., Sigmund, C. D., & Welsh, M. J. (2004). Overexpression of acid-sensing ion channel 1a in transgenic mice increases acquired fear-related behavior. Proceedings of the National Academy of Sciences of the United States of America, 101(10), 3621–6. http://doi.org/10.1073/pnas.0308753101

Wemmie, J. A., Chen, J., Askwith, C. C., Hruska-Hageman, A. M., Price, M. P., Nolan, B. C., … Welsh, M. J. (2002). The acid-activated ion channel ASIC contributes to synaptic plasticity, learning, and memory. Neuron, 34(3), 463–477. http://doi.org/10.1016/S0896-6273(02)00661-X

Wemmie, J. A., Price, M. P., & Welsh, M. J. (2006). Acid-sensing ion channels: advances, questions and therapeutic opportunities. Trends in Neurosciences, 29(10), 578–586. http://doi.org/10.1016/j.tins.2006.06.014

Wemmie, J. A., Taugher, R. J., & Kreple, C. J. (2013). Acid-sensing ion channels in pain and disease. Nature Reviews Neuroscience, 14(7), 461–471. http://doi.org/10.1038/nrn3529

White, J.G., Southgate, E., Thomson, J.N., Brenner, S. (1986). The Structure of the Nervous System of the Nematode Caenorhabditis elegans. Philosophical Transactions of the Royal Society of London. Series B, Biological Sciences, 314(1165), 1–340.

Winder, D. G., Mansuy, I. M., Osman, M., Moallem, T. M., & Kandel, E. R. (1998). Genetic and Pharmacological Evidence for a Novel , Intermediate Phase of Long-Term Potentiation Suppressed by Calcineurin, 92, 25–37.

Yamamura, H., Ugawa, S., Ueda, T., Nagao, M., & Shimada, S. (2004). Protons Activate the ??-Subunit of the Epithelial Na+ Channel in Humans. Journal of Biological Chemistry, 279(13), 12529–12534. http://doi.org/10.1074/jbc.M400274200

Younger, M. A., Müller, M., Tong, A., Pym, E. C., & Davis, G. W. (2013). A presynaptic ENaC channel drives homeostatic plasticity. Neuron, 79(6), 1183–1196. http://doi.org/10.1016/j.neuron.2013.06.048

Zha, X. (2013). Acid-sensing ion channels: trafficking and synaptic function. Molecular Brain, 6(1), 1. http://doi.org/10.1186/1756-6606-6-1

Zha, X., Wemmie, J. A., Green, S. H., & Welsh, M. J. (2006). Acid-sensing ion channel 1a is a postsynaptic proton receptor that affects the density of dendritic spines. Proceedings of the National Academy of Sciences of the United States of America, 103(44), 16556–16561. http://doi.org/10.1073/pnas.0608018103

Zhou, H. M., & Walthall, W. W. (1998). UNC-55, an Orphan Nuclear Hormone Receptor, Orchestrates Synaptic Specificity among Two Classes of Motor Neurons in Caenorhabditis elegans . The Journal of Neuroscience , 18(24), 10438–10444. Retrieved from http://www.jneurosci.org/content/18/24/10438.abstract

Ziemann, A. E., Allen, J. E., Dahdaleh, N. S., Drebot, I. I., Coryell, M. W., Wunsch, A. M., … Wemmie, J. A. (2009). The Amygdala Is a Chemosensor that Detects Carbon Dioxide and Acidosis to Elicit Fear Behavior. Cell, 139(5), 1012–1021. http://doi.org/10.1016/j.cell.2009.10.02

V. APPENDIX A

A transcriptionally regulated pathway selectively removes active zone proteins from remodeling GABAergic synapses.

Laura Manning[1], Tyne W Miller-Fleming[2], Janet Richmond[1], David M Miller III[2,3]

[1]Department of Biological Sciences, University of Illinois at Chicago, Chicago, United States;
[2]Neuroscience Program, Vanderbilt University, Nashville, United States;
[3]Department of Cell and Developmental Biology, Vanderbilt University, Nashville, United States;

Summary

Compared to the vast body of work devoted to synaptic development and assembly, less is known about the mechanisms that regulate synapse elimination. In *C. elegans,* a developmental remodeling program drives the activity-dependent removal of DD motor neurons from the ventral cord, recycling their existing synaptic components, and using them to build nascent synapses in the dorsal cord (Shan et al., 2005; Ou et al., 2010; Petersen et al., 2011; Miller-Fleming et al., 2016; Chapter 4). The transcription factor, *unc*-55, is a genetic suppressor of the remodeling program in VD neurons, which is partially mediated by the DEG/ENaC ion channel protein UNC-8. In an *unc-55* mutant, VD neurons undergo ectopic remodeling, and combined with the normal remodeling of DD neurons, all ventral GABAergic motor neuron synapses are eliminated (Figure 1A, Appendix A). We previously uncovered a role for the DEG/ENaC ion channel protein UNC-8 in driving activity-dependent synapse removal (Miller-Fleming et al., 2016, Chapter 4). UNC-8 is normally expressed in DD neurons, but in VD neurons, its expression is inhibited by *unc-55*. In an *unc-55;unc-8* double mutant, some ectopically remodeled VD synapses are restored to the ventral cord. Thus, we propose a model in which

unc-8 drives synaptic elimination in DD neurons, as well as *unc-55;unc-8* VD neurons (Miller-Fleming et al., 2016, Chapter 4) (Figure 1A, Appendix A). Briefly, active synapses experience elevated intracellular calcium levels that promote Calcineurin phosphorylation of UNC-8, thus activating sodium influx through UNC-8 channels that contributes to a positive feedback loop with UNC-2, TAX-6, and UNC-8. The resulting increase in intracellular Ca^{2+} can trigger activation of the canonical apoptotic pathway and dismantle the synapse (Miller-Fleming et al., 2016, Chapter 4, Meng et al., 2015).

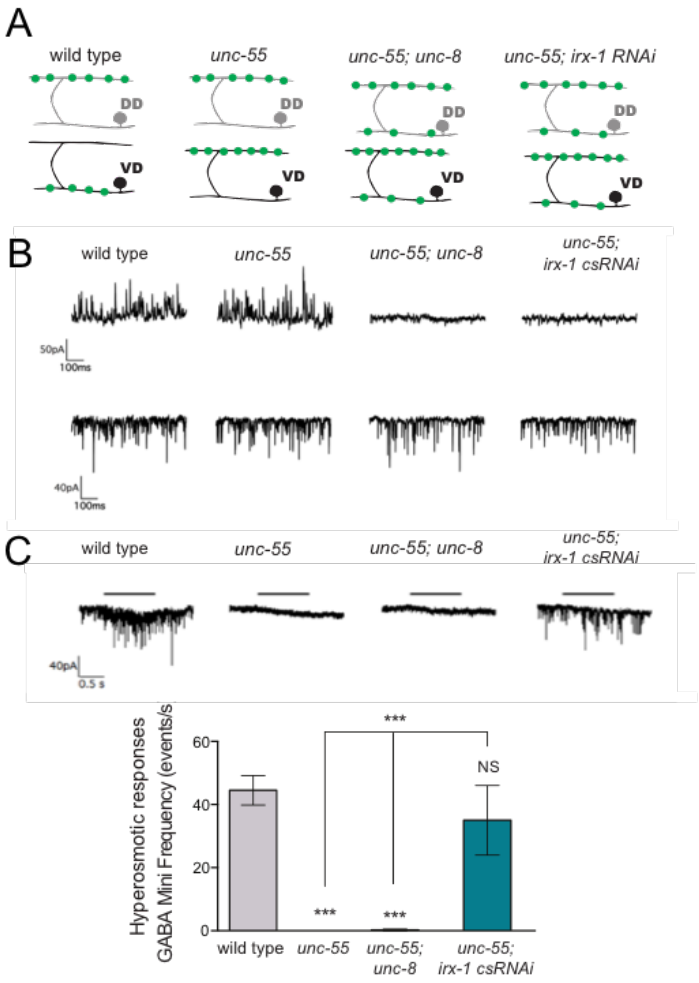

Appendix A, Figure 1. UNC-8 and IRX-1 have different effects on synaptic function in remodeling GABAergic neurons. A. Schematic of GABAergic motor neuron wiring in adult worms. DD neurons are pictured in the top row in gray. VD neurons are depicted in the bottom row in black. The ventral nerve cord contains the cell bodies of each class of neurons (black circles). Synapses are indicated by small green circles. In wild type animals, VD neurons form synapses in the ventral cord, while DD neurons synapse in the dorsal cord. In *unc-55* mutants, VD and DD synapses remodel to the dorsal cord. In both *unc-55;unc-8* and *unc-55;irx-1csRNAi* double mutants both DD and VD neurons retain synapses in the dorsal cord. B. Representative traces of ventral mini-iPSCs from each genotype (top row) and combined cholinergic and GABAergic mini PSCs (bottom row). C. Representative traces of ventral synapse response to application of hyperosmotic solution for each genotype in the presence of the cholinergic receptor blocker dTubocurare to isolate GABA minis. The high frequency response of wild type and *unc-55;irx-1 csRNAi* animals is not observed in *unc-55* or *unc-55;unc-8* mutants. Data collected by Janet Richmond.

In our recently published paper, summarized in Chapter 4 of this thesis, we demonstrated that UNC-8 promotes only partial removal of synapses during remodeling, and this finding is supported by studies that identify additional mechanisms and putative regulators of remodeling (see Chapter 4 Discussion). While some synapses could be observed at the light and EM level in the ventral cord of both *unc-8* and *unc-55;unc-8* mutants, electrophysiological recordings revealed that residual GABAergic *unc-55;unc-8* synapses were functionally defective, with spontaneous release virtually abolished (Figure 1B, Appendix A; Miller-Fleming et al., 2016; Chapter 4). Total mini release, measured as total cholinergic and GABAergic ventral responses, was relatively normal, indicating that this defect was specific to the residual ventral GABAergic synapses.

To understand the functional defect of *unc-55;unc-8*, we compared it to another established regulator of remodeling: Iroquouis family homeodomain transcription factor IRX-1 (Mukherjee and Burglin, 2007). Like UNC-8, IRX-1 promotes ventral DD synapse removal, in addition to helping build nascent dorsal synapses (Petersen et al., 2011). Because mutations for *irx-1* cause embryonic and early larval lethality, we used cell specific RNAi to induce *irx-1* knockdown in GABAergic neurons of adults*. unc-55;irx-1csRNAi* double mutant animals also exhibit a "rescue" of ventral GABAergic synapses that would otherwise remodel, as seen at the light and EM level (Figure 1A, Appendix A; see below**;** Petersen et al., 2011). While the residual

ventral synapses in *unc-55;unc-8* exhibit almost no spontaneous release, those in *unc-55;irx-1csRNAi* mutants show normal release frequency (Miller-Fleming et al., 2016; Chapter 4; Petersen et al., 2011) (Figure 1B, Appendix A). These results suggest that *unc-8* and *irx-1* regulate different aspects of synaptic disassembly during remodeling.

One possible explanation for the loss of spontaneous release in *unc-55;unc-8* animals is that their "rescued" ventral synapses do not possess the necessary release components to elicit detectable muscle responses. Another possibility is that while remaining ventral synapses are functional, there are not enough synapses present to produce normal release. We applied hyperosmotic saline to each set of mutant worms, which should elicit release of the primed pool of SVs (Kaeser and Regehr, 2014). While wild type and *unc-55;irx-1 csRNAi* animals both produced substantial responses to this stimulus, both *unc-55* and *unc-55;unc-8* double mutants showed virtually no response, suggesting that residual *unc-55;unc-8* synapses are in fact priming-defective (Figure 1C, Appendix A).

Before comparing the roles of *unc*-8 and *irx-1* in synapse removal during remodeling, we first needed to establish that they operate in parallel pathways. We counted ventral punc-25:SNB-1::GFP in *unc-55*;*unc-8* and *unc-55;irx-1csRNAi* double mutants, and compared that number to *unc-55;unc-8;irx-1csRNAi* triple mutants. Both double mutants partially rescued ventral puncta to the *unc-55* mutant background, although *irx-1* RNAi exerted a stronger rescue effect than *unc-8* (Figure 2A, B, Appendix A). Importantly, the triple mutant showed additive rescue of ventral puncta, indicating that each protein contributes to different functions in

synapse removal. We also examined the transcriptional UNC-8 reporter, punc-8::GFP in an *irx-1 csRNAi* mutant background and found that loss of *irx-1* did not affect levels of punc-8::GFP fluorescence (Figure 2C, D, Appendix A). Based on these results, we conclude that *unc-55* suppresses both *unc-8* and *irx-1*, which operate in parallel but distinct pathways that promote remodeling (Figure 2E, Appendix A).

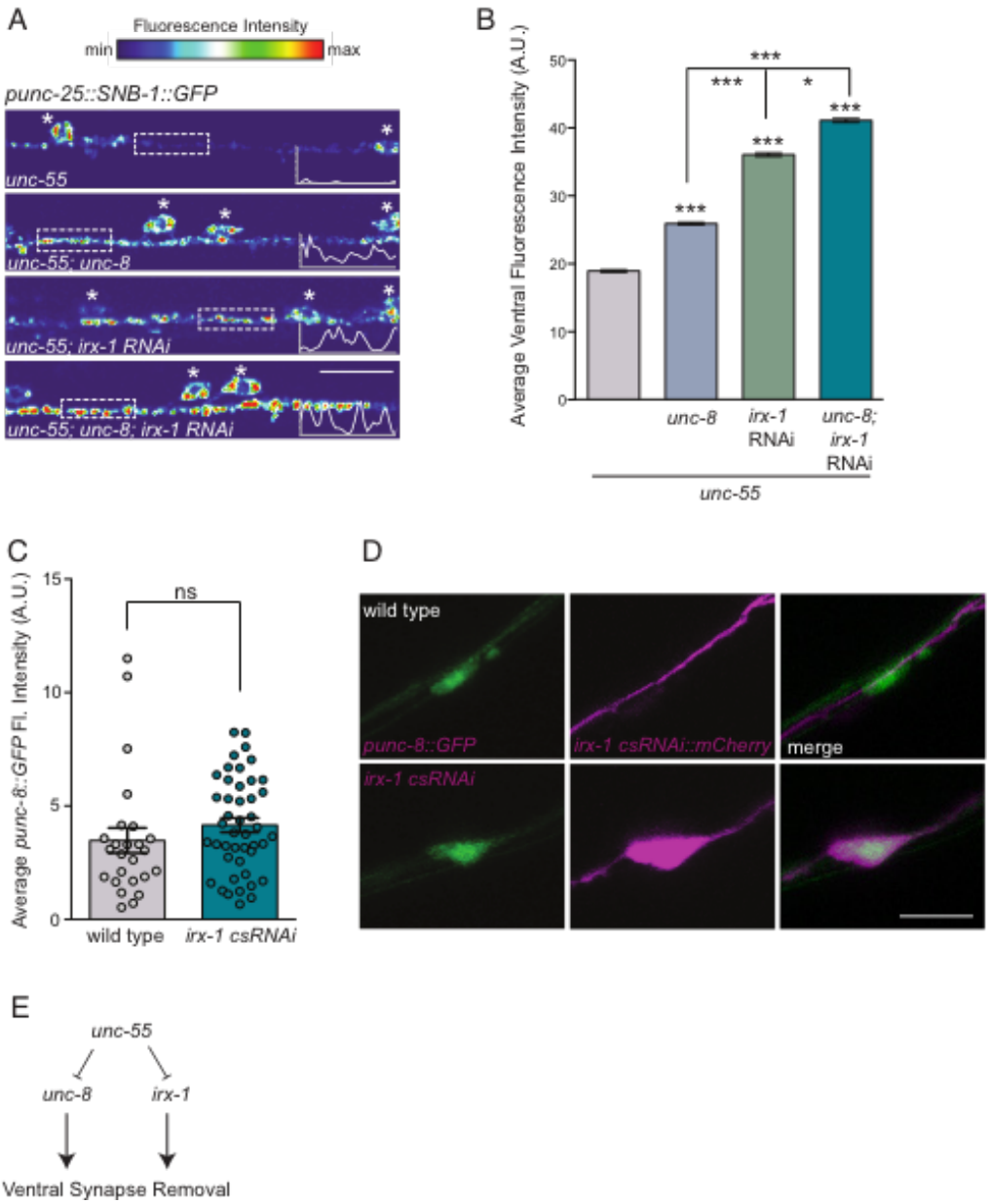

Appendix A, Figure 1. IRX-1 and UNC-8 drive synapse removal in distinct genetic pathways. A. Representative images and fluorescence intensity plots (generated from 20 mm dashed region) of SNB-1::GFP-marked ventral GABA neuron synapses in *unc-55*, *unc-55;unc-8*, *unc-55;irx-1 csRNAi*, and *unc-55;unc-8;irx-1 csRNAi* mutant animals. Scale bar is 10 mm. **B.** *unc-55;unc-8* and *unc-55;irx-1 csRNAi* have additive effects on the removal of ventral GABA synapses. Ventral GABA neuron synapses were quantified by measure SNB-1::GFP fluorescence intensity (*p<0.5, ***p<0.001). **C.** *irx-1 csRNAi* does not affect expression of punc-8::GFP reporter gene. Average punc-8::GFP intensity was quantified from images in (D). **D.** Representative images of punc-8::GFP reporter and *irx-1 csRNAi* reporter in wild type (top row) and *irx-1 csRNAi* mutants (bottom row). **E.** UNC-55 suppresses *unc-8* and *irx-1*, which function in parallel pathways to promote ventral synapse removal during remodeling. Data collected by Miller lab.

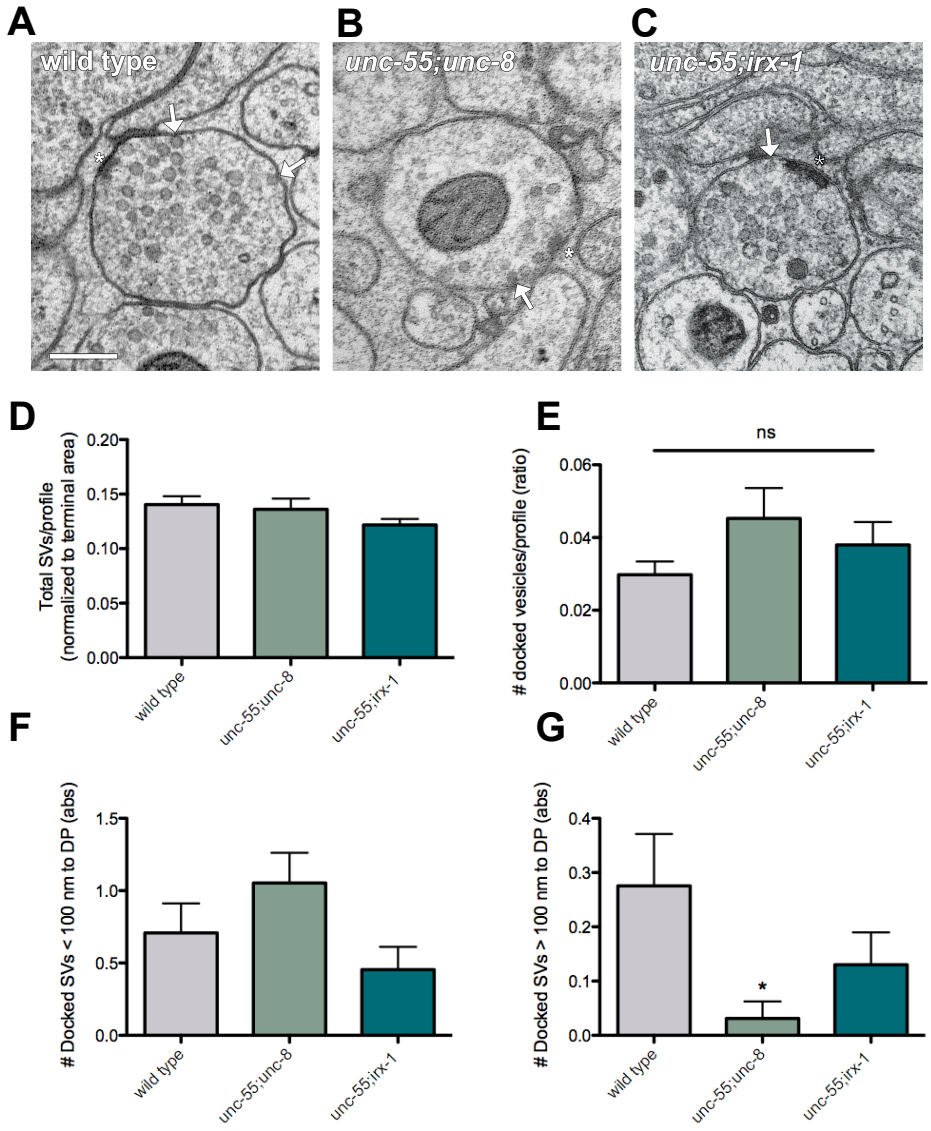

Appendix A, Figure 2. A-C. Electron micrographs of GABA synapses with ventral muscles in (A) wild type (B) *unc-55;unc-8*, and (C) *unc-55;irx-1 csRNAi* animals. Asterisks point to presynaptic densities, Arrows to docked SVs, scale bars are 200 nm. **D/E.** Total synaptic vesicles (D) and docked synaptic vesicles (E) were quantified in ventral GABAergic synapses. Synapses in wild-type, *unc-55;unc-8*, and *unc-55;irx-1 csRNAi* animals contain comparable numbers of synaptic vesicles. **E.** Docked synaptic vesicles were quantified in ventral GABAergic synapses. Synapses in wild-type, *unc-55;unc-8*, and *unc-55;irx-1 csRNAi* animals contain comparable numbers of synaptic vesicles. **F/G.** Distances between each docked synaptic vesicle and the presynaptic density were measured. The number of docked vesicles within 100 nm of the DP (F) were

slightly, though not significantly, reduced in *unc-55;irx-1* mutants. *unc-55;unc-8* animals showed slightly, though not significantly higher docking in this area than wild type. G. Docked vesicles further than 100 nm from the DP were slightly reduced in *unc-55;unc-8* animals. Data collected by Laura Manning.

Why do *unc-8* and *irx*-1 have different effects on synaptic function in remodeling neurons? To address this question, we performed HPF/FS EM analysis of ventral GABAergic neurons in *unc-55;unc-8* and *unc-55;irx-1csRNAi* mutants. We observed no significant changes in total number of docked or undocked SVs in *unc-55;unc-8* or *unc-55;irx-1csRNAi* mutant synapses compared to wild type (Figure 3-E, Appendix A) This was surprising because our electrophysiological data suggests priming should be eliminated in these synapses (Figure 1B, C, Appendix A, Miller-Fleming et al., 2016; Chapter 4 Results). Further examination indicated a shift in docked SV distribution relative to the AZ. Specifically, within 100 nm of the DP, *unc-55;unc*-8 mutants have slightly, though not significantly, more docked SVs than wild-type. *unc-55;irx-1* csRNAi mutant synapses show slightly, though not significantly reduced docked SVs compared to wild-type (Figure 3F, Appendix A). At a distance of greater than 100 nm, *unc-55;unc*-8 mutant synapses show slightly less docking than wild-type. *unc-55;irx-1csRNAi* mutants dock SVs at an intermediate level between wild type and *unc-55;unc-8* (Figure 3G, Appendix A) This 100 nm length of membrane near the DP represents a location where SVs can be docked and primed for release by the interaction of UNC-13, UNC-10, and RAB-3 (Gracheva et al., 2008). Importantly, UNC-10 and RAB-3 can still dock SVs in the absence of UNC-13, but UNC-13 is required for SV priming and release (Weimer et al., 2006; Gracheva et al., 2008). The current data are drawn from a small number of synapses and worms (N2: 3 worms, 6 synapses, 43 profiles; *unc-55;unc-8* 2 worms, 5 synapses, 37 profiles; *unc-55;irx-1csRNAi* 2 worms, 7 synapses, 59 profiles). Ongoing

analysis is required to expand this data set and provide an accurate characterization of these ultrastructural phenotypes.

Based on this ultrastructural and functional data, we predicted that ventral GABAergic synapses in *unc-55;unc-8* mutants would contain normal levels of AZ proteins required for docking, including UNC-10 as well as its vesicle docking partner RAB-3, but loss of the priming factor UNC-13. Furthermore, ventral GABAergic synapses in *unc-55;irx-1csRNAi* animals should contain all of these proteins. Previously, we measured ventral puncta in *unc-55;unc-8* using markers for SNB-1, RAB-3, UNC-57, and SYD-2 expressed in GABAergic neurons under the *unc-25* promoter. With each of these markers, we observed a pattern in which *unc-55* mutants displayed a severe reduction in ventral puncta number, and *unc-55;unc-8* double mutants partially restored them, though not to wild-type levels (Miller-Fleming et al., 2016, Chapter 4). Re-analysis of GABA-expressed mCherry::RAB-3 confirmed the partial restoration of ventral puncta in *unc-55;unc-8* mutants, while *unc-55;irx-1csRNAi* restored ventral puncta to almost wild-type levels (Figure 4A, Appendix A). We were surprised to find the intensity of GABAergic UNC-10::GFP fluorescence was nearly equal in the ventral cord of both wild-type and *unc-55* animals (Figure 4B, Appendix A). This was the only AZ marker we imaged that did not disassemble in *unc-55* mutant ventral synapses. Interestingly, no ventral GABAergic synapses were identified at the EM level in *unc-55* mutants (Miller-Fleming et al., 2016, Chapter 4). *unc-55;unc-8* and *unc-55;irx-1csRNAi* mutants did exhibit a reduction in UNC-10::GFP fluorescence in the ventral cord. These findings are currently difficult to interpret, but suggest that UNC-8 and IRX-1 activity may influence the localization of UNC-10 in GABAergic motor neurons.

We next examined a marker for the long isoform of UNC-13, which localizes near the DP and is important for priming and synchronous release (Hu et al., 2013). As we predicted, ventral UNC-13L::GFP puncta were nearly eliminated from ventral synapses in *unc-55;unc*-8 animals (Figure 4C, D, Appendix A). In fact, while *unc*-55 mutants showed the expected reduction in UNC-13L::GFP puncta, *unc-55;unc*-8 mutant ventral puncta count was even further reduced than in an *unc-55* single mutant alone. *unc-55;irx-1csRNAi* animals did show partial restoration of ventral puncta, though to a level lower than wild-type. These data support the hypothesis that residual ventral synapses in *unc-55;unc-8* animals are priming defective because they fail to retain UNC-13L, while those in *unc-55;irx-1csRNAi* animals do.

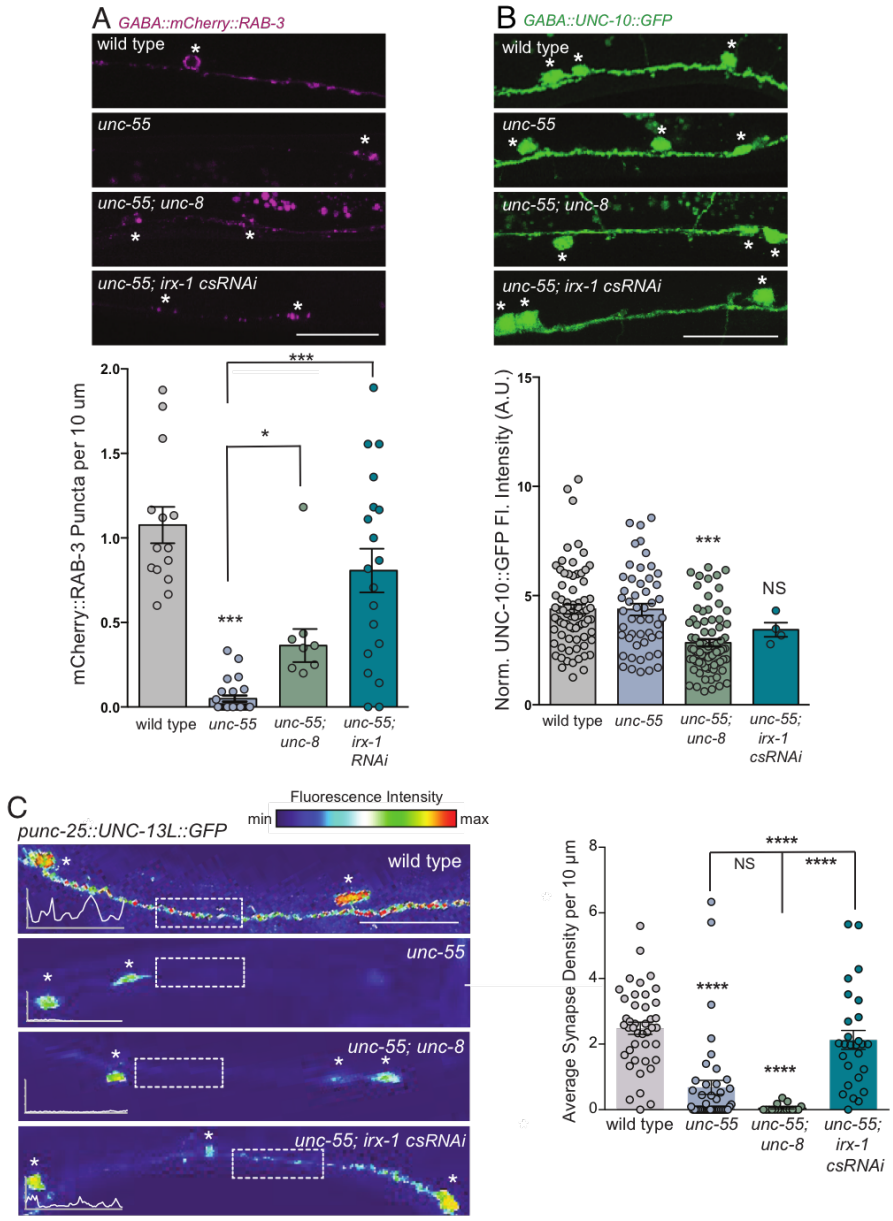

Appendix A, Figure 3. Differential retention of RAB-3, UNC-10, and UNC-13 in ventral GABAergic synapses of *unc-55;unc-8* and *unc-55;irx-1 csRNAi* mutant backgrounds. Fluorescent puncta for presynaptic proteins (mCherry::RAB-3 and UNC-13L::GFP) were counted in the ventral nerve cord from VD3 to VD11. Fluorescence intensity was measured for UNC-10::GFP. **A.** Representative images (top) and quantification (bottom) indicate that UNC-8 and IRX-1 promote ventral removal of RAB-3 in remodeling neurons. **B.** Representative images (top) and quantification (bottom) indicate that UNC-8 promote ventral removal of UNC-55 in remodeling neurons. **C.** Representative images (left) and quantification (right) indicate that UNC-8 promotes ventral removal of UNC-13L in remodeling neurons. Data collected by Miller Lab.

We observed a similar pattern of ELKS-1::tdTomato punctal expression in our double mutants (Figure 5A, B, Appendix A). *unc-55* single mutants showed a dramatic reduction of ventral puncta, reflecting synapse loss from the cord. In the *unc-55;unc*-8 double mutant, ventral ELKS-1::GFP puncta were even further reduced and practically eliminated from the cord. *unc-55;irx-1csRNAi* animals restored some ventral ELKS-1::tdTomato puncta, but not to wild-type levels. These results indicate that ELKS-1 localization in remodeling GABAergic neurons is dependent on UNC-8, and to some extent IRX-1. Because *unc-55;irx-1csRNAi* mutants showed partial and full restoration of other synaptic markers, we interpret the rescue of ELKS-1::GFP signal as a restoration of overall number of ventral synapses.

Finally, SYD-2::GFP puncta were restored to wild-type levels in both *unc-55;unc-8* and *unc-55;irx-1csRNAi* mutants (Figure 5C, D, Appendix A). These data suggest that while residual synapses in *unc-55;unc-8* likely contain important AZ scaffolding and SVs, fewer synapses remain in the ventral cord. In *unc-55;irx-1csRNAi* double mutants, however, ventral synapse numbers are restored closer to wild-type levels.

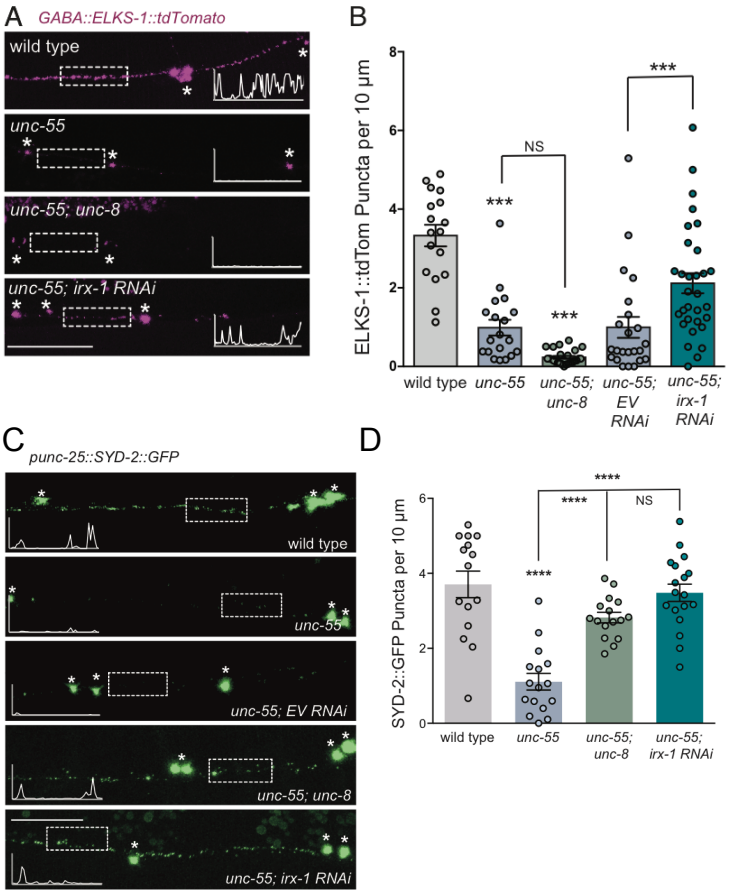

Appendix A, Figure 4. Differential retention of ELKS-1 and SYD-2 in ventral GABAergic synapses of *unc-55;unc-8* and *unc-55;irx-1 csRNAi* mutant backgrounds. Fluorescent puncta for presynaptic proteins (ELKS-1::dtTomato and SYD-2::GFP) were counted in the ventral nerve cord from VD3 to VD11. **A/B.** Representative images (A) and quantification (B) of ventral ELKS-1::tdTomato puncta. **C/D.** Representative images (A) and quantification (B) of ventral SYD-2::GFP puncta. Data collected from Miller lab.

Together these fluorescent imaging results support our electrophysiological and ultrastructural findings. Since UNC-13 is absolutely required for priming (Richmond and Jorgensen, 1999), the priming defects in *unc-55;unc-8* ventral synapses presumably reflect its absence, while *unc-55;irx-1csRNAi* synapses that contained some UNC-13L partially restored priming based on the partial rescue of responses to hyperosmotic saline. UNC-13 is also thought

to form a tripartite complex with UNC-10 and RAB-3 near the DP, but in *unc-13* mutants, docking is still observed in this area (Gracheva et al., 2008; Dulubova et al., 2005; Hu et al., 2013). We therefore suggest that in *unc-55;unc*-8 mutants, RAB-3 and UNC-10 are present at ventral synapses at a level that can mediate docking in the absence of UNC-13L (Weimer et al., 2006, Gracheva et al., 2008) (Figure 6, Appendix A). Without the ability to prime vesicles, spontaneous release is severely impaired in these mutants, as opposed to *unc-55;irx-1csRNAi* synapses where release is partially restored. Although ventral ELKS-1::GFP puncta were also drastically reduced in *unc-55;unc-8* animals, loss of *elks-1* has been shown to have almost no effect on synapse ultrastructure or release properties (Kittelmann et al., 2013). Additional EM data will be collected to bolster these results and examine other ultrastructural features including DP size.

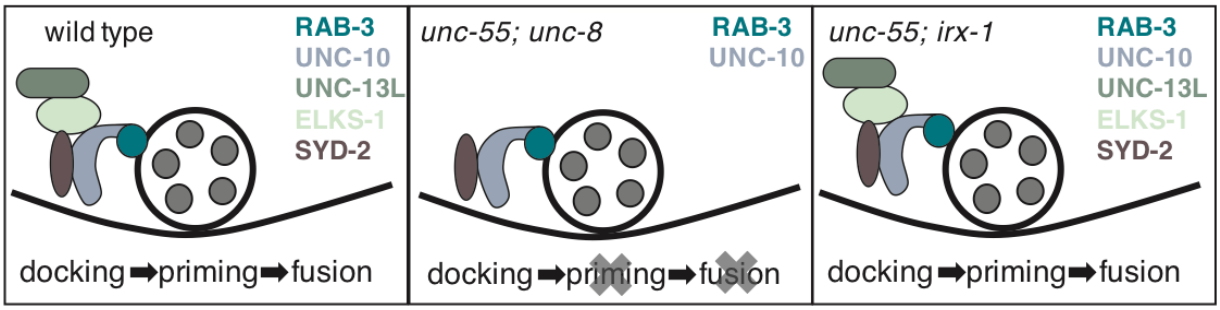

Appendix A, Figure 5. Model of molecular basis of release defects in *unc-55;unc-8* and *unc-55;irx-1* mutant ventral GABAergic synapses. In wild type animals, ventral synapses contain RAB-3, UNC-10, UNC-13L, ELKS-1, and SYD-2 that all promote SV localization to the active zone, docking, priming, and fusion. In *unc-55;unc-8* synapses, many of these proteins are absent, but RAB-3 and UNC-10 are present at sufficient levels to dock vesicles. In the absence of UNC-13, these SVs cannot be primed or released. In *unc-55;irx-1* mutants, active zone proteins are present at levels sufficient to mediate release.

A wide variety of proteins contribute to the structure and function of synapses, and their relationship to UNC-8 and IRX-1 activity is largely unknown. The results presented here indicate

that UNC-8 and IRX-1 may exert differential effects on the dismantling and transport of different AZ proteins. Importantly, synaptic localization of UNC-10, ELKS-1, and UNC-13L in remodeling GABAergic synapses all appear to absolutely require UNC-8, while RAB-3, UNC-10, and SYD-2 depend on UNC-8 to a lesser extent. IRX-1 is also required to localize some of these proteins, but to a lesser extent than UNC-8. Because IRX-1 is a transcriptional regulator, it may influence many downstream targets, potentially including these AZ proteins. Thus, it is likely that additional active zone proteins that have not yet been examined are involved in synapse removal during remodeling.

CITED LITERATURE

Dulubova, I., Lou, X., Lu, J., Huryeva, I., Alam, A., Schneggenburger, R., … Rizo, J. (2005). A Munc13/RIM/Rab3 tripartite complex: from priming to plasticity. The EMBO Journal, 24(16), 2839–2850. http://doi.org/10.1038/sj.emboj.7600753

Gracheva, E. O., Burdina, A. O., Holgado, A. M., Berthelot-Grosjean, M., Ackley, B. D., Hadwiger, G., … Richmond, J. E. (2006). Tomosyn inhibits synaptic vesicle priming in Caenorhabditis elegans. PLoS Biology, 4(8), e261. http://doi.org/10.1371/journal.pbio.0040261

Gracheva, E. O., Hadwiger, G., Nonet, M. L., & Richmond, J. E. (2008). Direct interactions between C. elegans RAB-3 and Rim provide a mechanism to target vesicles to the presynaptic density. Neuroscience Letters, 444(2), 137–142. http://doi.org/10.1016/j.neulet.2008.08.026

Hu, Z., Tong, X.-J., & Kaplan, J. M. (2013). UNC-13L, UNC-13S, and Tomosyn form a protein code for fast and slow neurotransmitter release in Caenorhabditis elegans. eLife, 2, e00967. http://doi.org/10.7554/eLife.00967

Kittelmann, M., Hegermann, J., Goncharov, A., Taru, H., Ellisman, M. H., Richmond, J. E., … Eimer, S. (2013). Liprin-α/SYD-2 determines the size of dense projections in presynaptic active zones in C. elegans. Journal of Cell Biology, 203(5), 849–863. http://doi.org/10.1083/jcb.201302022

Meng, L., Mulcahy, B., Cook, S. J., Neubauer, M., Wan, A., Jin, Y., & Yan, D. (2015). The Cell Death Pathway Regulates Synapse Elimination through Cleavage of Gelsolin in Caenorhabditis elegans Neurons. Cell Reports, 11(11), 1737–1748. http://doi.org/10.1016/j.celrep.2015.05.031

Miller-Fleming, T. W., Petersen, S. C., Manning, L., Matthewman, C., Gornet, M., Beers, A., … Miller, D. M. (2016). The DEG/ENaC cation channel protein UNC-8 drives activity-dependent synapse removal in remodeling GABAergic neurons. eLife, 5(JULY), 1–28. http://doi.org/10.7554/eLife.14599

Ou, C., Poon, V. Y., Maeder, C. I., Watanabe, S., Emily, K., Fu, A. K. Y., … Ip, N. Y. (2011). NIH Public Access, 141(5), 846–858. http://doi.org/10.1016/j.cell.2010.04.011

Petersen, S. C., Watson, J. D., Richmond, J. E., Sarov, M., Walthall, W. W., & Miller, D. M. (2011). A Transcriptional Program Promotes Remodeling of GABAergic Synapses in Caenorhabditis elegans. The Journal of Neuroscience , 31(43), 15362–15375. http://doi.org/10.1523/JNEUROSCI.3181-11.2011

Richmond, J. E., Davis, W. S., & Jorgensen, E. M. (1999). UNC-13 is required for synaptic vesicle fusion in C. elegans Janet. Nature Neuroscience, 2(11), 959–964. http://doi.org/10.1038/14755

Shan, G., Kim, K., Li, C., & Walthall, W. W. (2005). Convergent genetic programs regulate similarities and differences between related motor neuron classes in Caenorhabditis elegans. Developmental Biology, 280(2), 494–503. http://doi.org/http://dx.doi.org/10.1016/j.ydbio.2005.01.032

Weimer, R. M., Gracheva, E. O., Meyrignac, O., Miller, K. G., Richmond, J. E., & Bessereau, J.-L. (2006). UNC-13 and UNC-10/Rim Localize Synaptic Vesicles to Specific Membrane Domains. The Journal of Neuroscience , 26(31), 8040–8047. http://doi.org/10.1523/JNEUROSCI.2350-06.2006

VI. APPENDIX B

Statement of publisher's permission:

"Unless otherwise indicated, the articles and journal content published by eLife on the eLife Sites are licensed under a Creative Commons Attribution license (also known as a CC-BY license). This means that you are free to use, reproduce and distribute the articles and related content (unless otherwise noted), for commercial and noncommercial purposes, subject to citation of the original source in accordance with the CC-BY license."

VII. CITED LITERATURE

Ackermann, F., Waites, C. L., & Garner, C. C. (2015). Presynaptic active zones in invertebrates and vertebrates. EMBO Reports, 16(8), 1–16. http://doi.org/10.15252/embr.201540434

Ackley, B. D. (2005). The Two Isoforms of the Caenorhabditis elegans Leukocyte-Common Antigen Related Receptor Tyrosine Phosphatase PTP-3 Function Independently in Axon Guidance and Synapse Formation. Journal of Neuroscience, 25(33), 7517–7528. http://doi.org/10.1523/JNEUROSCI.2010-05.2005

Altun, Z. F., & Hall, D. H. (2011). Nervous system, general description. WormAtlas. http://doi.org/10.3908/wormatlas.1.18

Arancillo, M., Min, S.-W., Gerber, S., Munster-Wandowski, A., Wu, Y.-J., Herman, M., … Rosenmund, C. (2013). Titration of Syntaxin1 in Mammalian Synapses Reveals Multiple Roles in Vesicle Docking, Priming, and Release Probability. Journal of Neuroscience, 33(42), 16698–16714. http://doi.org/10.1523/JNEUROSCI.0187-13.2013

Aravamudan, B., Fergestad, T., Davis, W. S., Rodesch, C. K., & Broadie, K. (1999). Drosophila Unc-13 is essential for synaptic transmission. Nat Neurosci, 2(11), 965–971. Retrieved from http://dx.doi.org/10.1038/14764

Augustin, I., Rosenmund, C., Sudhof, T. C., & Brose, N. (1999). Munc13-1 is essential for fusion competence of glutamatergic synaptic vesicles. Nature, 400(6743), 457–461. Retrieved from http://dx.doi.org/10.1038/22768

Baas, P. W., Vidya Nadar, C., & Myers, K. A. (2006). Axonal Transport of Microtubules: the Long and Short of It. Traffic, 7(5), 490–498. http://doi.org/10.1111/j.1600-0854.2006.00392.x

Baas, P. (1998). The role of motor proteins in establishing the microtubule arrays of axons and dendrites. J Chem Neuroanat, 14, 175–180.

Banerjee, N., Bhattacharya, R., Gorczyca, M., Collins, K. M., & Francis, M. M. (2017). Local neuropeptide signaling modulates serotonergic transmission to shape the temporal organization of C. elegans egg-laying behavior. PLoS Genetics, 13(4). http://doi.org/10.1371/journal.pgen.1006697

Baumgärtel, K., & Mansuy, I. M. (2012). Neural functions of calcineurin in synaptic plasticity and memory. Learning & Memory (Cold Spring Harbor, N.Y.), 19(9), 375–84. http://doi.org/10.1101/lm.027201.112

Betz, A., Ashery, U., Rickmann, M., Augustin, I., Neher, E., Südhof, T. C., … Brose, N. (2017). Munc13-1 Is a Presynaptic Phorbol Ester Receptor that Enhances Neurotransmitter Release. Neuron, 21(1), 123–136. http://doi.org/10.1016/S0896-6273(00)80520-6

Bhattacharya, R., & Francis, M. M. (2015). during food searching, (September), 1–5.

Bhattacharya, R., Touroutine, D., Barbagallo, B., Climer, J., Lambert, C. M., Clark, C. M., … Francis, M. M. (2014). A Conserved Dopamine-Cholecystokinin Signaling Pathway Shapes Context???Dependent Caenorhabditis elegans Behavior. PLoS Genetics, 10(8). http://doi.org/10.1371/journal.pgen.1004584

Bianchi, L., & Driscoll, M. (2002). Protons at the Gate: DEG/ENaC Ion Channels Help Us Feel and Remember. Neuron, 34(3), 337–340. http://doi.org/http://dx.doi.org/10.1016/S0896-6273(02)00687-6

Blasi, J., Chapman, E. R., Yamasaki, S., Binz, T., Niemann, H., & Jahn, R. (1993). Botulinum neurotoxin C1 blocks neurotransmitter release by means of cleaving HPC-1/syntaxin. The EMBO Journal, 12(12), 4821–4828. Retrieved from http://www.ncbi.nlm.nih.gov/pmc/articles/PMC413934/

Blasi, J., Chapman, E. R., Link, E., Binz, T., Yamasaki, S., Camilli, P. De, … Jahn, R. (1993). Botulinum neurotoxin A selectively cleaves the synaptic protein SNAP-25. Nature, 365(6442), 160–163. Retrieved from http://dx.doi.org/10.1038/365160a0

Bono, M. de, & Villu Maricq, A. (2005). NEURONAL SUBSTRATES OF COMPLEX BEHAVIORS IN C. ELEGANS. Annual Review of Neuroscience, 28(1), 451–501. http://doi.org/10.1146/annurev.neuro.27.070203.144259

Brenner, S. (1974). The genetics of Caenorhabditis elegans. Genetics, 77(1), 71–94. http://doi.org/10.1002/cbic.200300625

Broadie, K., Prokop, A., Bellen, H. J., O'Kane, C. J., Schulze, K. L., & Sweeney, S. T. (1995). Syntaxin and synaptohrevin function downstream of vesicle docking in drosophila. Neuron, 15(3), 663–673. http://doi.org/10.1016/0896-6273(95)90154-X

Bruckner, J. J., Gratz, S. J., Slind, J. K., Geske, R. R., Cummings, A. M., Galindo, S. E., … O'Connor-Giles, K. M. (2012). Fife, a Drosophila Piccolo-RIM homolog, promotes active zone organization and neurotransmitter release. The Journal of Neuroscience : The Official Journal of the Society for Neuroscience, 32(48), 17048–58. http://doi.org/10.1523/JNEUROSCI.3267-12.2012

Bruckner, J. J., Zhan, H., & O'Connor-Giles, K. M. (2015). Advances in imaging ultrastructure yield new insights into presynaptic biology. Frontiers in Cellular Neuroscience, 9(May), 196. http://doi.org/10.3389/fncel.2015.00196

Bruckner, Joseph J., 1 Zhan, Hong 2 Gratz, Scott J., 2 Rao, Monica, 1 Ukken, Fiona, 2 Zilberg, Gregory, 2 and, & O'Connor-Giles, Kate M.1, 2, 3. (2016). Fife organizes synaptic vesicles and calcium channels for high-probablility neurotransmitter release. J. Cell Biol, 216(1), 231–246. http://doi.org/10.1083/jcb.201601098

Bruns, D., & Jahn, R. (1995). Real-time measurement of transmitter release from single synaptic vesicles. Nature, 377(6544), 62–65. Retrieved from http://dx.doi.org/10.1038/377062a0

Bury, L. A. D., & Sabo, S. L. (2011). Coordinated trafficking of synaptic vesicle and active zone proteins prior to synapse formation. Neural Development, 6(1), 24. http://doi.org/10.1186/1749-8104-6-24

Cases-Langhoff, C., B, V., AM, G., Appeltauer, U., Takei, K., Kindler, S., … Garner, C. (1996). Piccolo, a novel 420 kDA protein associated within the presynaptic cytomatrix. European Journal of Cell Biology, 69, 214–233.

Catterall, W. A., & Few, A. P. (2008). Calcium Channel Regulation and Presynaptic Plasticity. Neuron, 59(6), 882–901. http://doi.org/10.1016/j.neuron.2008.09.005

Chen, D., Taylor, K. P., Hall, Q., & Kaplan, J. M. (2016). elegans locomotion. Genetics, 204(3), 1151–1159. http://doi.org/10.1534/genetics.116.192898

Chen, D., Wilkinson, C. R. M., Watt, S., Penkett, C. J., Toone, W. M., Jones, N., & Bähler, J. (20016). High-Resolution Crystal Structure and In Vivo Function of a Kinesin-2 Homologue in Giardia intestinalis. Molecular Biology of the Cell, 19(1), 308–317. http://doi.org/10.1091/mbc.E07

Chia, P. H., Chen, B., Li, P., Rosen, M. K., & Shen, K. (2014). Local F-actin network links synapse formation and axon branching. Cell, 156(0), 208–220. http://doi.org/10.1016/j.cell.2013.12.009

Chia, P. H., Li, P., & Shen, K. (2013). Cellular and molecular mechanisms underlying presynapse formation. Journal of Cell Biology, 203(1), 11–22. http://doi.org/10.1083/jcb.201307020

Chia, P. H., Patel, M. R., & Shen, K. (2012). NAB-1 instructs synapse assembly by linking adhesion molecules and F-actin to active zone proteins. Nature Neuroscience, 15(2), 234–242. http://doi.org/10.1038/nn.2991

Cho, J.-H., & Askwith, C. C. (2008). Presynaptic Release Probability Is Increased in Hippocampal Neurons From ASIC1 Knockout Mice. Journal of Neurophysiology, 99(2), 426–441. http://doi.org/10.1152/jn.00940.2007

Choi, S., Taylor, K. P., Chatzigeorgiou, M., Hu, Z., Schafer, W. R., & Kaplan, J. M. (2015). Sensory Neurons Arouse C. elegans Locomotion via Both Glutamate and Neuropeptide Release. PLoS Genetics, 11(7), 1–20. http://doi.org/10.1371/journal.pgen.1005359

Coppola, T., Magnin-Lüthi, S., Perret-Menoud, V., Gattesco, S., Schiavo, G., & Regazzi, R. (2001). Direct Interaction of the Rab3 Effector RIM with Ca2+ Channels, SNAP-25, and Synaptotagmin. Journal of Biological Chemistry, 276(35), 32756–32762. http://doi.org/10.1074/jbc.M100929200

Crump, J. G., Zhen, M., Jin, Y., & Bargmann, C. I. (2001). The SAD-1 kinase regulates presynaptic vesicle clustering and axon termination. Neuron, 29(1), 115–129. http://doi.org/10.1016/S0896-6273(01)00184-2

Dai, Z., & Peng, H. B. (1996). Dynamics of synaptic vesicles in cultured spinal cord neurons in relationship to synaptogenesis. Mol Cell Neurosci, 7. http://doi.org/10.1006/mcne.1996.0032

Dani, A., Huang, B., Bergan, J., Dulac, C., & Zhuang, X. (2010). Superresolution Imaging of Chemical Synapses in the Brain. Neuron, 68(5), 843–856. http://doi.org/10.1016/j.neuron.2010.11.021

Deák, F., Schoch, S., Liu, X., Südhof, T. C., & Kavalali, E. T. (2004). Synaptobrevin is essential for fast synaptic-vesicle endocytosis. Nature Cell Biology, 6(11), 1102–1108. http://doi.org/10.1038/ncb1185

Deidda, G., Allegra, M., Cerri, C., Naskar, S., Bony, G., Zunino, G., … Cancedda, L. (2014). Early depolarizing GABA controls critical-period plasticity in the rat visual cortex. Nature Neuroscience, 18(1), 87–96. http://doi.org/10.1038/nn.3890

Deken, S. L. (2005). Redundant Localization Mechanisms of RIM and ELKS in Caenorhabditis elegans. Journal of Neuroscience, 25(25), 5975–5983. http://doi.org/10.1523/JNEUROSCI.0804-05.2005

Deng, L., Chávez, A. E., Liu, X., Castillo, P. E., Südhof, T. C., & Kaeser, P. S. (2009). ELKS2alpha/CAST deletion selectively increases neurotransmitter release at inhibitory synapses. Neuron, 64(2), 227–239. Retrieved from http://linkinghub.elsevier.com/retrieve/pii/S0896627309007193%0Afile:///Articles/2009/Kaeser/Neuron 2009 Kaeser.pdf%0Apapers3://publication/doi/10.1016/j.neuron.2009.09.019

Dickinson, D. J., Pani, A. M., Heppert, J. K., Higgins, C. D., & Goldstein, B. (2015). Streamlined genome engineering with a self-excising drug selection cassette. Genetics, 200(4), 1035–1049. http://doi.org/10.1534/genetics.115.178335

Dorf, M. E., Rao, A., Davidson, L., Boschetti, E., Hess, S. D., Doroshenko, P. A., & Augustinet, G. J. (2017). A Functional Role for GTP-Binding Proteins in Synaptic Vesicle Cycling Author (s): S . D . Hess , P . A . Doroshenko and G . J . Augustine Published by : American Association for the Advancement of Science Stable URL : http://www.jstor.org/stable/288075, 259(5098), 1169–1172.

Dulubova, I., Sugita, S., Hill, S., Hosaka, M., Fernandez, I., Südhof, T. C., … Forman-Kay, J. (1999). A conformational switch in syntaxin during exocytosis: role of munc18. The EMBO Journal, 18(16), 4372–4382. http://doi.org/10.1093/emboj/18.16.4372

Dulubova, I., Lou, X., Lu, J., Huryeva, I., Alam, A., Schneggenburger, R., … Rizo, J. (2005). A Munc13/RIM/Rab3 tripartite complex: from priming to plasticity? The EMBO Journal, 24(16), 2839–2850. http://doi.org/10.1038/sj.emboj.7600753

Erni, R., Rossell, M. D., Kisielowski, C., & Dahmen, U. (2009). Atomic-resolution imaging with a sub-50-pm electron probe. Physical Review Letters, 102(9). http://doi.org/10.1103/PhysRevLett.102.096101

Erturk, A., Wang, Y., & Sheng, M. (2014). Local Pruning of Dendrites and Spines by Caspase-3-Dependent and Proteasome-Limited Mechanisms. Journal of Neuroscience, 34(5), 1672–1688. http://doi.org/10.1523/JNEUROSCI.3121-13.2014

Etchberger, J. F., Lorch, A., Sleumer, M. C., Zapf, R., Jones, S. J., Marra, M. a, … Hobert, O. (2007). The molecular signature and cis -regulatory architecture of a C . elegans gustatory neuron. Genes & Development, 21, 1653–1674. http://doi.org/10.1101/gad.1560107.tatory

Farsad, K., Ringstad, N., Takei, K., Floyd, S. R., Rose, K., & De Camilli, P. (2001). Generation of high curvature membranes mediated by direct endophilin bilayer interactions. Journal of Cell Biology, 155(2), 193–200. http://doi.org/10.1083/jcb.200107075

Fasshauer, D., Sutton, R. B., Brunger, A. T., & Jahn, R. (1998). Conserved structural features of the synaptic fusion complex: SNARE proteins reclassified as Q- and R-SNAREs. Proceedings of the National Academy of Sciences, 95(26), 15781–15786. http://doi.org/10.1073/pnas.95.26.15781

Fenster, S. D., Chung, W. J., Zhai, R., Cases-Langhoff, C., Voss, B., Garner, A. M., … Garner, C. C. (2000). Piccolo, a Presynaptic Zinc Finger Protein Structurally Related to Bassoon. Neuron, 25(1), 203–214. http://doi.org/10.1016/S0896-6273(00)80883-1

Flavell, S. W., & Greenberg, M. E. (2008). Signaling Mechanisms Linking Neuronal Activity to Gene Expression and Plasticity of the Nervous System. Annual Review of Neuroscience, 31(1), 563–590. http://doi.org/10.1146/annurev.neuro.31.060407.125631

Fujimoto, K., Shibasaki, T., Yokoi, N., Kashima, Y., Matsumoto, M., Sasaki, T., … Seino, S. (2002). Piccolo, a Ca2+ Sensor in Pancreatic β-Cells: INVOLVEMENT OF cAMP-GEFII·Rim2·PICCOLO COMPLEX IN cAMP-DEPENDENT EXOCYTOSIS . Journal of Biological Chemistry , 277(52), 50497–50502. http://doi.org/10.1074/jbc.M210146200

Gage, P. W. (1998). Signal transmission in ligand-gated receptors. Immunology and Cell Biology, 76(5), 436–440. http://doi.org/10.1046/j.1440-1711.1998.00763.x

Gally, C., & Bessereau, J.-L. (2003). GABA is dispensable for the formation of junctional GABA receptor clusters in Caenorhabditis elegans. The Journal of Neuroscience : The Official Journal of the Society for Neuroscience, 23(7), 2591–2599.

Gao, J., Duan, B., Wang, D. G., Deng, X. H., Zhang, G. Y., Xu, L., & Xu, T. Le. (2005). Coupling between NMDA receptor and acid-sensing ion channel contributes to ischemic neuronal death. Neuron, 48(4), 635–646. http://doi.org/10.1016/j.neuron.2005.10.011

Gengyo-Ando, K., & Mitani, S. (2000). Characterization of mutations induced by ethyl methanesulfonate, UV, and trimethylpsoralen in the nematode Caenorhabditis elegans. Biochemical and Biophysical Research Communications, 269(1), 64–69. http://doi.org/10.1006/bbrc.2000.2260

Gerber, S. H., Rah, J.-C., Min, S.-W., Liu, X., de Wit, H., Dulubova, I., … Sudhof, T. C. (2008). Conformational Switch of Syntaxin-1 Controls Synaptic Vesicle Fusion. Science, 321(5895), 1507–1510. http://doi.org/10.1126/science.1163174

Giraldez, T., Domínguez, J., & Alvarez de la Rosa, D. (2013). ENaC in the brain--future perspectives and pharmacological implications. Current Molecular Pharmacology, 6(1), 44–9. Retrieved from http://www.ncbi.nlm.nih.gov/pubmed/23547934

Gracheva, E. O., Burdina, A. O., Holgado, A. M., Berthelot-Grosjean, M., Ackley, B. D., Hadwiger, G., … Richmond, J. E. (2006). Tomosyn inhibits synaptic vesicle priming in Caenorhabditis elegans. PLoS Biology, 4(8), e261. http://doi.org/10.1371/journal.pbio.0040261

Gracheva, E. O., Hadwiger, G., Nonet, M. L., & Richmond, J. E. (2008). Direct interactions between C. elegans RAB-3 and Rim provide a mechanism to target vesicles to the presynaptic density. Neuroscience Letters, 444(2), 137–142. http://doi.org/10.1016/j.neulet.2008.08.026

Gracheva, E. O., Hadwiger, G., Nonet, M. L., & Richmond, J. E. (2008). Direct interactions between C. elegans RAB-3 and Rim provide a mechanism to target vesicles to the presynaptic density. Neuroscience Letters, 444(2), 137–142. http://doi.org/10.1016/j.neulet.2008.08.026

Hallam, S. J., & Jin, Y. (1998). lin-14 regulates the timing of synaptic remodelling in Caenorhabditis elegans. Nature, 395(6697), 78–82. http://doi.org/10.1038/25757

Harlow, M. L., Ress, D., Stoschek, A., Marshall, R. M., & McMahan, U. J. (2001). The architecture of active zone material at the frog's neuromuscular junction. Nature, 409(6819), 479–484. http://doi.org/10.1038/35054000

Harris, T. W., Hartwieg, E., Horvitz, H. R., & Jorgensen, E. M. (2000). Mutations in synaptojanin disrupt synaptic vesicle recycling. Journal of Cell Biology, 150(3), 589–599. http://doi.org/10.1083/jcb.150.3.589

Haucke, V., & De Camilli, P. (1999). AP-2 Recruitment to Synaptotagmin Stimulated by Tyrosine-Based Endocytic Motifs. Science, 285(5431), 1268–1271. http://doi.org/10.1126/science.285.5431.1268

He, S., Philbrook, A., McWhirter, R., Gabel, C. V., Taub, D. G., Carter, M. H., … Miller, D. M. (2015). Transcriptional control of synaptic remodeling through regulated expression of an immunoglobulin superfamily protein. Current Biology, 25(19), 2541–2548. http://doi.org/10.1016/j.cub.2015.08.022

Hensch, T. K. (1998). Local GABA Circuit Control of Experience-Dependent Plasticity in Developing Visual Cortex. Science, 282(5393), 1504–1508. http://doi.org/10.1126/science.282.5393.1504

Hong, W. (2005). SNAREs and traffic. Biochimica et Biophysica Acta - Molecular Cell Research, 1744(2), 120–144. http://doi.org/10.1016/j.bbamcr.2005.03.014

Howell, K., White, J. G., & Hobert, O. (2015). Spatiotemporal control of a novel synaptic organizer molecule. Nature, 523(7558), 83–87. http://doi.org/10.1038/nature14545

Hu, Z., Vashlishan-Murray, a. B., & Kaplan, J. M. (2015). NLP-12 Engages Different UNC-13 Proteins to Potentiate Tonic and Evoked Release. Journal of Neuroscience, 35(3), 1038–1042. http://doi.org/10.1523/JNEUROSCI.2825-14.2015

Hu, Z., Pym, E. C. G., Babu, K., Vashlishan Murray, A. B., & Kaplan, J. M. (2011). A Neuropeptide-Mediated Stretch Response Links Muscle Contraction to Changes in Neurotransmitter Release. Neuron, 71(1), 92–102. http://doi.org/10.1016/j.neuron.2011.04.021

Hu, Z., Tong, X.-J., & Kaplan, J. M. (2013). UNC-13L, UNC-13S, and Tomosyn form a protein code for fast and slow neurotransmitter release in Caenorhabditis elegans. eLife, 2, e00967. http://doi.org/10.7554/eLife.00967

Hunt, J. M., Bommert, K., Charlton, M. P., Kistner, A., Habermann, E., Augustine, G. J., & Betzt, H. (1994). A post-docking role for synaptobrevin in synaptic vesicle fusion. Neuron, 12(6), 1269–1279. http://doi.org/10.1016/0896-6273(94)90443-X

Huttner, W. B., & Schmidt, A. (2000). Lipids, lipid modification and lipid-protein interaction in membrane budding and fission - Insights from the roles of endophilin A1 and synaptophysin in synaptic vesicle endocytosis. Current Opinion in Neurobiology, 10(5), 543–551. http://doi.org/10.1016/S0959-4388(00)00126-4

Imig, C., Min, S. W., Krinner, S., Arancillo, M., Rosenmund, C., Südhof, T. C., … Cooper, B. H. (2014). The Morphological and Molecular Nature of Synaptic Vesicle Priming at Presynaptic Active Zones. Neuron, 84(2), 416–431. http://doi.org/10.1016/j.neuron.2014.10.009

Jahn, R., & Scheller, R. H. (2006). SNAREs — engines for membrane fusion. Nature Reviews Molecular Cell Biology, 7(9), 631–643. http://doi.org/10.1038/nrm2002

Jin, Y., & Garner, C. C. (2008). Molecular Mechanisms of Presynaptic Differentiation. Annual Review of Cell and Developmental Biology, 24(1), 237–262. http://doi.org/10.1146/annurev.cellbio.23.090506.123417

Jin, Y., Jorgensen, E., Hartwieg, E., & Horvitz, H. R. (1999). The Caenorhabditis elegans gene unc-25 encodes glutamic acid decarboxylase and is required for synaptic transmission but not synaptic development. The Journal of Neuroscience : The Official Journal of the Society for Neuroscience, 19(2), 539–548.

Jung, N., & Haucke, V. (2007). Clathrin-mediated endocytosis at synapses. Traffic, 8(9), 1129–1136. http://doi.org/10.1111/j.1600-0854.2007.00595.x

Kaeser, P. S., Deng, L., Chávez, A. E., Liu, X., Castillo, P. E., & Südhof, T. C. (2009). ELKS2α/CAST Deletion Selectively Increases Neurotransmitter Release at Inhibitory Synapses. Neuron, 64(2), 227–239. http://doi.org/10.1016/j.neuron.2009.09.019

Kaeser, P. S., Deng, L., Wang, Y., Dulubova, I., Liu, X., Rizo, J., & Südhof, T. C. (2011). RIM proteins tether Ca2+ channels to presynaptic active zones via a direct PDZ-domain interaction. Cell, 144(2), 282–295. http://doi.org/10.1016/j.cell.2010.12.029

Kakizawa, S., Yamasaki, M., Watanabe, M., & Kano, M. (2000). Critical period for activity-dependent synapse elimination in developing cerebellum. The Journal of Neuroscience : The Official Journal of the Society for Neuroscience, 20(13), 4954–4961. http://doi.org/20/13/4954 [pii]

Kaufmann, N., DeProto, J., Ranjan, R., Wan, H., & Van Vactor, D. (2002). Drosophila Liprin-α and the Receptor Phosphatase Dlar Control Synapse Morphogenesis. Neuron, 34(1), 27–38. http://doi.org/https://doi.org/10.1016/S0896-6273(02)00643-8

Khvotchev, M., Dulubova, I., Sun, J., Dai, H., Rizo, J., & Sudhof, T. C. (2007). Dual modes of Munc18-1/SNARE interactions are coupled by functionally critical binding to syntaxin-1 N terminus. J Neurosci, 27(45), 12147–12155. http://doi.org/27/45/12147 [pii]\r10.1523/JNEUROSCI.3655-07.2007

Kittelmann, M., Hegermann, J., Goncharov, A., Taru, H., Ellisman, M. H., Richmond, J. E., … Eimer, S. (2013). Liprin-α/SYD-2 determines the size of dense projections in presynaptic active zones in C. elegans. Journal of Cell Biology, 203(5), 849–863. http://doi.org/10.1083/jcb.201302022

Ko, J., Kim, S., Valtschanoff, J. G., Shin, H., Lee, J.-R., Sheng, M., … Kim, E. (n.d.). Interaction between liprin-alpha and GIT1 is required for AMPA receptor targeting. The Journal of Neuroscience : The Official Journal of the Society for Neuroscience, 23(5), 1667–1677. http://doi.org/23/5/1667 [pii]

Ko, J., Na, M., Kim, S., Lee, J. R., & Kim, E. (n.d.). Interaction of the ERC Family of RIM-binding Proteins with the Liprin-?? Family of Multidomain Proteins. Journal of Biological Chemistry, 278(43), 42377–42385. http://doi.org/10.1074/jbc.M307561200

Koch, H., Hofmann, K., & Brose, N. (2000). Definition of Munc13-homology-domains and characterization of a novel ubiquitously expressed Munc13 isoform. Biochem. J, 349, 247–253. http://doi.org/10.1042/0264-6021:3490247

Kohn, R. E., Duerr, J. S., McManus, J. R., Duke, A., Rakow, T. L., Maruyama, H., … Rand, J. B. (2000). Expression of multiple UNC-13 proteins in the Caenorhabditis elegans nervous system. Molecular Biology of the Cell, 11(10), 3441–52. Retrieved from http://www.pubmedcentral.nih.gov/articlerender.fcgi?artid=15005&tool=pmcentrez&rendertype=abstract

Koushika, S. P., Richmond, J. E., Hadwiger, G., Weimer, R. M., Erik, M., & Nonet, M. L. (2008). NIH Public Access, 4(10), 997–1005. http://doi.org/10.1038/nn732.A

Kreple, C. J., Lu, Y., Taugher, R. J., Schwager-Gutman, A. L., Du, J., Stump, M., … Wemmie, J. A. (2014). Acid-sensing ion channels contribute to synaptic transmission and inhibit cocaine-evoked plasticity. Nature Neuroscience, 17(8), 1083–1091. http://doi.org/10.1038/nn.3750

Kuo, C. T., Zhu, S., Younger, S., Jan, L. Y., & Jan, Y. N. (2006). Identification of E2/E3 Ubiquitinating Enzymes and Caspase Activity Regulating Drosophila Sensory Neuron Dendrite Pruning. Neuron, 51(3), 283–290. http://doi.org/10.1016/j.neuron.2006.07.014

Kupfermann, I. (1991). Functional studies of cotransmission. Physiological Reviews, 71(3), 683 LP-732. Retrieved from http://physrev.physiology.org/content/71/3/683.abstract

Lee, H. K., Kameyama, K., Huganir, R. L., & Bear, M. F. (1998). NMDA induces long-term synaptic depression and dephosphorylation of the GluR1 subunit of AMPA receptors in hippocampus. Neuron, 21(5), 1151–1162. http://doi.org/10.1016/S0896-6273(00)80632-7

Li, C., & Kim, K. (2008). Neuropeptides. WormBook, 1–36. http://doi.org/10.1895/wormbook.1.142.1

Li, F., Pincet, F., Perez, E., Eng, W. S., Melia, T. J., Rothman, J. E., & Tareste, D. (2007). Energetics and dynamics of SNAREpin folding across lipid bilayers. Nature Structural & Molecular Biology, 14(10), 890–896. http://doi.org/10.1038/nsmb1310

Li, L., Tian, X., Zhu, M., Bulgari, D., Böhme, M. A., Goettfert, F., … Wu, C. (2014). Drosophila Syd-1, Liprin-α, and Protein Phosphatase 2A B′ Subunit Wrd Function in a Linear Pathway to Prevent Ectopic Accumulation of Synaptic Materials in Distal Axons. The Journal of Neuroscience, 34(25), 8474 LP-8487. Retrieved from http://www.jneurosci.org/content/34/25/8474.abstract

Li, Z., Jo, J., Jia, J. M., Lo, S. C., Whitcomb, D. J., Jiao, S., … Sheng, M. (2010). Caspase-3 activation via mitochondria is required for long-term depression and AMPA receptor internalization. Cell, 141(5), 859–871. http://doi.org/10.1016/j.cell.2010.03.053

Lim, M. A., Chitturi, J., Laskova, V., Meng, J., Findeis, D., Wiekenberg, A., … Zhen, M. (2016). Neuroendocrine modulation sustains the C. elegans forward motor state. eLife, 5(NOVEMBER2016), 1–33. http://doi.org/10.7554/eLife.19887

Liu, Q., Hollopeter, G., & Jorgensen, E. M. (2009). Graded synaptic transmission at the Caenorhabditis elegans neuromuscular junction. Proceedings of the National Academy of Sciences of the United States of America, 106(26), 10823–10828. http://doi.org/10.1073/pnas.0903570106

Liu, T., Kim, K., Li, C., & Barr, M. M. (2007). FMRFamide-like neuropeptides and mechanosensory touch receptor neurons regulate male sexual turning behavior in Caenorhabditis elegans. J Neurosci, 27(27), 7174–7182. http://doi.org/10.1523/JNEUROSCI.1405-07.2007

Liu, Z., Kanzawa, N., & Ono, S. (2011). Calcium-sensitive activity and conformation of Caenorhabditis elegans gelsolin-like protein 1 are altered by mutations in the first gelsolin-like domain. Journal of Biological Chemistry, 286(39), 34051–34059. http://doi.org/10.1074/jbc.M111.237404

Ma, C., Su, L., Seven, A. B., Xu, Y., & Rizo, J. (2013). Reconstitution of the Vital Functions of Munc18 and Munc13 in Neurotransmitter Release. Science (New York, N.Y.), 339(6118), 421–425. http://doi.org/10.1126/science.1230473

Maas, C., Torres, V. I., Altrock, W. D., Leal-Ortiz, S., Wagh, D., Terry-Lorenzo, R. T., … Garner, C. C. (2012). Formation of Golgi-Derived Active Zone Precursor Vesicles. Journal of Neuroscience, 32(32), 11095–11108. http://doi.org/10.1523/JNEUROSCI.0195-12.2012

Martens, S., Kozlov, M. M., & McMahon, H. T. (2007). How Synaptotagmin Promotes Membrane Fusion. Science, 316(5828), 1205–1208. http://doi.org/10.1126/science.1142614

Maruyama, I. N., & Brenner, S. (1991). A phorbol ester/diacylglycerol-binding protein encoded by the unc-13 gene of Caenorhabditis elegans. Proceedings of the National Academy of Sciences of the United States of America, 88(13), 5729–33. http://doi.org/10.1073/pnas.88.13.5729

Mathews, E. A., Garcia, E., Santi, C. M., Mullen, G. P., Thacker, C., Moerman, D. G., & Snutch, T. P. (2003). Critical residues of the Caenorhabditis elegans unc-2 voltage-gated calcium channel that affect behavioral and physiological properties. J Neurosci, 23(16), 6537–6545. Retrieved from http://www.ncbi.nlm.nih.gov/pubmed/12878695

McEwen, J. M., Madison, J. M., Dybbs, M., & Kaplan, J. M. (2006). Antagonistic Regulation of Synaptic Vesicle Priming by Tomosyn and UNC-13. Neuron, 51(3), 303–315. http://doi.org/10.1016/j.neuron.2006.06.025

McIntire, S. L., Jorgensen, E., Kaplan, J., & Horvitz, H. R. (1993). The GABAergic nervous system of Caenorhabditis elegans. Nature, 364, 337–341. http://doi.org/10.1038/364337a0

Meng, L., Mulcahy, B., Cook, S. J., Neubauer, M., Wan, A., Jin, Y., & Yan, D. (2015). The Cell Death Pathway Regulates Synapse Elimination through Cleavage of Gelsolin in Caenorhabditis elegans Neurons. Cell Reports, 11(11), 1737–1748. http://doi.org/10.1016/j.celrep.2015.05.031

Miller-Fleming, T. W., Petersen, S. C., Manning, L., Matthewman, C., Gornet, M., Beers, A., … Miller, D. M. (2016). The DEG/ENaC cation channel protein UNC-8 drives activity-dependent synapse removal in remodeling GABAergic neurons. eLife, 5(JULY), 1–28. http://doi.org/10.7554/eLife.14599

Miller, T. M., & Heuser, J. E. (1984). Endocytosis of synaptic vesicle membrane at the frog neuromuscular junction. Journal of Cell Biology, 98(2), 685–698. http://doi.org/10.1083/jcb.98.2.685

Mittelstaedt, T., & Schoch, S. (2007). Structure and evolution of RIM-BP genes: Identification of a novel family member. Gene, 403(1–2), 70–79. http://doi.org/10.1016/j.gene.2007.08.004

Moor, H. (1987). Theory and Practice of High Pressure Freezing. Cryotechniques in Biological Electron Microscopy, 175–191. http://doi.org/10.1007/978-3-642-72815-0_8

Müller, M., & Davis, G. W. (2012). Transsynaptic control of presynaptic Ca 2+ influx achieves homeostatic potentiation of neurotransmitter release. Current Biology, 22(12), 1102–1108. http://doi.org/10.1016/j.cub.2012.04.018

Nakata, T., Kitamura, Y., Shimizu, K., Tanaka, S., Fujimori, M., Yokoyama, S., … Emi, M. (1999). Fusion of a novel gene, ELKS, to RET due to translocation t(10;12)(q11;p13) in a papillary thyroid carcinoma. Genes Chromosomes and Cancer, 25(2), 97–103. http://doi.org/10.1002/(SICI)1098-2264(199906)25:2<97::AID-GCC4>3.0.CO;2-L

Nakata, T., Yokota, T., Emi, M., & Minami, S. (2002). Differential expression of multiple isoforms of the ELKS mRNAs involved in a papillary thyroid carcinoma. Genes Chromosomes and Cancer, 35(1), 30–37. http://doi.org/10.1002/gcc.10095

Nonet, M. L., Saifee, O., Zhao, H., Rand, J. B., & Wei, L. (1998). Synaptic transmission deficits in Caenorhabditis elegans synaptobrevin mutants. The Journal of Neuroscience : The Official Journal of the Society for Neuroscience, 18(1), 70–80.

Nonet, M. L. (1999). Visualization of synaptic specializations in live C. elegans with synaptic vesicle protein-GFP fusions. Journal of Neuroscience Methods, 89(1), 33–40. http://doi.org/10.1016/S0165-0270(99)00031-X

O'Connor, V., Heuss, C., De Bello, W. M., Dresbach, T., Charlton, M. P., Hunt, J. H., … Schäfer, T. (1997). Disruption of syntaxin-mediated protein interactions blocks neurotransmitter secretion. Proceedings of the National Academy of Sciences of the United States of America, 94(22), 12186–91. http://doi.org/10.1073/pnas.94.22.12186

Ohtsuka, T., Takao-Rikitsu, E., Inoue, E., Inoue, M., Takeuchi, M., Matsubara, K., … Takai, Y. (2002). CAST: A novel protein of the cytomatrix at the active zone of synapses that forms a ternary complex with RIM1 and Munc13-1. Journal of Cell Biology, 158(3), 577–590. http://doi.org/10.1083/jcb.200202083

Ou, C., Poon, V. Y., Maeder, C. I., Watanabe, S., Emily, K., Fu, A. K. Y., … Ip, N. Y. (2011). NIH Public Access, 141(5), 846–858. http://doi.org/10.1016/j.cell.2010.04.011.Two

Owald, D., & Sigrist, S. J. (2009). Assembling the presynaptic active zone. Current Opinion in Neurobiology, 19(3), 311–318. http://doi.org/10.1016/j.conb.2009.03.003

Park, M., Watanabe, S., Poon, V. Y. N., Ou, C. Y., Jorgensen, E. M., & Shen, K. (2011). CYY-1/Cyclin Y and CDK-5 Differentially Regulate Synapse Elimination and Formation for Rewiring Neural Circuits. Neuron, 70(4), 742–757. http://doi.org/10.1016/j.neuron.2011.04.002

Petersen, S. C., Watson, J. D., Richmond, J. E., Sarov, M., Walthall, W. W., & Miller, D. M. (2011). A Transcriptional Program Promotes Remodeling of GABAergic Synapses in Caenorhabditis

elegans. The Journal of Neuroscience , 31(43), 15362–15375. http://doi.org/10.1523/JNEUROSCI.3181-11.2011

Pinan-Lucarre, B., Gabel, C. V., Reina, C. P., Hulme, S. E., Shevkoplyas, S. S., Slone, R. D., … Driscoll, M. (2012). The core apoptotic executioner proteins CED-3 and CED-4 promote initiation of neuronal regeneration in caenorhabditis elegans. PLoS Biology, 10(5). http://doi.org/10.1371/journal.pbio.1001331

Pobbati, A. V. (2006). N- to C-Terminal SNARE Complex Assembly Promotes Rapid Membrane Fusion. Science, 313(5787), 673–676. http://doi.org/10.1126/science.1129486

Praitis, V., Casey, E., Collar, D., & Austin, J. (2001). Creation of low-copy integrated transgenic lines in Caenorhabditis elegans. Genetics, 157(3), 1217–1226.

Renden, R., Berwin, B., Davis, W., Ann, K., Chin, C.-T., Kreber, R., … Broadie, K. (2017). Drosophila CAPS Is an Essential Gene that Regulates Dense-Core Vesicle Release and Synaptic Vesicle Fusion. Neuron, 31(3), 421–437. http://doi.org/10.1016/S0896-6273(01)00382-8

Richmond, J. (2006). Synaptic function. WormBook, 1–15. http://doi.org/10.1895/wormbook.1.69.1

Richmond, J. E., Davis, W. S., & Jorgensen, E. M. (1999). UNC-13 is required for synaptic vesicle fusion in C. elegans Janet. Nature Neuroscience, 2(11), 959–964. http://doi.org/10.1038/14755

Richmond, J. E., & Jorgensen, E. M. (1999). One GABA and two acetylcholine receptors function at the. America, 791–798.

Rizzoli, S. O., Bethani, I., Zwilling, D., Wenzel, D., Siddiqui, T. J., Brandhorst, D., & Jahn, R. (2006). Evidence for early endosome-like fusion of recently endocytosed synaptic vesicles. Traffic, 7(9), 1163–1176. http://doi.org/10.1111/j.1600-0854.2006.00466.x

Rizzoli, S. O., & Jahn, R. (2007). Kiss-and-run, collapse and “readily retrievable” vesicles. Traffic, 8(9), 1137–1144. http://doi.org/10.1111/j.1600-0854.2007.00614.x

Robinson, L. J., & Martin, Thomas, F. (1998). Docking and fusion in neurosecretion. Current Opinion in Cell Biology, (10), 483–492.

Rostaing, P., Weimer, R. M., Jorgensen, E. M., Triller, A., & Bessereau, J.-L. (2004). Preservation of Immunoreactivity and Fine Structure of Adult C. elegans Tissues Using High-pressure Freezing. Journal of Histochemistry & Cytochemistry, 52(1), 1–12. http://doi.org/10.1177/002215540405200101

Saheki, Y., & Bargmann, C. I. (2009). Presynaptic CaV2 calcium channel traffic requires CALF-1 and the α2δ subunit UNC-36. Nature Neuroscience, 12(10), 1257–1265. http://doi.org/10.1038/nn.2383

Saifee, O., Wei, L., & Nonet, M. L. (1998). The Caenorhabditis elegans unc-64 locus encodes a syntaxin that interacts genetically with synaptobrevin. Molecular Biology of the Cell, 9(6), 1235–52. Retrieved from http://www.pubmedcentral.nih.gov/articlerender.fcgi?artid=25346&tool=pmcentrez&rendertype=abstract

Sanderson, J. L., Gorski, J. a., Gibson, E. S., Lam, P., Freund, R. K., Chick, W. S., & Dell'Acqua, M. L. (2012). AKAP150-Anchored Calcineurin Regulates Synaptic Plasticity by Limiting Synaptic Incorporation of Ca2+-Permeable AMPA Receptors. Journal of Neuroscience, 32(43), 15036–15052. http://doi.org/10.1523/JNEUROSCI.3326-12.2012

Schiavo, G., Poulain, B., Rossetto, O., Benfenati, F., Tauc, L., & Montecucco, C. (1992). Tetanus toxin is a zinc protein and its inhibition of neurotransmitter release and protease activity depend on zinc. The EMBO Journal, 11(10), 3577–83. Retrieved from http://www.pubmedcentral.nih.gov/articlerender.fcgi?artid=556816&tool=pmcentrez&rendertype=abstract

Schmid, S. L. (1997). Clathrin-coated vesicle formation and protein sorting: An Integrated Process. Annual Review of Biochemistry, 66(1), 511–548. http://doi.org/10.1146/annurev.biochem.66.1.511

Schoch, S., Deák, F., Königstorfer, A., Mozhayeva, M., Sara, Y., Südhof, T. C., & Kavalali, E. T. (2001). SNARE Function Analyzed in Synaptobrevin/VAMP Knockout Mice. Science, 294(5544), 1117 LP-1122. Retrieved from http://science.sciencemag.org/content/294/5544/1117.abstract

Schoch, S., & Gundelfinger, E. (2006). Molecular organization of the presynaptic active zone. Cell and Tissue Research, 326(2), 379–391. http://doi.org/10.1007/s00441-006-0244-y

Schuske, K., Beg, A. A., & Jorgensen, E. M. (2004). The GABA nervous system in C. elegans. Trends in Neurosciences, 27(7), 407–414. http://doi.org/10.1016/j.tins.2004.05.005

Schuske, K. R., Richmond, J. E., Matthies, D. S., Davis, W. S., Runz, S., Rube, D. A., … Jorgensen, E. M. (2003). Endophilin is required for synaptic vesicle endocytosis by localizing synaptojanin. Neuron, 40(4), 749–762. http://doi.org/10.1016/S0896-6273(03)00667-6

Shan, G., Kim, K., Li, C., & Walthall, W. W. (2005). Convergent genetic programs regulate similarities and differences between related motor neuron classes in Caenorhabditis elegans. Developmental Biology, 280(2), 494–503. http://doi.org/http://dx.doi.org/10.1016/j.ydbio.2005.01.032

Shapira, M., Zhai, R. G., Dresbach, T., Bresler, T., Torres, V. I., Gundelfinger, E. D., … Garner, C. C. (2003). Unitary assembly of presynaptic active zones from Piccolo-Bassoon transport vesicles. Neuron, 38(2), 237–252. http://doi.org/10.1016/S0896-6273(03)00207-1

Shibasaki, T., Sunaga, Y., Fujimoto, K., Kashima, Y., & Seino, S. (2004). Interaction of ATP Sensor, cAMP Sensor, Ca2+ Sensor, and Voltage-dependent Ca2+ Channel in Insulin Granule Exocytosis. Journal of Biological Chemistry, 279(9), 7956–7961. http://doi.org/10.1074/jbc.M309068200

Shin, H., Wyszynski, M., Huh, K. H., Valtschanoff, J. G., Lee, J. R., Ko, J., … Kim, E. (2003). Association of the kinesin motor KIF1A with the multimodular protein liprin-α. Journal of Biological Chemistry, 278(13), 11393–11401. http://doi.org/10.1074/jbc.M211874200

Sieburth, D., Madison, J. M., & Kaplan, J. M. (2006). PKC-1 regulates secretion of neuropeptides. Nature Neuroscience, 10(1), 49–57. http://doi.org/10.1038/nn1810

Siksou, L., Rostaing, P., Lechaire, J.-P., Boudier, T., Ohtsuka, T., Fejtova, A., … Marty, S. (2007). Three-Dimensional Architecture of Presynaptic Terminal Cytomatrix. Journal of Neuroscience, 27(26), 6868–6877. http://doi.org/10.1523/JNEUROSCI.1773-07.2007

Siksou, L., Varoqueaux, F., Pascual, O., Triller, A., Brose, N., & Marty, S. (2009). A common molecular basis for membrane docking and functional priming of synaptic vesicles. European Journal of Neuroscience, 30(1), 49–56. http://doi.org/10.1111/j.1460-9568.2009.06811.x

Silacci, P., Mazzolai, L., Gauci, C., Stergiopulos, N., Yin, H. L., & Hayoz, D. (2004). Gelsolin superfamily proteins: Key regulators of cellular functions. Cellular and Molecular Life Sciences, 61(19–20), 2614–2623. http://doi.org/10.1007/s00018-004-4225-6

Smith, C. J., Watson, J. D., Spencer, W. C., O'Brien, T., Cha, B., Albeg, A., … Miller, D. M. (2010). Time-lapse imaging and cell-specific expression profiling reveal dynamic branching and molecular determinants of a multi-dendritic nociceptor in C. elegans. Developmental Biology, 345(1), 18–33. http://doi.org/10.1016/j.ydbio.2010.05.502

Smith, J. E., & Reese, T. S. (1980). Use of aldehyde fixatives to determine the rate of synaptic transmitter release. The Journal of Experimental Biology, 89(1), 19–29. Retrieved from http://www.ncbi.nlm.nih.gov/pubmed/6110693

Snydman, D. R., Walker, M., Kublin, J. G., & Zunt, J. R. (2006). Parasitic Central Nervous System Infections in Immunocompromised Hosts: Malaria, Microsporidiosis, Leishmaniasis, and African Trypanosomiasis. Clinical Infectious Diseases, 42(1), 115–125. http://doi.org/Snydman, D. R., Walker, M., Kublin, J. G., & Zunt, J. R. (2006). Parasitic Central Nervous System Infections in Immunocompromised Hosts: Malaria, Microsporidiosis,

Leishmaniasis, and African Trypanosomiasis. Clinical Infectious Diseases, 42(1), 115–125. http://doi.org/10.1086/498510

Söllner, T., Whiteheart, S. W., Brunner, M., Erdjument-Bromage, H., Geromanos, S., Tempst, P., & Rothman, J. E. (1993). SNAP receptors implicated in vesicle targeting and fusion. Nature, 362(6418), 318–324. http://doi.org/10.1038/362318a0

Sossin, W. S., & Scheller, R. H. (1991). Biosynthesis and sorting of neuropeptides. Current Opinion in Neurobiology, 1(1), 79–83. http://doi.org/10.1016/0959-4388(91)90013-W

Spangler, S. A., Schmitz, S. K., Kevenaar, J. T., De Graaff, E., De Wit, H., Demmers, J., … Hoogenraad, C. C. (2013). Liprin-alpha 2 promotes the presynaptic recruitment and turnover of RIM1/CASK to facilitate synaptic transmission. Journal of Cell Biology, 201(6), 915–928. http://doi.org/10.1083/jcb.201301011

Speese, S., Petrie, M., Schuske, K., Ailion, M., Ann, K., Iwasaki, K., … Martin, T. F. J. (2007). UNC-31 (CAPS) is required for dense-core vesicle but not synaptic vesicle exocytosis in Caenorhabditis elegans. The Journal of Neuroscience : The Official Journal of the Society for Neuroscience, 27(23), 6150–62. http://doi.org/10.1523/JNEUROSCI.1466-07.2007

Stevens, C. F., & Tsujimoto, T. (1995). Estimates for the pool size of releasable quanta at a single central synapse and for the time required to refill the pool. Proceedings of the National Academy of Sciences of the United States of America, 92(January), 846–849. http://doi.org/10.1073/pnas.92.3.846

Stevens, D. R., Wu, Z.-X., Matti, U., Junge, H. J., Schirra, C., Becherer, U., … Rettig, J. (2005). Identification of the Minimal Protein Domain Required for Priming Activity of Munc13-1. Current Biology, 15(24), 2243–2248. http://doi.org/10.1016/j.cub.2005.10.055

Stretton, A. O. (1976). Anatomy and development of the somatic musculature of the nematode Ascaris. The Journal of Experimental Biology, 64(3), 773–88. Retrieved from http://www.ncbi.nlm.nih.gov/pubmed/932637

Stroud, R. M., McCarthy, M. P., & Shuster, M. (1990). Nicotinic acetylcholine receptor superfamily of ligand gated ion channels. Biochem., 29, 11009–11023.

Südhof, T. C. (2012). The presynaptic active zone. Neuron, 75(1), 11–25. http://doi.org/10.1016/j.neuron.2012.06.012

Sulston, J. E. (1977). Post-embryonic Cell Lineages of the Nematode , Caenorhabditis elegans. Developmental Biology, 156, 110–156.

Sulston, J. E., & Brenner, S. (1974). The DNA of Caenorhabditis elegans. Genetics, 77(1), 95–104.

Sutton, R. B., Fasshauer, D., Jahn, R., & Brunger, A. T. (1998). Crystal structure of a SNARE complex involved in synaptic exocytosis at 2.4 A resolution. Nature, 395(6700), 347–353. http://doi.org/10.1038/26412

Sweitzer, S. M., & Hinshaw, J. E. (1998). Dynamin undergoes a GTP-dependent conformational change causing vesiculation. Cell, 93(6), 1021–1029. http://doi.org/10.1016/S0092-8674(00)81207-6

T, K., S, Y., & S, O. (2008). Caenorhabditis elegans gelsolin-like protein 1 (GSNL-1) is a novel actin filament severing protein with four gelsolin-like repeats. J Biol Chem. Retrieved from http://www.wormbase.org/db/misc/paper?name=WBPaper00032034

Takao-Rikitsu, E., Mochida, S., Inoue, E., Deguchi-Tawarada, M., Inoue, M., Ohtsuka, T., & Takai, Y. (2004). Physical and functional interaction of the active zone proteins, CAST, RIM1, and Bassoon, in neurotransmitter release. Journal of Cell Biology, 164(2), 301–311. http://doi.org/10.1083/jcb.200307101

Tandon, A., Bannykh, S., Kowalchyk, J. A., Banerjee, A., Martin, T. F. J., & Balch, W. E. (2017). Differential Regulation of Exocytosis by Calcium and CAPS in Semi-Intact Synaptosomes. Neuron, 21(1), 147–154. http://doi.org/10.1016/S0896-6273(00)80522-X

Tao-Cheng, J. H. (2007). Ultrastructural localization of active zone and synaptic vesicle proteins in a preassembled multi-vesicle transport aggregate. Neuroscience, 150. http://doi.org/10.1016/j.neuroscience.2007.09.031

Thompson-Peer, K. L., Bai, J., Hu, Z., & Kaplan, J. (2012). HBL-1 patterns synaptic remodeling in C.elegans. Neuron, 73(3), 453–465. http://doi.org/10.1016/j.neuron.2011.11.025

Tom Dieck, S., Sanmartí-Vila, L., Langnaese, K., Richter, K., Kindler, S., Soyke, A., … Gundelfinger, E. D. (1998). Bassoon, a novel zinc-finger CAG/glutamine-repeat protein selectively localized at the active zone of presynaptic nerve terminals. Journal of Cell Biology, 142(2), 499–509. http://doi.org/10.1083/jcb.142.2.499

Tursun, B., Cochella, L., Carrera, I., & Hobert, O. (2009). A toolkit and robust pipeline for the generation of fosmid-based reporter genes in C. elegans. PLoS ONE, 4(3). http://doi.org/10.1371/journal.pone.0004625

Ungewickell, E., Ungewickell, H., Holstein, S. E. H., Lindner, R., Prasad, K., Barouch, W., … Eisenberg, E. (1995). Role of auxilin in uncoating clathrin-coated vesicles. Nature, 378(6557), 632–635. http://doi.org/10.1038/378632a0

Verhage, M., McMahon, H. T., Ghijsen, W. E. J. M., Boomsma, F., Scholten, G., Wiegant, V. M., & Nicholls, D. G. (1991). Differential release of amino acids, neuropeptides, and

catecholamines from isolated nerve terminals. Neuron, 6(4), 517–524. http://doi.org/10.1016/0896-6273(91)90054-4

Voglis, G., & Tavernarakis, N. (2008). A synaptic DEG/ENaC ion channel mediates learning in C. elegans by facilitating dopamine signalling. The EMBO Journal, 27(24), 3288–3299. http://doi.org/10.1038/emboj.2008.252

Waites, C. L., Leal-Ortiz, S. A., Okerlund, N., Dalke, H., Fejtova, A., Altrock, W. D., … Garner, C. C. (2013). Bassoon and Piccolo maintain synapse integrity by regulating protein ubiquitination and degradation. The EMBO Journal, 32(7), 954–969. http://doi.org/10.1038/emboj.2013.27

Waldmann, R., Champigny, G., Bassilana, F., Voilley, N., & Lazdunski, M. (1995). Molecular Cloning and Functional Expression of a Novel Amiloride-sensitive Na + Channel. Journal of Biological Chemistry, 270(46), 27411–27414. http://doi.org/10.1074/jbc.270.46.27411

Walthall, W. W., & Plunkett, J. A. (1995). Genetic transformation of the synaptic pattern of a motoneuron class in Caenorhabditis elegans. The Journal of Neuroscience : The Official Journal of the Society for Neuroscience, 15(2), 1035–1043.

Wang, H., & Sieburth, D. (2013). PKA controls calcium influx into motor neurons during a rhythmic behavior. PLoS Genetics, 9(9), e1003831. http://doi.org/10.1371/journal.pgen.1003831

Wang, J. Y., Chen, F., Fu, X. Q., Ding, C. S., Zhou, L., Zhang, X. H., & Luo, Z. G. (2014). Caspase-3 cleavage of dishevelled induces elimination of postsynaptic structures. Developmental Cell, 28(6), 670–684. http://doi.org/10.1016/j.devcel.2014.02.009

Wang, S. S. H., Held, R. G., Wong, M. Y., Liu, C., Karakhanyan, A., & Kaeser, P. S. (2016). Fusion Competent Synaptic Vesicles Persist upon Active Zone Disruption and Loss of Vesicle Docking. Neuron, 91(4), 777–791. http://doi.org/10.1016/j.neuron.2016.07.005

Wang, X., Hu, B., Zieba, A., Neumann, N. G., Kasper-Sonnenberg, M., Honsbein, A., … Kilimann, M. W. (2009). A Protein Interaction Node at the Neurotransmitter Release Site: Domains of Aczonin/Piccolo, Bassoon, CAST, and Rim Converge on the N-Terminal Domain of Munc13-1. Journal of Neuroscience, 29(40), 12584–12596. http://doi.org/10.1523/JNEUROSCI.1255-09.2009

Wang, Y., Okamoto, M., Schmitz, F., Hofmann, K., & Südhof, T. C. (1997). Rim is a putative Rab3 effector in regulating synaptic-vesicle fusion. Nature, 388(6642), 593–598. http://doi.org/10.1038/41580

Wang, Y., Liu, X., Biederer, T., & Südhof, T. C. (2002). A family of RIM-binding proteins regulated by alternative splicing: Implications for the genesis of synaptic active zones. Proceedings of

the National Academy of Sciences of the United States of America, 99(22), 14464–14469. http://doi.org/10.1073/pnas.182532999

Washbourne, P., Cansino, V., Mathews, J. R., Graham, M., Burgoyne, R. D., & Wilson, M. C. (2001). Cysteine residues of SNAP-25 are required for SNARE disassembly and exocytosis, but not for membrane targeting. Biochemical Journal, 357(Pt 3), 625–634. Retrieved from http://www.ncbi.nlm.nih.gov/pmc/articles/PMC1221993/

Watanabe, S., Liu, Q., Davis, M. W., Hollopeter, G., Thomas, N., Jorgensen, N. B., & Jorgensen, E. M. (2013). Ultrafast endocytosis at Caenorhabditis elegans neuromuscular junctions. eLife, 2013(2), 1–24. http://doi.org/10.7554/eLife.00723

Weber, T., Zemelman, B. V., McNew, J. A., Westermann, B., Gmachl, M., Parlati, F., … Rothman, J. E. (1998). SNAREpins: Minimal machinery for membrane fusion. Cell, 92(6), 759–772. http://doi.org/10.1016/S0092-8674(00)81404-X

Weimer, R. M., Gracheva, E. O., Meyrignac, O., Miller, K. G., Richmond, J. E., & Bessereau, J.-L. (2006). UNC-13 and UNC-10/Rim Localize Synaptic Vesicles to Specific Membrane Domains. The Journal of Neuroscience , 26(31), 8040–8047. http://doi.org/10.1523/JNEUROSCI.2350-06.2006

Wemmie, J. A., Askwith, C. C., Lamani, E., Cassell, M. D., Freeman, J. H., & Welsh, M. J. (2003). Acid-sensing ion channel 1 is localized in brain regions with high synaptic density and contributes to fear conditioning. The Journal of Neuroscience : The Official Journal of the Society for Neuroscience, 23(13), 5496–5502. http://doi.org/23/13/5496 [pii]

Wemmie, J. A., Coryell, M. W., Askwith, C. C., Lamani, E., Leonard, A. S., Sigmund, C. D., & Welsh, M. J. (2004). Overexpression of acid-sensing ion channel 1a in transgenic mice increases acquired fear-related behavior. Proceedings of the National Academy of Sciences of the United States of America, 101(10), 3621–6. http://doi.org/10.1073/pnas.0308753101

Wemmie, J. A., Chen, J., Askwith, C. C., Hruska-Hageman, A. M., Price, M. P., Nolan, B. C., … Welsh, M. J. (2002). The acid-activated ion channel ASIC contributes to synaptic plasticity, learning, and memory. Neuron, 34(3), 463–477. http://doi.org/10.1016/S0896-6273(02)00661-X

Wemmie, J. A., Price, M. P., & Welsh, M. J. (2006). Acid-sensing ion channels: advances, questions and therapeutic opportunities. Trends in Neurosciences, 29(10), 578–586. http://doi.org/10.1016/j.tins.2006.06.014

Wemmie, J. A., Taugher, R. J., & Kreple, C. J. (2013). Acid-sensing ion channels in pain and disease. Nature Reviews Neuroscience, 14(7), 461–471. http://doi.org/10.1038/nrn3529

Wentzel, C., Sommer, J. E., Nair, R., Stiefvater, A., Sibarita, J. B., & Scheiffele, P. (2013). MSYD1A, a Mammalian Synapse-Defective-1 Protein, Regulates Synaptogenic Signaling and Vesicle Docking. Neuron, 78(6), 1012–1023. http://doi.org/10.1016/j.neuron.2013.05.010

White, J.G., Southgate, E., Thomson, J.N., Brenner, S. (1986). The Structure of the Nervous System of the Nematode Caenorhabditis elegans. Philosophical Transactions of the Royal Society of London. Series B, Biological Sciences, 314(1165), 1–340.

Winder, D. G., Mansuy, I. M., Osman, M., Moallem, T. M., & Kandel, E. R. (1998). Genetic and Pharmacological Evidence for a Novel , Intermediate Phase of Long-Term Potentiation Suppressed by Calcineurin, 92, 25–37.

Wucherpfennig, T., Wilsch-Bräuninger, M., & González-Gaitán, M. (2003). Role of Drosophila Rab5 during endosomal trafficking at the synapse and evoked neurotransmitter release. Journal of Cell Biology, 161(3), 609–624. http://doi.org/10.1083/jcb.200211087

Wyszynski, M., Kim, E., Dunah, A. W., Passafaro, M., Valtschanoff, J. G., Serra-Pagès, C., … Sheng, M. (2002). Interaction between GRIP and liprin-alpha/SYD2 is required for AMPA receptor targeting. Neuron, 34(1), 39–52. http://doi.org/S0896627302006402 [pii]

Yamamura, H., Ugawa, S., Ueda, T., Nagao, M., & Shimada, S. (2004). Protons Activate the ??-Subunit of the Epithelial Na+ Channel in Humans. Journal of Biological Chemistry, 279(13), 12529–12534. http://doi.org/10.1074/jbc.M400274200

Younger, M. A., Müller, M., Tong, A., Pym, E. C., & Davis, G. W. (2013). A presynaptic ENaC channel drives homeostatic plasticity. Neuron, 79(6), 1183–1196. http://doi.org/10.1016/j.neuron.2013.06.048

Zha, X. (2013). Acid-sensing ion channels: trafficking and synaptic function. Molecular Brain, 6(1), 1. http://doi.org/10.1186/1756-6606-6-1

Zha, X., Wemmie, J. A., Green, S. H., & Welsh, M. J. (2006). Acid-sensing ion channel 1a is a postsynaptic proton receptor that affects the density of dendritic spines. Proceedings of the National Academy of Sciences of the United States of America, 103(44), 16556–16561. http://doi.org/10.1073/pnas.0608018103

Zhai, R. G., Vardinon-Friedman, H., Cases-Langhoff, C., Becker, B., Gundelfinger, E. D., Ziv, N. E., & Garner, C. C. (2001). Assembling the presynaptic active zone: a characterization of an active one precursor vesicle. Neuron, 29. http://doi.org/10.1016/S0896-6273(01)00185-4

Zhai, R. G., Vardinon-Friedman, H., Cases-Langhoff, C., Becker, B., Gundelfinger, E. D., Ziv, N. E., & Garner, C. C. (2001). Assembling the presynaptic active zone: A characterization of an active zone precursor vesicle. Neuron, 29(1), 131–143. http://doi.org/10.1016/S0896-6273(01)00185-4

Zhou, H. M., & Walthall, W. W. (1998). UNC-55, an Orphan Nuclear Hormone Receptor, Orchestrates Synaptic Specificity among Two Classes of Motor Neurons in Caenorhabditis elegans . The Journal of Neuroscience , 18(24), 10438–10444. Retrieved from http://www.jneurosci.org/content/18/24/10438.abstract

Ziemann, A. E., Allen, J. E., Dahdaleh, N. S., Drebot, I. I., Coryell, M. W., Wunsch, A. M., … Wemmie, J. A. (2009). The Amygdala Is a Chemosensor that Detects Carbon Dioxide and Acidosis to Elicit Fear Behavior. Cell, 139(5), 1012–1021. http://doi.org/10.1016/j.cell.2009.10.029

Zucker, R. S. (1996). Exocytosis: A molecular and physiological perspective. Neuron, 17(6), 1049–1055. http://doi.org/10.1016/S0896-6273(00)80238-X

Zuo, Y., Yang, G., Kwon, E., & Gan, W.-B. (2005). Long-term sensory deprivation prevents dendritic spine loss in primary somatosensory cortex. Nature, 436(7048), 261–265. http://doi.org/10.1038/nature03715

VIII. VITA

Laura Manning

EDUCATION

University of Illinois at Chicago (UIC) August 2012 - Dec 2017
Ph.D. in Biological Sciences with a concentration in Neurobiology– December 2017
GPA: 4.0/4.0

- Advisor: Janet Richmond
- Certificate in The Foundations of College Instruction

University of Illinois Urbana-Champaign 2008-2012
B.S. in Psychology - 2012
GPA 3.6/4.0

RESEARCH EXPERIENCE

Chicago, IL
Graduate Research Assistant at University of Illinois Chicago 2012-present

- Mastered highly specialized skills in high-pressure freeze and freeze substitution electron microscopy *C. elegans* whole animal tissue
- Prepare fixed samples for morphological analysis as well as immunogold labeling and imaging using ultramicrotomy and customized post-staining procedures
- Prepare serial section reconstructions of nerve cord acquire high-resolution images for ultrastructural tissue analysis on JEOL JEM-1220 transmission electron microscope
- Implemented critical enhancement of quantitative analysis methods using custom scripts in ImageJ and scripts in MATLAB
- Mastered skills in molecular genetics to study synaptic structure and function in *C. elegans*
- Mastered skills in confocal microscopy for *in vivo* imaging of fluorescent markers in worms
- Collaborate with the labs of David Miller, Kang Shen, Daniel Colon-Ramos, and Ken Miller by generating and analyzing electron microscopy data critical to respective projects
- Wrote custom macros in FIJI for analysis of fluorescence data

Georg-August-Universtität Götttingen, Germany
Goethe-Universität, Frankfurt, Germany Summer 2013, 2014
Visiting Reseach Assistant

- Learned and developed specialized skills in high-pressure freeze electron microscopy and automatic freeze substitution alongside experts in the technique Visiting Student at Georg-August-Universtität Götttingen and Johann Wolfgang Goethe-Universität Frankfurt

- Prepared samples using state-of-the-art equipment that were later analyzed for collaborative projects
- Elevated scientific understanding and awareness by participating in lab meetings and events and communicating with international students and faculty

RESEARCH AWARDS AND FUNDING

UIC Biological Sciences Award for Research Achievement	April 2016
Bodmer International Travel Award	July 2013
LAS PhD Student Travel Award	June 2013

PUBLICATIONS

Xuan, Z., **Manning, L.**, Nelson, J., Richmond, J., Colón-Ramos, D., Shen, K., Kurshan, P. Clarinet (CLA-1), a novel active zone protein required for synaptic vesicle clustering and release. Elife, *in press*. (equally contributing first author)

Morrison, L., Edwards, S., **Manning, L.**, Stec, Natalia., Richmond, J., Miller, K. Sentryn and SAD Kinase Link Dense Core Vesicle Axonal Transport and Synaptic Capture. *Manuscript in preparation*.

Edwards, S., Morrison, L., **Manning, L**., Stec, Natalia., Richmond, J., Miller, K. Sentryn Acts with a Subset of Active Zone Proteins to Link the Guided Transport and Capture of Synaptic Vesicles. *Manuscript in preparation.*

Miller-Fleming, T. W., Petersen, S.C., **Manning, L**., Matthewman, C., Gornet, M., Beers, A., Mitani, S., Bianchi, L., Richmond, J., Miller, D. The DEG/ENaC cation channel protein UNC-8 drives activity-dependent synapse removal in remodeling GABAergic neurons. Elife 5, 1–28 (2016).

POSTERS

Manning, L. & Richmond, J. in C. elegans: Methods and Applications (eds. Biron, D. & Haspel, G.) 121–140 (Humana Press, 2015). doi:10.1007/978-1-4939-2842-2_10

Manning, L., Martin, A., Bhetuwal, O., Richmond, J. "Investigating the role of the G ↓s pathway in neurotransmission." Society for Neuroscience Annual Meeting, Chicago, IL. Oct 12-18, 2015.

Manning, LM., Martin, AM., Bhetuwal, O., Richmond, JE. "Investigating the synaptic role of the Gαs pathway" International C. Elegans Meeting, Los Angeles, CA. June 26-30, 2015.

Manning, LM., Martin, AM., Takaki, S., Richmond, JE. "Investigating the synaptic role of the Gαs pathway" Midwest C. Elegans Meeting. Grand Rapid, MI. April 11, 2015.

Manning, LM., Martin, AM., Takaki, S., Richmond, JE. "Investigating the synaptic role of the Gαs pathway" C. elegans Topic Meeting. Madison, WI. Jul 7-10, 2014.

TEACHING AWARDS

- UIC Excellence in Undergraduate Mentoring for Graduate Students Award - Recognized by the Dean of the Graduate College (2017)
- Teaching Excellence Award - Recognized by the UIC Biological Sciences Department (2015 and 2017)

TEACHING EXPERIENCE

University of Illinois at Chicago

Teaching Assistant for Neuroscience I and II (BIOS 484 and 485) 2014-present

- Designed and implemented feedback surveys to improve course curriculum and syllabus
- Implemented key changes in design of course and major class project
- Conducted heavily attended office hours and supplemental review sessions to help students master concepts, review old exams
- Used technology to broadly expand student access to my time, including extensive use of Blackboard communication tools
- Designed and delivered guest lectures on acetylcholine reception

Teaching Assistant for various courses in Biological Sciences 2012-present

- Prepared weekly presentations and worksheets to review class material
- Led students through lab procedure and discussion
- Compiled and graded weekly quizzes, graded lab reports and exams, kept records of grades using Excel and Blackboard
- Provided informal advising to students in Biological Sciences courses in college success, course selection, career counseling, and stress management
- Provided support for medical school and graduate school applications, including:
    - Interviewing and writing recommendation letters
    - Advising in pre-health career options and alternatives to medical school
    - Reviewing personal statements

Guest Lecturer/Speaker:

- BIOS 184 – The Basics of Neuroscience – *"The Mind of a Worm," (2017)*
- UIC New TA Orientation – *"How to Survive and Excel as a Graduate Student Who Teaches"* (2017)
- BIOS 386 – Seminar in Neurobiology – *Neuroscience of Sex: Mating behavior in* C. elegans (2016)
- HON 201 – Biomedical Discovery and the Media – *Obesity* (2016)
- BIOS 184 – The Basics of Neuroscience – *The nervous system of the worm* (2015)
- BIOS 484 – Foundations of Neuroscience – *Acetylcholine reception* (2016)

MENTORING EXPERIENCE

University of Illinois at Chicago

Undergraduate Research Supervisor 2012-2016

- Mentored two pre-health undergraduate students in BIOS 399 Independent Research

projects
- Guided students in:
    - Goal-setting and project management skills to complete Capstone Project
    - Learning and performing research techniques, data analysis, literature review
    - Writing successfully funded LASURI Award ($2,250) and Undergraduate Honors College Research Grant ($733)
    - Designing and presenting posters at Student Research Forum and Chicago Area Undergraduate Research Symposium

Northwestern University
Science Club Mentor 2015-present
- Mentor middle school children from underserved groups once/week at the True Value Boys and Girls Club
- Guide students through hands-on science projects to encourage critical thinking and writing skills
- Complete quarterly training in mentor development, including classroom management strategies, curriculum standards and implementation, and working with diverse students
- Recruited additional mentors from UIC colleagues for newly developed program

University of Illinois at Chicago
Mentor for UIC Women in Science and Engineering (WISE) 2016-present
- Engage in monthly mentoring sessions with pre-health undergraduate regarding:
    - course progress and selection
    - identifying resources on and off campus for MCAT/GRE prep, volunteering and networking opportunities
    - managing work-life balance and career planning

SERVICE AND LEADERSHIP

University of Illinois at Chicago
Founder and Editor-in-Chief of The Science Café 2016-present
- Initiated and created monthly email newsletter and website to create an online community that connects the UIC Biological Sciences graduate students with department and broader UIC community
- Recruited team of student writers and faculty/staff advisors
- Grew readership to over 100 subscribers
- Publish monthly issues containing original student content and resources for readers

Chicago, IL
Co-President of Expanding Your Horizons Chicago 2013-present
- Lead efforts to organize annual conference for over 200 6-8th grade girls to promote women in STEM careers

- Structured and manage subcommittee chairs in efforts to coordinate conference, including selecting workshop leaders, training volunteers, recruiting student participants, event organizing, and fundraising
- Raised and managed $5000 budget
- Initiate and develop broad vision and long-term goals to support our mission

University of Illinois at Chicago
Treasurer and Secretary of Biological Graduate Student Association 2016-2017

- spearheaded and organized efforts to obtain official recognition at university level that deems organization eligible for funding
- invited key speakers and helped organize career panel and lunch for graduate students
- developed community-building and professional development events such as a professional headshot session for students

Chicago, IL
Invited speaker

- Rauner College Prep STEM Expo – "Researching Neurobiology" - 2015 and 2016
- Loyola Neuroscience Society - "Talk Nerdy To Me: The importance of science outreach and communication," – 2015
- Women in Science and Engineering Career Panel - 2016